Transition Metal Complexes of Bis(carboranes) and their Potential as Catalyst Precursors

Antony P. Y. Chan

Submitted for the degree of Doctor of Philosophy at Heriot-Watt University, on completion of research in the School of Engineering and Physical Sciences.

February 2019

Abstract

Chapter 1 provides a short overview of heteroborane chemistry with particular attention on the areas of metallacarborane catalysts and bis(*o*-carborane). It also includes a more detailed scope of the thesis.

Chapter 2 reports the first examples of heterometalated bis(carboranes) using cobalt and ruthenium, specifically their preparation and characterisation. Tangential to this is the isolation of a novel 13-vertex/12-vertex species, the former of which possesses the first crystallographically-determined 4,5,1,12-$M_2C_2B_9$ architecture (where M = CoCp*).

Chapter 3 expands the range of heterometalated bis(carboranes) to include those with the catalytically-active rhodium fragment {$Rh(PPh_3)_2H$}. Additionally, the first example of a crystallographically-characterised rhodacarborane/carborane species is reported.

Chapter 4 discusses the catalytic activity of the rhodacarborane compounds in alkene isomerisation and ketone hydrosilylation. The results of preliminary DFT calculations into the possible mechanisms of these catalytic reactions are also included.

Chapter 5 contains the experimental procedures and spectroscopic details for all novel compounds discussed.

Appendix A explores the use of phosphites as ligands in rhodacarboranes and *Appendix B* details the preliminary results in the deboronation/metalation of bis(*m*-carborane). *Appendix C* summarises the crystallographic tables of all compounds studied by *X*RD in this thesis.

Acknowledgements

First and foremost, I would like express my sincerest thanks and gratitude to Professor Alan J. Welch for his continual guidance, dedication and enthusiasm throughout my PhD. His keen interest in carborane chemistry during my MChem project was a key factor for my pursuit in a PhD position within the Heteroborane Group. I am grateful not only for the chemistry knowledge he has imparted but also skills in critical thinking, grammar and well-constructed PowerPoint slides. I would also like to acknowledge the CRITICAT Centre for Doctoral Training program for funding and the additional training opportunities I was able to experience.

Special thanks goes to Dr Wing Y. Man for my induction into the Heteroborane Group as well as her patience whilst supervising over my MChem project. I must also thank Dr Alasdair P. M. Robertson for the extensive knowledge and support he provided during his time in the group. I would also like to thank all the previous group members and project students who have had a positive impact on my time in the group, especially my fumehood neighbour Dr Laura E. Riley (Woodward). Many thanks to Amanda Benton for her continually positive self and Rebekah J. Jeans for tolerating my sense of humour enough to return for a PhD.

Additionally, I must also thank all the technical staff for their services, in particular Dr David Ellis for countless helpful discussions and his expertise in NMR spectroscopy, and Dr Georgina M. Rosair for dealing with my frequently poor crystal samples. I would also like to acknowledge Prof. Stuart A. Macgregor for the DFT calculations presented in Chapter 4 and his help in my understanding of these results. I must also thank my fellow PhD and postdoctoral colleagues for enriching my PhD experience, especially those who studied alongside me during my undergraduate degree.

Finally, I wish to thank my family for accepting my decision to pursue further education as opposed to settling down in a career, something that I presume will be expected of me now.

ACADEMIC REGISTRY

Research Thesis Submission

Please note this form should be bound into the submitted thesis.

Name*:*	Antony P. Y. Chan		
School:	Engineering and Physical Sciences		
Version: *(i.e. First, Resubmission, Final)*	Final	Degree Sought:	PhD

Declaration

In accordance with the appropriate regulations I hereby submit my thesis and I declare that:

1. The thesis embodies the results of my own work and has been composed by myself
2. Where appropriate, I have made acknowledgement of the work of others
3. Where the thesis contains published outputs under Regulation 6 (9.1.2) these are accompanied by a critical review which accurately describes my contribution to the research and, for multi-author outputs, a signed declaration indicating the contribution of each author (complete Inclusion of Published Works Form – see below)
4. The thesis is the correct version for submission and is the same version as any electronic versions submitted*.
5. My thesis for the award referred to, deposited in the Heriot-Watt University Library, should be made available for loan or photocopying and be available via the Institutional Repository, subject to such conditions as the Librarian may require
6. I understand that as a student of the University I am required to abide by the Regulations of the University and to conform to its discipline.
7. Inclusion of published outputs under Regulation 6 (9.1.2) shall not constitute plagiarism.
8. I confirm that the thesis has been verified against plagiarism via an approved plagiarism detection application e.g. Turnitin.

* *Please note that it is the responsibility of the candidate to ensure that the correct version of the thesis is submitted.*

Signature of Candidate*:*		Date:	

Submission

Submitted By *(name in capitals):*	ANGELA FONG
Signature of Individual Submitting:	
Date Submitted:	

For Completion in the Student Service Centre (SSC)

Received in the SSC by *(name in capitals):*			
Method of Submission *(Handed in to SSC; posted through internal/external mail):*			
*E-thesis Submitted (**mandatory for final theses**)*			
Signature:		Date:	

ACADEMIC REGISTRY

Inclusion of Published Works

Declaration

This thesis contains one or more multi-author published works. In accordance with Regulation 6 (9.1.2) I hereby declare that the contributions of each author to these publications is as follows:

Citation details	G. Thiripuranathar, W. Y. Man, C. Palmero, A. P. Y. Chan, B. T. Leube, D. Ellis, D. McKay, S. A. Macgregor, L. Jourdan, G. M. Rosair and A. J. Welch, Icosahedral Metallacarborane/Carborane Species Derived from 1,1′-bis(*o*-carborane), *Dalton Trans.*, 2015, **44**, 5628-5637.
Authors 1-5	Synthesis and characterisation
Author 6	NMR Spectroscopy
Author 7	Computational
Authors 9,10	Crystallography
Authors 8, 11	Supervisor
Signature:	
Date:	

Citation details	L. E. Riley, A. P. Y. Chan, J. Taylor, W. Y. Man, D. Ellis, G. M. Rosair, A. J. Welch and I. B. Sivaev, Unprecedented Flexibility of the 1,1'-bis(o-carborane) Ligand: Catalytically-Active Species Stabilised by B-agostic B-H→Ru Interactions, *Dalton Trans.*, 2016, **45**, 1127-1137.
Authors 1-4	Synthesis and characterisation
Author 5	NMR Spectroscopy
Author 6	Crystallography
Authors 7,8	Supervisor
Signature:	
Date:	

Citation details	G. Thiripuranathar, A. P. Y. Chan, D. Mandal, W. Y. Man, M. Argentari, G. M. Rosair and A. J. Welch, Double Deboronation and Homometalation of 1,1′-bis(*ortho*-carborane), *Dalton Trans.*, 2017, **46**, 1811-1821.
Authors 1-5	Synthesis and characterisation
Author 6	Crystallography
Author 7	Supervisor
Signature:	
Date:	

Citation details	A. P. Y. Chan, G. M. Rosair and A. J. Welch, Heterometalation of 1,1′-bis(*o*-carborane), *Inorg. Chem.*, 2018, **57**, 8002-8011.
Author 1	Synthesis and characterisation
Author 2	Crystallography
Author 3	Supervisor
Signature:	
Date:	

Table of Contents

Chapter 4 – Rhodacarboranes in Catalysis

Chapter 5 – Experimental

Abbreviations and Acronyms

2c-2e	Two-Centre-Two-Electron
BHD	Boron-to-Hydrogen Distance
Bis(*o*-carborane)	[1-(1′-*closo*-1′,2′-$C_2B_{10}H_{11}$)-*closo*-1,2-$C_2B_{10}H_{11}$]
Bis(*m*-carborane)	[1-(1′-*closo*-1′,7′-$C_2B_{10}H_{11}$)-*closo*-1,7-$C_2B_{10}H_{11}$]
BNCT	Boron Neutron Capture Therapy
BTMA	Benzyltrimethylammonium
Cp	Cyclopentadienyl
Cp*	Pentamethylcyclopentadienyl
DCM	Dichloromethane
DEI	Direct Electrophilic Insertion
DFT	Density Functional Theory
DME	1,2-Dimethoxyethane
DSD	Diamond-Square-Diamond
EI	Electron Ionisation
ELO	Exo-Polyhedral Ligand Orientation
ESI	ElectroSpray Ionisation
FMO	Frontier Molecular Orbital
MS	Mass Spectrum
NBO	Natural Bond Orbital
NMR	Nuclear Magnetic Resonance

Petrol	Petroleum Ether 40-60 °C
PSEP	Polyhedral Skeletal Electron Pair
PSEPT	Polyhedral Skeletal Electron Pair Theory
SC*X*RD	Single Crystal *X*-Ray Diffraction
STE	Structural Trans Effect
TFR	Triangular Face Rotation
THF	Tetrahydrofuran
TLC	Thin Layer Chromatography
U_{eq}	Equivalent Isotropic Thermal Displacement Parameter
VCD	Vertex-to-Centroid Distance

Abbreviations for Selected Compounds

VIII [3-H-3,3-$(PPh_3)_2$-*closo*-3,1,2-$RhC_2B_9H_{11}$]

XXX [2-H-2,2-$(PPh_3)_2$-*closo*-2,1,12-$RhC_2B_9H_{11}$]

1 [$HNMe_3$][8-(7′-*nido*-7′,8′-$C_2B_9H_{11}$)-2-(*p*-cymene)-*closo*-2,1,8-$RuC_2B_9H_{10}$]

2*α* *α*-[8-(1′-3′-Cp-*closo*-3′,1′,2′-$CoC_2B_9H_{10}$)-2-(*p*-cymene)-*closo*-2,1,8-$RuC_2B_9H_{10}$]

2*β* *β*-[8-(1′-3′-Cp-*closo*-3′,1′,2′-$CoC_2B_9H_{10}$)-2-(*p*-cymene)-*closo*-2,1,8-$RuC_2B_9H_{10}$]

3 [$HNMe_3$][8-(7′-*nido*-7′,8′-$C_2B_9H_{11}$)-2-Cp-*closo*-2,1,8-$CoC_2B_9H_{10}$]

4 [1-(1′-*closo*-1′,2′-$C_2B_{10}H_{11}$)-3-Cp*-*closo*-3,1,2-$CoC_2B_9H_{10}$]

5 [8-(1′-*closo*-1′,2′-$C_2B_{10}H_{11}$)-2-Cp*-*closo*-2,1,8-$CoC_2B_9H_{10}$]

6 [12-(1′-*closo*-1′,2′-$C_2B_{10}H_{11}$)-4,5-Cp^*_2-*closo*-4,5,1,12-$Co_2C_2B_9H_{10}$]

7 [$HNMe_3$][8-(7′-*nido*-7′,8′-$C_2B_9H_{11}$)-2-Cp*-*closo*-2,1,8-$CoC_2B_9H_{10}$]

8 [8-(1′-3′-(*p*-cymene)-*closo*-3′,1′,2′-$RuC_2B_9H_{10}$)-2-Cp*-*closo*-2,1,8-$CoC_2B_9H_{10}$]

9 [8-(8′-2′-(*p*-cymene)-*closo*-2′,1′,8′-$RuC_2B_9H_{10}$)-2-Cp*-*closo*-2,1,8-$CoC_2B_9H_{10}$]

10 [8-(1′-*closo*-1′,2′-$C_2B_{10}H_{11}$)-2-H-2,2-$(PPh_3)_2$-*closo*-2,1,8-$RhC_2B_9H_{10}$]

11*α* *α*-[8-(8′-2′-(*p*-cymene)-*closo*-2′,1′,8′-$RuC_2B_9H_{10}$)-2-H-2,2-$(PPh_3)_2$-*closo*-2,1,8-$RhC_2B_9H_{10}$]

11*β* *β*-[8-(8′-2′-(*p*-cymene)-*closo*-2′,1′,8′-$RuC_2B_9H_{10}$)-2-H-2,2-$(PPh_3)_2$-*closo*-2,1,8-$RhC_2B_9H_{10}$]

12*α* *α*-[8-(8′-2′-Cp*-*closo*-2′,1′,8′-$CoC_2B_9H_{10}$)-2-H-2,2-$(PPh_3)_2$-*closo*-2,1,8-$RhC_2B_9H_{10}$]

12*β* *β*-[8-(8′-2′-Cp*-*closo*-2′,1′,8′-$CoC_2B_9H_{10}$)-2-H-2,2-$(PPh_3)_2$-*closo*-2,1,8-$RhC_2B_9H_{10}$]

13 [3-H-3,3-$\{P(OPh)_3\}_2$-*closo*-3,1,2-$RhC_2B_9H_{11}$]

14 [8-(1′-*closo*-1′,2′-$C_2B_{10}H_{11}$)-2-H-2,2-$\{P(OPh)_3\}_2$-*closo*-2,1,8-$RhC_2B_9H_{10}$]

15 [$HNMe_3$][7-(1′-*closo*-1′,7′-$C_2B_{10}H_{11}$)-*nido*-7,9-$C_2B_9H_{11}$]

Chapter 1

Introduction

1.1 Boron

The name 'boron' is derived from a combination of borax, the most common boron-containing mineral, and carbon, its adjacent element in the Periodic Table. Despite its low atomic weight and simplicity, boron only constitutes roughly 0.001% of the Earth's crust and does not exists naturally in its elemental state. The metalloid was not recognised as an element until 1808 when it was independently isolated by the English Davy,[1] and the French Gay-Lussac and Thenard.[2]

There are two naturally occurring isotopes of boron, ^{10}B and ^{11}B. Both isotopes are stable indefinitely and have a natural abundance of 19.9% and 80.1%, respectively. There are 14 radioisotopes of boron currently discovered, ranging from a mass number of 6 to 21, the longest half-life of which is ^{8}B (λ = 770 ms). Both stable isotopes of boron are NMR-active but ^{11}B NMR is exclusively used in research due to its greater abundance and higher receptivity. Further to this, the smaller nuclear spin of ^{11}B (I = 3/2) compared to ^{10}B (I = 3) reduces the splitting observed from boron coupling, simplifying the NMR spectra.[3] However, ^{10}B NMR is commonly used for ^{10}B-enriched compounds for BNCT.

1.2 Boranes

Boron possesses three valence electrons available for bonding and typically forms trigonal planar compounds. However, these BX_3 species are coordinatively unsaturated as there is a vacant p_z orbital on the B atom (Figure 1.1, left). The empty orbital can accept a lone pair from a Lewis base to stabilise the species by achieving a stable octet around the boron centre (Figure 1.1, right). Consequently, it is not surprising that the simplest boron containing compound BH_3 does not exist as a free entity.

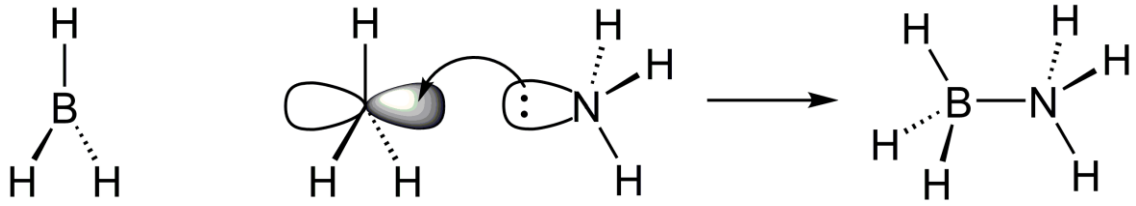

Figure 1.1 Predicted structure of borane (BH_3) and general schematic of Lewis adduct formation.

Boron hydrides, colloquially known as boranes, are simply compounds derived from solely boron and hydrogen. The first examples of these compounds were reported by Alfred Stock in the 1930s with diborane (B_2H_6) as the simplest species (Figure 1.2, left).[4] Two general families of boranes were noted; B_nH_{n+4} and B_nH_{n+6}.

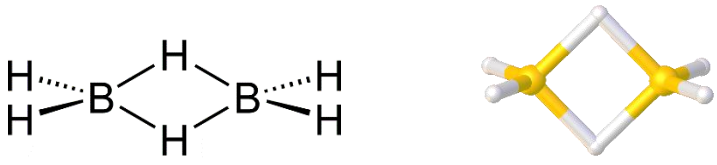

Figure 1.2 Structure of diborane (B_2H_6) predicted by Bauer and Schomaker, subsequently confirmed crystallographically by Lipscomb. Selected bond lengths: B–$H_{terminal}$ 1.09(2) Å, B–$H_{bridging}$ 1.24(2) Å.

Due to limitations in spectroscopic techniques, full characterisation of these compounds was not completed. It was assumed that these boranes were structural analogues of the related carbon hydrides with the difference of being electron-deficient as there are fewer valence electrons.[5] However, an ethane-like structure was ruled out following further analytical investigation leading to the proposal of a bridging B_2H_6 structure.[6,7] With the development of Single Crystal *X*-Ray Diffraction (SC*X*RD) in the 1950s, the structure of diborane was confirmed to be a dimeric species possessing bridging-H atoms (Figure 1.2, right).[8] This supports the proposal by Longuet-Higgins who conceptualised 3-centre-2-electron (3c-2e) bonding to account for the missing electrons required for classical 2c-2e bonding.[9] Additionally, through theoretical studies, the icosahedral structure of $[B_{12}H_{12}]^{2-}$ was predicted by Longuet-Higgins[10] and the species later isolated in 1960 by Hawthorne (Figure 1.3).[11]

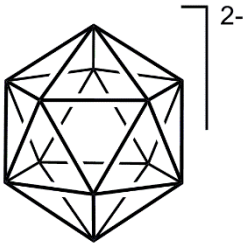

Figure 1.3 Structure of the icosahedral dianion $[B_{12}H_{12}]^{2-}$. Unlabelled vertices in clusters are treated as BH throughout.

Subsequently, *styx* rules were developed by Lipscomb as a general methodology for rationalising and predicting the structure of boranes.[12] A localised bonding schematic can be deduced by solving a set of equations that accounts for the number of B–H–B (*s*), B–B–B (*t*), B–B (*y*) and BH_2 (*x*) units. Though useful for relatively small boranes, predicting the exact structure of larger clusters becomes challenging.

In the 1970s, Williams recognised the structures of open boranes and carboranes were not simply fragments of an icosahedron but rather related to their own parent structure after classifying each species as either closo (parent polyhedron), nido (one missing vertex) or arachno (two missing vertices).[13] Based on this, a set of rules was proposed by Wade,[14]

consequently extended by Mingos,[15] relating the structure of the cluster and the number of skeletal electron pairs known as Wade's rules or Wade-Mingos rules (also commonly referred to as Polyhedral Skeletal Electron Pair Theory, PSEPT). This approach does not discriminate the elements in the cluster and thus can also be applied to heteroboranes and metal clusters.

The number of PSEPs is calculated by breaking the cluster into individual fragments and the electron contribution of each fragment (*s*) to the skeletal framework is determined and summed.

For main group vertex $s = v + x - 2$

For transition metal vertex (18e) $s = v + x - 12$

For transition metal vertex (16e) $s = v + x - 10$

where v = no. of valence electrons of the vertex atom; x = no. of electrons provided by exopolyhedral substituents.

The total number of skeletal electrons is divided by two to obtain the number of PSEPs. The geometry of the cluster can then be deduced by comparison of the number of PSEPs and the number of vertices present (n):

$(n + 1)$ PSEPs ≡ closo structure i.e. parent polyhedron

$(n + 2)$ PSEPs ≡ nido structure i.e. one vertex removed from parent polyhedron

$(n + 3)$ PSEPs ≡ arachno structure i.e. two adjacent vertices removed from parent polyhedron

1.3 Carboranes

Carboranes are a subclass of boron clusters and can contain up to five carbon atoms. The most prominent species is the icosahedral $C_2B_{10}H_{12}$ cluster first prepared by Heying[16] in 1963 and subsequently structurally characterised by Bohn in 1971 *via* electron diffraction studies.[17] The 12-vertex species can exist as three structural isomers based on the location of the cage C atoms, the first of which was *ortho*-carborane (*closo*-1,2-$C_2B_{10}H_{12}$) prepared *via* the insertion of acetylene into decaborane (*nido*-$B_{10}H_{14}$) in the presence of a Lewis base (Figure 1.4). This synthetic procedure has been adapted to prepare a variety of C-substituted *ortho*-carboranes.[18]

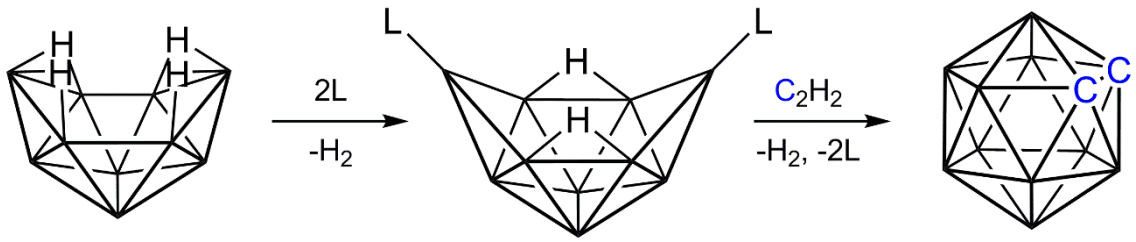

Figure 1.4 General schematic for the preparation of *ortho*-carborane from decaborane *nido*-$B_{10}H_{14}$ *via* the *arachno*-$L_2B_{10}H_{12}$ intermediate complex. Cage C vertices treated as CH unless specified throughout.

Isomerisation of *ortho*-carborane can be induced thermally to produce the meta-[16,19] and para-[20] isomers, *closo*-1,7-$C_2B_{10}H_{12}$ and *closo*-1,12-$C_2B_{10}H_{12}$ respectively (Figure 1.5). The increased separation of the cage C atoms is thermodynamically favoured due to the electrostatic repulsion of the electronegative carbon vertices relative to the boron vertices.

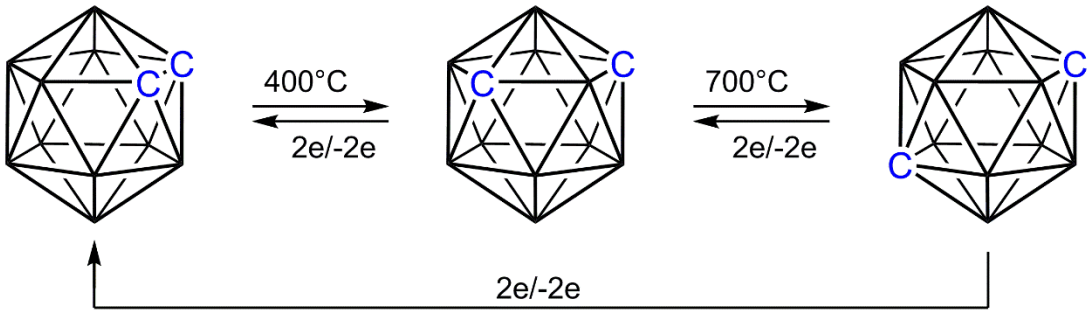

Figure 1.5 The three isomers of $C_2B_{10}H_{12}$ and their isomerisation pathways.

This isomerisation can be reversed by a reduction/oxidation process where two electrons are added to the cage to produce a [*nido*-$C_2B_{10}H_{12}$]$^{2-}$ species which is subsequently re-oxidised.[21,22] These air-sensitive reduced carborane species are the most common precursors for polyhedral expansion where reduction is followed by capitation with an appropriate fragment.

The mechanism for the isomerisation of *o*-carborane to both *m*- and *p*-carborane has yet to be definitively proven as the high temperatures involved prevents the isolation of intermediates. The most widely accepted mechanisms for this process are the Diamond-Square-Diamond (DSD)[23] rearrangement and Triangular Face Rotation (TFR).[24]

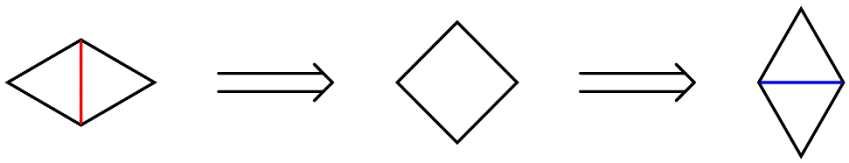

Figure 1.6 The DSD mechanism; connectivity cleaved (red) and formed (blue) highlighted.

The DSD rearrangement proposes the cleavage of a common connectivity shared by two triangular faces to form a square-faced intermediate (Figure 1.6). Subsequent formation of a new connectivity perpendicular to the previously broken edge regenerates two triangular faces where the vertices have shifted. Low activation energies and minimal bond stretching for one DSD transition are the main reasons for the credibility of this mechanism. Using DSD, Lipscomb proposed a cuboctahedral intermediate in an attempt to rationalise the isomerisation of *o*- to *m*-carborane (Figure 1.7). This intermediate would be accessed *via* six simultaneous DSD transformations.

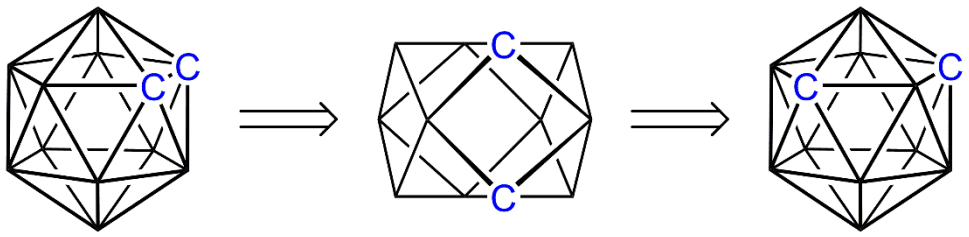

Figure 1.7 Proposed mechanism for the isomerisation of *o*-carborane to *m*-carborane through a cuboctahedral intermediate.

Though plausible, the *para*-isomer cannot be formed by the same mechanism starting from either *o*- or *m*-carborane. Additionally, the proposed intermediate was deemed too high energy to access by Wales[25] who argued that the isomerisation was likely to proceed *via* sequential DSD rearrangements producing several low-symmetry intermediates with relatively lower activation energies. Isolation of a non-icosahedral metallacarborane intermediate (**I**) by Welch[26] further supports Wales' proposal (Figure 1.8). Interestingly, a distorted cuboctahedral carborane was structurally characterised by Hosmane however this species is the result of additional skeletal electron pairs (14 PSEPs) stabilised by bulky substituents.[27]

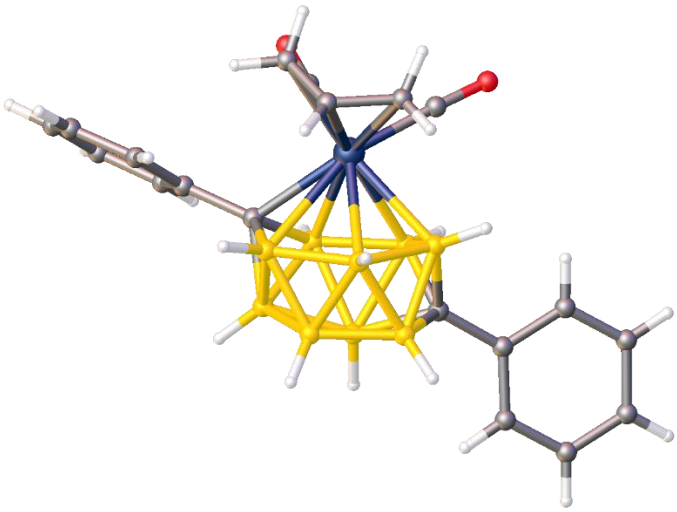

Figure 1.8 Perspective view of $[Ph_2(CO)_2(\eta^3\text{-}C_3H_5)MoC_2B_9H_9]^-$ (**I**) where the cluster displays a non-icosahedral geometry. The cation has been omitted for clarity.

The alternative accepted mechanism is quite simply the 120° rotation of a triangular face of the polyhedron, hence TFR (Figure 1.9). Recent theoretical studies have shown TFR to be a low energy process for the isomerisation of *o*- to *m*-carborane.[28] The energy required is equivalent to three DSD rearrangements, the same number of DSD steps required to replicate a TFR, and is thus widely accepted to be effectively the same process. As such, both mechanisms are equally acknowledged and applied.

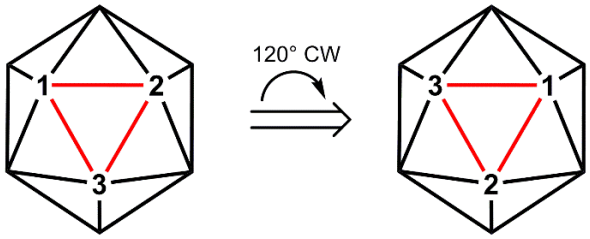

Figure 1.9 The TFR rearrangement mechanism

1.3.1 Numbering and Nomenclature

Polyhedral boranes are named similarly to the oxa-aza replacement protocol for organic chemistry where replacement of one or more boron atoms with a heteroatom or transition metal affixes the appropriate prefix, e.g. carborane for carbon and rhodaborane for rhodium. As discussed in Section 1.2, the structure is denoted with closo- for a closed polyhedron and nido- or arachno- for species in which one or two vertices, respectively, are missing.

The clusters are numbered according to the highest-order symmetry axis of the closed parent polyhedron, numbering successive belts in a clockwise direction where the first vertex to be numbered in the following belt must be clockwise relative to the first vertex numbered in the preceding belt. Priority is assigned to the highest atomic number if multiple elements are incorporated into the cluster. However, there is an exception to this general rule that is particularly relevant in this work; in metallacarboranes, C atoms take precedence over M atoms. For example, [3-Cp-*closo*-3,1,2-$CoC_2B_9H_{11}$] is numbered accordingly (Figure 1.10) as it is derived from *closo*-1,2-$C_2B_{10}H_{12}$ by replacement of the B3 vertex with a {CoCp} fragment whereas, if applying the 'highest atomic number' rule, the nomenclature would be [1-Cp-*closo*-1,2,3-$CoC_2B_9H_{11}$]. Whilst this rule is not certified by IUPAC, it simplifies the discussion of metallacarboranes and is adopted by all in this field.

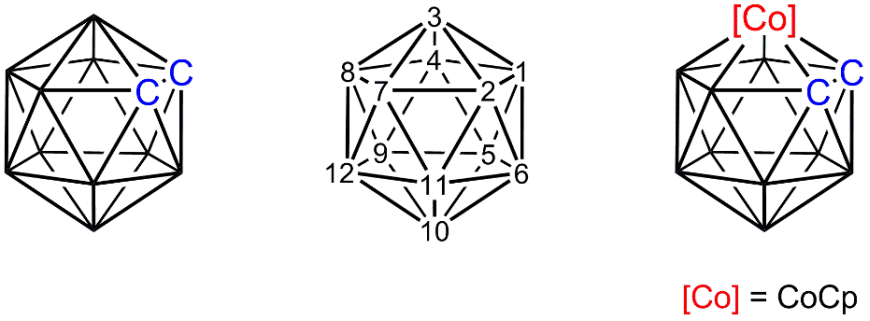

Figure 1.10 The structures of *closo*-1,2-$C_2B_{10}H_{12}$ and [3-Cp-*closo*-3,1,2-$CoC_2B_9H_{11}$] and their related numbering scheme (centre).

When numbering *nido*-C_2B_9 species, the vertex antipodal to the open face is designated 1. Successive belts are then numbered in the same fashion where the C atoms are assigned the lowest number possible (Figure 1.11).

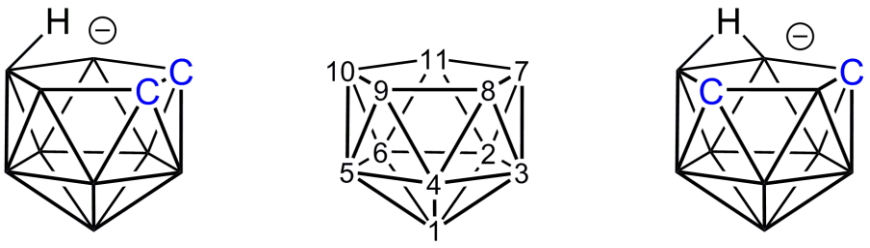

Figure 1.11 The structures of [*nido*-7,8-$C_2B_9H_{12}$]$^-$ and [*nido*-7,9-$C_2B_9H_{12}$]$^-$ and their related numbering scheme (centre).

1.3.2 Reactivity of Carboranes

There are three main types of reactions that carboranes can undergo: substitution at a cage vertex, polyhedral subrogation and polyhedral expansion.

Aside from utilising substituted acetylenes,[18] nucleophilic substitution is an alternative method for adding exopolyhedral groups to the cage C atoms.[29-32] The greater electronegativity of carbon over boron generates a higher delta positive charge on the attached H atom relative to the H atoms attached to boron. Deprotonation at the cage C position, typically *via* an alkyl lithium reagent, generates an anionic nucleophile that can attack an appropriate reagent, such as an alkyl halide, to afford the *C*-substituted carborane. By adjusting the stoichiometry, both mono- and di-substituted products can be obtained. The lithio salt $Li[C_2B_{10}H_{11}]$ however has a tendency to disproportionate into $Li_2[C_2B_{10}H_{10}]$ and $C_2B_{10}H_{12}$ often leading to formation of both mono- and di-substituted products as well as regenerating starting materials (Figure 1.12).[33] In addition to organic functional groups, many main group and transition metal substituents can also be tethered to the C vertex by this general approach.

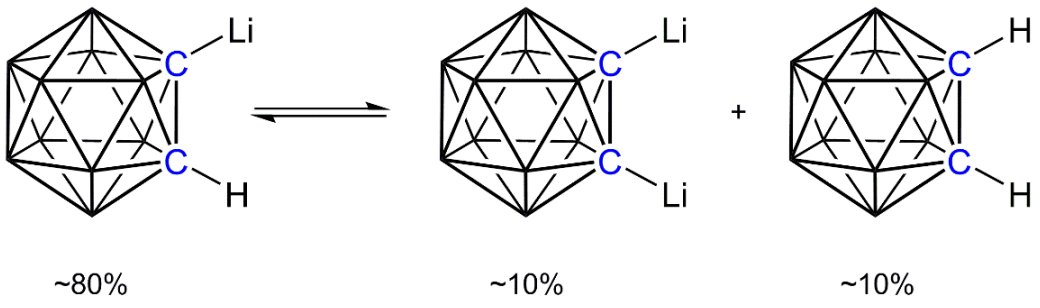

Figure 1.12 The disproportionation of monolithiated *o*-carborane.

Parallel to this, the polarisation of the molecule also causes the H atoms on the antipodal positions to bear a delta negative charge. These can undergo electrophilic halogenation to produce a range of *B*-substituted carboranes.[29,31,34] In the case of *o*-carborane, the antipodal positions B9 and B12 are the easiest to substitute followed by B8 and B10. These halogenated carborane derivatives are commonly used in Grignard reactions to introduce functional groups to the B vertices.

Polyhedral subrogation, often referred to as decapitation/capitation, firstly involves removal of one vertex from the cluster followed by insertion of an isolobal fragment. Typically, a metal fragment is inserted affording a metallacarborane[35] but main group fragments have also been utilised for synthesising novel heteroboranes.[36] By insertion of a {BR} fragment, it is possible to effectively substitute the B atoms at positions 3 and 6 which cannot be done directly. Degradation of *o*-carborane was first reported by Hawthorne in 1964 where the most positive boron vertex (B3 or B6) was selectively removed in basic conditions.[37] The [*nido*-7,8-$C_2B_9H_{12}$]$^-$ anion isolated possesses a bridging/endo-H formally located on B10 but typically asymmetrically-bridged between B9 or B11.[38,39] Deprotonation of the *endo*-H is required to reveal the open face, generating a [*nido*-7,8-$C_2B_9H_{11}$]$^{2-}$ dianion, and subsequent capitation/metalation will afford the new closo species (Figure 1.13).

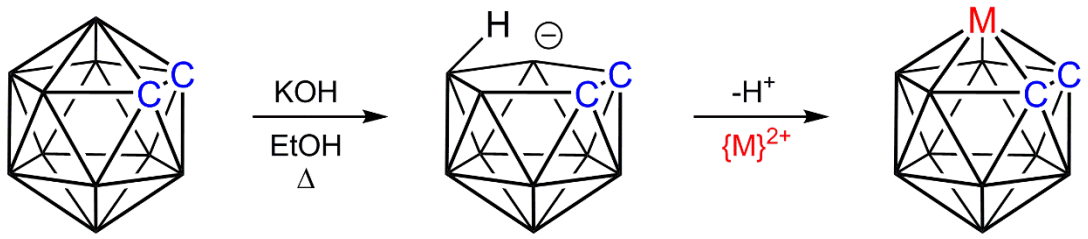

Figure 1.13 General procedure for the deboronation of *o*-carborane followed by metalation to afford metallacarborane products.

Supraicosahedral clusters (greater than 12 vertices) are formed *via* polyhedral expansion. Insertion of two electrons into a C_2B_n cage will afford the nido form of the expanded C_2B_{n+1} cluster, as implied by Wade's rules. This reduction process typically causes separation of the cage C atoms. Capitation/metalation of the dianionic nido species will then generate the closo expanded cluster (Figure 1.14). The first example of a supraicosahedral metallacarborane was prepared by Hawthorne in 1971 following the outlined reduction/metalation protocol.[40] The 13-vertex compound has a docosahedral shape in which the metal is located at one of the degree-6 vertices and one of the cage carbon atoms is located at the unique degree-4 vertex.

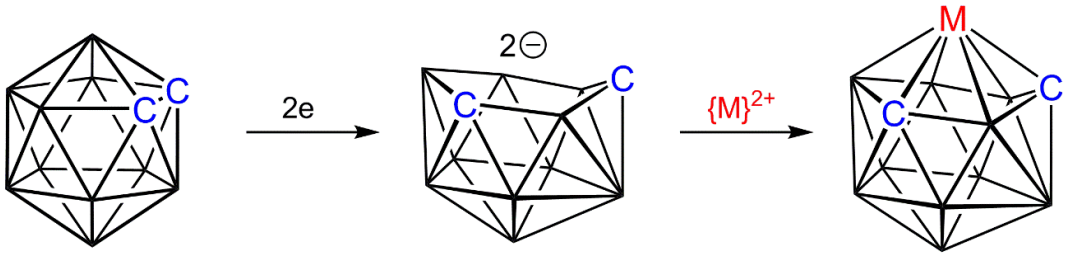

Figure 1.14 General procedure for the reduction/metalation of *o*-carborane.

More recently in 2014, Welch utilises an alternative route for polyhedral expansion using Direct Electrophilic Insertion (DEI) to synthesise novel 14-vertex metallacarboranes.[41] This process, first reported by Kudinov,[42] involves the reaction between an anionic closo metallacarborane and a cationic metal fragment to afford a neutral bimetallic cluster (Figure 1.15). Currently, the largest known clusters are 15-vertices for a metallacarborane[43,44] and 16-vertices for a metallaborane.[45]

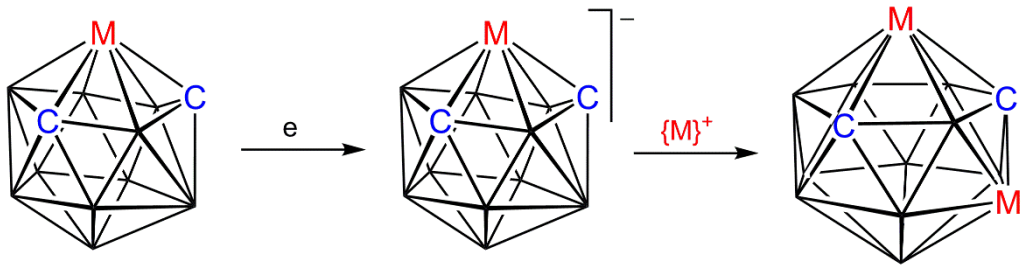

Figure 1.15 General procedure for DEI of 13-vertex metallacarboranes to afford 14-vertex dimetallacarboranes.

1.3.3 Characterisation of Carboranes

Carboranes and metallacarboranes can be readily analysed by an array of techniques. The common quantitative analysis employed is elemental analysis (commonly referred to as microanalysis or CHN analysis). This is particularly useful for insoluble carborane derivatives which precludes the majority of spectroscopic techniques.

Mass spectrometry is often used in conjunction with microanalysis for determining chemical composition. Due to the large number of boron atoms present within a cluster relative to organoboron compounds and the two possible isotopes of boron, the mass ion peaks are typically observed as broad envelopes.

Infrared spectroscopy is a common technique used for analysing carboranes. A distinctive strong broad band between 2500 and 2660 cm^{-1} corresponding to $B–H_{terminal}$ vibrations can be easily observed. When present, the $C–H_{terminal}$ stretch can be found between 2900 and 3160 cm^{-1}.[46]

One of the most useful techniques for characterising carboranes and metallacarboranes is NMR spectroscopy. Of the two stable isotopes of boron, the more abundant ^{11}B is exclusively used in research with the exception of analysing ^{10}B-enriched compounds. The ^{11}B NMR experiment is typically performed in tandem with the decoupled $^{11}B\{^{1}H\}$ NMR experiment which removes the splitting observed from the exo-H atoms. Comparison of the two spectra can rapidly identify boron atoms bearing non-H substituents. Although ^{11}B is a spin-active nucleus (I = 3/2), boron-boron coupling is not observed due to its large quadrupolar moment which instead results in broadened resonances.[3] The relative integrals of resonances can also be used to gain information on the symmetry of the compound. However, full assignment of these one-dimensional spectra is challenging as geometrical relationships between cage atoms can produce anomalies in the chemical shifts of the resonances. The most notable example is the antipodal effect where the vertex directly opposite influences its chemical shift. This is

particularly evident in *nido*-C_2B_9 species where vertex opposite the open face (B1) is typically shifted upfield to *ca.* δ -30 to -40 ppm.[38,47]

Although considerable information can be obtained from these techniques, the ultimate analytical method is *X*-ray crystallography as it can definitively determine not only the overall structure but also the precise isomer of the species. However, certain limitations are present in this technique. In highly symmetrical species, such as *o*-carborane, the data collected typically reveals a fully disordered structure. Use of coordinating agents to produce co-crystals can overcome this problem.[48]

1.3.4 Distinguishing Carbon and Boron Vertices in *X*RD Studies

Due to adjacency of boron and carbon in the Periodic Table, the ability to discern the two in *X*-ray diffraction studies has always been of great challenge. This is especially relevant when dealing with carborane clusters where neither atom bears a substituent other than H. Conventional methods involve identification of shorter cage connectivities (where B–B > B–C > C–C) and low U_{eq} values when all cage atoms are refined as boron (where the lowest U_{eq} values are assigned as C atoms). However, these methods are not always reliable especially in cases where vertices have varying degrees (number of connectivities) or if heavy atoms are bound to the vertices.[49] More recently, two new approaches have been devised by Welch that can be used in parallel to confidently assign carbon and boron atoms.

The Vertex-to-Centroid Distance (VCD) method[41,50] utilises the difference in atomic radii between carbon and boron. By initial refinement of all unassigned vertices as boron to obtain a prostructure, the centroid of the cluster is then generated. The distance between the centroid and all vertices can then be tabulated and compared. The atomic radius of carbon is smaller than that of boron and so a carbon vertex will lie closer to the centroid. The resulting shorter VCD can thus be used to identify the atom as carbon for subsequent final refinement.

The location of the centroid is key in this approach and therefore care must be applied when selecting the vertices used for its generation. For C_2B_{10} icosahedra, all twelve vertices are used to determine the location of the centroid whereas for MC_2B_9 species the metal vertex and its antipodal vertex are omitted. This is due to the larger atomic radii of all metals which will bias the centroid towards the M vertex. The exclusion of the antipodal vertex is required to counteract the new bias towards this vertex from the omission of the metal vertex (Figure 1.16).

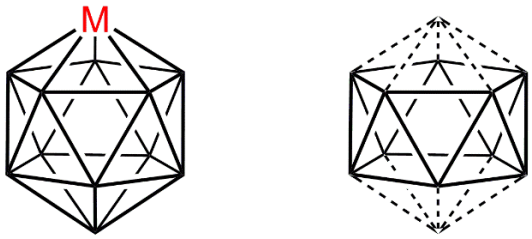

Figure 1.16 The ten vertices used to determine the position of the centroid in MC_2B_9 species.

The Boron-Hydrogen Distance (BHD) method[41,51] also requires use of the prostructure. Additionally, the cage H atoms are freely refined to obtain the vertex–H bond length. Vertices incorrectly modelled as boron will have excess electron density unaccounted for (as carbon possesses one more electron) and thus the bound H atom will migrate closer to the vertex to compensate. The resulting shortened "B–H" distance can be easily identified and the carbon vertex therefore located.

1.4 Metallacarboranes

The first metallacarborane was isolated in 1965 by Hawthorne following reaction between two equivalents of deboronated *o*-carborane with $FeCl_2$ to afford [3,3-Fe-(*closo*-1,2-$FeC_2B_9H_{11})_2]^{n-}$ (where n = 1 or 2).[52] The [*nido*-7,8-$C_2B_9H_{11}]^{2-}$ unit of the metallacarborane is comparable to a cyclopentadienide $[Cp]^-$ ligand since each possesses five π Frontier Molecular Orbitals (FMOs) bearing a total of six electrons. Additionally, the similarity in energy means these two ligands are essentially isolobal.[53] The orientation of the FMOs in the open pentagonal face of [*nido*-7,8-$C_2B_9H_{11}]^{2-}$ point slightly inwards due to the inclination of the *exo*-H atoms as opposed to parallel to each other as in $[Cp]^-$ (Figure 1.17). This provides a greater overlap with the bonding orbitals of the metal centre. As such, metallacarborane sandwich complexes $[M(C_2B_9H_{11})_2]^{n-}$ are more robust than their metallocene $[MCp_2]$ counterparts. This is particularly evident in the case of copper where the metallocene analogue of [3,3-Cu-(*closo*-1,2-$C_2B_9H_{11})_2]^-$ is not known.[54] Aside from icosahedral C_2B_{10} systems, 12-vertex metallacarboranes are the most extensively studied topic within carborane chemistry. This is due to the accessibility of *o*-carborane and the simplicity of their synthesis.

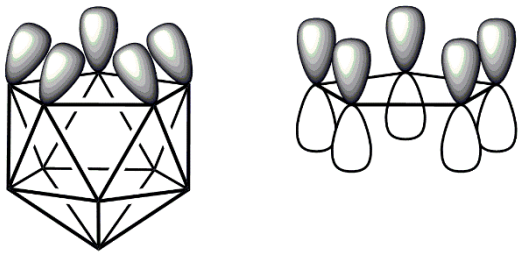

Figure 1.17 The totally symmetric FMOs of [*nido*-7,8-$C_2B_9H_{11}]^{2-}$ and $[Cp]^-$ (cage C unlabelled for clarity).

Following the report of sandwich complexes $[M(C_2B_9H_{11})_2]^{n-}$, half-sandwich complexes $[MC_2B_9H_{11}]$ were swiftly isolated.[55] The first crystallographically studied species was [3-Cp-*closo*-3,1,2-$FeC_2B_9H_{11}$] which confirmed Hawthorne's proposed sandwich-type bonding exhibited by the [*nido*-7,8-$C_2B_9H_{11}]^{2-}$ dianion.[56] Interestingly, despite only possessing 25 skeletal electrons, the icosahedral geometry is retained in the paramagnetic

species [3-Cp-*closo*-3,1,2-$FeC_2B_9H_{11}$] with only minor distortions from the differing covalent radii of the cage atoms. The endurance to structural change is due to the favourable icosahedral architecture as well as the availability of non-bonding orbitals on the metal centre. This allows the addition and removal of electrons without compromising the skeletal electrons, thus minimising structural deformation. The scope of isolobal fragments to {BH} has led to a vast array of icosahedral metallacarboranes encompassing elements in all four blocks of the Periodic Table.[35]

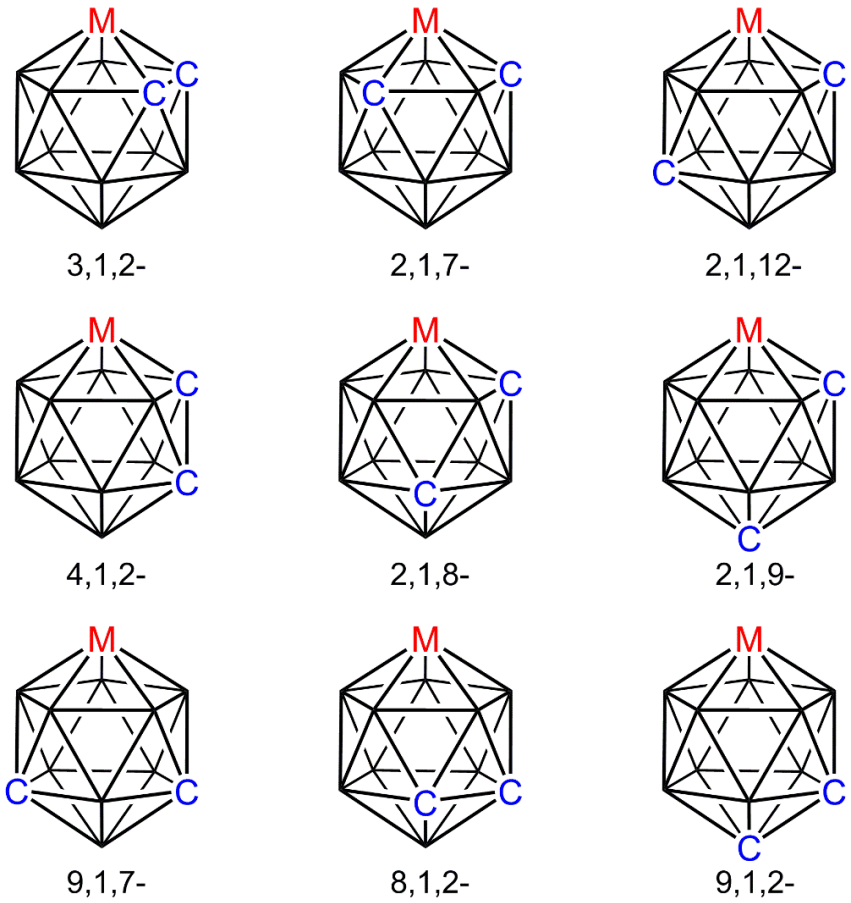

Figure 1.18 The nine possible isomers of MC_2B_9 where the first two rows have been synthesised and crystallographically characterised and the final row has been detected spectroscopically from high temperature thermolysis.

There are nine possible isomers of MC_2B_9 (Figure 1.18) whereas the parent C_2B_{10} cluster only has three. Of these nine isomers, using {CoCp} as the example M fragment, only six have been synthesised through standard laboratory conditions and confirmed

crystallographically.[57] The "missing" three isomers (Figure 1.18, bottom row) are reported to form from gas phase thermolysis of either [*closo*-3,1,2-CoC_2B_9] or its μ-$(CH_2)_3$ tethered analogue with temperatures excess of 600°C and have been assigned solely by spectroscopic means.[58] These compounds are important as they give a further insight into the isomerisation mechanism of carboranes.

Sterics have a major influence in the isomerisation behaviour of a carborane. The use of bulky *C*-substituted carboranes has been shown to lower the temperature required to induce isomerisation. In some cases, metalation of [*nido*-7,8-$R_2C_2B_9H_9$]$^{2-}$ (where R = alkyl or aryl) at ambient temperatures affords only the isomerised metallacarborane product.[59]

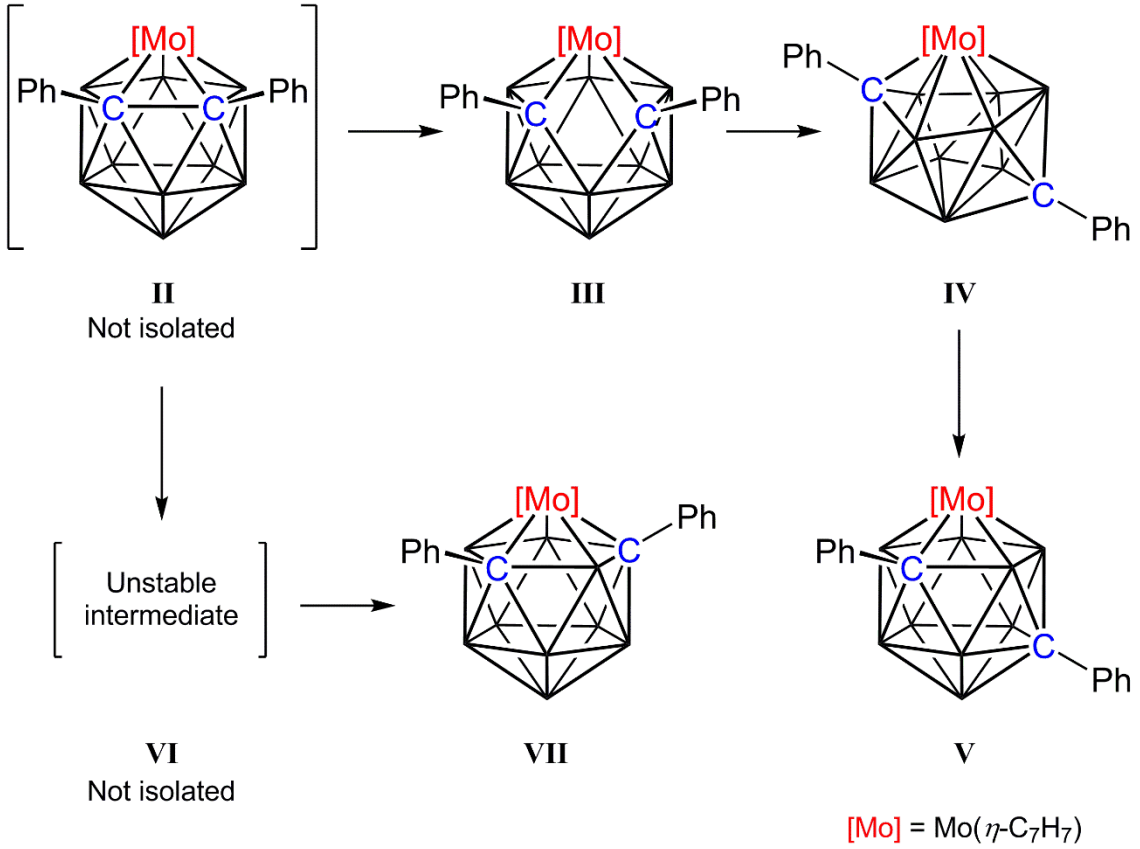

Figure 1.19 Isomerisation pathways of [3-(η-C_7H_7)-*closo*-3,1,2-$MoC_2B_9H_{11}$] (**II**) to [2-(η-C_7H_7)-*closo*-2,1,7-$MoC_2B_9H_{11}$] (**V**) and [2-(η-C_7H_7)-*closo*-2,1,8-$MoC_2B_9H_{11}$] (**VII**).

A notable study of this phenomena by Welch reports five products from the metalation of [*nido*-7,8-$Ph_2C_2B_9H_9$]$^{2-}$ with the {Mo(η-C_7H_7)} fragment (Figure 1.19).[60] The pseudocloso species **III** is isolated where the geometry is effectively identical to the expected *closo*-3,1,2-MC_2B_9 (**II**) with the exception of the missing cage C–C connectivity. Prolonged stirring affords the non-icosahedral intermediate **IV** which subsequently yields the isomerised *closo*-2,1,8-MC_2B_9 thermodynamic product **V**. The non-icosahedral geometry was predicted by Wales through theoretical studies as an intermediate for the isomerisation of *o*- to *m*-carborane. The final intermediate (**VI**) is unstable and readily converts to *closo*-2,1,7-MC_2B_9 (**VII**), precluding structural studies. Nevertheless, this demonstrates that different isomerisation pathways are required for the formation of 2,1,7- and 2,1,8-metallacarboranes and the isolated intermediates support the mechanisms proposed by Wales.

1.4.1 Metallacarboranes in Catalysis

Due to the isolobal nature of [*nido*-7,8-$C_2B_9H_{11}$]$^{2-}$ to [Cp]$^-$ and their extensive capability to be modified, metallacarborane catalysts are an attractive target for highly tailored systems. Further advantages include increased robustness of the ligand and wide variety in solubility relative to [Cp]$^-$, crucial for catalytic applications especially at industrial levels.

Among the reported metallacarborane catalysts, one of the most extensively studied species is [3-H-3,3-(PPh_3)$_2$-*closo*-3,1,2-$RhC_2B_9H_{11}$] (**VIII**, Figure 1.20, left). First reported in 1974 together with the 2,1,7-isomer,[61] the rhodacarborane was demonstrated to catalyse the isomerisation and hydrogenation of 1-hexene. Additionally, it was noted to promote the hydrosilylation of acetophenone. Subsequently, a series of papers was published expanding the reaction scope to include the hydrogenolysis[62] and hydrosilylanolysis[63] of alkenyl acetates as well as kinetic studies to determine the active catalyst.[62,64,65] Parallel to this, the hydrosilylation scope was expanded to alkenes and alkynes by Zakharkin where use of *B*-fluorosubstituted rhodacarboranes was also investigated.[66]

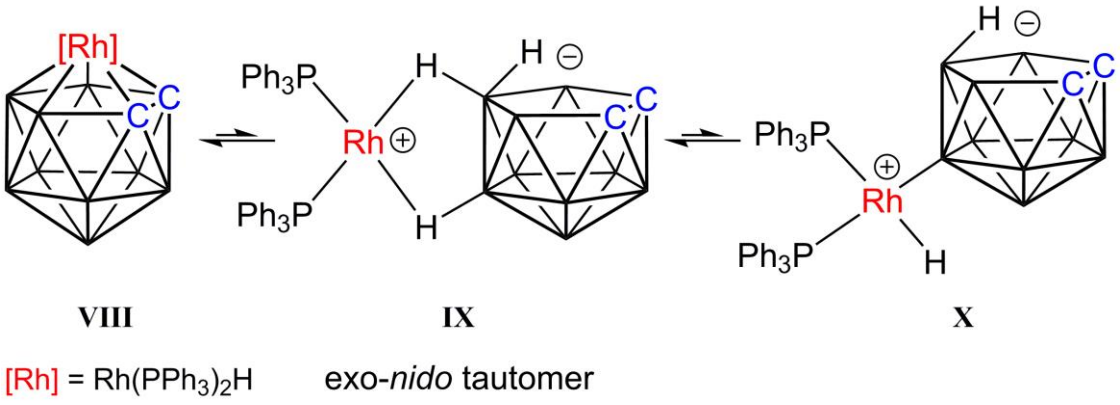

Figure 1.20 Tautomerisation of [3-H-3,3-(PPh_3)$_2$-*closo*-3,1,2-$RhC_2B_9H_{11}$] (**VIII**) to the exo-*nido* form (**IX**) followed by oxidative addition of a BH unit to afford a Rh(III) hydride species (**X**).

Deuterium-labelling studies of the isomerisation of 1-hexene showed only partial H/D scrambling of the hydride ligand when employing [3-D-3,3-$(PPh_3)_2$-*closo*-3,1,2-$RhC_2B_9H_{11}$] as the catalyst precursor, indicating the hydride ligand is not heavily involved in the catalytic cycle.[64] However, in a subsequent publication, no deuterium exchange was observed from the same experiment.[62] Based on this result, Hawthorne proposed an exo-*nido* tautomer (**IX**) as the possible active catalyst where the $\{Rh(PPh_3)_2\}$ fragment has migrated exo to the cluster supported by B–H–Rh *B*-agostic interactions and the formerly hydride H atom has transferred to the open face (Figure 1.20). This zwitterionic species now possesses a 16e Rh(I) centre capable of losing up to two phosphine ligands, comparable to classic rhodium catalysts such as Wilkinson's catalyst $[Rh(PPh_3)_3Cl]$. The exo-*nido* tautomer was subsequently characterised crystallographically where the use of bulky *C*-substituted carboranes was sufficient to force the tautomer to be the preferred geometry. The forced exo-*nido* was found to be catalytically-active in the same reactions. However, against expectations, an increased rate was not necessarily observed.

Although the proposed exo-*nido* tautomer **IX** was a viable explanation for the hydrogenation of alkenes, the lack of a rhodium hydride prohibits the standard alkene isomerisation pathway of migratory insertion to form an M(alkyl) intermediate and subsequent β-H elimination. An η^3-allyl intermediate was instead postulated *via* oxidative addition of the alkene to generate the M(allyl)H intermediate which can then undergo reductive elimination to afford the isomerised product (Figure 1.21). Oxidative addition of a cage BH bond following exo-*nido* tautomerisation to form a 14e Rh(III) monohydride species (**X**) was considered but deuterium labelling experiments showed BH to BD formation was minimal or absent.[64]

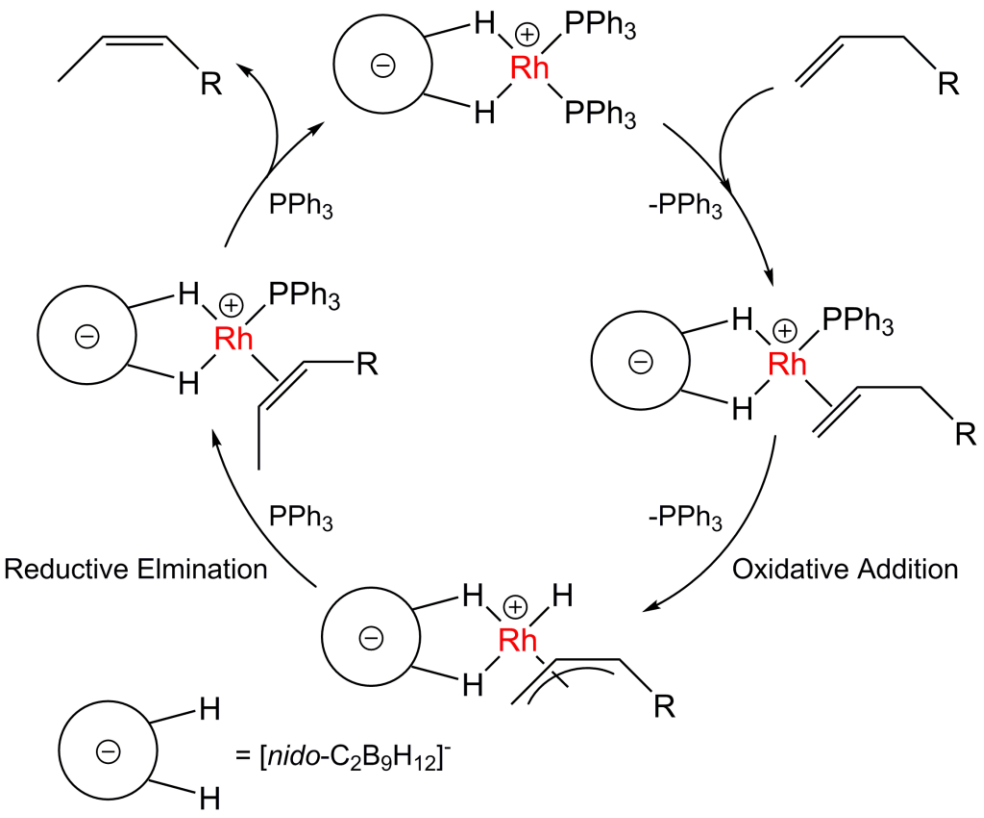

Figure 1.21 Proposed alkene isomerisation mechanism *via* an allyl intermediate.

However, studies into the hydrogenolysis of alkenyl acetates revealed that the formation of a monohydride intermediate must be occurring.[62] Alkenyl acetates can react *via* two pathways leading to two sets of products depending on the number of metal hydride ligands (Figure 1.22). With two metal hydrides present, alkyl acetates are afforded through catalytic hydrogenation (Pathway **A**) whereas, with one metal hydride ligand, ethene is released whilst generating an M(OAc) species (Pathway **B**). In both cases, H_2 is then used to complete the catalytic cycle to regenerate the dihydride or the monohydride species along with one equivalent of acetic acid. Employing the rhodacarborane **VIII** as the catalyst precursor, the latter set of products is observed. Coupled with the lack of rate dependence on the concentration of H_2, the reaction must proceed *via* a monohydride intermediate.

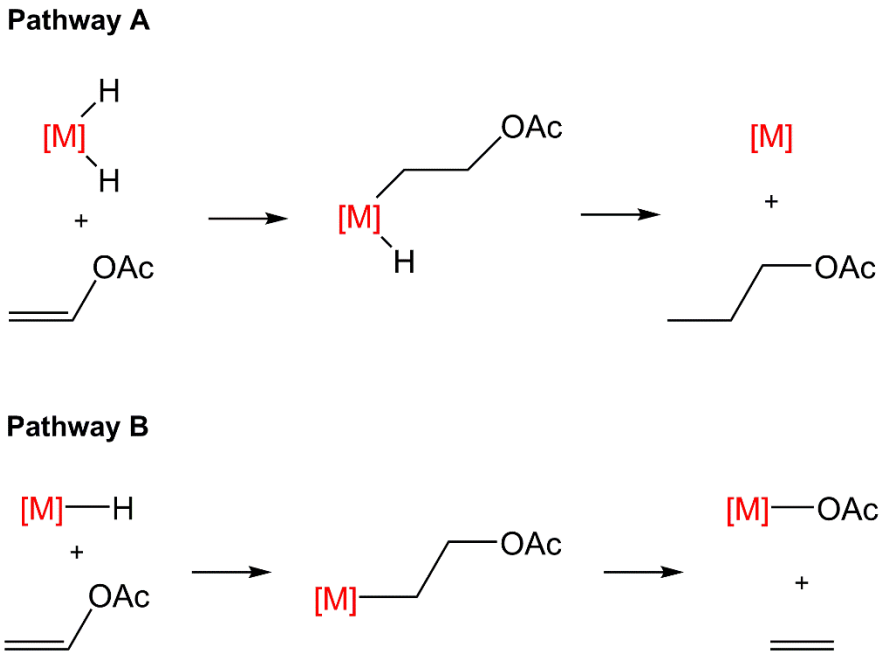

Figure 1.22 The two possible reaction pathways of the reaction between alkenyl acetates and H_2 dependent on the number of available hydride ligands attached to the metal centre.

This prompted the re-evaluation of the 14e Rh(III) monohydride species **X** where the minimal BH/BD conversion was rationalised by the likely short lifetime of the species and the high reactivity of the species. Complete regiospecific H/D exchange was observed at vertices B9, B10 and B12 when the isomerisation reaction was scaled up to 600 turnovers.[62] This demonstrates the validity of **X** as an intermediate for the catalytic cycle. Additionally, this explains the lack of BH/BD conversion observed previously due to the small scale of the experiments (*ca.* 13 turnovers). Thus, the proposed tautomerisation and B–H oxidative addition products (Figure 1.20) are currently the accepted active catalysts when employing rhodacarboranes as catalyst precursors.

1.5 Bis(carboranes)

Bis(carboranes) are simply molecules in which two carborane units are linked together. Although there exists a large number of potential isomers, the most common species are linked through the cage C vertex. Of the three possible C–C linked bis(carboranes), the most extensively studied species is [1-(1′-*closo*-1′,2′-$C_2B_{10}H_{11}$)-*closo*-1,2-$C_2B_{10}H_{11}$], trivially named bis(*o*-carborane) (Figure 1.23), due to the accessibility of *o*-carborane.

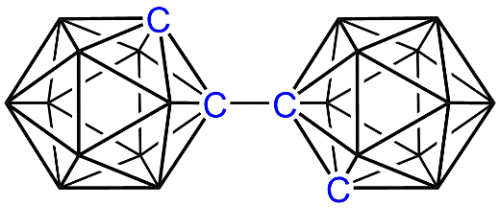

Figure 1.23 The structure of 1,1′-bis(*ortho*-carborane).

Bis(*o*-carborane) was first reported in 1964 by Hawthorne utilising a similar approach to that employed in preparing *o*-carborane.[67] Diacetylene was inserted into decaborane in lieu of acetylene to afford the desired bis(carborane) product (4%) and the alkyne-substituted *o*-carborane (35%). The latter product can be further reacted with decaborane to yield bis(*o*-carborane) (60%) giving a combined total yield of 25%.

By switching the Lewis base from acetonitrile to diethylsulfide and performing the initial reaction at low temperatures (-25°C), Hawthorne enhanced the yield of the reaction to *ca.* 60%.[68] In 1995, an alternative route was reported, again by Hawthorne, where the dilithiated *o*-carborane $Li_2[C_2B_{10}H_{10}]$ was coupled using copper (II) chloride as a coupling agent.[69] Three products were identified from this reaction where one is the desired 1,1′-bis(*o*-carborane) and the other two are the 1,3′- and 1,4′- C-B coupled bis(carboranes). These were characterised by their unique CH resonance in their ^{1}H NMR spectra. The combined total yield for this reaction however was only 31%.

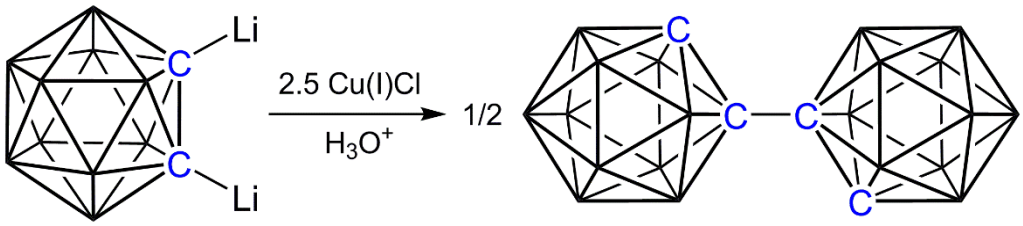

Figure 1.24 Synthetic procedure of 1,1′-bis(*ortho*-carborane) *via* Cu-mediated coupling.

This methodology was adapted by Xie in 2008 by substituting copper (II) chloride with copper (I) chloride, [70] a concept previously explored by Zakharkin in 1973 and Hawthorne in 1992,[71,72] to enhance the yield up to 83% (Figure 1.24). An additional advantage of using copper (I) chloride is that it inhibits the formation of C-B coupled products.

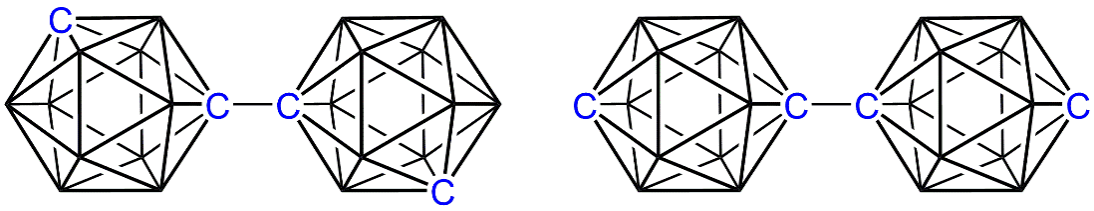

Figure 1.25 The structure of 1,1′-bis(*meta*-carborane) (left) and 1,1′-bis(*para*-carborane) (right).

The remaining C–C linked bis(carboranes), [1-(1′-*closo*-1′,7′-$C_2B_{10}H_{11}$)-*closo*-1,7-$C_2B_{10}H_{11}$] and [1-(1′-*closo*-1′,12′-$C_2B_{10}H_{11}$)-*closo*-1,12-$C_2B_{10}H_{11}$], also abbreviated to bis(*m*-carborane) and bis(*p*-carborane) respectively (Figure 1.25), can also be synthesised from Cu-mediated coupling of the lithiated parent cluster. These were first reported by Zakharkin in 1973 and later by Hawthorne in 1992 with complete spectroscopic analysis.[71,72] The definitive crystal structures of bis(*o*-carborane) and bis(*m*-carborane) were subsequently reported by Welch in 2014.[73,74]

1.5.1 Reactivity of Bis(*o*-carborane)

Analogous to *o*-carborane, bis(*o*-carborane) can undergo the same three main categories of reactivity: substitution at a cage vertex, polyhedral subrogation and polyhedral expansion.[75] However, the chemistry is relatively understudied in comparison to its single-cage parent largely due to the low yields in its preparation. The comparatively recent enhanced protocol has led to a resurgence in interest in this species with just under half of the publications involving bis(carborane) being published in this decade.

Substitution at a cage C vertex is performed in the same manner *via* nucleophilic substitution. Due to the orientation of the two CH vertices, bis(*o*-carborane) can also be used as a chelating species to bind to transition metal or main group fragments in a κ^2 fashion. This was first demonstrated by Hawthorne in 1970 where two equivalents of dilithiated bis(*o*-carborane) $[LiC_2B_{10}H_{10}]_2$ were reacted with a transition metal to afford $[M(bis)_2]^{n-}$ products where M = Cu, Ni, Co or Zn and n = 1 or 2 (Figure 1.26).[76] The geometry of these complexes can range from tetrahedral to square planar at the metal centre.

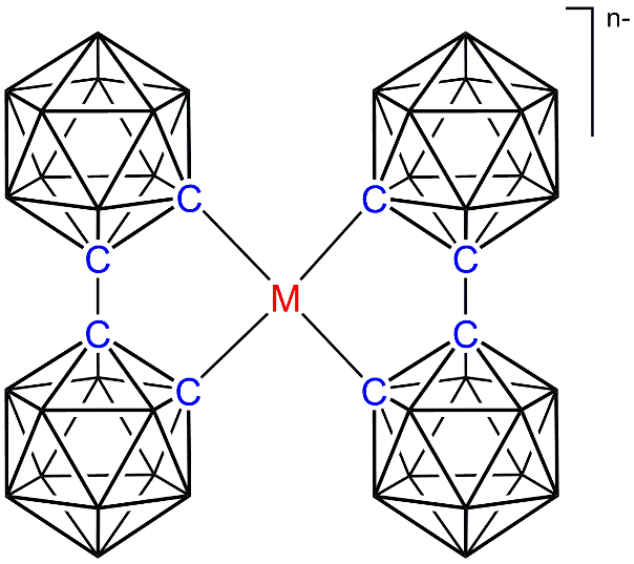

Figure 1.26 Transition metals (M = Cu, Ni, Co or Zn) chelated by two bis(*o*-carborane) units through the cage carbon atoms. Charge n = 1 or 2 depending on the oxidation state of the metal centre.

By using just one equivalent of $[LiC_2B_{10}H_{10}]_2$, Welch extended the product types to L_nM(bis) where $L_nM = (PR_3)_2Ni$, (*p*-cymene)Ru or $(PR_3)_2Ru$ (Figure 1.27).[77,78] The ruthenium chelates, in addition to novel binding modes, exhibit the ability to catalyse Diels-Alder cycloadditions. Subsequently, further examples were reported by Jin (M = Rh or Ir) and Spokoyny (M = Pd or Pt).[79,80] There are currently only five non-transition metal elements shown to be chelated by bis(*o*-carborane); arsenic,[81,82] phosphorus,[81,83,84] magnesium, tin[85] and boron.[86]

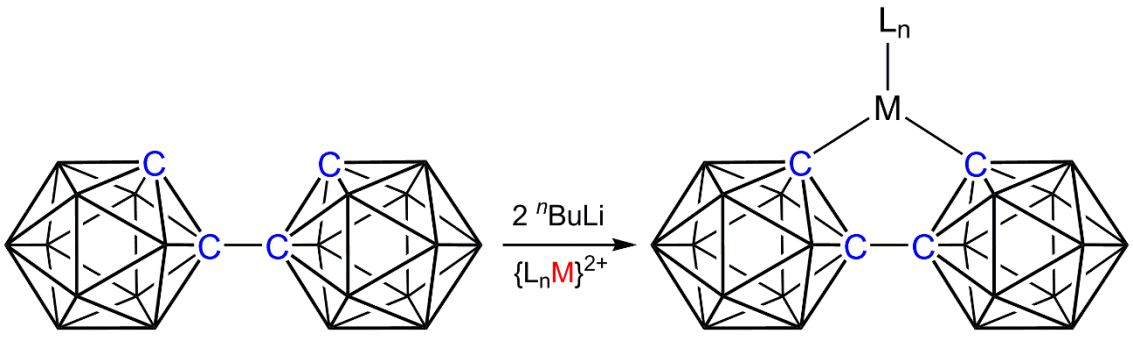

Figure 1.27 General procedure for the synthesis of L_nM(bis) products.

Much as with *o*-carborane, the same decapitation/capitation methodology can be applied to bis(*o*-carborane). Degradation of one cage ([**XI**]$^-$) was first achieved by Hawthorne in 1971 using potassium hydroxide (KOH) in an ethanol medium at reflux temperature for 90 minutes (Figure 1.28).[87] Extended reaction times (120 h) yielded the doubly-deboronated product ([**XII**]$^{2-}$). Both products can be isolated in high yields (80%) as either the caesium or trimethylammonium ($[HNMe_3]^+$) salts.

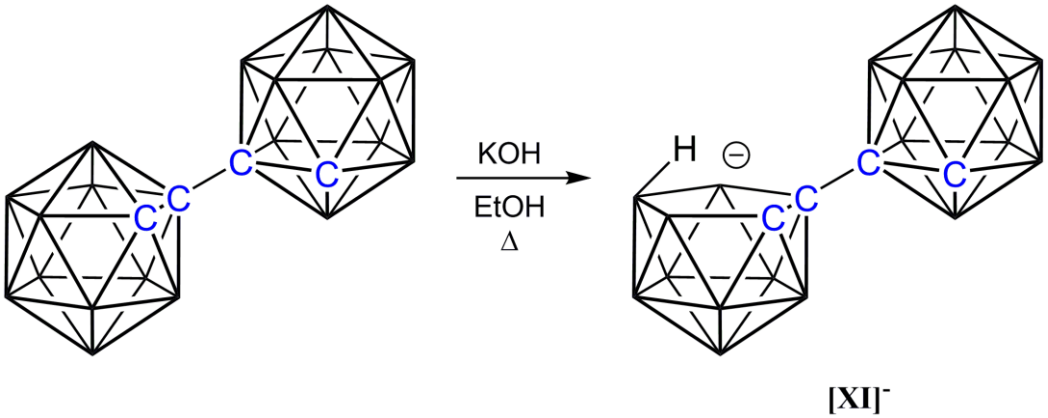

[XI]$^{-}$

Figure 1.28 Single deboronation of bis(*o*-carborane) to afford the [7-(1′-*closo*-1′,2′-$C_2B_{10}H_{11}$)-*nido*-7,8-$C_2B_9H_{11}$]$^{-}$ anion ([**XI**]$^{-}$).

Removal of the second {BH} fragment can occur at positions B3′ or B6′ leading to a diastereomeric product mixture (Figure 1.29). Hawthorne postulated the meso isomer would be formed selectively due to a higher stability. No evidence of diastereoisomers was observed in the ^{11}B and ^{1}H NMR spectra, supporting his hypothesis. However, in 1983, Hawthorne briefly remarks that two distinct isomers can be observed in ^{11}B NMR spectroscopy but no further details are given.[88]

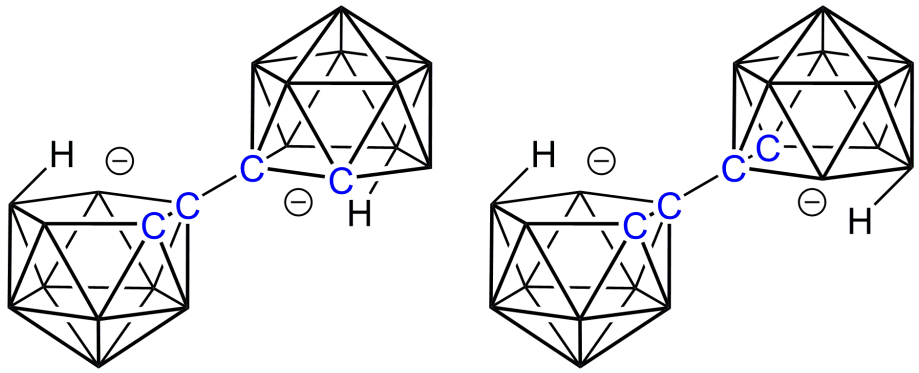

[XIIa]$^{2-}$ *rac*-form

[XIIb]$^{2-}$ *meso*-form

Figure 1.29 The two diastereoisomers of doubly-deboronated bis(*o*-carborane).

The double deboronation was replicated in 2017 by Welch and it was found that similar yields can be achieved with shorter reaction times (18-48 h) and a higher equivalence of KOH.[89] The product was isolated as salts of benzyltrimethylammonium $[BTMA]^+$, $[HNMe_3]^+$ and thallium $[Tl]^+$. Additionally, evidence for a diastereomeric product mixture was observed in the $^{11}B\{^1H\}$ NMR spectrum which displayed additional minor resonances integrating *ca.* 1:2 relative to the major resonances. This is consistent with two $C_{cage}H$ resonances noted in the ^1H NMR spectrum with the same 1:2 ratio of relative integrals. A crystallographic study of $[BTMA]_2$[7-(7′-*nido*-7′,8′-$C_2B_9H_{11}$)-*nido*-7,8-$C_2B_9H_{11}$] ($[BTMA]_2$[**XII**]) revealed B/C disorder between vertices 8 and 11, preventing the assignment of the major and minor product.

The mono-deboronated bis(*o*-carborane) anion [7-(1′-*closo*-1′,2′-$C_2B_{10}H_{11}$)-*nido*-7,8-$C_2B_9H_{11}$]$^-$ ([**XI**]$^-$) was also confirmed crystallographically by Welch in 2015.[90] An alternative synthetic route was reported by Sivaev in 2016 utilising the electron-withdrawing nature of a *C*-bound $C_2B_{10}H_{11}$ substituent for selective mono-deboronation achieved at ambient temperatures using a water/acetonitrile mixture.[91] Extended reaction times and even reflux temperatures do not induce the second deboronation.

The first example of a metallacarborane/carborane product was reported by Hawthorne in 1984.[92] The salt $[Ir(COD)(PPh_3)_2]$[7-(1′-*closo*-1′,2′-$C_2B_{10}H_{11}$)-*nido*-7,8-$C_2B_9H_{11}$] ($[Ir(COD)(PPh_3)_2]$[**XI**]) was heated to reflux in cyclohexane for 7 days to afford the closo product [8-(1′-*closo*-1′,2′-$C_2B_{10}H_{11}$)-2-H-2,2-$(PPh_3)_2$-*closo*-2,1,8-$IrC_2B_9H_{10}$] (**XIII**) in 41% yield. In the same year, Hawthorne reported the second example of a metallacarborane/carborane species prepared in a similar fashion.[93] Reaction of [Tl][**XI**] with $[Rh(PPh_3)_3Cl]$ afforded the cation-exchanged product $[Rh(PPh_3)_3]$[7-(1′-*closo*-1′,2′-$C_2B_{10}H_{11}$)-*nido*-7,8-$C_2B_9H_{11}$] ($[Rh(PPh_3)_3]$[**XI**]) and subsequent addition of triethylphosphine (PEt_3) in benzene at reflux conditions forms the product [8-(1′-*closo*-1′,2′-$C_2B_{10}H_{11}$)-2-H-2,2-$(PEt_3)_2$-*closo*-2,1,8-$RhC_2B_9H_{10}$] (**XIV**) in 65% yield. In both cases, the 2,1,8-geometry (Figure 1.30) was assigned by analogy with the substituted single-cage derivatives [2-H-2,2-$(PPh_3)_2$-8-Ph-*closo*-2,1,8-$IrC_2B_9H_{11}$] and [1-Me-2-H-2,2-$(PEt_3)_2$-8-Ph-*closo*-2,1,8-$RhC_2B_9H_{11}$], respectively.

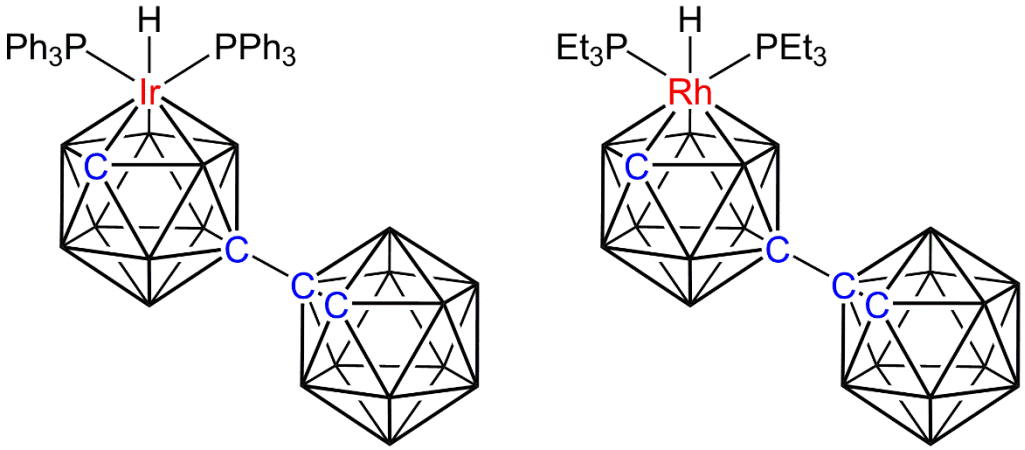

XIII **XIV**

Figure 1.30 The proposed structure of the first two metallacarborane/carborane complexes.

The scope of fragments inserted into mono-deboronated bis(*o*-carborane) was not expanded until two decades later by Welch.[94] A trace product from the 2e reduction and metalation of bis(*o*-carborane) afforded [1-(1′-*closo*-1′,2′-$C_2B_{10}H_{11}$)-8-Cp-*closo*-8,1,2-$CoC_2B_9H_{10}$] (**XV**), the first metallacarborane/carborane species confirmed crystallographically (Figure 1.31).

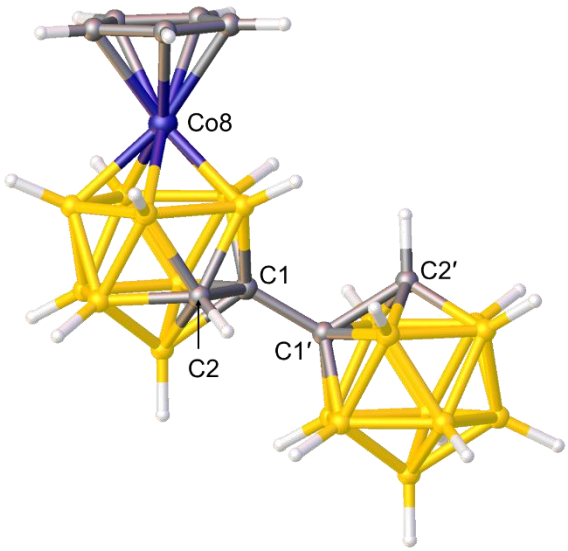

Figure 1.31 Perspective view of [1-(1′-*closo*-1′,2′-$C_2B_{10}H_{11}$)-8-Cp-*closo*-8,1,2-$CoC_2B_9H_{10}$] (**XV**).

In 2015, Welch targeted these compounds deliberately from the same anion [**XI**]$^-$ reported by Hawthorne.[90] Deprotonation of the endo-H with ^{n}BuLi to generate the dianion [7-(1′-*closo*-1′,2′-$C_2B_{10}H_{11}$)-*nido*-7,8-$C_2B_9H_{10}$]$^{2-}$ is required before addition of the metal fragment. Use of the {Ru(*p*-cymene)} fragment affords two isomeric products; [1-(1′-*closo*-1′,2′-$C_2B_{10}H_{11}$)-3-(*p*-cymene)-*closo*-3,1,2-$RuC_2B_9H_{10}$] (**XVI**) and [8-(1′-*closo*-1′,2′-$C_2B_{10}H_{11}$)-2-(*p*-cymene)-*closo*-2,1,8-$RuC_2B_9H_{10}$] (**XVII**) in 8% and 19% yields respectively. The geometry was confirmed crystallographically for both compounds (Figure 1.32). Isomerisation of **XVI** to **XVII** can be induced thermally upon a 2 h reflux in THF in quantitative yields.

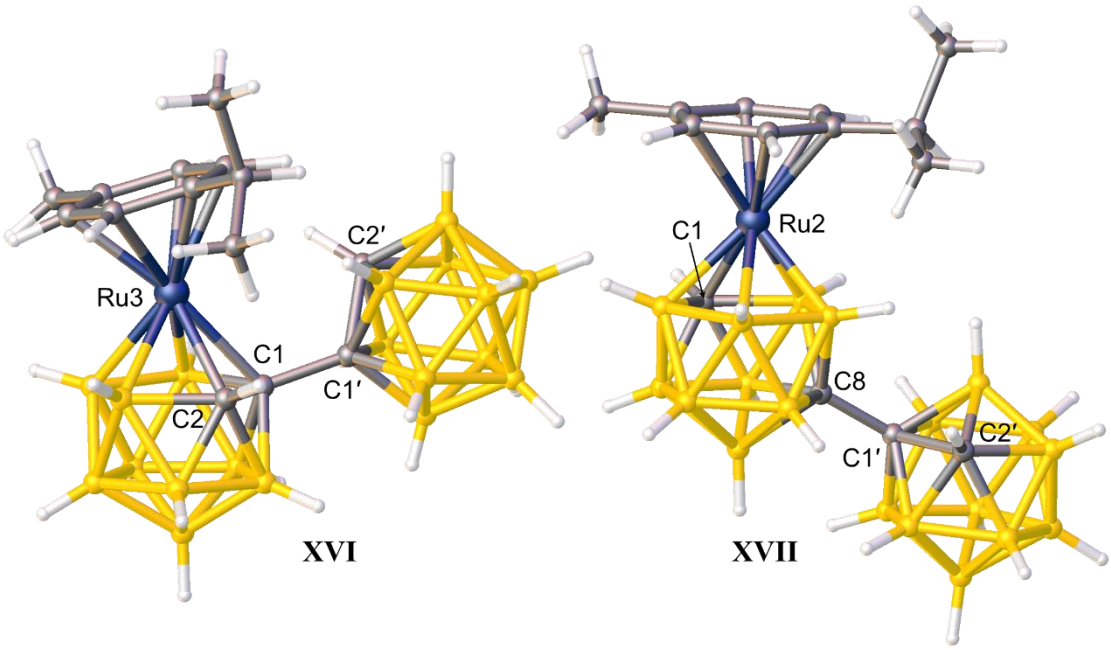

Figure 1.32 Perspective view of [1-(1′-*closo*-1′,2′-$C_2B_{10}H_{11}$)-3-(*p*-cymene)-*closo*-3,1,2-$RuC_2B_9H_{10}$] (**XVI**) and [8-(1′-*closo*-1′,2′-$C_2B_{10}H_{11}$)-2-(*p*-cymene)-*closo*-2,1,8-$RuC_2B_9H_{10}$] (**XVII**).

Similar products can also be obtained using the {CoCp} fragment. Interestingly, the product observed is dependent on the metal fragment source; [CoCp(CO)I_2] affords [1-(1′-*closo*-1′,2′-$C_2B_{10}H_{11}$)-3-Cp-*closo*-3,1,2-$CoC_2B_9H_{10}$] whereas $CoCl_2$/NaCp affords [8-(1′-*closo*-1′,2′-$C_2B_{10}H_{11}$)-2-Cp-*closo*-2,1,8-$CoC_2B_9H_{10}$]. It is important to note that a trace of the alternate isomer can be detected by spot TLC in both cases. Isomerisation from 3,1,2 to 2,1,8 cannot be induced thermally even at 110°C but can be readily achieved

by a 1e redox process. This is consistent with the trend observed in the product distribution as the *in situ* generated {CoCp} fragment from $CoCl_2$/NaCp would be formally Co^{II}, leading to the initial formation of 1e-reduced product. This will facilitate the isomerisation to the 2,1,8-isomer which is subsequently isolated upon aerial oxidation and work-up.

Following this, Welch reported a range of novel nickelacarborane/carborane species, the most notable of which are [1-(1′-*closo*-1′,2′-$C_2B_{10}H_{11}$)-4-dppe-*closo*-4,1,2-$NiC_2B_9H_{10}$] (dppe = 1,2-bis(diphenylphosphino)ethane) and [1-(1′-*closo*-1′,2′-$C_2B_{10}H_{11}$)-4,4-$(PMePh_2)_2$-*closo*-4,1,2-$NiC_2B_9H_{10}$], the only two examples of the 4,1,2-isomer of metallacarborane/carborane species.[95] This brings the total number of known isomers of singly-metalated bis(*o*-carborane) up to four.

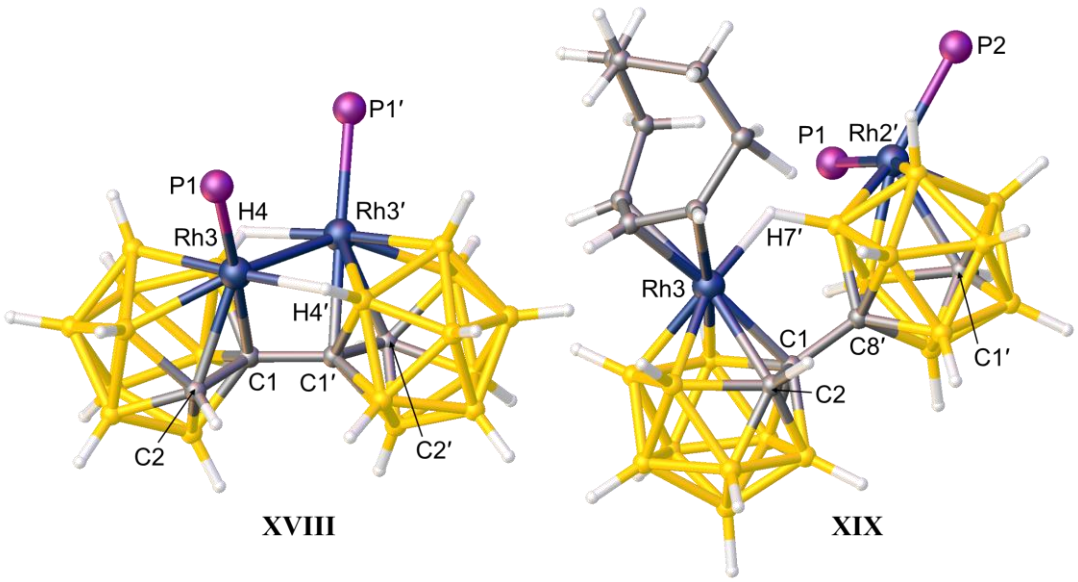

Figure 1.33 Perspective view of [1-(1′-3′-PEt_3-*closo*-3′,1′,2′-$RhC_2B_9H_{10}$)-3-PEt_3-*closo*-3,1,2-$RhC_2B_9H_{10}$] (**XVIII**) and [1-(8′-2′-H-2′,2′-$(PEt_3)_2$-*closo*-2′,1′,8′-$RhC_2B_9H_{10}$)-3-η^3-CODH-*closo*-3,1,2-$RhC_2B_9H_{10}$] (**XIX**). Ethyl groups of the phosphines are omitted for clarity.

Metallacarborane/metallacarborane compounds derived from the doubly-deboronated bis(*o*-carborane) were first reported in Hawthorne in 1983 with a subsequent publication in 1985.[88,96] Reaction of [7-(7′-*nido*-7′,8′-$C_2B_9H_{11}$)-*nido*-7,8-$C_2B_9H_{11}$]$^{2-}$ ([**XII**]$^{2-}$) as the caesium salt with [Rh(COD)(PEt_3)Cl] affords two products; [1-(1′-3′-PEt_3-*closo*-3′,1′,2′-$RhC_2B_9H_{10}$)-3-PEt_3-*closo*-3,1,2-$RhC_2B_9H_{10}$] (**XVIII**) and [1-(8′-2′-H-2′,2′-(PEt_3)$_2$-*closo*-2′,1′,8′-$RhC_2B_9H_{10}$)-3-η^3-CODH-*closo*-3,1,2-$RhC_2B_9H_{10}$] (**XIX**) in 23% and 19% yields respectively. Interestingly, both products were confirmed crystallographically to only contain a single stereoisomer despite being derived from a diastereomeric source (Figure 1.33).

The former of the two products **XVIII**, in addition to the C1–C1′ linkage, possesses three further interactions between the two icosahedra; a Rh3-Rh3′ interaction and two B–H–Rh *B*-agostic interactions from vertices B4 and B4′. Hawthorne notes that the alternate diastereoisomer can be observed in the $^{31}P\{^1H\}$ NMR spectrum but this species was not isolated and fully characterised. The latter product **XIX** also possesses a B–H–Rh *B*-agostic interaction from the B7′ vertex to Rh3 to electronically saturate the metal centre.

Further examples of metallacarborane/metallacarborane compounds were not reported until 2017 by Welch.[89] Deprotonation and subsequent metalation of [**XII**]$^{2-}$ using the {Ru(*p*-cymene)} fragment afforded both diastereoisomers of [1-(8′-2′-(*p*-cymene)-*closo*-2′,1′,8′-$RuC_2B_9H_{10}$)-3-(*p*-cymene)-*closo*-3,1,2-$RuC_2B_9H_{10}$] (**XX**) where one cage has isomerised (Figure 1.34). The two diastereoisomers are denoted with either by α- or β-prefix to distinguish the two species. Analogous products (**XXI**) can be formed upon metalation with the {CoCp} fragment when using the $CoCl_2$/NaCp source as well as the unique [8-(8′-2′-Cp-*closo*-2′,1′,8′-$CoC_2B_9H_{10}$)-2-Cp-*closo*-2,1,8-$CoC_2B_9H_{10}$] species (**XXII**, Figure 1.35) as an inseparable diastereomeric mixture. Crystallographic study of the doubly isomerised product shows that the molecule possesses C_{2h} symmetry and a 50%C/50%B disorder in vertex 1, suggesting both diastereoisomers may be present.

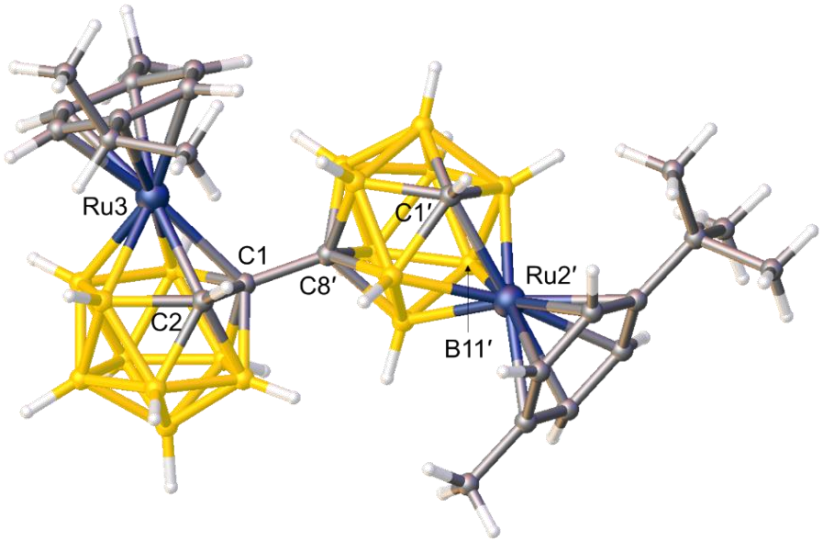

Figure 1.34 Perspective view of *α*-[1-(8′-2′-(*p*-cymene)-*closo*-2′,1′,8′-$RuC_2B_9H_{10}$)-3-(*p*-cymene)-*closo*-3,1,2-$RuC_2B_9H_{10}$] (**XXa**). The complimentary diastereoisomer **XXb** is isostructural with the exception of the cage C1′ in position B11′.

A 2e redox of either diastereomerically-pure **XXI** both afforded **XXII**, confirmed spectroscopically and crystallographically, consistent with **XXII** being an inseparable and indistinguishable diastereomeric mixture. Use of [CoCp(CO)I_2] as the metal source yields a single product; *rac*-[1-(1′-3′-Cp-*closo*-3′,1′,2′-$CoC_2B_9H_{10}$)-3-Cp-*closo*-3,1,2-$CoC_2B_9H_{10}$] (**XXIII**, Figure 1.35). Thermolysis of this affords exclusively **XXIa**, allowing all products of the *α*-form to be related to the rac precursors and, conversely, the *β*-form to the meso precursors.

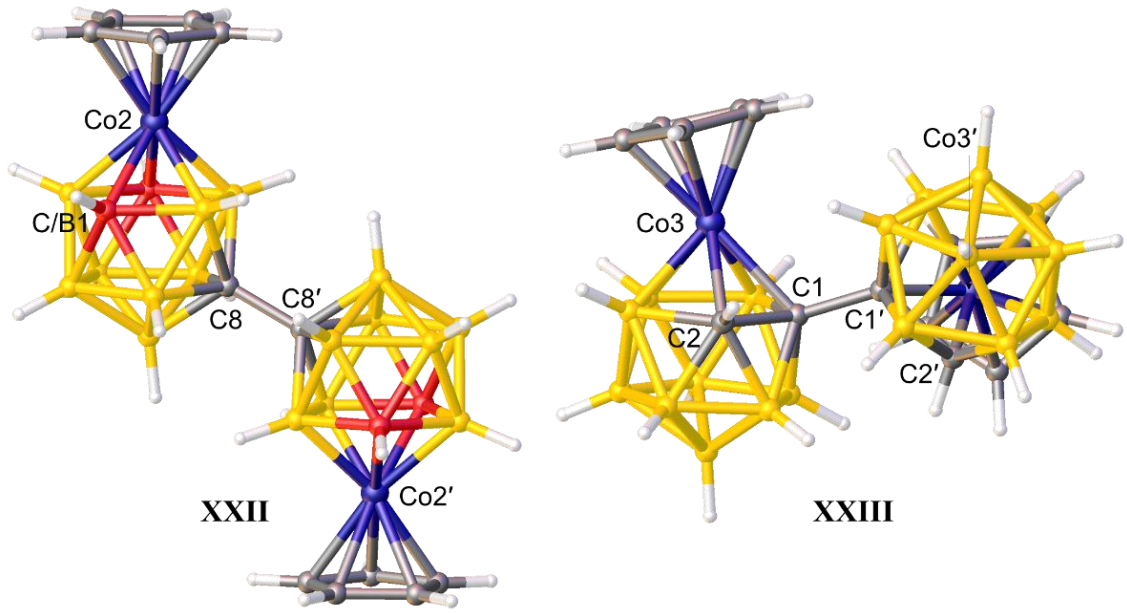

Figure 1.35 Perspective view of [8-(8′-2′-Cp-*closo*-2′,1′,8′-$CoC_2B_9H_{10}$)-2-Cp-*closo*-2,1,8-$CoC_2B_9H_{10}$] (**XXII**) and *rac*-[1-(1′-3′-Cp-*closo*-3′,1′,2′-$CoC_2B_9H_{10}$)-3-Cp-*closo*-3,1,2-$CoC_2B_9H_{10}$] (**XXIII**). Atoms shown in red are disordered 50%C/50%B.

Polyhedral expansion of bis(*o*-carborane) remains a heavily understudied area. The first report of a reduced bis(carborane) species was in 1990 by Hawthorne where 2e-reduced product (**XXIV**) was isolated as a methyltriphenylphosphonium $[PMePh_3]^+$ salt.[97] Crystallographic study revealed partial opening of both cages indicating an extent of delocalisation between the two icosahedra. This is believed to exist in equilibrium with the *nido*-12-vertex/*closo*-12-vertex in solution (Figure 1.36). Four electron reduction produces the expected *nido*-12-vertex geometry in both cages.[98]

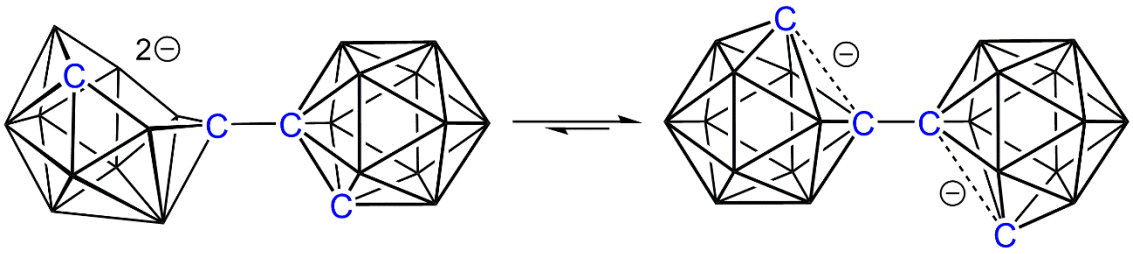

Figure 1.36 Equilibrium of the two-electron reduced 1,1′-bis(*o*-carborane) (**XXIV**).

In 2010, Welch reported the first supraicosahedral bis(carborane) derivative where metalation with the {Ru(*p*-cymene)} following a 4e reduction yields the 13-vertex/12-vertex flyover complex [1-(1′-*closo*-1′,2′-$C_2B_{10}H_{11}$)-4-{$C_{10}H_{14}$Ru(*p*-cymene)}-*closo*-4,1,6-$RuC_2B_{10}H_{11}$] (**XXV**, Figure 1.37).[99] Through theoretical studies, Welch postulates an internal redox process where the reduced carborane substituent transfers two electrons to the central arene of a carborane–Ru–arene–Ru–arene triple deck which can subsequently isomerise to the isolated product.

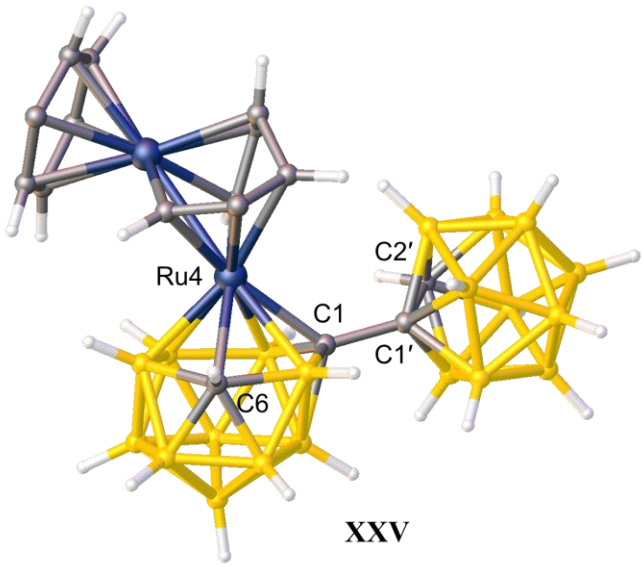

Figure 1.37 Perspective view of the fly-over complex [1-(1′-*closo*-1′,2′-$C_2B_{10}H_{11}$)-4-{$C_{10}H_{14}$Ru(*p*-cymene)}-*closo*-4,1,6-$RuC_2B_{10}H_{11}$] (**XXV**). Isopropyl and methyl groups of the *p*-cymene ligands omitted for clarity.

In the same year, Welch also reported the analogous reduction/metalation reaction using the {CoCp} fragment formed *in situ* from $CoCl_2$/NaCp to afford the expected 13-vertex/13-vertex product.[100] Both rac and meso isomers of [1-(1′-4′-Cp-*closo*-4′,1′,6′-$CoC_2B_{10}H_{11}$)-4-Cp-*closo*-4,1,6-$CoC_2B_{10}H_{11}$] was isolated. In 2015, both species were independently isomerised to [1-(1′-4′-Cp-*closo*-4′,1′,12′-$CoC_2B_{10}H_{11}$)-4-Cp-*closo*-4,1,12-$CoC_2B_{10}H_{11}$] by heating to 180°C.[101]

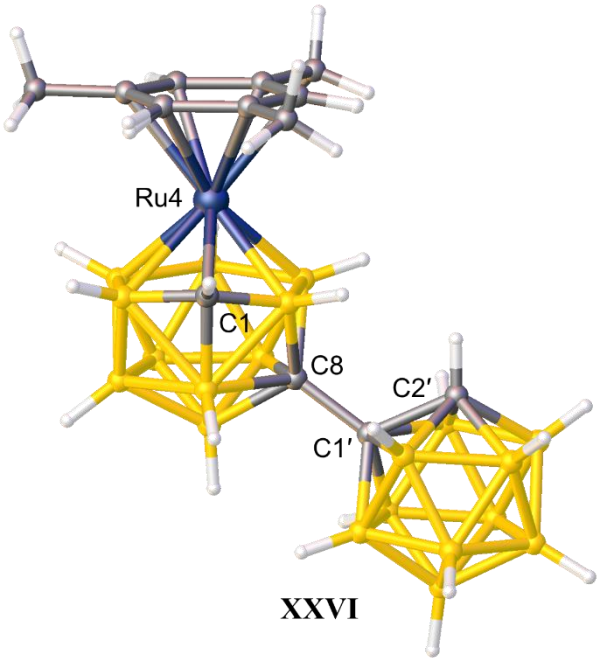

Figure 1.38 Perspective view of [8-(1′-*closo*-1′,2′-$C_2B_{10}H_{11}$)-4-mesitylene-*closo*-4,1,8-$CoC_2B_{10}H_{11}$] (**XXVI**).

Following on, Welch reported the results of stepwise reduction/metalation where only two electrons are inserted sequentially.[102] Metalation with {Ru(mesitylene)} affords the isomerised 13-vertex/12-vertex species [8-(1′-*closo*-1′,2′-$C_2B_{10}H_{11}$)-4-mesitylene-*closo*-4,1,8-$CoC_2B_{10}H_{11}$] (**XXVI**, Figure 1.38) whereas smaller arene ligands (C_6H_6 and *p*-cymene) yield the non-isomerised 4,1,6/1′,2′-product.

Metallacarboranes of the form 4,1,8-MC_2B_{10} are known to be susceptible to reduction/metalation to afford 1,14,2,9-$M_2C_2B_{10}$ 14-vertex products. Additionally, **XXVI** has the potential to be reduced at the C_2B_{10} unit leading to a second potential 13-vertex/13-vertex product.

Reduction/metalation of **XXVI** with {Ru(arene)}, where arene = C_6H_6, *p*-cymene or mesitylene, afforded [9-(1′-*closo*-1′,2′-$C_2B_{10}H_{11}$)-1-mesitylene-13-arene-*closo*-1,13,2,9-$Ru_2C_2B_{10}H_{11}$] (**XXVII**), a different isomer from the anticipated 1,14,2,9-$Ru_2C_2B_{10}$ geometry.

A perspective view of the mesitylene species (**XXVIIc**) is shown in Figure 1.39. Additionally, a minor 13-vertex/12-vertex [6-(1′-*closo*-1′,2′-$C_2B_{10}H_{11}$)-4-mesitylene-5-arene-*closo*-4,5,1,6-$Ru_2C_2B_9H_{11}$] co-product is also formed by loss of a {BH} fragment. The 1,13,2,9-$Ru_2C_2B_{10}$ geometry observed is typically seen from DEI into 4,1,8-MC_2B_{10}, suggesting the metalation mechanism must proceed through DEI as opposed to reduction/metalation. Thus, Welch proposed the second reduction must result in a partitioning of the two electrons to each cage resulting in a monoanionic RuC_2B_{10} cage which is required for DEI.

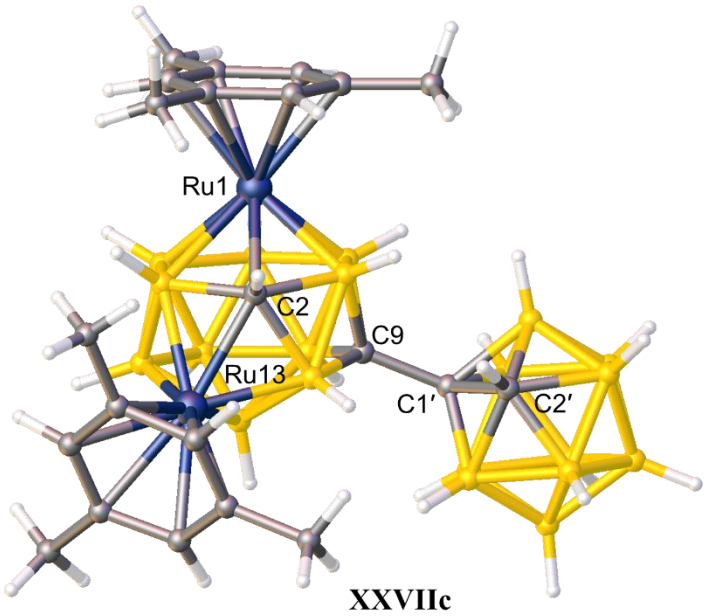

Figure 1.39 Perspective view of [9-(1′-*closo*-1′,2′-$C_2B_{10}H_{11}$)-1,13-(mesitylene)$_2$-*closo*-1,13,2,9-$Ru_2C_2B_{10}H_{11}$] (**XXVIIc**).

1.6 Scope of Thesis

This chapter has described the reactivity of *o*-carborane with particular emphasis on deboronation/metalation chemistry. Focus was given to the catalytically-active rhodacarborane [3-H-3,3-$(PPh_3)_2$-*closo*-3,1,2-$RhC_2B_9H_{11}$] and the chemistry surrounding bis(*o*-carborane) upon which the results in forthcoming chapters are based.

Chapter 2 describes the development of a new protocol for synthesising novel heterometalated derivatives of bis(*o*-carborane). Stepwise deboronation/metalation requires investigation into milder deboronation conditions for producing the suitable metallacarborane/*nido*-carborane precursor for subsequent metalation. In conjunction with this, two new metallacarborane/carborane species are reported along with an unexpected 13-vertex/12-vertex product arising from DEI.

Chapter 3 explores incorporating the catalytically-active {$Rh(PPh_3)_2H$} fragment into bis(*o*-carborane) as both metallacarborane/carborane and metallacarborane/ metallacarborane species. Four further examples of heterometalated derivatives of bis(*o*-carborane) are reported which were all characterised crystallographically.

Chapter 4 discusses the employment of all newly reported rhodacarborane species in various catalytic reactions. Comparison of reaction rates against the original [3-H-3,3-$(PPh_3)_2$-*closo*-3,1,2-$RhC_2B_9H_{11}$] (**VIII**) allows a ranking order of performance to be formed. Trends observed and preliminary DFT calculations provides an insight into the possible mechanistic cycles of the catalyst precursors.

Chapter 5 outlines the experimental procedures and characterisation of all previously discussed novel compounds.

1.7 References

1. H. Davy, *Phil. Trans. R. Soc. Lond.*, 1809, **99**, 39-104.
2. J. L. Gay-Lusaac and L. J. Thenard, *Annales de chimie*, 1808, **68**, 169-174.
3. W. L. Smith, *J. Chem. Educ.*, 1977, **54**, 469-473.
4. A. Stock, *Hydrides of Boron and Silicon*, Cornell University Press, Ithaca, New York, 1933.
5. S. H. Bauer, *J. Am. Chem. Soc.*, 1937, **59**, 1096-1103.
6. S. H. Bauer, *Chem. Rev.*, 1942, **31**, 43-75.
7. K. Hedberg and V. Schomaker, *J. Am. Chem. Soc.*, 1951, **73**, 1482-1487.
8. H. W. Smith and W. N. Lipscomb, *J. Chem. Phys.*, 1965, **43**, 1060-1064.
9. H. C. Longuet-Higgins, *J. Chim. Phys.*, 1949, **46**, 268-275.
10. H. C. Longuet-Higgins and M. D. Roberts, *Proc. Roy. Soc. Lond.*, 1955, **A230**, 110-119.
11. A. R. Pitochelli and M. F. Hawthorne, *J. Am. Chem. Soc.*, 1960, **82**, 3228-3229.
12. W. N. Lipscomb, *Boron Hydrides*, W. A. Benjamin Inc., New York, 1963.
13. R. E. Williams, *Inorg. Chem.*, 1971, **10**, 210-214.
14. K. Wade, *J. Chem. Soc. D*, 1971, 792-793.
15. D. M. P. Mingos, *Acc. Chem. Res.*, 1984, **17**, 311-319.
16. T. L. Heying, J. W. Ager, S. L. Clark, D. J. Mangold, H. L. Goldstein, M. Hillman, R. J. Polak and J. W. Szymanski, *Inorg. Chem.*, 1963, **2**, 1089-1092.
17. R. K. Bohn and M. D. Bohn, *Inorg. Chem.*, 1971, **10**, 350-355.
18. M. F. Hawthorne, T. D. Andrews, P. M. Garrett, F. P. Olsen, M. Reintjes, F. N. Tebbe, L. F. Warren, P. A. Wegner and D. C. Young, *Inorg. Synth.*, 1967, **10**, 91-118.
19. D. Grafstein and J. Dvorak, *Inorg. Chem.*, 1963, **2**, 1128-1133.
20. S. Papetti and T. L. Heying, *J. Am. Chem. Soc.*, 1964, **86**, 2295.
21. G. B. Dunks, R. J. Wiersema and M. F. Hawthorne, *J. Am. Chem. Soc.*, 1973, **95**, 3174-3179.
22. V. A. Brattsev and V. I. Stanko, *J. Organomet. Chem.*, 1973, **55**, 205-207.
23. W. N. Lipscomb, *Science*, 1966, **153**, 373-378.

24. E. L. Muetterties and W. N. Knoth, *Polyhedral Boranes*, Marcel Dekker, New York, 1968.

25. D. J. Wales, *J. Am. Chem. Soc.*, 1993, **115**, 1557-1567.

26. S. Dunn, G. M. Rosair, Rh. Ll. Thomas, A. S. Weller and A. J. Welch, *Angew. Chem., Int. Ed.*, 1997, **36**, 645-647.

27. N. S. Hosmane, H. Zhang, J. A. Maguire, Y. Wang, C. J. Thomas and T. G. Gray, *Angew. Chem., Int. Ed.*, 1996, **35**, 1000-1002.

28. C. A. Brown and M. L. McKee, *J. Mol. Model.*, 2006, **12**, 653-664.

29. V. I. Bregadze, *Chem. Rev.*, 1992, **92**, 209-223.

30. J. Cai, H. Nemoto, B. Singaram and Y. Yamamoto, *Tetrahedron Lett.*, 1996, **37**, 3383-3386.

31. V. N. Kalinin and V. A. Ol'shevskaya, *Russ. Chem. Bull.*, 2008, **57**, 815-836.

32. Z. Qiu, *Tetrahedron Lett.*, 2015, **56**, 963-971.

33. L. I. Zakharkin, A. V. Grebennikov and A. V. Kazantsev, *Bull. Acad. Sci. USSR, Div. Chem. Sci.*, 1967, **16**, 1991-1993.

34. D. Olid, R. Núñez, C. Viñas and F. Teixidor, *Chem. Soc. Rev.*, 2013, **42**, 3318-3336.

35. M. F. Hawthorne, *J. Organomet. Chem.*, 1975, **100**, 97-110.

36. L. Wesemann, *Comprehensive Organometallic Chemistry III, Chapter 3.03*, Elsevier, Oxford, 2007.

37. R. A. Wiesboeck and M. F. Hawthorne, *J. Am. Chem. Soc.*, 1964, **86**, 1642-1643.

38. J. Buchanan, E. J. M. Hamilton, D. Reed and A. J. Welch, *J. Chem. Soc., Dalton Trans.*, 1990, 677-680.

39. M. A. Fox, A. E. Goeta, J. A. K. Howard, A. K. Hughes, A. L. Johnson, D. A. Keen, K. Wade and C. C. Wilson, *Inorg. Chem.*, 2001, **40**, 173-175.

40. G. B. Dunks, M. M. McKown and M. F. Hawthorne, *J. Am. Chem. Soc.*, 1971, **93**, 2541-2453.

41. A. McAnaw, M. E. Lopez, D. Ellis, G. M. Rosair and A. J. Welch, *Dalton Trans.*, 2014, **43**, 5095-5105.

42. A. R. Kudinov, D. S. Perekalin, S. S. Rynin, K. A. Lyssenko, G. V. Grintselev-Knyazev and P. V. Petrovskii, *Angew. Chem., Int. Ed.*, 2002, **41**, 4112-4114.

43. R. D. McIntosh, D. Ellis, G. M. Rosair and A. J. Welch, *Angew. Chem., Int. Ed.*, 2006, **45**, 4313-4316.

44. L. Deng, J. Zhang, H. S. Chan and Z. Xie, *Angew. Chem., Int. Ed.*, 2006, **45**, 4309-4313.

45. D. K. Roy, S. K. Bose, R. S. Anju, B. Mondal, V. Ramkumar and S. Ghosh, *Angew. Chem., Int. Ed.*, 2013, **52**, 3222-3226.

46. L. A. Leites, *Chem. Rev.*, 1992, **92**, 279-323.

47. M. A. Fox, A. E. Goeta, A. K. Hughes and A. L. Johnson, *Dalton Trans.*, 2002, 2132-2141.

48. M. G. Davidson, T. G. Hibbert, J. A. K. Howard, A. Mackinnon and K. Wade, *Chem. Commun.*, 1996, 2285-2286.

49. A. J. Welch, *Crystals*, 2017, **7**, 234.

50. A. McAnaw, G. Scott, L. Elrick, G. M. Rosair and A. J. Welch, *Dalton Trans.*, 2013, **42**, 645-664.

51. A. McAnaw, M. E. Lopez, D. Ellis, G. M. Rosair and A. J. Welch, *Dalton Trans.*, 2014, **43**, 5095-5105.

52. M. F. Hawthorne, D. C. Young and P. A. Wegner, *J. Am. Chem. Soc.*, 1965, **87**, 1818-1819.

53. M. Elian, M. M. L. Chen, D. M. P. Mingos and R. Hoffmann, *Inorg. Chem.*, 1976, **15**, 1148-1155.

54. L. F. Warren and M. F. Hawthorne, *J. Am. Chem. Soc.*, 1968, **90**, 4823-4828.

55. M. F. Hawthorne and T. D. Andrews, *J. Am. Chem. Soc.*, 1965, **87**, 2496.

56. A. Zalkin, D. H. Templeton and T. E. Hopkins, *J. Am. Chem. Soc.*, 1965, **87**, 3988-3990.

57. W. Y. Man, G. M. Rosair and A. J. Welch, *Dalton Trans.*, 2015, **44**, 15417-15419.

58. M. K. Kaloustian, R. J. Wiersema and M. F. Hawthorne, *J. Am. Chem. Soc.*, 1972, **94**, 6679-6686.

59. S. Robertson, R. M. Garrioch, D. Ellis, T. D. McGrath, B. E. Hodson, G. M. Rosair and A. J. Welch, *Inorg. Chim. Acta*, 2005, **358**, 1485-1493.

60. R. D. McIntosh, D. Ellis, B. T. Giles, S. A. Macgregor, G. M. Rosair and A. J. Welch, *Inorg. Chim. Acta*, 2006, **359**, 3745-3753.

61. T. E. Paxson and M. F. Hawthorne, *J. Am. Chem. Soc.*, 1974, **96**, 4674-4676.

62. J. A. Belmont, J. Soto, R. E. King III, A. J. Donaldson, J. D. Hewes and M. F. Hawthorne, *J. Am. Chem. Soc.*, 1989, **111**, 7475-7486.

63. H. C. Kang and M. F. Hawthorne, *Organometallics*, 1990, **9**, 2327-2332.

64. P. E. Behnken, J. A. Belmont, D. C. Busby, M. S. Delaney, R. E. King III, C. W. Kreimendahl, T. B. Marder, J. J. Wilczynski and M. F. Hawthorne, *J. Am. Chem. Soc.*, 1984, **106**, 3011-3025.

65. P. E. Behnken, D. C. Busby, M. S. Delaney, R. E. King III, C. W. Kreimendahl, T. B. Marder, J. J. Wilczynski and M. F. Hawthorne, *J. Am. Chem. Soc.*, 1984, **106**, 7444-7450.

66. V. N. Lebedev, E. V. Balagurova, F. M. Dolgushin, A. I. Yanovskii and L. I. Zakharkin, *Russ. Chem. Bull.*, 1997, **46**, 550-558.

67. J. A. Dupont and M. F. Hawthorne, *J. Am. Chem. Soc.*, 1964, **86**, 1643.

68. T. E. Paxson, K. P. Callahan and M. F. Hawthorne, *Inorg. Chem.*, 1973, **12**, 708-709.

69. X. Yang, W. Jiang, C. B. Knobler, M. D. Mortimer and M. F. Hawthorne, *Inorg. Chim. Acta*, 1995, **240**, 371-378.

70. S. Ren and Z. Xie, *Organometallics*, 2008, **27**, 5167-5168.

71. L. I. Zakharkin and A. I. Kovredov, *Bull. Acad. Sci. USSR, Div. Chem. Sci.*, 1973, **22**, 1396.

72. X. Yang, W. Jiang, C. B. Knobler and M. F. Hawthorne, *J. Am. Chem. Soc.*, 1992, **114**, 9719-9721.

73. W. Y. Man, G. M. Rosair and A. J. Welch, *Acta Cryst.*, 2014, **E70**, 462-465.

74. L. Elrick, G. M. Rosair and A. J. Welch, *Acta Cryst.*, 2014, **E70**, 376-378.

75. I. B. Sivaev, *Commun. Inorg. Synth.* , 2016, **4**, 21-28.

76. D. A. Owen and M. F. Hawthorne, *J. Am. Chem. Soc.*, 1971, **93**, 873-880.

77. M. J. Martin, W. Y. Man, G. M. Rosair and A. J. Welch, *J. Organomet. Chem.*, 2015, **798**, 36-40.

78. L. E. Riley, A. P. Y. Chan, J. Taylor, W. Y. Man, D. Ellis, G. M. Rosair, A. J. Welch and I. B. Sivaev, *Dalton Trans.*, 2016, **45**, 1127-1137.

79. Z.-J. Yao, Y.-Y. Zhang and G.-X. Jin, *J. Organomet. Chem.*, 2015, **798**, 274-277.

80. K. O. Kirlikovali, J. C. Axtell, A. Gonzalez, A. C. Phung, S. I. Khan and A. M. Spokoyny, *Chem. Sci.*, 2016, **7**, 5132-5138.

81. L. I. Zakharkin and N. F. Shemyakin, *Bull. Acad. Sci. USSR, Div. Chem. Sci.*, 1978, **27**, 1267-1268.

82. A. I. Yanovskii, N. G. Furmanova, Y. T. Struchkov, N. F. Shemyakin and L. I. Zakharkin, *Bull. Acad. Sci. USSR, Div. Chem. Sci.*, 1979, **28**, 1412-1417.

83. S. E. Johnson and C. B. Knobler, *Phosphorus, Sulfur, Silicon, Relat. Elem.*, 1996, **115**, 227-240.

84. L. E. Riley, T. Krämer, C. L. McMullin, D. Ellis, G. M. Rosair, I. B. Sivaev and A. J. Welch, *Dalton Trans.*, 2017, **46**, 5218-5228.

85. J. C. Axtell, K. O. Kirlikovali, R. M. Dziedzic, M. Gembicky, A. L. Rheingold and A. M. Spokoyny, *Eur. J. Inorg. Chem.*, 2017, **2017**, 4411-4416.

86. S. Yruegas, J. C. Axtell, K. O. Kirlikovali, A. M. Spokoyny and C. D. Martin, *Chem. Commun.*, 2019, **55**, 2892-2895.

87. M. F. Hawthorne, D. A. Owen and J. W. Wiggins, *Inorg. Chem.*, 1971, **10**, 1304-1306.

88. P. E. Behnken, C. B. Knobler and M. F. Hawthorne, *Angew. Chem., Int. Ed.*, 1983, **22**, 722-723.

89. G. Thiripuranathar, A. P. Y. Chan, D. Mandal, W. Y. Man, M. Argentari, G. M. Rosair and A. J. Welch, *Dalton Trans.*, 2017, **46**, 1811-1821.

90. G. Thiripuranathar, W. Y. Man, C. Palmero, A. P. Y. Chan, B. T. Leube, D. Ellis, D. McKay, S. A. Macgregor, L. Jourdan, G. M. Rosair and A. J. Welch, *Dalton Trans.*, 2015, **44**, 5628-5637.

91. G. S. Kazakov, I. B. Sivaev, K. Y. Suponitsky, A. D. Kirilin, V. I. Bregadze and A. J. Welch, *J. Organomet. Chem.*, 2016, **805**, 1-5.

92. J. A. Doi, E. A. Mizusawa, C. B. Knobler and M. F. Hawthorne, *Inorg. Chem.*, 1984, **23**, 1482-1484.

93. J. A. Long, T. B. Marder, P. E. Behnken and M. F. Hawthorne, *J. Am. Chem. Soc.*, 1984, **106**, 2979-2989.

94. W. Y. Man, S. Zlatogorsky, H. Tricas, D. Ellis, G. M. Rosair and A. J. Welch, *Angew. Chem., Int. Ed.*, 2014, **53**, 12222-12225.

95. D. Mandal, W. Y. Man, G. M. Rosair and A. J. Welch, *Dalton Trans.*, 2016, **45**, 15013-15025.

96. P. E. Behnken, T. B. Marder, R. T. Baker, C. B. Knobler, M. R. Thompson and M. F. Hawthorne, *J. Am. Chem. Soc.*, 1985, **107**, 932-940.

97. T. D. Getman, C. B. Knobler and M. F. Hawthorne, *J. Am. Chem. Soc.*, 1990, **112**, 4593-4594.

98. T. D. Getman, C. B. Knobler and M. F. Hawthorne, *Inorg. Chem.*, 1992, **31**, 101-105.

99. D. Ellis, D. McKay, S. A. Macgregor, G. M. Rosair and A. J. Welch, *Angew. Chem., Int. Ed.*, 2010, **49**, 4943-4945.

100. D. Ellis, G. M. Rosair and A. J. Welch, *Chem. Commun.*, 2010, **46**, 7394-7396.

101. D. Mandal, W. Y. Man, G. M. Rosair and A. J. Welch, *Acta Cryst.*, 2015, **C71**, 793-798.

102. W. Y. Man, D. Ellis, G. M. Rosair and A. J. Welch, *Angew. Chem., Int. Ed.*, 2016, **55**, 4596-4599.

Chapter 2

Ruthenium/Cobalt Heterometalated Bis(carboranes)

2.1 Introduction

The metalation of either one or both cages of bis(*o*-carborane) was recently established affording MC_2B_9-C_2B_{10} and MC_2B_9-MC_2B_9 products, respectively.[1,2] Single deboronation of bis(*o*-carborane) was first reported by Hawthorne,[3] and subsequently optimised by Welch,[1] using an alkoxide. An alternative route utilising the electron-withdrawing properties of the carboranyl (-$C_2B_{10}H_{11}$) substituent was reported by Sivaev using wet acetonitrile to perform the mono-deboronation.[4] The resulting anion [7-(1′-*closo*-1′,2′-$C_2B_{10}H_{11}$)-*nido*-7,8-$C_2B_9H_{11}$]$^-$ [**XI**]$^-$ is the precursor for all metallacarborane/carborane complexes (Figure 2.1).

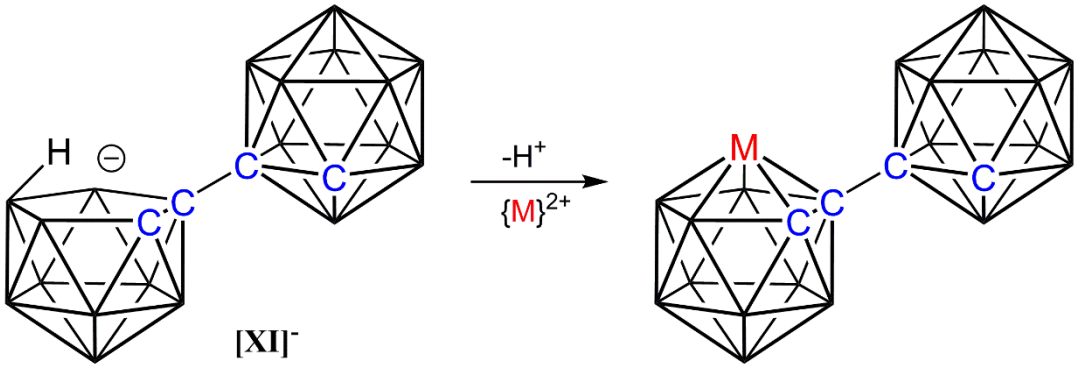

Figure 2.1 General protocol for synthesising metallacarborane/carborane products.

Double deboronation, again first reported by Hawthorne[3] and optimised by Welch,[2] affords the dianion [7-(7′-*nido*-7′,8′-$C_2B_9H_{11}$)-*nido*-7,8-$C_2B_9H_{11}$]$^{2-}$ ([**XII**]$^{2-}$). The product exists as a diastereomeric mixture and thus all metalated products can exist as diastereoisomers. Similarly, this is the precursor for all metallacarborane/ metallacarborane species. Due to the one-step nature of the metalation process, all products isolated are necessary homometalated (Figure 2.2).

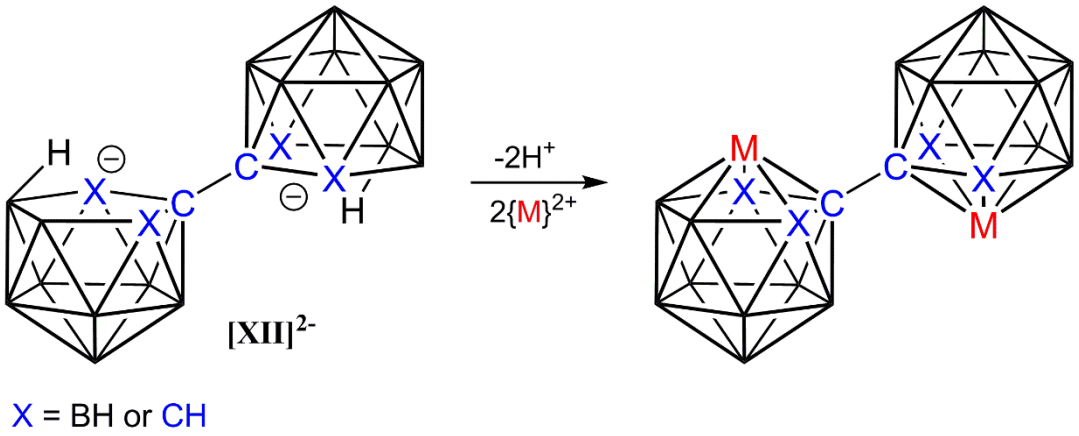

Figure 2.2 General procedure for synthesising metallacarborane/metallacarborane products.

In this chapter, we aim to synthesise novel heterometalated bis(carboranes) with the commonly used metal fragments {CoCp} and {Ru(*p*-cymene)} by two stepwise decapitation/metalation processes.

2.2 Synthesis of [HNMe$_3$][8-(7′-*nido*-7′,8′-$C_2B_9H_{11}$)-2-(*p*-cymene)-*closo*-2,1,8-$RuC_2B_9H_{10}$] (1)

[8-(1′-*closo*-1′,2′-$C_2B_{10}H_{11}$)-2-(*p*-cymene)-*closo*-2,1,8-$RuC_2B_9H_{10}$] (**XVII**) was deboronated using KF in a THF/H_2O mixture (10:1) at reflux overnight. The initial potassium salt formed was metathesised in H_2O with NMe_3.HCl to isolate the target compound **1** as the $[HNMe_3]^+$ salt (Figure 2.3). The white powder was characterised by microanalysis and NMR spectroscopy. The product exists as an inseparable diastereomeric mixture (1:1) from which single crystals could not be grown, precluding the use of *X*-ray diffraction studies as a characterisation method.

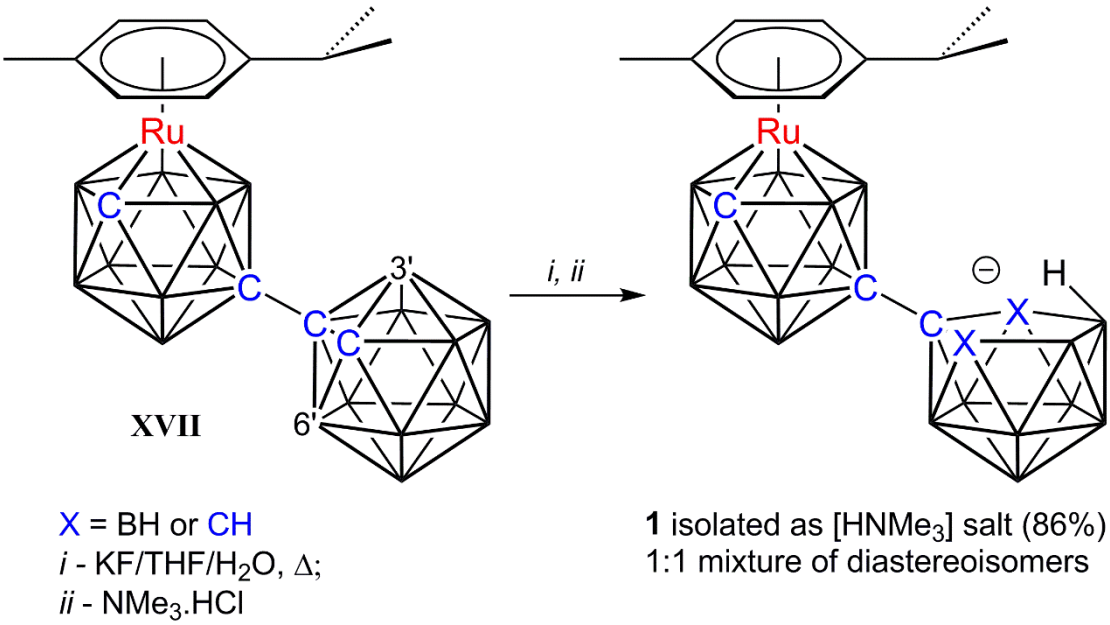

Figure 2.3 Deboronation of [8-(1′-*closo*-1′,2′-$C_2B_{10}H_{11}$)-2-(*p*-cymene)-*closo*-2,1,8-$RuC_2B_9H_{10}$] (**XVII**) using KF to afford **1**.

The elemental analysis is in good agreement with the predicted formula $C_{17}H_{45}B_{18}NRu$. Diastereoisomers are expected as deboronations at positions B3′ or B6′ are both possible as they are chemically equivalent.

The ^{1}H NMR spectrum displays the expected chemical shifts for the *p*-cymene ligand and the methyl groups of the trimethylammonium cation. The $C_{cage}H$ shifts were observed at δ 2.64 and 1.93 ppm as broad singlets, the former of which is typical for an isomerised metallacarborane and the latter a *nido*-$C_2B_9H_{12}$ cage. A number of resonances of the *p*-cymene double up to display an overlapped signal, most notable in the resonances related to the ^{i}Pr substituent (Figure 2.4, left), indicative of diastereoisomers. The most diagnostic evidence for this is the overlapping broad singlets observed for the bridging/endo-*H* of the deboronated cage (Figure 2.4, right). Relative integrals of these duplicate signals suggest a 1:1 ratio of the two diastereoisomers.

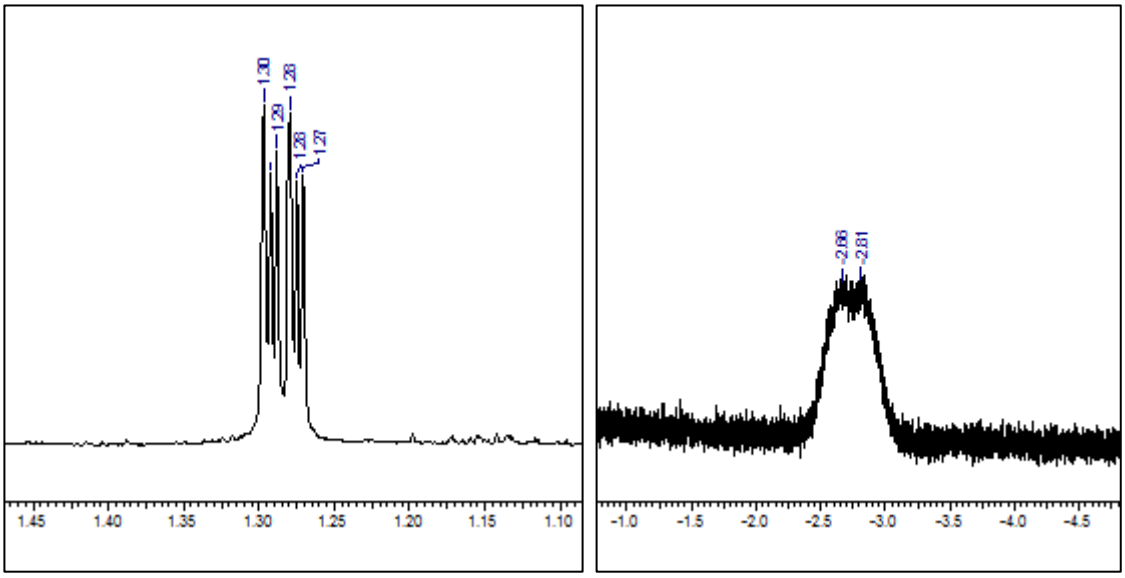

Figure 2.4 Selected ^{1}H NMR resonances of **1**; overlapped pairs of doublets corresponding to CH_3 of the ^{i}Pr substituent (left) and overlapped broad singlets assigned to the μ-*H* of the *nido*-$C_2B_9H_{11}$ unit (right). Units in ppm.

The ^{11}B{^{1}H} NMR spectrum displays a 1:2:1:1:3:2:2:1:2:1:1:1 ratio of peaks. The lack of symmetry in this species indicates that any equivalent signals are purely coincidental. The two most upfield resonances at δ -33.5 and -35.9 ppm are characteristic of a nido cage and correspond to the B10′ and B1′ vertices respectively.

Prior to using KF as a deboronation reagent in the preparation of **1**, the typical KOH/EtOH conditions were trialled. Whilst the desired product can be isolated, in addition to minor decomposition, the limited solubility of **XVII** in ethanol prevented the scale-up of this process. Additionally, total decomposition was observed when using more fragile metal fragments i.e. {$Rh(PPh_3)_2H$}.

The milder acetonitrile/water conditions were also tested and found to afford **1**. However, the deboronation was too inefficient to be taken forward (*ca*. 30% conversion after 7 days at reflux temperatures). This prompted the use of 'wet' fluoride as it has been recognised to be mild and selective deboronation reagent.[5] The fluoride anion is typically supplied as tetrabutylammonium fluoride (TBAF) and the product is isolated as the $[NBu_4]^+$ salt. However, this counterion is impractical for the subsequent metalation step as direct generation of the dilithio-salt is not possible. Thus, $[HNMe_3]^+$ is normally the cation of choice. Unfortunately, there is no equivalent fluoride source with trimethylammonium therefore this was accessed indirectly from use of KF to initially form the potassium salt. Metathesis with NMe_3.HCl can then afford the desired compound **1** in good yield.

2.3 Synthesis of *α*-[8-(1′-3′-Cp-*closo*-3′,1′,2′-$CoC_2B_9H_{10}$)-2-(*p*-cymene)-*closo*-2,1,8-$RuC_2B_9H_{10}$] (2*α*) and *β*-[8-(1′-3′-Cp-*closo*-3′,1′,2′-$CoC_2B_9H_{10}$)-2-(*p*-cymene)-*closo*-2,1,8-$RuC_2B_9H_{10}$] (2*β*)

Deprotonation of **1** with ^{n}BuLi and subsequent reaction with $CoCl_2$/NaCp followed by aerial oxidation yields an orange band from column chromatography. Further purification by preparative TLC reveals two close-moving orange bands identified to be the two diastereoisomers of [8-(1′-3′-Cp-*closo*-3′,1′,2′-$CoC_2B_9H_{10}$)-2-(*p*-cymene)-*closo*-2,1,8-$RuC_2B_9H_{10}$] (**2*α*** and **2*β***), the first examples of heterometalated bis(carborane) (Figure 2.5). As no nomenclature rules have been published (to our knowledge), the primed cage has been assigned as that containing the second metal fragment to be inserted. Both compounds were analysed by mass spectrometry, microanalysis and NMR spectroscopy. Suitable crystals for *X*RD studies were grown from DCM/petrol diffusion at -20 °C.

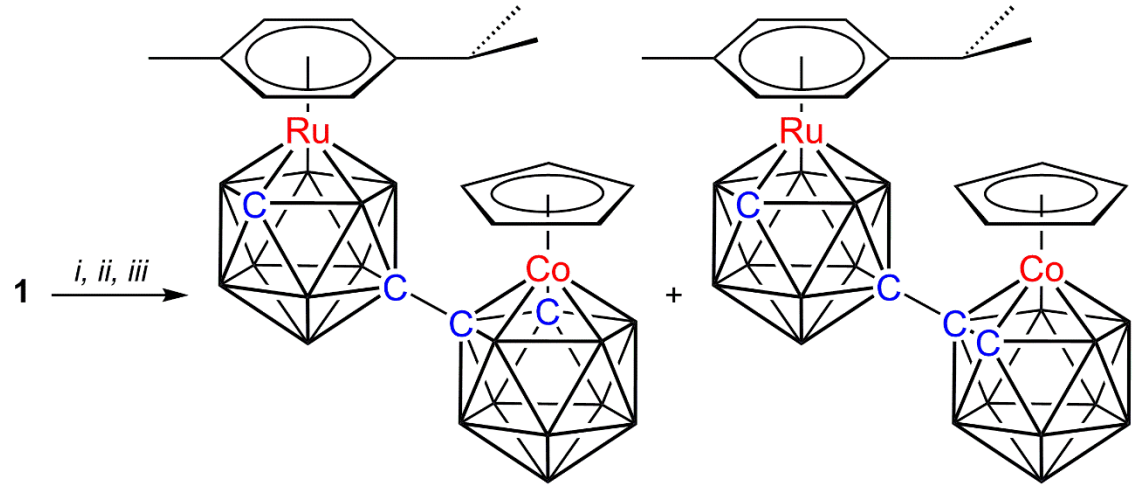

Figure 2.5 Metalation of **1** using $CoCl_2$/NaCp to afford **2*α*** and **2*β***.

Elemental analysis and mass spectrometry of **2*α*** are in good agreement with the formulated product $C_{19}H_{39}B_{18}CoRu$. The typical resonances are observed in the ^{1}H NMR spectrum for the *p*-cymene and Cp ligands in addition to the two $C_{cage}H$ shifts at δ 4.27

and 2.63 ppm, typical of a 3,1,2-MC_2B_9-1′,2′-C_2B_{10} and 2,1,8-MC_2B_9-1′,2′-C_2B_{10} geometry respectively. Starting with the isomerised architecture in **1**, we can assign the low frequency $C_{cage}H$ shift to the existing ruthenacarborane and the relatively high frequency $C_{cage}H$ shift to the new cobaltacarborane. From this, we tentatively formulate the product to have a 2,1,8-RuC_2B_9-3′,1′,2′-CoC_2B_9 geometry. As expected, the $^{11}B\{^1H\}$ NMR spectrum is largely uninformative due to its complexity. Nevertheless, several isolated resonances integrating to 1B can be identified to give a total of 18B atoms.

An *X*-ray diffraction study of the orange block crystals confirmed the structure to be *α*-[8-(1′-3′-Cp-*closo*-3′,1′,2′-$CoC_2B_9H_{10}$)-2-(*p*-cymene)-*closo*-2,1,8-$RuC_2B_9H_{10}$] (Figure 2.6), where the alpha denotes that the product is derived from the rac-diastereoisomer of [7-(7′-*nido*-7′,8′-$C_2B_9H_{11}$)-*nido*-7,8-$C_2B_9H_{11}$]$^{2-}$ [**XIIa**]$^{2-}$.[2] The location of the cage C atoms not involved in the bis(carborane) linkage was identified unambiguously by both the VCD and BHD methods.

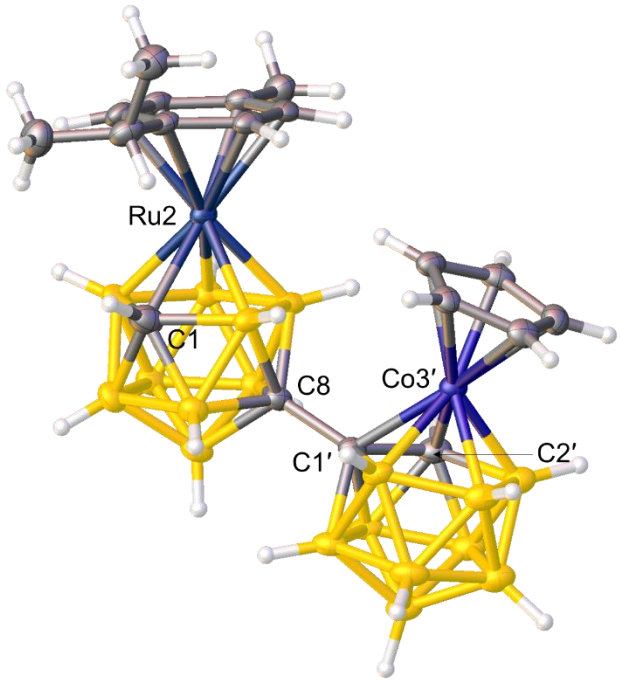

Figure 2.6 Perspective view of one of the two crystallographically independent molecules of *α*-[8-(1′-3′-Cp-*closo*-3′,1′,2′-$CoC_2B_9H_{10}$)-2-(*p*-cymene)-*closo*-2,1,8-$RuC_2B_9H_{10}$] (**2*α***).

The cobaltacarborane cage architecture is unexpected as previous work has shown {CoCp} generated *in situ* from $CoCl_2$/NaCp primarily affords the isomerised 2,1,8-CoC_2B_9 geometry.[1] This is due to the initial formation of a 1e-reduced product which has been shown to readily isomerise (Figure 2.7). This finding indicates subrogating the carboranyl substituent by a ruthenacarborane prevents the typically-observed redox isomerisation.

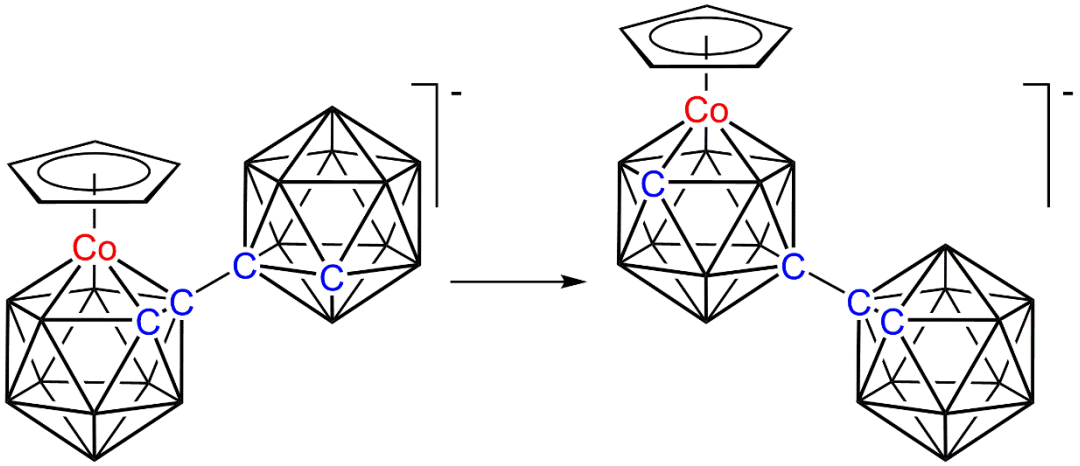

Figure 2.7 Reduction-promoted isomerisation of [1-(1′-*closo*-1′,2′-$C_2B_{10}H_{11}$)-3-Cp-*closo*-3,1,2-$CoC_2B_9H_{10}$].

There are two crystallographically independent molecules of **2*α*** in the unit cell. These are effectively superimposable with the exception of the orientation of the *p*-cymene ligand. In one of the independent molecules, the ^{i}Pr group of the *p*-cymene is partially disordered. As expected, both *p*-cymene ligands lie parallel to the lower pentagonal belt of the cages (C8B4B5B10B12) due to their isomerised architecture. In contrast to this, the non-isomerised cobaltacarborane displays significant bendback angles [θ = 13.93(18) and 13.97(18)°] of the Cp ligand relative to the B5′B6′B11′B12′B9′ plane. These are comparable to those in the singly-metalated species [1-(1′-*closo*-1′,2′-$C_2B_{10}H_{11}$)-3-Cp-*closo*-3,1,2-$CoC_2B_9H_{10}$] where the angles θ are 15.8 and 16.3°.

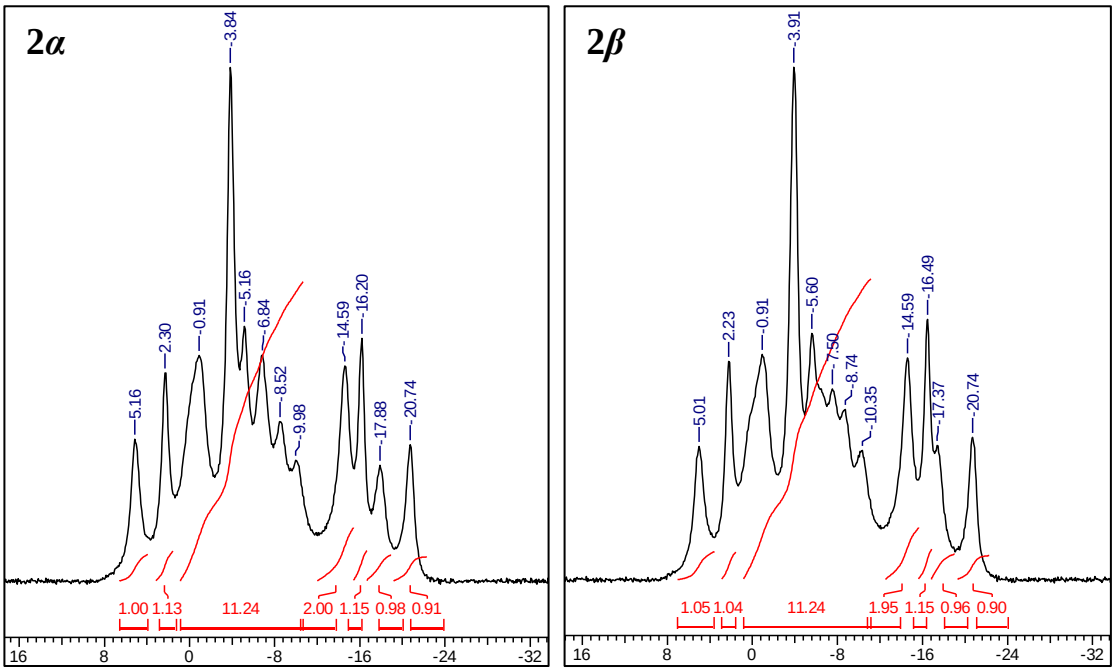

Figure 2.8 The $^{11}B\{^{1}H\}$ NMR spectra of **2*α*** (left) and **2*β*** (right). Units in ppm.

For **2*β***, microanalysis and mass spectrometry are consistent with the same $C_{19}H_{39}B_{18}CoRu$ formula, indicating that this must be an isomer of **2*α***. Additionally, the ^{1}H NMR spectrum is remarkably similar implying **2*β*** is likely to be the complementary diastereoisomer as opposed to a different architectural form. However, small differences in the ^{1}H NMR spectra can be observed, most notably the Cp resonance (δ 5.82 vs 5.80 ppm) and one of the $C_{cage}H$ resonance (δ 4.12 vs 4.27 ppm), allowing the two compounds to be distinguished. The remaining $C_{cage}H$ shift in **2*β*** is at δ 2.63 ppm which is identical to that in **2*α***. The $^{11}B\{^{1}H\}$ NMR spectrum again is equivocal but is essentially interchangeable with that of **2*α*** (Figure 2.8).

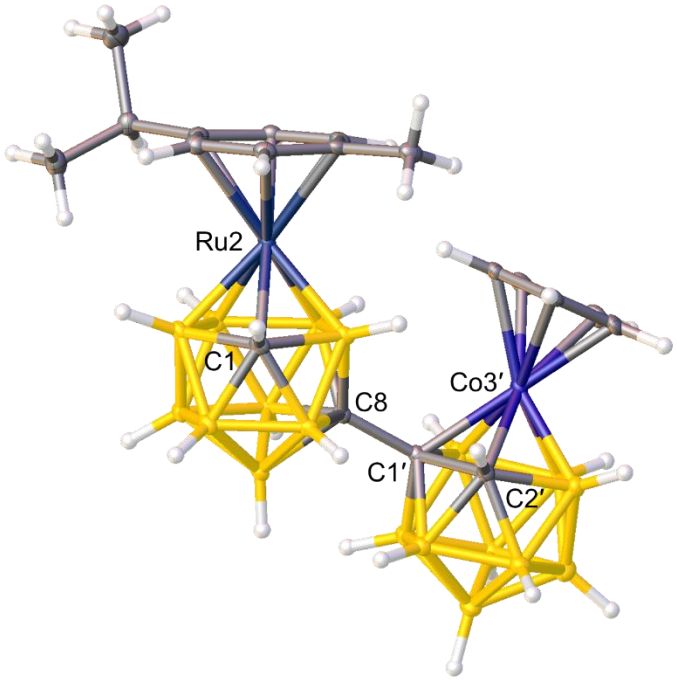

Figure 2.9 Perspective view of one of the two crystallographically independent molecules of *β*-[8-(1′-3′-Cp-*closo*-3′,1′,2′-$CoC_2B_9H_{10}$)-2-(*p*-cymene)-*closo*-2,1,8-$RuC_2B_9H_{10}$] (**2*β***).

To determine the precise structure of **2*β***, a crystallographic study was undertaken of the block orange crystals. The species was confirmed to be the expected *β*-[8-(1′-3′-Cp-*closo*-3′,1′,2′-$CoC_2B_9H_{10}$)-2-(*p*-cymene)-*closo*-2,1,8-$RuC_2B_9H_{10}$] (Figure 2.9). The unit cell comprises of two essentially superimposable molecules of **2*β*** and half a DCM molecule. The *p*-cymene unit lies effectively parallel to the reference plane whilst the Cp ligands subtend angles of θ 13.57(8) and 13.08(7)° to minimise the steric crowding. The VCD and BHD methods were successfully employed to identify the unassigned cage C atoms in all four cages.

2.4 Synthesis of [HNMe$_3$][8-(7′-*nido*-7′,8′-$C_2B_9H_{11}$)-2-Cp-*closo*-2,1,8-$CoC_2B_9H_{10}$] (3)

Analogous to the preparation of **1**, [8-(1′-*closo*-1′,2′-$C_2B_{10}H_{11}$)-2-Cp-*closo*-2,1,8-$CoC_2B_9H_{10}$] was treated with KF in a THF/H_2O mixture (10:1) at reflux overnight. Metathesis in H_2O with NMe_3.HCl afforded **3** as the $[HNMe_3]^+$ salt (Figure 2.10). The yellow powder was analysed by NMR spectroscopy and elemental analysis. Similar to **1**, the product exists as an inseparable diastereomeric mixture (1:1) from which single crystals were not successfully grown for a crystallographic study.

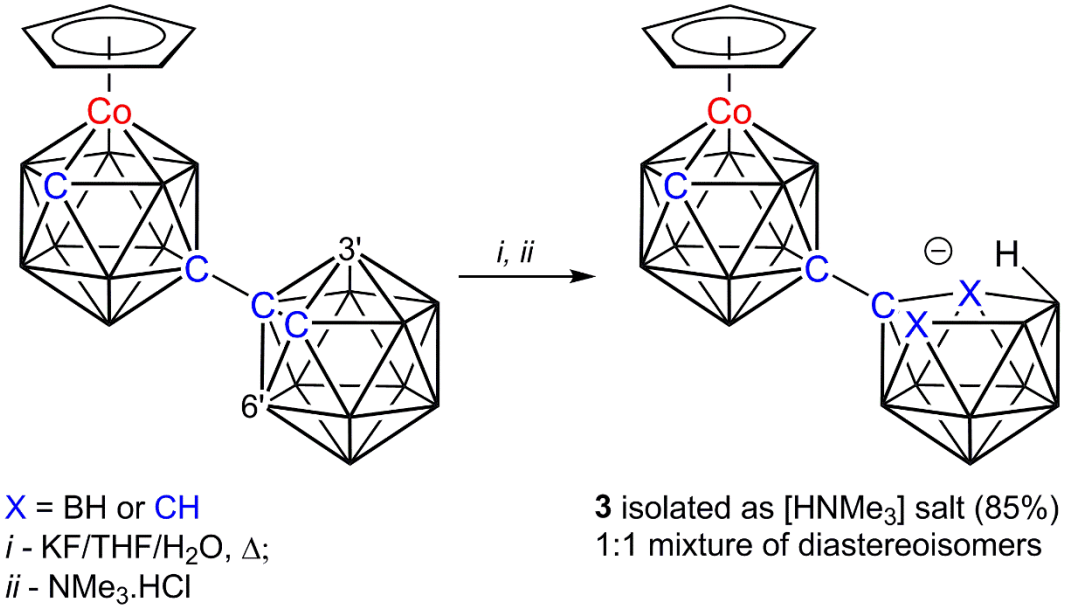

Figure 2.10 Deboronation of [8-(1′-*closo*-1′,2′-$C_2B_{10}H_{11}$)-2-Cp-*closo*-2,1,8-$CoC_2B_9H_{10}$] using KF to afford **3**.

The elemental analysis is consistent with the formula $C_{12}H_{36}B_{18}CoN$. A single resonance is observed for the C*H*$_3$ moieties of trimethylammonium cation in the ^{1}H NMR spectrum as expected. Broad $C_{cage}H$ resonances were observed at δ 2.84 and 1.88 ppm, again typical for an isomerised metallacarborane cage and a *nido*-$C_2B_9H_{12}$ cage, respectively.

Two singlets (δ 5.50 and 5.49 ppm) for the Cp ligand and overlapping broad singlets for the bridging/endo-*H* of the deboronated cage are observed confirming that the product is a mixture of diastereoisomers (Figure 11). Integration of the ^{1}H NMR spectrum suggests an equimolar mixture.

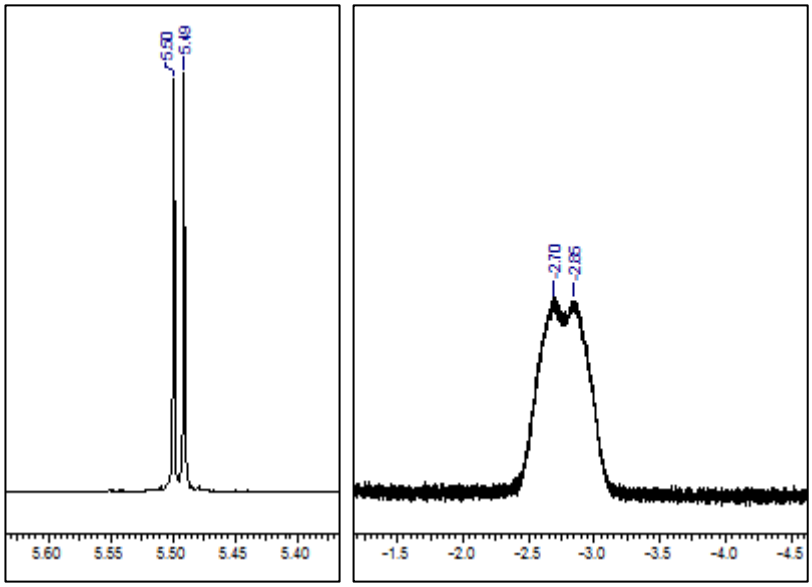

Figure 2.11 Selected ^{1}H NMR resonances of **3**; pair of singlets assigned to the Cp (left) and overlapped broad singlets assigned to the μ-*H* of the *nido*-$C_2B_9H_{11}$ unit (right). Units in ppm.

The ^{11}B{^{1}H} NMR spectrum displays a 3:1:2:1:1:1:2:2:1:1:1:1:1 ratio of peaks where all equivalent signals are coincidental due to the asymmetry of the anion. The characteristic nido resonances of B10′ and B1′ are observed at δ -33.3 and -35.7 ppm respectively.

Use of **3** as a precursor for heterometalated bis(carboranes) affords no neutral products following typical deprotonation and metalation protocols. Decomposition of **3** is suspected to occur upon deprotonation using ^{n}BuLi as an immediate darkening of the solution is observed. Reasoning that this has occurred due to attack on the Cp ligand by ^{n}BuLi, the more robust Cp* ligand was used in its place.

2.5 Synthesis of [1-(1′-*closo*-1′,2′-$C_2B_{10}H_{11}$)-3-Cp*-*closo*-3,1,2-$CoC_2B_9H_{10}$] (4), [8-(1′-*closo*-1′,2′-$C_2B_{10}H_{11}$)-2-Cp*-*closo*-2,1,8-$CoC_2B_9H_{10}$] (5), and [12-(1′-*closo*-1′,2′-$C_2B_{10}H_{11}$)-4,5-Cp*$_2$-*closo*-4,5,1,12-$Co_2C_2B_9H_{10}$] (6)

In THF, [$HNMe_3$][7-(1′-*closo*-1′,2′-$C_2B_{10}H_{11}$)-*nido*-7,8-$C_2B_9H_{11}$] [**XI**] was deprotonated using ^{n}BuLi to produce a pale yellow solution. Following addition of $CoCl_2$ and NaCp*, aerial oxidation and subsequent work-up affords three mobile bands (red, yellow and green) isolated by column chromatography (Figure 2.12). The red and yellow products (**4** and **5**, respectively) are structural isomers of Cp*$CoC_2B_9H_{10}$-$C_2B_{10}H_{11}$ whilst the trace green band (**6**) contains an additional {CoCp*} fragment.

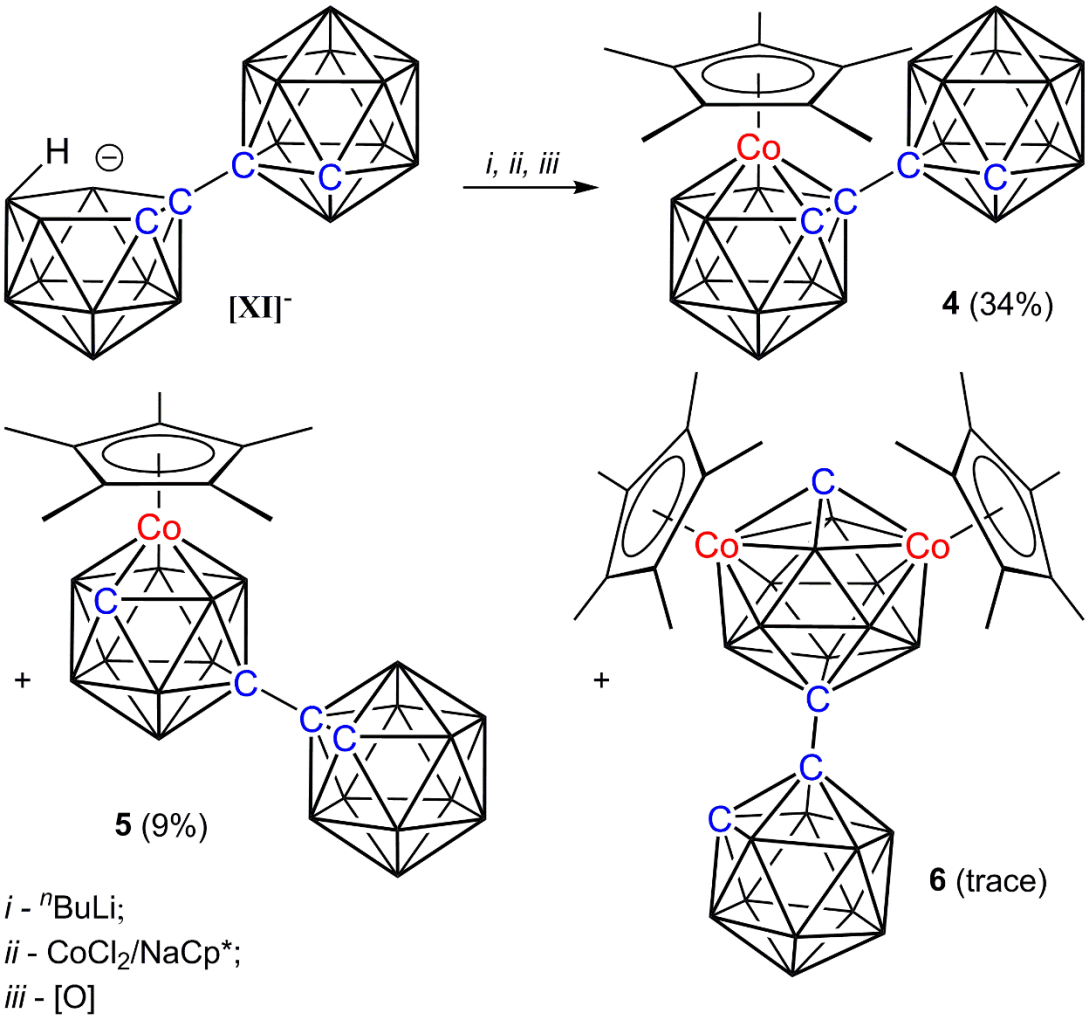

Figure 2.12 Formation of **4**, **5** and **6** from the metalation of [$HNMe_3$][7-(1′-*closo*-1′,2′-$C_2B_{10}H_{11}$)-*nido*-7,8-$C_2B_9H_{11}$] ([$HNMe_3$][**XI**]) with *in situ* generated {CoCp*} followed by oxidation.

Mass spectrometry of **4** is in good agreement with the formula $C_{14}H_{36}B_{19}Co$ as EIMS displays an envelope centred on *m/z* 469 (M^+) (GFM = 468.78 g mol^{-1}). The chemical composition is further supported by microanalysis.

The majority of the $^{11}B\{^1H\}$ NMR spectrum displays significant peak overlap however a single relatively high frequency 1B resonance is observed at δ 10.1 ppm, reminiscent of the Cp analogue with a 3,1,2-CoC_2B_9-1′,2′-C_2B_{10} architecture (δ 6.5 ppm). The ^1H NMR spectrum displays a singlet for the Cp* protons as well as two $C_{cage}H$ resonances at δ 4.10 and 3.37 ppm, the latter of which is ascribed to the cobaltacarborane cage. The Cp analogue $C_{cage}H$ resonances are not easily assigned due to their similarity (δ 4.24 and 4.03 ppm). The shift towards lower frequency (~0.6 ppm) in **4** is attributed to the inductive effect of the Cp* ligand.

The structure of **4** was confirmed crystallographically (Figure 2.13). Non-linking cage C atoms were assigned using the VCD and BHD methods independently. Substantial steric crowding is evident from the bendback angle of the Cp* [θ = 21.58(8)°] with reference to the lower pentagonal belt, significantly larger than that in the Cp analogue (θ = 15.8 and 16.3°). In addition to lengthening of the C1–Co3 connectivity [2.1670(19) Å compared to 2.118 and 2.124 Å], there is a reduced elevation of the carborane substituent with reference to the C1C2B7B8B4 plane [θ = 16.07(12)° *cf.* Cp analogue θ = 19.1 and 19.5°].

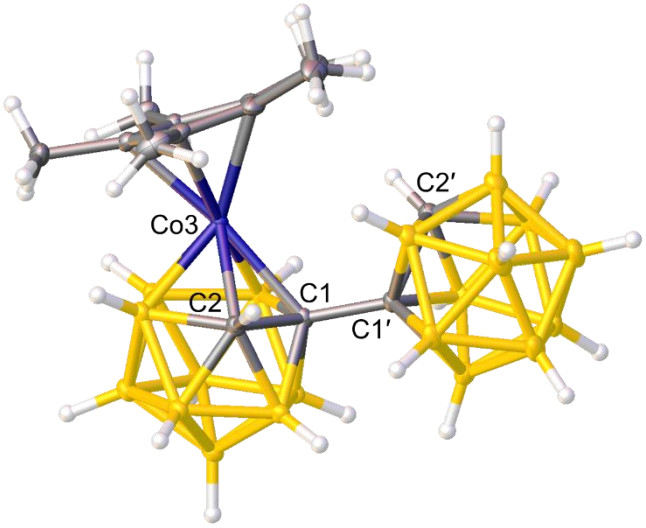

Figure 2.13 Perspective view of [1-(1′-*closo*-1′,2′-$C_2B_{10}H_{11}$)-3-Cp*-*closo*-3,1,2-$CoC_2B_9H_{10}$] (**4**).

Compound **5** was found to have the same chemical composition as **4** by mass spectrometry and elemental analysis, fully consistent with the proposal that it is a structural isomer.

A mixed solvent system ($CHCl_3$/CD_3CN, 1:10) was required to distinguish one of the $C_{cage}H$ resonances (δ 2.09 ppm) which is assigned to an isomerised cobaltacarborane cage from the Cp* protons (δ 1.84 ppm). An upfield shift of the same magnitude (~0.6 ppm) is noted in this cobaltacarborane $C_{cage}H$ resonance (δ 2.09 ppm) when compared to that in its Cp analogue (δ 2.73 ppm). As was the case with **4**, this is due to the inductive effect of the Cp* ligand. The remaining $C_{cage}H$ resonance is observed at δ 4.01 ppm, typical for a carboranyl substituent. Similar to **4**, the $^{11}B\{^1H\}$ NMR spectrum is largely uninformative due to a number of overlapped peaks. However, two relatively low frequency resonances (δ -18.0 and -18.6 ppm) integrating for 1B each and a singlet at δ -9.9 ppm (6B) allowed the spectrum to be fully integrated to account for a total of 19B atoms. Additionally, the same features [δ -9.9 (6B), -16.8 (1B) and -17.7 (1B)] can be observed in the Cp analogue, supporting the implication of an isomerised 2,1,8-CoC_2B_9 structure.

The structure of **5** was definitively determined crystallographically to be [8-(1′-*closo*-1′,2′-$C_2B_{10}H_{11}$)-2-Cp*-*closo*-2,1,8-$CoC_2B_9H_{10}$] (Figure 2.14). Two superimposable crystallographically-independent molecules are present in the asymmetric fraction of the unit cell. As expected, the Cp* ligand lies effectively parallel to the reference plane as the steric crowding has been removed. The structure is unremarkable and fully comparable to its Cp analogue.

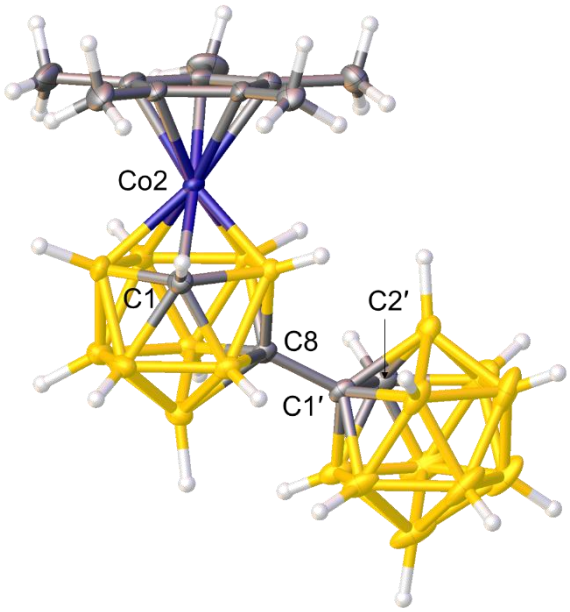

Figure 2.14 Perspective view of one of the two crystallographically-independent molecules of [8-(1′-*closo*-1′,2′-$C_2B_{10}H_{11}$)-2-Cp*-*closo*-2,1,8-$CoC_2B_9H_{10}$] (**5**).

The formation of both **4** and **5** is somewhat surprising as previous synthesis of the Cp analogue has shown *in situ* generation of the {CoCp} fragment affords predominantly the isomerised product.[1] Overnight reaction yields **4** in 34% yield and **5** in only 9% yield, a reversal in product preference. However, extended reaction times (3 days) affords **4** and **5** in yields of 6% and 27%, respectively, suggesting the reduction-induced isomerisation is much slower.

EIMS of the trace co-product **6** displayed envelopes centred on *m/z* 663 (M^+) and 469 (M^+ - {CoCp*}) suggesting the incorporation of two {CoCp*} fragments to give a species with the formula $C_{24}H_{51}B_{19}Co_2$ (GFM = 662.94 g mol^{-1}). The limited availability of **6** precluded the use of elemental analysis to confirm its chemical composition.

Two broad singlets corresponding to the $C_{cage}H$ resonances can be observed in the ^1H NMR spectrum at δ 3.80 and 1.26 ppm. Interestingly, only one singlet is observed for the Cp* protons integrating for 30H suggesting an equivalent environment. The $^{11}B\{^1H\}$ NMR spectrum displays one relatively high frequency resonance (δ 7.6 ppm) that can be confidently integrated for 1B atom allowing the full spectrum to be assigned a total integral of 19B atoms.

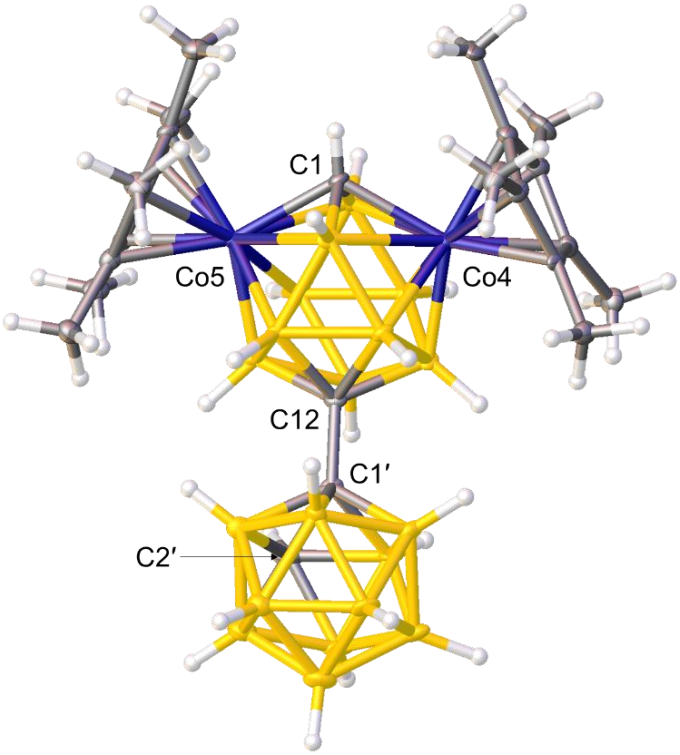

Figure 2.15 Perspective view of [12-(1′-*closo*-1′,2′-$C_2B_{10}H_{11}$)-4,5-Cp*$_2$-*closo*-4,5,1,12-$Co_2C_2B_9H_{10}$] (**6**).

The structure of **6** was deduced crystallographically to be the 13-vertex/12-vertex species [12-(1′-*closo*-1′,2′-$C_2B_{10}H_{11}$)-4,5-Cp*$_2$-*closo*-4,5,1,12-$Co_2C_2B_9H_{10}$] (Figure 2.15). The cage C atom positions were determined independently by the VCD and BHD methods (Figure 2.16). Both metal vertices occupy the degree-6 sites (4 and 5) of the docosahedron, typical of bimetallic 13-vertex metallacarboranes. The cage C atoms are located in vertices 1 and 12 giving the complex a plane of symmetry bisecting these two vertices. Thus the two metal fragments are equivalent leading to only one Cp* resonance observed in the ^{1}H NMR spectrum.

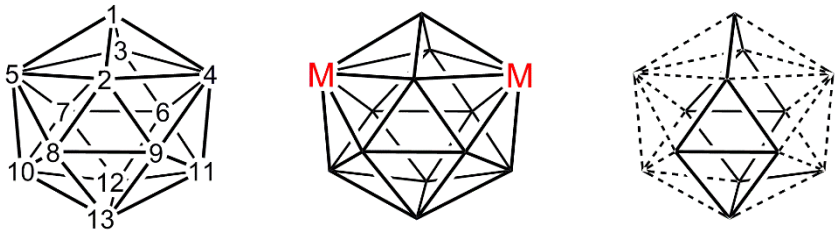

Figure 2.16 The numbering scheme of a docosahedron (left) and the nine vertices used to determine the position of the centroid in $M_2C_2B_9$ species (right).

Bimetallic docosahedral metallacarboranes are known but all structurally determined species possess cage C atoms in positions 1 and 6 or 2 and 3. In all cases, both metal vertices occupy the degree-6 vertices 4 and 5.[6-9] Thus, **6** is the first structurally confirmed example of a 4,5,1,12-$M_2C_2B_9$ architecture although this has been a suggested structure of one reported isomer of $Cp_2Co_2C_2B_9H_{11}$.[10] Compound **6** is postulated to be formed from DEI of a $\{CoCp^*\}^+$ fragment into the 1e-reduced species [**5**]$^-$ prior to the latter's aerial oxidation (Figure 2.17).

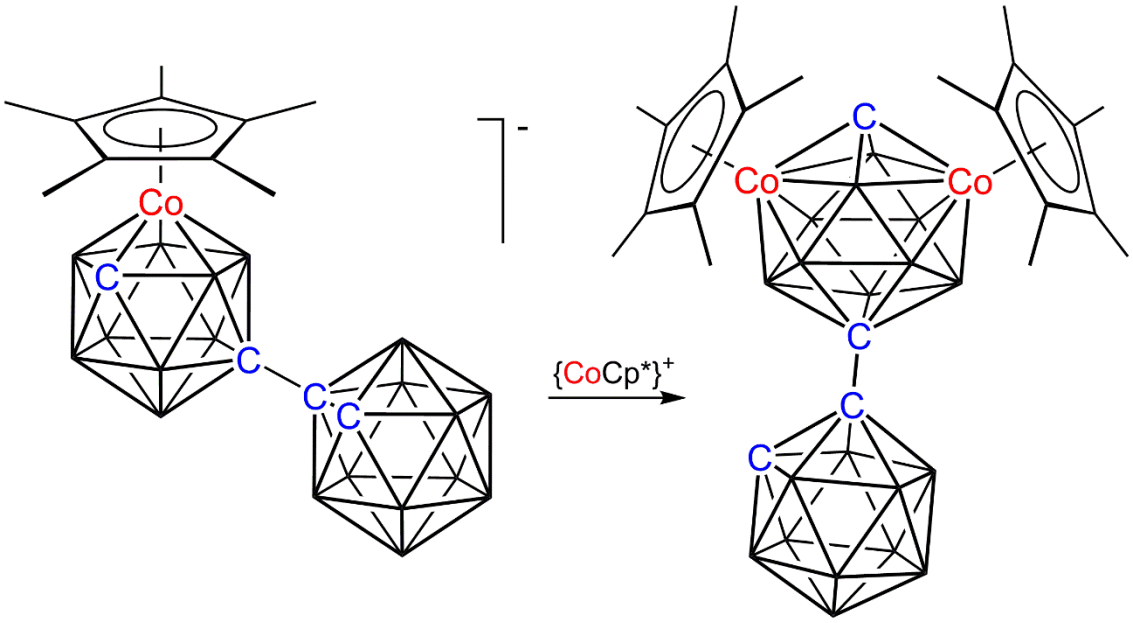

Figure 2.17 Proposed DEI mechanism for the formation of **6**.

2.6 Isomerisation of 4 to 5

Compound **4** was reduced by 1e supplied by sodium naphthalenide and subsequently aerially oxidised after 1 h. Preparative TLC of the mixture affords the starting material **4** (40%) and the isomerised product **5** (45%), confirmed spectroscopically. Under the same conditions, the Cp analogue is quantitatively converted to the isomerised product. The partial conversion is consistent with both Cp* products observed from *in situ* synthesis whereas the Cp analogue affords only the isomerised product.[1]

Isomerisation can also be induced thermally in toluene at reflux temperature (110 °C) overnight, monitored by $^{11}B\{^{1}H\}$ NMR spectroscopy. Interestingly, the Cp analogue does not isomerise under the same conditions. This observation is attributed to extended steric crowding, evident from the exopolyhedral ligand distortion in the solid state, sufficiently reducing the energy required for thermal isomerisation.

2.7 Synthesis of [HNMe$_3$][8-(7′-*nido*-7′,8′-$C_2B_9H_{11}$)-2-Cp*-*closo*-2,1,8-$CoC_2B_9H_{10}$] (7)

Analogous to the preparation of **1** and **3**, compound **5** was deboronated using KF overnight in a THF/H_2O mixture (10:1) at reflux temperatures. Compound **7** was afforded upon metathesis with NMe_3.HCl in H_2O as a yellow powder which was analysed by microanalysis and NMR spectroscopy. Unfortunately, no suitable crystals could be grown for a diffraction study. The product exists as an equimolar mixture of diastereoisomers.

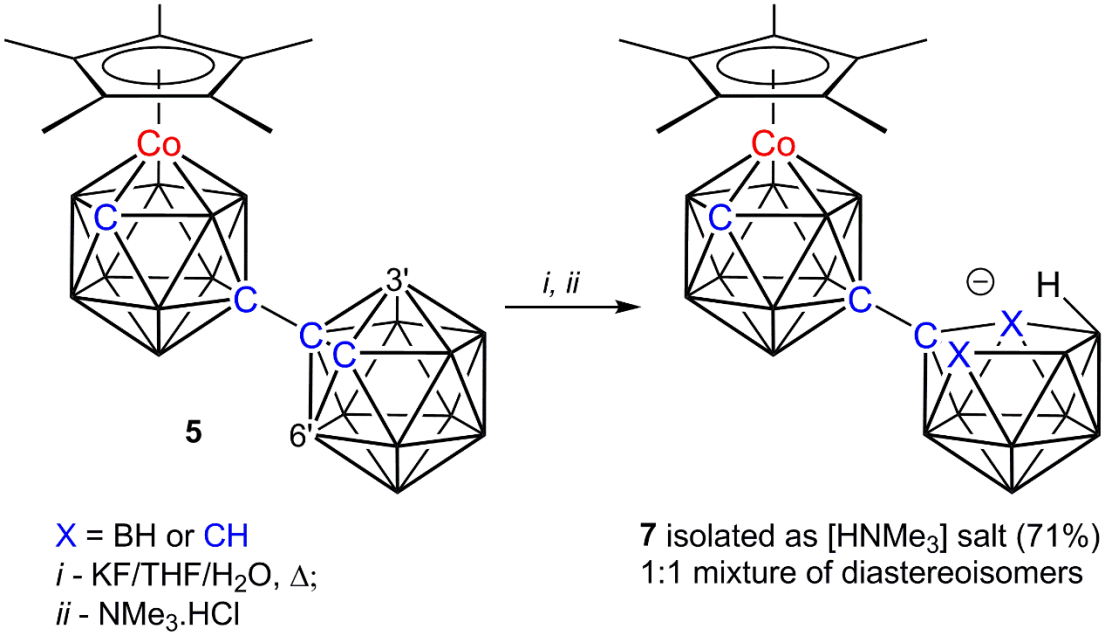

Figure 2.18 Deboronation of **5** using KF to afford **7**.

Microanalysis of **7** is in good agreement with the anticipated formula $C_{17}H_{46}B_{18}CoN$. The ^{1}H NMR spectrum displays a sharp singlet for the methyl groups of the trimethylammonium cation at δ 3.18 ppm and two broad $C_{cage}H$ resonances at δ 1.96 and 1.88 ppm. The latter corresponds to a *nido*-$C_2B_9H_{12}$ cage and is identical to the chemical shift observed in **3**. Thus, the remaining $C_{cage}H$ shift is assigned to the isomerised CoC_2B_9 metallacarborane where the signal has shifted upfield relative to its Cp analogue **3** (δ 2.84 ppm).

Relative integrals of the two singlets observed for the Cp* ligand (δ 1.85 and 1.84 ppm) reveal an equimolar mixture. Overlapping broad singlets for the bridging/endo-*H* of the deboronated cage are also observed supporting a mixture of diastereoisomers.

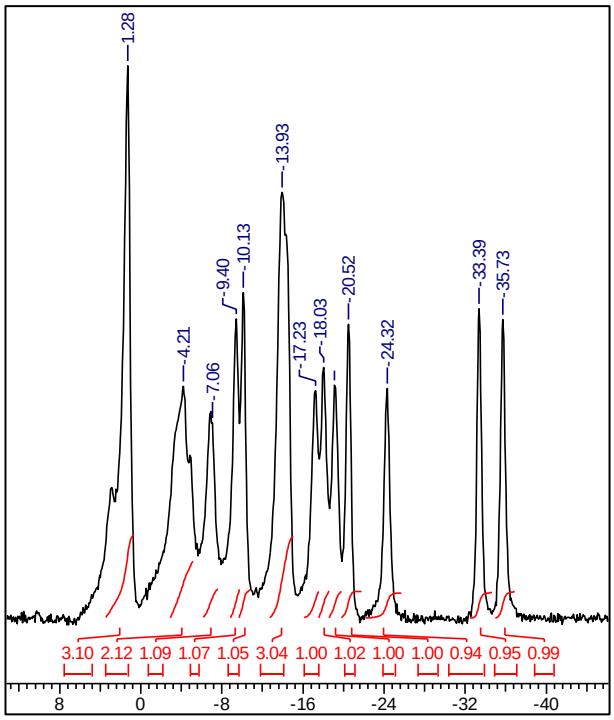

Figure 2.19 The $^{11}B\{^{1}H\}$ NMR spectra of **7**. Units in ppm.

The $^{11}B\{^{1}H\}$ NMR spectrum (Figure 2.19) displays a 3:2:1:1:1:3:1:1:1:1:1:1:1 ratio of peaks where all equivalent signals are coincidental given the asymmetry of the anion. The nido resonances (B10′ and B1′) are observed at δ -33.4 and -35.7 ppm respectively.

2.8 Synthesis of [8-(1′-3′-(*p*-cymene)-*closo*-3′,1′,2′-$RuC_2B_9H_{10}$)-2-Cp*-*closo*-2,1,8-$CoC_2B_9H_{10}$] (8)

Deprotonation of **7** by ^{n}BuLi and subsequent reaction with [Ru(*p*-cymene)Cl_2]$_2$ affords a yellow band isolated from column chromatography (Figure 2.20). Spot TLC of the product **8** revealed two overlapped bands that could not be separated despite exhaustive attempts. The product was analysed by microanalysis, EIMS and NMR spectroscopy. Suitable single crystals could not be grown from the product mixture preventing crystallographic study.

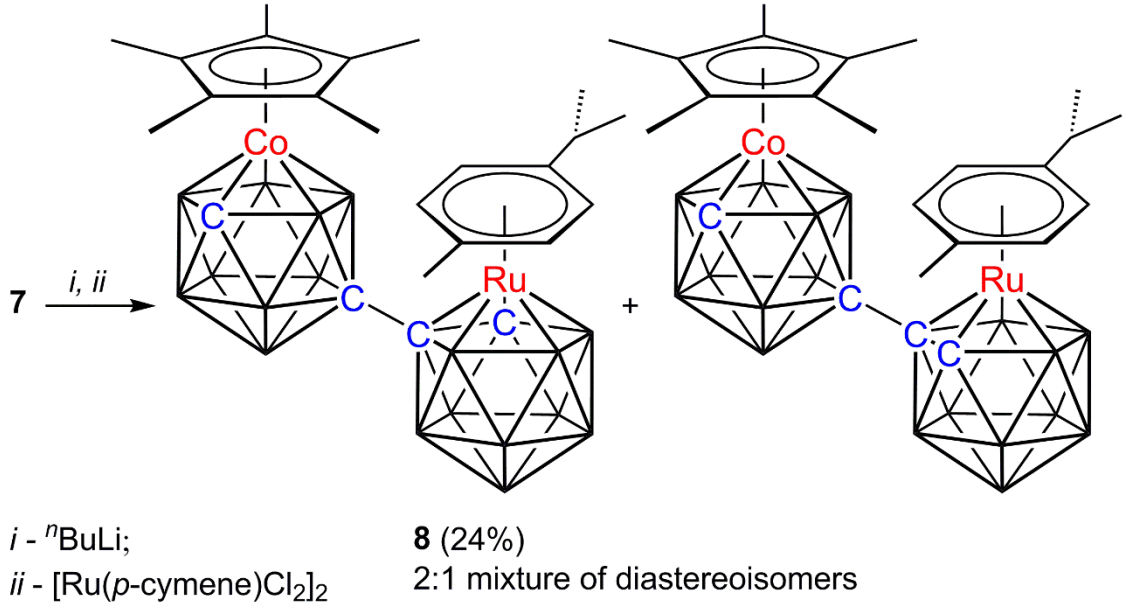

Figure 2.20 Metalation of **7** with {Ru(*p*-cymene)} to afford the product mixture **8**.

Elemental analysis and mass spectrometry of **8** are both in good agreement with the formulated product $C_{24}H_{49}B_{18}CoRu$. Although the $^{11}B\{^{1}H\}$ NMR spectrum is largely uninformative, the ^{1}H NMR spectrum reveals two $C_{cage}H$ shifts as well as the typical resonances observed for the *p*-cymene and Cp* ligands indicating both metal fragments are present. Of these, the methyl group of the *p*-cymene, the Cp* and the high frequency $C_{cage}H$ are displayed as two signals, confirming a mixture of products (Figure 2.21).

Relative integrals of these resonances suggest a *ca.* 2:1 ratio of products. It is surprising to note the ~2:1 ratio of diastereoisomers of **8** whilst the precursor **7** is an equimolar mixture. The low frequency shared $C_{cage}H$ resonance (δ 1.79 ppm) is attributed to the isomerised 2,1,8-CoC_2B_9 cobaltacarborane cage from the precursor **7**. The high frequency $C_{cage}H$ shifts (δ 3.88 and 3.75 ppm) are therefore ascribed to the new ruthenacarborane. Comparison with the $C_{cage}H$ shifts of 3,1,2-MC_2B_9-1′,2′-C_2B_{10} (δ 4.03 or 3.91 ppm) and 2,1,8-MC_2B_9-1′,2′-C_2B_{10} (δ 2.63 ppm) where M = {Ru(*p*-cymene)} suggests the new ruthenacarborane exhibits the non-isomerised 3′,1′,2′-RuC_2B_9 geometry. Thus, **8** is formulated as a diastereomeric mixture of [8-(1′-3′-(*p*-cymene)-*closo*-3′,1′,2′-$RuC_2B_9H_{10}$)-2-Cp*-*closo*-2,1,8-$CoC_2B_9H_{10}$].

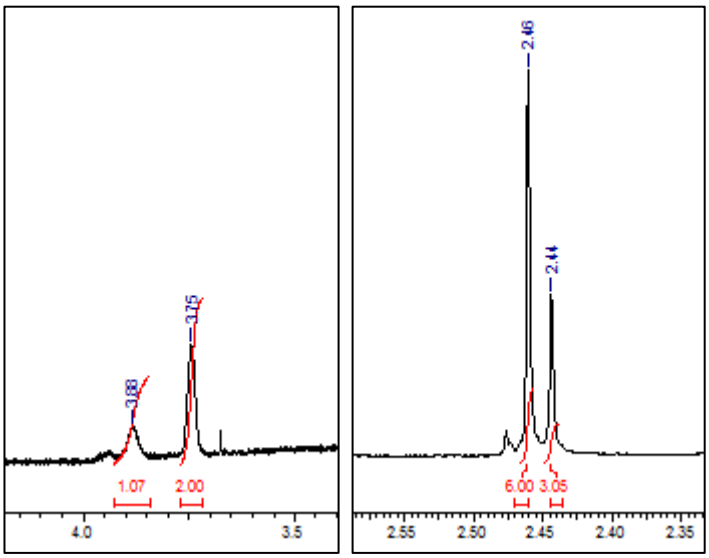

Figure 2.21 Selected ^{1}H NMR resonances of **8**; $C_{cage}H$ resonances of the two diastereoisomers of the 3′,1′,2′-$RuC_2B_9H_{10}$ cage (left) and pair of singlets assigned to the methyl substituent of the *p*-cymene ligand (right). Units in ppm.

2.9 Isomerisation of 8 to [8-(8′-2′-(*p*-cymene)-*closo*-2′,1′,8′-$RuC_2B_9H_{10}$)-2-Cp*-*closo*-2,1,8-$CoC_2B_9H_{10}$] (9)

Compound **8** was heated to reflux in dimethoxyethane (DME) overnight and purification of the resultant yellow solution afforded one yellow band **9**, isolated by preparative TLC (Figure 2.22). Due to the diastereomeric precursor **8**, two products are expected but exhaustive chromatography did not yield any separation. Thus, compound **9** is tentatively assigned as a diastereomeric mixture similar to **8**.

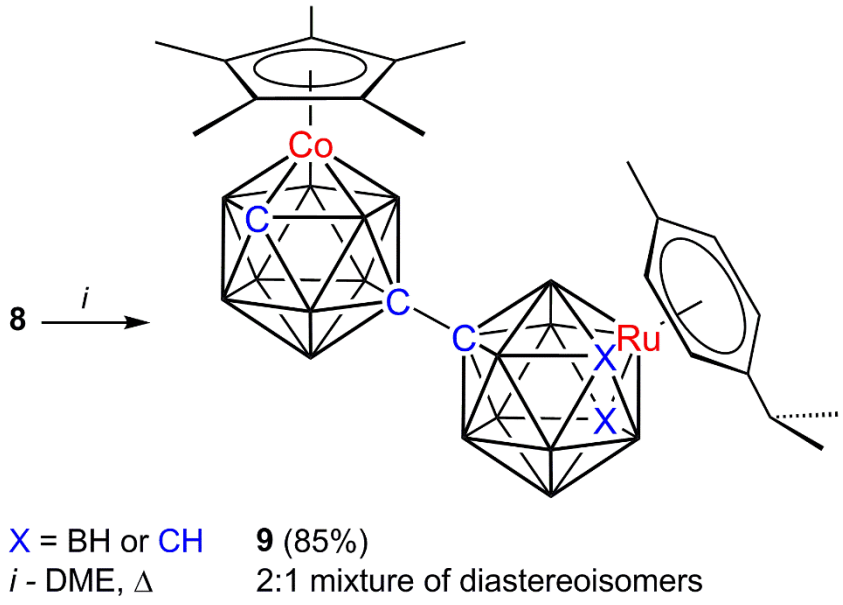

Figure 2.22 Thermal isomerisation of **8** to afford **9**.

Elemental analysis and mass spectrometry confirmed that **9** bears the same chemical composition as **8**. Again like **8**, the $^{11}B\{^1H\}$ spectrum is complex due to multiple products and overlapping resonances but the ^1H NMR spectrum reveals upfield shifts of the ruthenacarborane $C_{cage}H$ atoms from δ 3.88 and 3.75 ppm to δ 2.62 and 2.59 ppm. This suggests a 2′,1′,8′-RuC_2B_9 architecture to give the formula [8-(8′-2′-(*p*-cymene)-*closo*-2′,1′,8′-$RuC_2B_9H_{10}$)-2-Cp*-*closo*-2,1,8-$CoC_2B_9H_{10}$] for compound **9**. Relative integrals of these $C_{cage}H$ resonances and the Cp* signals (δ 1.84 and 1.83 ppm) give the same ~2:1 ratio of diastereoisomers as **8** (Figure 2.23).

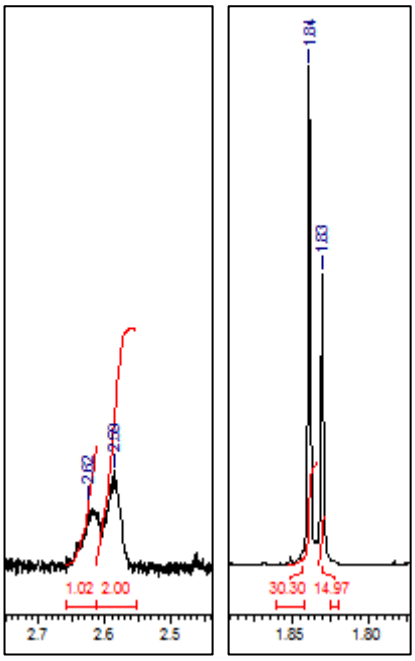

Figure 2.23 Selected ^{1}H NMR resonances of **9**; $C_{cage}H$ resonances of the two diastereoisomers of the 2′,1′,8′-$RuC_2B_9H_{10}$ cage (left) and pair of singlets assigned to the Cp* (right). Units in ppm.

Diffraction-quality crystals of **9** were successfully grown from DCM/petrol and the *X*RD study reveals both diastereoisomers crystallise together to give a partially disordered structure (Figure 2.24). This was suggested by VCD and BHD analyses and confirmed following refinement. In both cages, the cage C atom not involved in the bis(carborane) linkage is disordered over vertices 1 and 11 (or 1′ and 11′). The occupancy ratio in the cobaltacarborane cage is 0.52(2):0.48(2) and in the ruthenacarborane cage is 0.31(2):0.69(2). The former ratio suggests both diastereoisomers are present in the crystal in equal amounts. Nonetheless, the structure confirms the assigned formula in which the ruthenacarborane cage has isomerised. Compound **9** is the first heterometalated bis(carborane) exhibiting a 2,1,8-MC_2B_9-2′,1′,8′-M′C_2B_9 structure and, as expected of 2,1,8-MC_2B_9 architectures, both ligands are effectively parallel with respect to their reference planes.

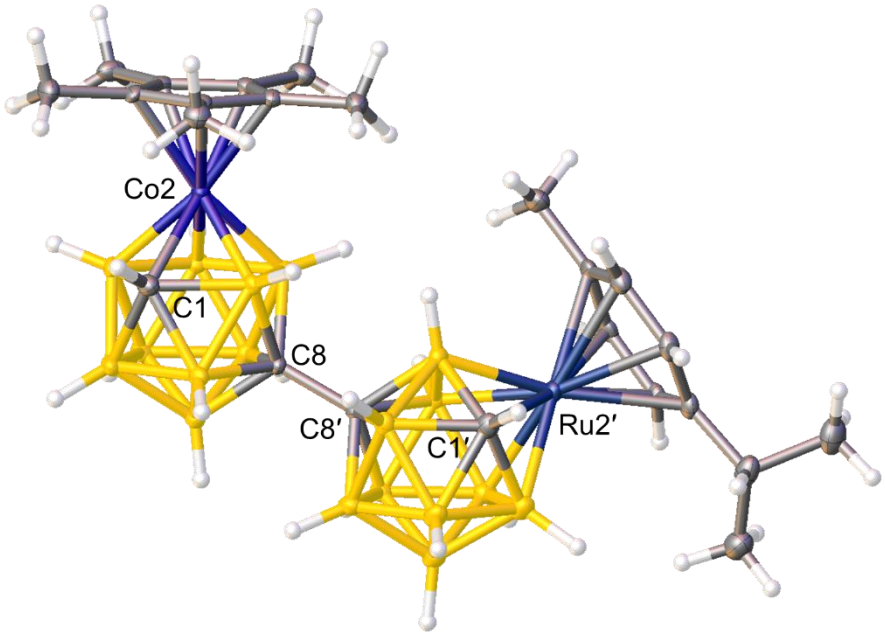

Figure 2.24 Perspective view of one arbitrary diastereoisomer of [8-(8′-2′-(*p*-cymene)-*closo*-2′,1′,8′-$RuC_2B_9H_{10}$)-2-Cp*-*closo*-2,1,8-$CoC_2B_9H_{10}$] (**9**).

2.10 Discussion

The first metallacarborane was reported by Hawthorne in 1965 following his perceptive recognition that the [*nido*-$C_2B_9H_{11}$]$^{2-}$ unit was analogous to a [Cp]$^-$ ligand.[11] This breakthrough led to the rapid expansion of metallacarborane chemistry where it is now the second most studied subarea of carborane chemistry. In fact, essentially all transition metal elements have been successfully incorporated into a carborane framework. The range and versatility of metallacarboranes has led to their applications in catalysis,[12] medicine[13] and polymeric materials.[14]

Although substantial research has been reported on single-cage metallacarborane systems, minimal work has been published on the related bis(carboranes), an obvious avenue for further development. The single deboronation[3] and metalation[15] of bis(*o*-carborane) was first reported by Hawthorne and the product was identified spectroscopically. This was recently developed further by Welch, expanding the scope of metal fragments inserted and establishing a standard synthetic protocol.[1,16]

Similarly, the double deboronation and metalation of bis(*o*-carborane) was studied initially by Hawthorne[3] and subsequently extended by Welch.[2] All reported doubly-metalated products were necessarily homometalated due to the one-step nature of the metalation. The drive for synthesising heterometalated bis(carborane) compounds, aside from their intrinsic academic interest, is that it affords a novel means of derivatisation, showcasing the flexibility of the bis(carborane) framework. This is especially relevant with respect to catalytic applications where cooperative or even tandem systems could potentially be achieved with a heterobimetallic complex.

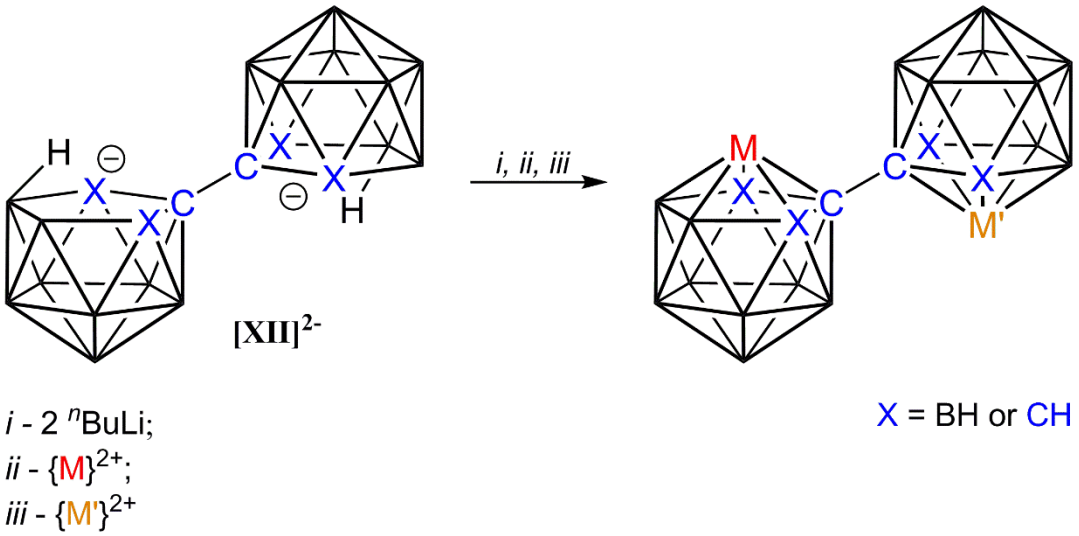

Figure 2.25 Proposed one-pot stepwise synthesis of heterometalated bis(carboranes).

Unpublished initial attempts at synthesising heterometalated species in our laboratory involved reacting the anionic [**XII**]$^{2-}$ with two different metal fragments in a stepwise manner (Figure 2.25). However, the only products isolated from these reactions were the previously reported homometalated compounds. We attribute this to the relative insolubility of the precursor [**XII**]$^{2-}$. Following the metalation of one cage, the MC_2B_9-C_2B_9 intermediate will be more soluble than the starting material [**XII**]$^{2-}$, leading to a rapid second metalation to yield the homometalated products.

Subsequently, simultaneous mixed metalation was attempted where one equivalent of each metal fragment was reacted with [**XII**]$^{2-}$ at the same time. Theoretically, a statistical distribution of products would be obtained, notwithstanding geometrical differences, with 50% of the targeted heterometalated species and 25% of each of the two homometalated species (Figure 2.26). Disappointingly, this was not achieved and instead only the homometalated products were isolated. We postulate that the difference in reactivity between the metal fragments likely dictates the order of metalation, leading only to homometalated complexes.

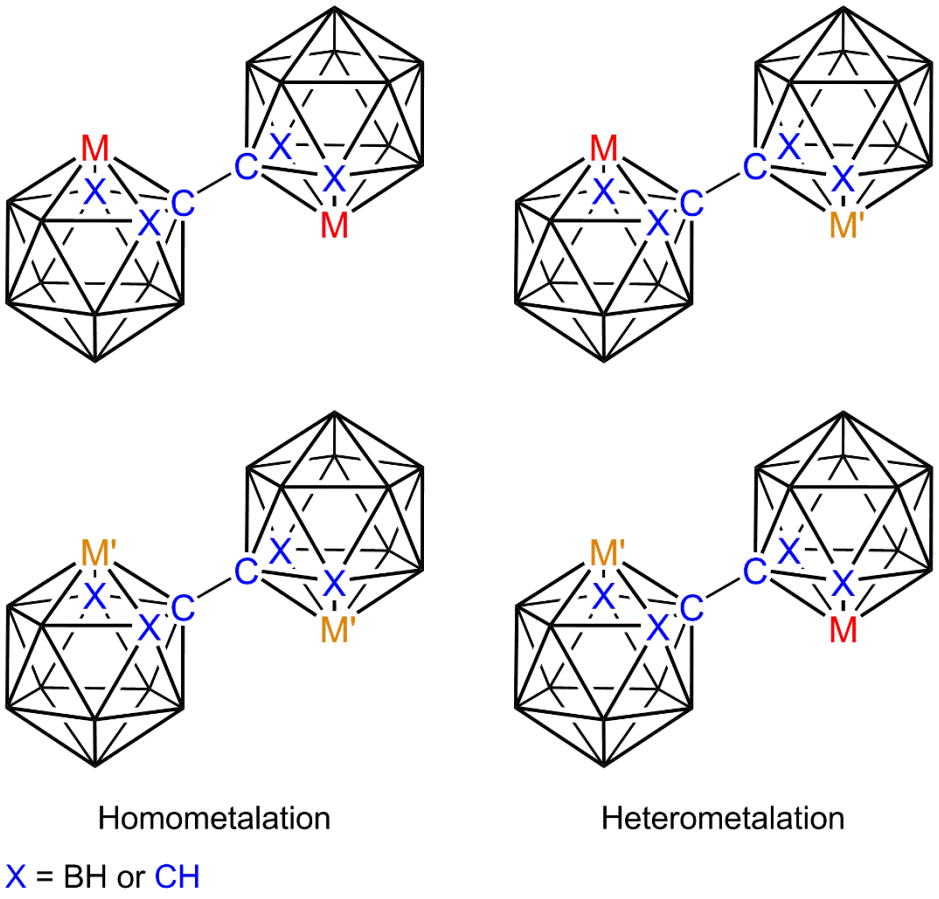

Figure 2.26 The four possible products from simultaneous metalation with two different metal fragments where the two heterometalated products are identical (rotamers).

Ultimately, two consecutive deboronation and metalation steps were required to synthesise the target bimetallic species. Crucial to this procedure was the second deboronation process. Typically, a range of nucleophiles can be used to initiate the deboronation such as amines,[17] 'wet' fluoride[18] and even acetonitrile.[4] The most frequently employed method is the use of potassium hydroxide in alcoholic medium.[3]

Both KOH/EtOH and acetonitrile were found to be capable to generating MC_2B_9-C_2B_9 salts. However, the former was found to be too harsh, leading to minor decomposition, and the poor solubility of the metallacarborane/carborane starting materials in ethanol inhibited scale-up of the reaction. Conversely, acetonitrile was too mild a deboronating agent, requiring excessive reaction times for even poor to moderate yields.

Therefore, the intermediate deboronation reagent 'wet' fluoride was selected. By utilising potassium fluoride instead of the typical TBAF as the fluoride source,[18] the initially formed potassium salt could be easily metathesised to the more synthetically useful $[HNMe_3]^+$ salt.

The new deboronation protocol for metallacarborane/carborane compounds afforded three novel *nido*-carborane salts of the form [8-(7′-*nido*-7′,8′-$C_2B_9H_{11}$)-*closo*-2,1,8-$MC_2B_9H_{10}]^-$ [where M = Ru(*p*-cymene); **1**, CoCp; **3** and CoCp*; **7**] in good yields. These species were isolated as an equimolar mixture of diastereoisomers. All three salts are potential precursors to heterometalated products but, due to the fragility of the Cp ligand to ^{n}BuLi, only **1** and **7** were used for subsequent metalations.

Prior to the preparation of **7**, the synthesis of the Cp* derivatives of the metallacarborane/carborane starting material had to be undertaken. Two isomers of Cp*$CoC_2B_9H_{10}$-$C_2B_{10}H_{11}$ (**4** and **5**) was successfully isolated and fully characterised as well as the unexpected bimetallic docosahedral species [12-(1′-*closo*-1′,2′-$C_2B_{10}H_{11}$)-4,5-Cp*$_2$-*closo*-4,5,1,12-$Co_2C_2B_9H_{10}$] (**6**). Both compounds **4** and **5** are comparable to their Cp analogues with the exception of the 3,1,2-isomer (**4**) displaying extended bendback angles of the Cp* ligand due to its increased size relative to Cp. Additionally, the cobaltacarborane $C_{cage}H$ resonances in the ^{1}H NMR spectra of both species shift upfield relative to their Cp analogues from the larger inductive effect of the Cp* ligand. Compound **6** is the first example of a 4,5,1,12-$M_2C_2B_9$ isomer confirmed crystallographically and is postulated to form from DEI of a $\{CoCp^*\}^+$ fragment into the 1-e reduced $[\mathbf{5}]^-$ generated prior to aerial oxidation of the reaction mixture.

Metalation of **1** with the {CoCp} fragment afforded the heterometalated [8-(1′-3′-Cp-*closo*-3′,1′,2′-$CoC_2B_9H_{10}$)-2-(*p*-cymene)-*closo*-2,1,8-$RuC_2B_9H_{10}$] (**2**) which was successfully separated into its two diastereomeric components (**2*α*** and **2*β***), confirmed crystallographically. Metalation of **7** with the {Ru(*p*-cymene)} fragment afforded the heterometalated product **8** which could not be separated into its distinct diastereoisomers. Thermolysis of mixture **8** afforded the isomerised product **9** which was successfully

studied by *X*-ray diffraction and found to contain both diastereoisomers. Compounds **2*α***, **2*β***, **8** and **9** represent the first examples of heterometalated bis(carboranes) and have been shown to exhibit both 2,1,8-3′,1′,2′ and 2,1,8-2′,1′,8′ geometries.

The ability to synthesise mixed metal cobalt/ruthenium complexes independent of the order the metal fragment are inserted demonstrates the generality of this protocol. Providing that the initial fragment can tolerate the deprotonation step prior to metalation, this methodology serves as a potential route to synthesising an array of heterometalated derivatives which can utilise the tunability of the bis(carborane) framework.

2.11 References

1. G. Thiripuranathar, W. Y. Man, C. Palmero, A. P. Y. Chan, B. T. Leube, D. Ellis, D. McKay, S. A. Macgregor, L. Jourdan, G. M. Rosair and A. J. Welch, *Dalton Trans.*, 2015, **44**, 5628-5637.

2. G. Thiripuranathar, A. P. Y. Chan, D. Mandal, W. Y. Man, M. Argentari, G. M. Rosair and A. J. Welch, *Dalton Trans.*, 2017, **46**, 1811-1821.

3. M. F. Hawthorne, D. A. Owen and J. W. Wiggins, *Inorg. Chem.*, 1971, **10**, 1304-1306.

4. G. S. Kazakov, I. B. Sivaev, K. Y. Suponitsky, A. D. Kirilin, V. I. Bregadze and A. J. Welch, *J. Organomet. Chem.*, 2016, **805**, 1-5.

5. M. A. Fox, W. R. Gill, P. L. Herbertson, J. A. H. MacBride, K. Wade and H. M. Colquhoun, *Polyhedron*, 1996, **15**, 565-571.

6. A. R. Kudinov, D. S. Perekalin, S. S. Rynin, K. A. Lyssenko, G. V. Grintselev-Knyazev and P. V. Petrovskii, *Angew. Chem., Int. Ed.*, 2002, **41**, 4112-4114.

7. B. Grüner, B. Štíbr, R. Kivekäs, R. Sillanpää, P. Stopka, F. Teixidor and C. Viñas, *Chem. – Eur. J.*, 2003, **9**, 6115-6121.

8. A. R. Kudinov, M. I. Rybinskaya, D. S. Perekalin, V. I. Meshcheryakov, Y. A. Zhuravlev, P. V. Petrovskii, A. A. Korlyukov, D. G. Golovanov and K. A. Lyssenko, *Russ. Chem. Bull.*, 2004, **53**, 1958-1962.

9. M. E. Lopez, M. J. Edie, D. Ellis, A. Horneber, S. A. Macgregor, G. M. Rosair and A. J. Welch, *Chem. Commun.*, 2007, 2243-2245.

10. D. F. Dustin and M. F. Hawthorne, *J. Am. Chem. Soc.*, 1974, **96**, 3462-3467.

11. M. F. Hawthorne, D. C. Young and P. A. Wegner, *J. Am. Chem. Soc.*, 1965, **87**, 1818-1819.

12. Z. Yinghuai and N. S. Hosmane, *J. Organomet. Chem.*, 2013, **747**, 25-29.

13. M. Scholz and E. Hey-Hawkins, *Chem. Rev.*, 2011, **111**, 7035-7062.

14. R. Núñez, I. Romero, F. Teixidor and C. Viñas, *Chem. Soc. Rev.*, 2016, **45**, 5147-5173.

15. J. A. Doi, E. A. Mizusawa, C. B. Knobler and M. F. Hawthorne, *Inorg. Chem.*, 1984, **23**, 1482-1484.

16. D. Mandal, W. Y. Man, G. M. Rosair and A. J. Welch, *Dalton Trans.*, 2016, **45**, 15013-15025.

17. L. I. Zakharkin and V. N. Kalinin, *Tetrahedron Lett.*, 1965, **6**, 407-409.

18. M. A. Fox, W. R. Gill, P. L. Herbertson, J. A. H. MacBride. K. Wade and H. M. Colquhoun, *Polyhedron*, 1996, **15**, 565-571.

Chapter 3

Rhodium Derivatives of Bis(carborane)

3.1 Introduction

The insertion of the {Rh(PPh$_3$)$_2$H} fragment into deboronated *o*-carborane is achieved by direct reaction of [Rh(PPh$_3$)$_3$Cl] with the monoanionic form of the carborane [*nido*-7,8-C$_2$B$_9$H$_{12}$]$^-$ typically as the [HNMe$_3$]$^+$ salt (Figure 3.1).[1] In contrast with archetypal metalations, removal of the bridging/endo-H is not required but instead is utilised to generate the hydride ligand in the product [3-H-3,3-(PPh$_3$)$_2$-*closo*-3,1,2-RhC$_2$B$_9$H$_{11}$] (**VIII**).

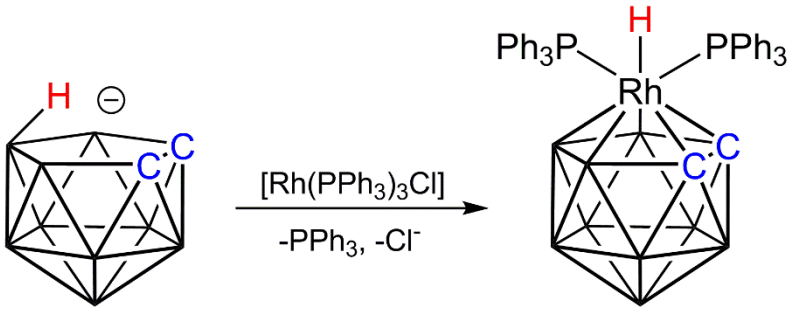

VIII

Figure 3.1 Insertion of the {Rh(PPh$_3$)$_2$H} fragment where migration of the bridging/endo-H is required to afford the hydride ligand.

However, the same methodology for inserting the {Rh(PPh$_3$)$_2$H} fragment into singly-deboronated bis(*o*-carborane) [**XI**]$^-$ affords simply the cation-exchanged product [Rh(PPh$_3$)$_3$][7-(1′-*closo*-1′,2′-C$_2$B$_{10}$H$_{11}$)-*nido*-7,8-C$_2$B$_9$H$_{11}$].[2,3] Presumably the additional steric crowding from the carboranyl substituent on the open face of the nido carborane prevents the capitation.

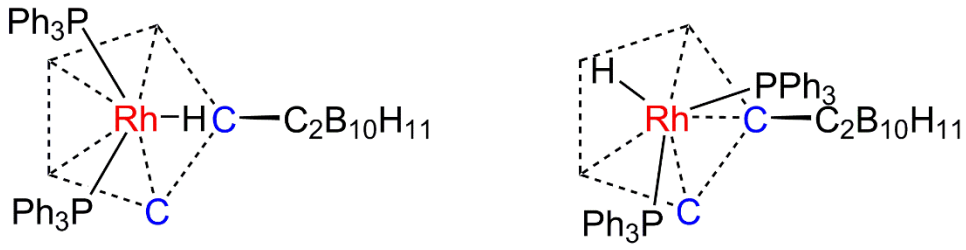

Figure 3.2 Top-down view of the rhodacarborane of the hypothetical product [1-(1′-*closo*-1′,2′-$C_2B_{10}H_{11}$)-3-H-3,3-$(PPh_3)_2$-*closo*-3,1,2-$RhC_2B_9H_{10}$] and the possible orientations of the exopolyhedral ligands; minimal steric interactions (left) and preferred orientation (right).

Although it could be envisioned that the hydride ligand would occupy a position adjacent to the carborane substituent to minimise the steric congestion (Figure 3.2, left), the preferred ELO of the hydride within the {$Rh(PPh_3)_2H$} fragment is trans to the C-C connectivity of the C_2B_3 face (Figure 3.2, right).[4] As such, the bulky PPh_3 ligands are forced towards the carboranyl group which presumably prevents the formation of the target rhodacarborane/carborane product.

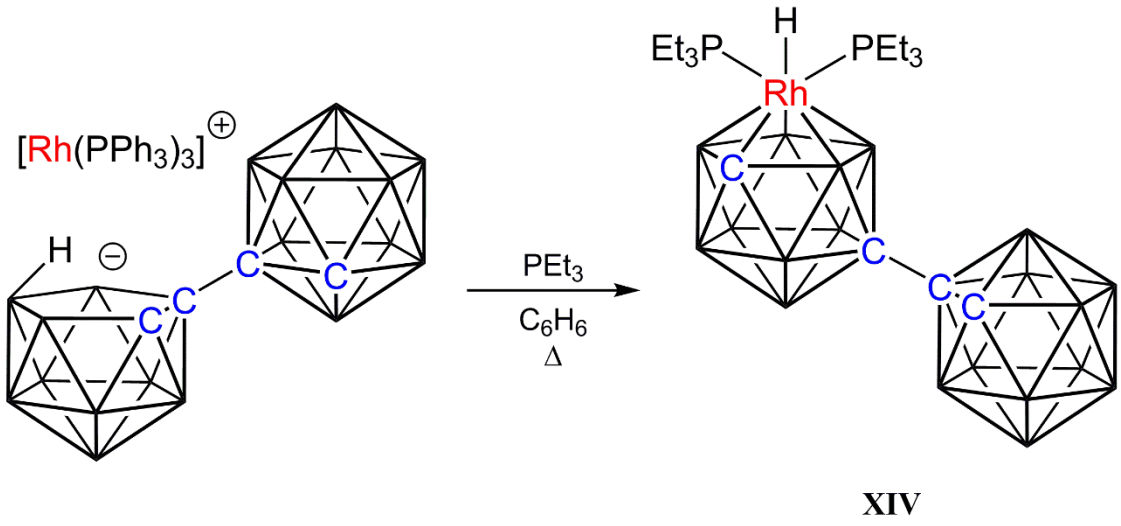

XIV

Figure 3.3 Metalation of $[Rh(PPh_3)_3]$[**XI**] following the addition of triethylphosphine at elevated temperatures.

Addition of PEt_3 to the $[Rh(PPh_3)_3]$[**XI**] salt in benzene at reflux temperature affords the closo species [8-(1′-*closo*-1′,2′-$C_2B_{10}H_{11}$)-2-H-2,2-$(PEt_3)_2$-*closo*-2,1,8-$RhC_2B_9H_{10}$] (**XIV**), confirmed by NMR spectroscopy (Figure 3.3).[2] The isomerisation of the rhodacarborane cage effectively removes all steric crowding.

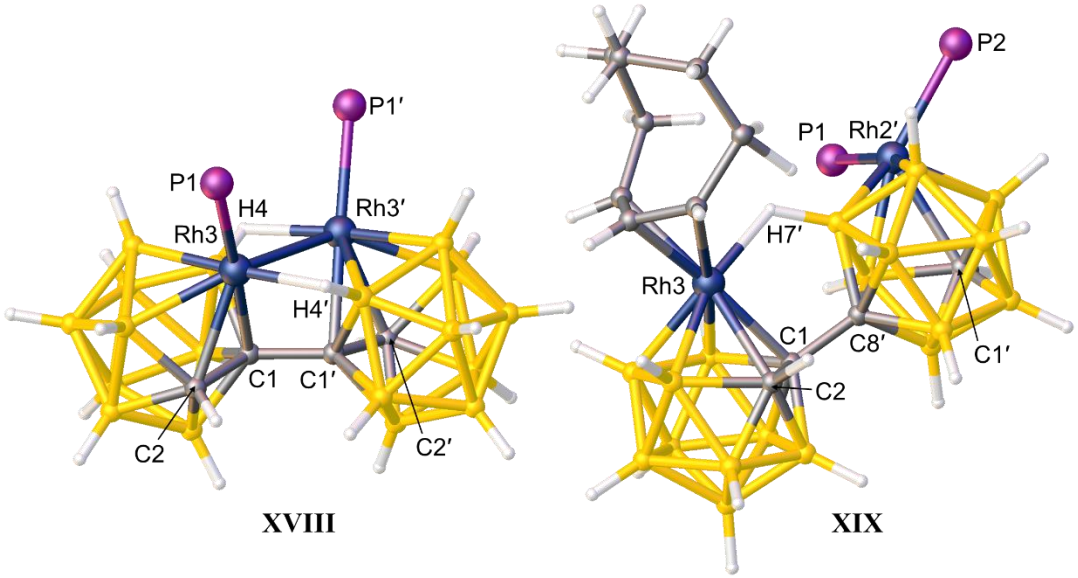

Figure 3.4 Perspective view of **XVIII** and **XIX**. Ethyl groups of the phosphines are omitted for clarity.

Two further examples of rhodium derivatives of bis(carborane) are known (Figure 3.4); [1-(1′-3′-PEt_3-*closo*-3′,1′,2′-$RhC_2B_9H_{10}$)-3-PEt_3-*closo*-3,1,2-$RhC_2B_9H_{10}$] (**XVIII**) and [1-(8′-2′-H-2′,2′-$(PEt_3)_2$-*closo*-2′,1′,8′-$RhC_2B_9H_{10}$)-3-η^3-CODH-*closo*-3,1,2-$RhC_2B_9H_{10}$] (**XIX**), previously discussed in Chapter 1.5.1. Both species are formed from the reaction between doubly-deboronated bis(*o*-carborane) [**XII**]$^{2-}$ and [Rh(COD)(PEt_3)Cl] and feature B–H–Rh *B*-agostic interactions.[5,6]

These four species are currently the only known rhodium derivatives of bis(carborane). This chapter explores further metalation chemistry with the {$Rh(PPh_3)_2H$} fragment with bis(*o*-carborane) to expand the scope of these products and produce new species with the potential to act as homogeneous catalyst precursors.

3.2 Synthesis of [8-(1′-*closo*-1′,2′-$C_2B_{10}H_{11}$)-2-H-2,2-$(PPh_3)_2$-*closo*-2,1,8-$RhC_2B_9H_{10}$] (10)

Salt [$HNMe_3$][**XI**] was deprotonated with ^{n}BuLi following which addition of [$Rh(PPh_3)_3Cl$] produces a dark brown solution. Purification of the mixture by column chromatography yields a single yellow fraction, subsequently identified as [8-(1′-*closo*-1′,2′-$C_2B_{10}H_{11}$)-2-H-2,2-$(PPh_3)_2$-*closo*-2,1,8-$RhC_2B_9H_{10}$] (**10**). The product was characterised by elemental analysis, NMR spectroscopy and *X*RD studies. Note that the rhodacarborane cage has been designated as the unprimed cage in this and all subsequent rhodium derivatives of bis(carborane) to simplify future discussion.

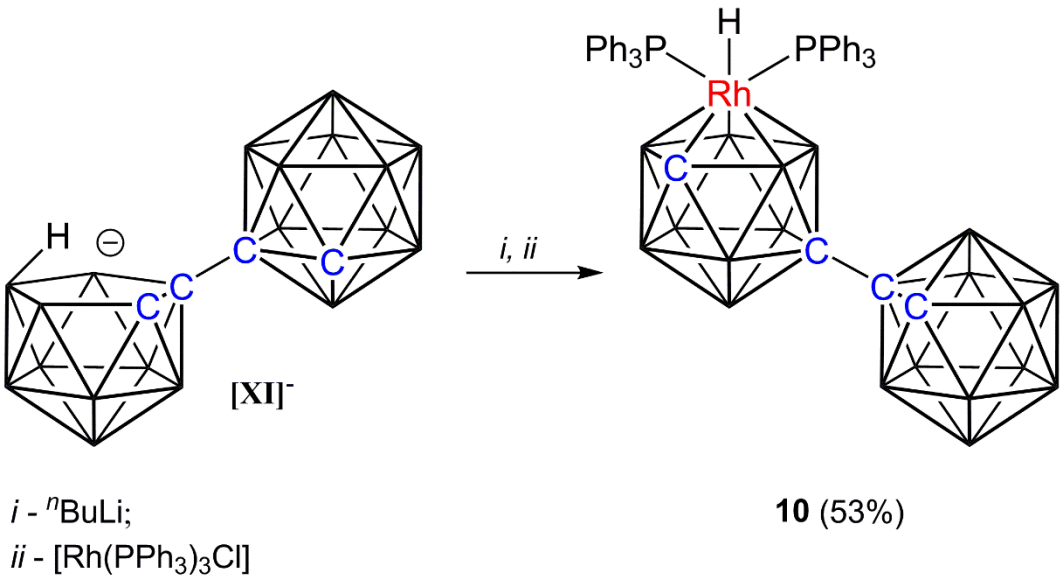

Figure 3.5 Metalation of [$HNMe_3$][**XI**] with [$Rh(PPh_3)_3Cl$] to form **10**.

Contrary to the typical insertion of a {$Rh(PPh_3)_2H$} fragment, a deprotonation step was carried out prior to the addition of the metal fragment source. By generating a dianionic open face, the greater coulombic attraction between the nido carborane and the cationic rhodium fragment is postulated to overcome the steric factors previously described leading only to the formation of [$Rh(PPh_3)_3$][**XI**]. In the synthesis of **10**, the origin of the hydride ligand observed in the product is attributed to protonation from solvent during the reaction or work-up.

Microanalysis of **10** is consistent with the expected formula $C_{40}H_{52}B_{19}P_2Rh$. Despite repeated attempts to analyse **10** by mass spectrometry using both EI and ESI techniques, no meaningful data could be obtained.

The ^1H NMR spectrum displays a complex multiplet centred on δ 7.40 ppm, assigned to the aromatic protons of the PPh_3 ligands. Two broad singlets corresponding to the $C_{cage}H$ protons are observed at δ 1.95 and 1.84 ppm. Due to the proximity of the two resonances, assignments cannot be made confidently. However, by comparison with other metallacarborane/carborane species, the relatively downfield signal is tentatively assigned to the $C_2B_{10}H_{11}$ cage. A final resonance is observed at δ -8.70 ppm (Figure 3.6, left) arising from the hydride ligand split by the rhodium centre and two inequivalent phosphorus atoms to give a doublet of doublet of doublets splitting pattern ($J_{Rh\text{-}H}$ = 26.9 Hz, $J_{P\text{-}H}$ = 26.9 and 15.4 Hz).

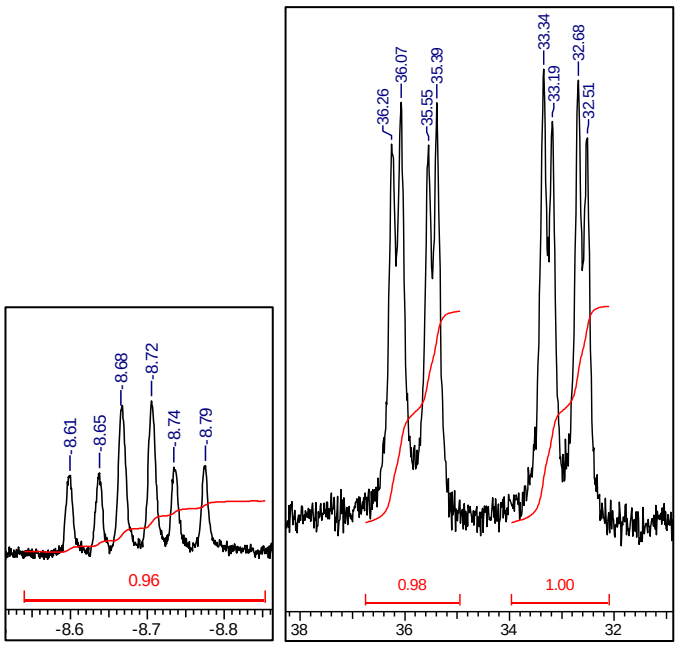

Figure 3.6 The ^1H NMR signal of the hydride ligand of **10** displayed as a doublet of doublet of doublets (left). The $^{31}P\{^1H\}$ NMR spectrum of **10** showing two sets of doublet of doublets in a 1:1 ratio (right). Units in ppm.

As anticipated, $^{11}B\{^{1}H\}$ NMR data yields little meaningful information. However, the $^{31}P\{^{1}H\}$ NMR spectrum (Figure 3.6, right) reveals two signals split into doublet of doublets ($J_{Rh\text{-}P}$ = 114.9 Hz, $J_{P\text{-}P}$ = 27.7 Hz and $J_{Rh\text{-}P}$ = 107.0 Hz, $J_{P\text{-}P}$ = 27.7 Hz) indicating two unique phosphorus environments, consistent with the nature of the hydride signal in the ^{1}H NMR spectrum.

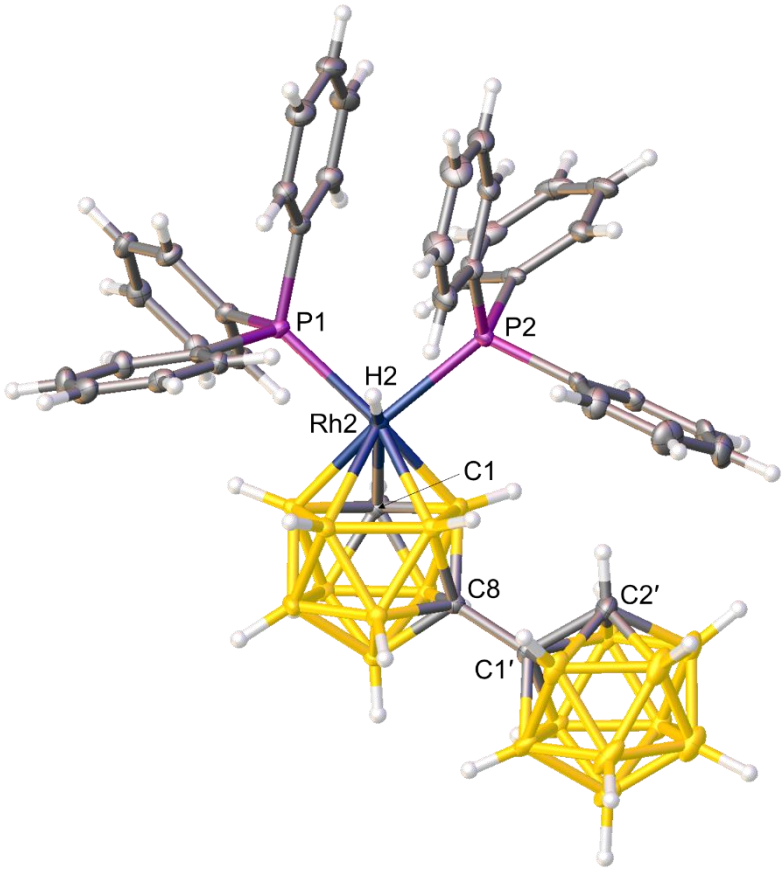

Figure 3.7 Perspective view of [8-(1′-*closo*-1′,2′-$C_2B_{10}H_{11}$)-2-H-2,2-$(PPh_3)_2$-*closo*-2,1,8-$RhC_2B_9H_{10}$] (**10**).

Yellow needle crystals of **10** were grown from a DCM/petrol diffusion and a diffraction study confirmed the species to be [8-(1′-*closo*-1′,2′-$C_2B_{10}H_{11}$)-2-H-2,2-$(PPh_3)_2$-*closo*-2,1,8-$RhC_2B_9H_{10}$] (Figure 3.7). The cage C atoms were identified using both the VCD and BHD methods independently. As expected for an isomerised species, minimal steric interactions are observed between the exopolyhedral ligands and the carboranyl substituent. The orientation of the hydride is trans to the cage C atom of the CB_4 face, as

predicted from ELO considerations. A Structural Trans Effect (STE)[7] can be observed in the elongation of the C1–Rh2 connectivity [2.306(4) Å] relative to the remaining four cage to rhodium connectivities [2.175(4)-2.215(4) Å] even though carbon has a smaller atomic radius than boron.

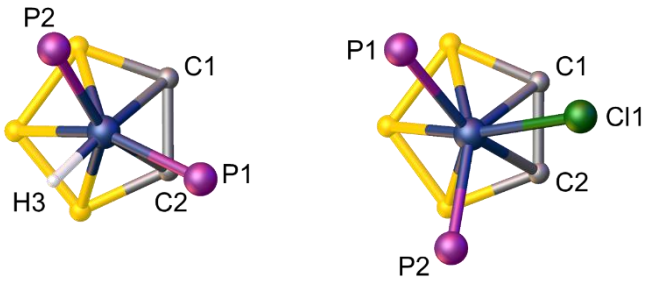

Figure 3.8 Top-down view of the molecular structures of [3-X-3,3-$(PPh_3)_2$-*closo*-3,1,2-$RhC_2B_9H_{11}$] where X = H (left) or Cl (right). Phenyl rings and lower portion of cage omitted for clarity.

Additionally, the upfield shift of the rhodacarborane $C_{cage}H$ resonance (δ 1.84 ppm) relative to analogous 2,1,8-MC_2B_9-1′,2′-C_2B_{10} species [M = {CoCp}; δ 2.73 ppm, {Ru(*p*-cymene)}; δ 2.63 ppm][8] is attributed to the ELO of the hydride ligand. As noted in the molecular structure of **10**, the hydride ligand is positioned trans to the cage C atom in the CB_4 face which leads to a relatively weak C1–Rh2 connectivity, evidenced by its length. As a result, we postulate a relatively strong C1–H bond is formed, reflected in the low-frequency resonance observed in the ^{1}H NMR spectrum.

This is particularly evident by comparison of the single-cage analogues [3-X-3,3-$(PPh_3)_2$-*closo*-3,1,2-$RhC_2B_9H_{11}$] where X = H or Cl. The orientation of the hydride ligand is effectively trans to the cage C1 atom whereas the chloride ligand lies cisoid to the C–C connectivity (Figure 3.8), resulting in a downfield $C_{cage}H$ resonance (δ 3.77 ppm)[9] relative to the hydride species (δ 2.24 ppm).[1] The same phenomenon can be observed in the isoelectronic and isostructural species [NEt_4][3-X-3,3-$(PPh_3)_2$-*closo*-3,1,2-$RuC_2B_9H_{11}$] (X = H, Cl) in which the $C_{cage}H$ can be observed at δ 1.63 and 2.90 ppm respectively.[10]

3.3 Synthesis of *α*-[8-(8′-2′-(*p*-cymene)-*closo*-2′,1′,8′-$RuC_2B_9H_{10}$)-2-H-2,2-$(PPh_3)_2$-*closo*-2,1,8-$RhC_2B_9H_{10}$] (11*α*) and *β*-[8-(8′-2′-(*p*-cymene)-*closo*-2′,1′,8′-$RuC_2B_9H_{10}$)-2-H-2,2-$(PPh_3)_2$-*closo*-2,1,8-$RhC_2B_9H_{10}$] (11*β*)

Deprotonation of **1** with ^{n}BuLi followed by reaction with $[Rh(PPh_3)_3Cl]$ in THF at reflux temperatures affords a dark brown mixture. Purification by preparative TLC affords, among an array of coloured trace bands, two colourless mobile bands identified as two diastereoisomers of [8-(8′-2′-(*p*-cymene)-*closo*-2′,1′,8′-$RuC_2B_9H_{10}$)-2-H-2,2-$(PPh_3)_2$-*closo*-2,1,8-$RhC_2B_9H_{10}$] (**11**). Both species were analysed by elemental analysis, mass spectrometry and NMR spectroscopy. Single crystals of both **11*α*** and **11*β*** were successfully grown and these were employed in *X*RD studies to elucidate their precise structures.

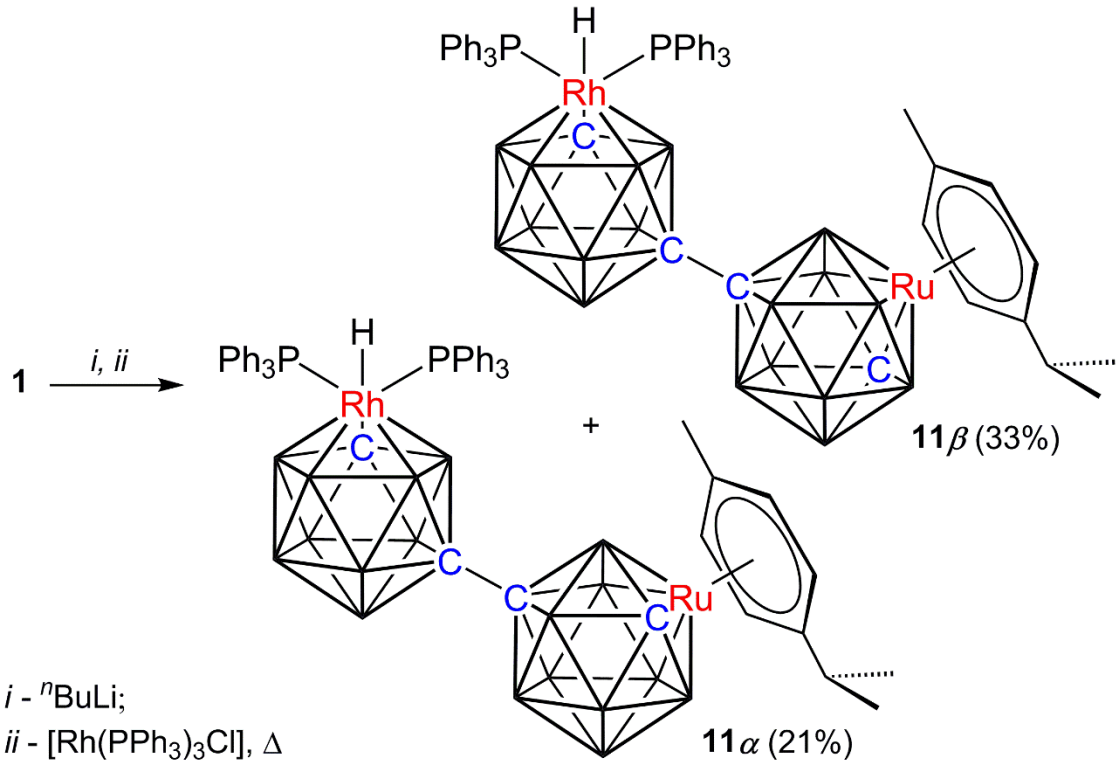

Figure 3.9 Metalation of salt **1** with $[Rh(PPh_3)_3Cl]$ to afford both diastereoisomers of **11**.

Microanalysis of the slower moving band **11*α*** was in good agreement with the expected formula $C_{50}H_{65}B_{18}P_2RhRu$. Analysis by mass spectrometry displayed no parent mass ion peak but an envelope centred on *m/z* 603 was observed, corresponding to the anticipated product after the loss of two PPh_3 ligands. This suggests that the rhodium has been successfully incorporated but, analogous to **10**, the rhodium fragment is fragile upon analysis by mass spectrometry.

A complex multiplet ranging from δ 7.43-7.09 ppm can be observed in the ^{1}H NMR spectrum, assigned to the phenyl protons of the phosphine ligands. Typical chemical shifts can also be noted relating to the *p*-cymene unit. Two $C_{cage}H$ resonances can be observed as broad singlets at δ 2.45 and 1.31 ppm attributed to the ruthenacarborane cage and rhodacarborane cage respectively. The rhodium hydride exhibits a similar ddd splitting pattern (Figure 3.10, left) to that observed in **10** at δ -8.56 ppm ($J_{Rh\text{-}H}$ = 29.8 Hz, $J_{P\text{-}H}$ = 23.7 and 15.4 Hz).

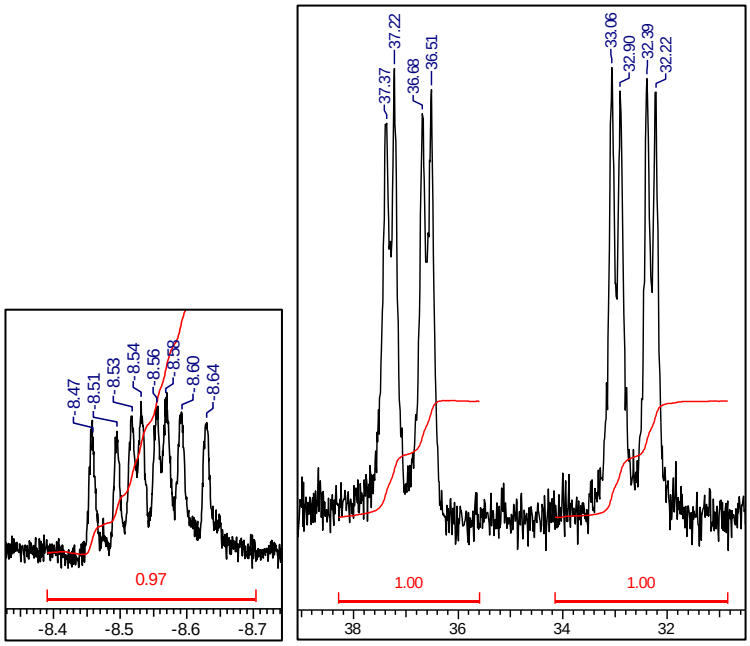

Figure 3.10 The ^{1}H NMR signal of the hydride ligand of **11*α*** exhibiting a doublet of doublet of doublets splitting pattern (left). The $^{31}P\{^1H\}$ NMR spectrum of **11*α*** displaying two sets of doublet of doublets in a 1:1 ratio (right). Units in ppm.

The $^{11}B\{^{1}H\}$ NMR spectrum displays two regions of overlapped resonances from δ 0.2 to -8.6 and -15.7 to -21.0 ppm with relative integrals of 12 and 6 respectively, totalling to the anticipated 18B atoms. Similar to **10**, two doublet of doublets can be observed in the $^{31}P\{^{1}H\}$ NMR spectrum at δ 36.95 and 32.65 ppm (Figure 3.10, right).

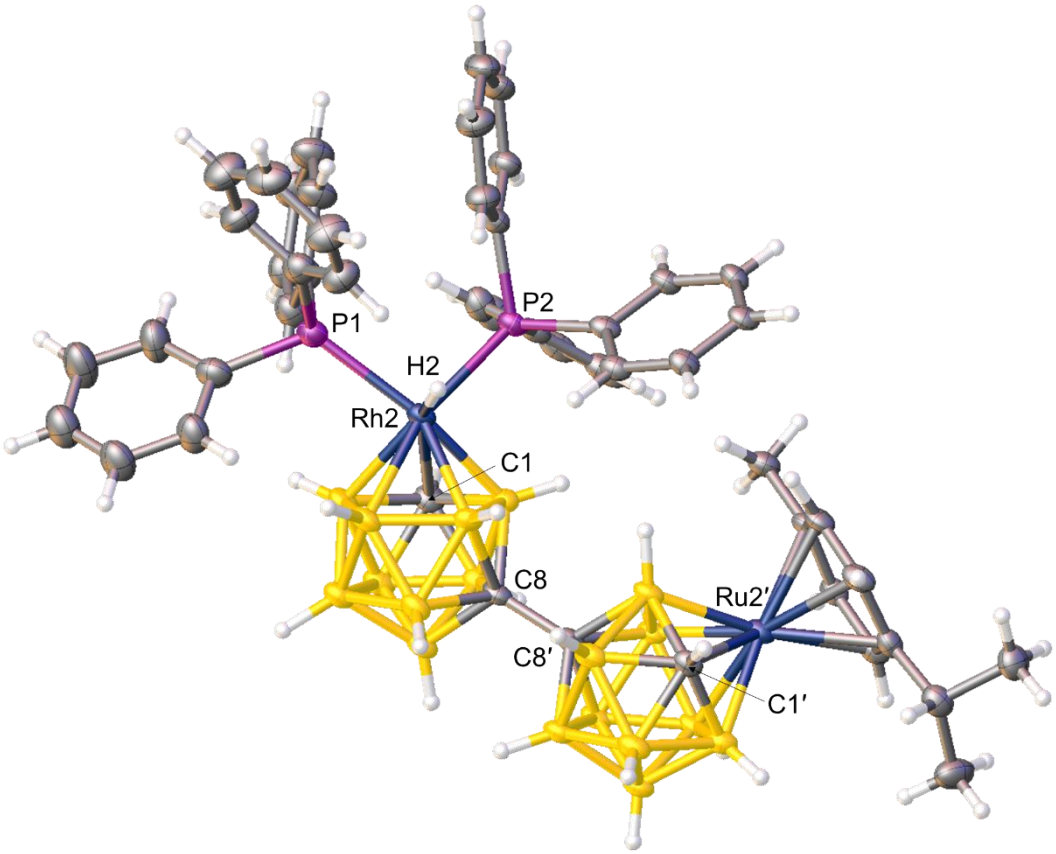

Figure 3.11 Perspective view of *α*-[8-(8′-2′-(*p*-cymene)-*closo*-2′,1′,8′-$RuC_2B_9H_{10}$)-2-H-2,2-$(PPh_3)_2$-*closo*-2,1,8-$RhC_2B_9H_{10}$] (**11*α***).

To determine the precise diastereoisomer, single crystals of **11*α*** were grown and a crystallographic study was undertaken. The structure was confirmed to be the alpha form of the isomerised species [8-(8′-2′-(*p*-cymene)-*closo*-2′,1′,8′-$RuC_2B_9H_{10}$)-2-H-2,2-$(PPh_3)_2$-*closo*-2,1,8-$RhC_2B_9H_{10}$] (Figure 3.11). As expected, the *p*-cymene ligand lies effectively parallel to the lower pentagonal belt (C8′B4′B5′B10′B12′) with a plane-plane angle of 4.65(16)°.

Minimal steric distortions can be observed in the exopolyhedral ligands of the rhodacarborane and, as previously noted in **10**, the hydride ligand lies effectively trans to the cage C atom of the CB_4 face. Additionally, elongation of the C1–Rh2 connectivity [2.287(5) Å] relative to the four cage B–Rh connectivities [2.184(6)-2.228(5) Å] is observed. This is particularly apparent when compared to the ruthenacarborane where the C1′–Ru2′ connectivity [2.163(5) Å] is comparable to the shortest B′–Ru′ distance [2.160(6)-2.214(5) Å].

Elemental analysis of compound **11*β*** reveals comparable results indicating the same chemical composition and thus implying that **11*β*** a structural isomer of **11*α***. The identical fragment ($M^+ - 2 \times PPh_3$) is noted in the EI mass spectrum.

The ^1H NMR spectrum is virtually identical to that of **11*α*** with the exception of slight differences of several signals by *ca.* 0.05 ppm allowing the two species to be distinguished. Unsurprisingly, the $^{11}B\{^1H\}$ and $^{31}P\{^1H\}$ NMR spectra are also essentially superimposable on those of **11*α*** (Figure 3.12 and 3.13).

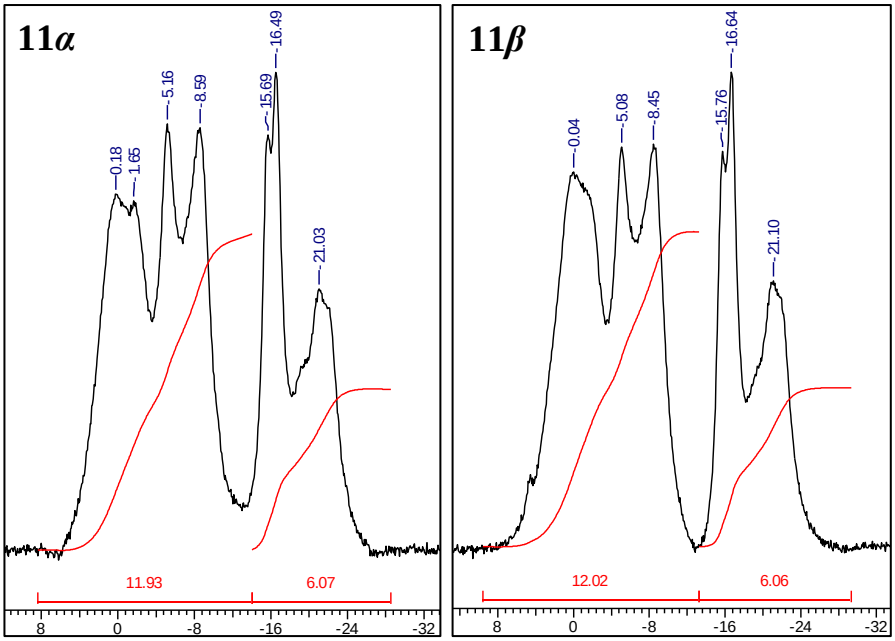

Figure 3.12 The $^{11}B\{^1H\}$ NMR spectra of **11*α*** (left) and **11*β*** (right). Units in ppm.

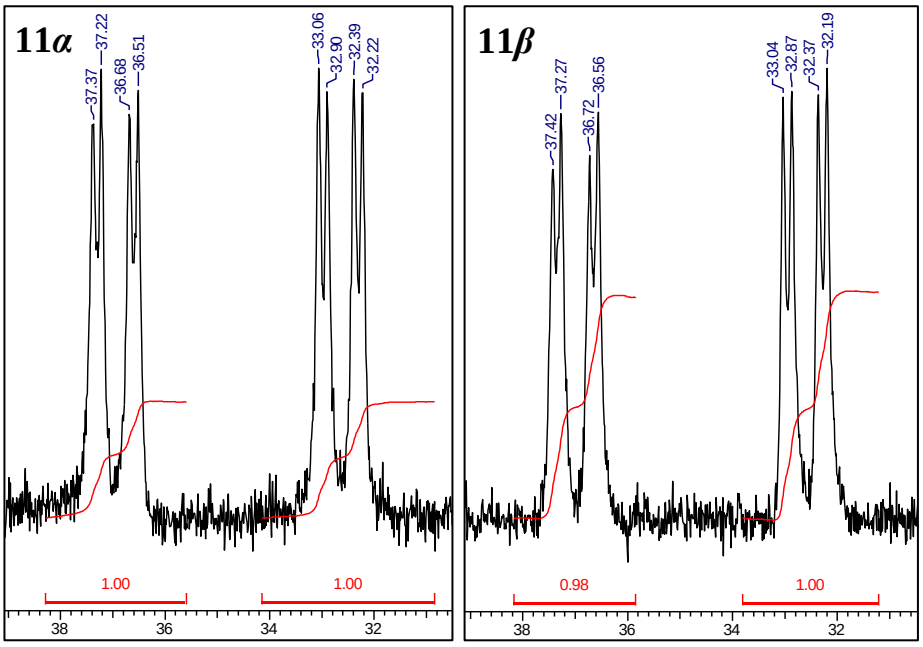

Figure 3.13 The $^{31}P\{^{1}H\}$ NMR spectra of **11*α*** (left) and **11*β*** (right). Units in ppm.

A diffraction study of **11*β*** revealed the species to be the expected complementary beta form of [8-(8′-2′-(*p*-cymene)-*closo*-2′,1′,8′-$RuC_2B_9H_{10}$)-2-H-2,2-$(PPh_3)_2$-*closo*-2,1,8-$RhC_2B_9H_{10}$] (Figure 3.14). The structure of **11*β*** is effectively superimposable on that of **11*α***, with the exception of a cage C vertex, despite being a different morphology. The cage C atoms were identified unambiguously by both the VCD and BHD methods independently. The *p*-cymene ligand lies effectively parallel to the lower pentagonal belt of the ruthenacarborane cage [θ = 5.87(19)°] and minimal distortion is noted in the ELO of the rhodacarborane cage. Again, the hydride ligand is positioned effectively trans to the cage C atom of the CB_4 face. Considerable lengthening of the C1–Rh2 connectivity is apparent [2.278(5) Å] relative to the B–Rh2 connectivities [2.172(5)-2.246(4) Å]. In contrast to this, the length of the C1′–Ru2′ connectivity [2.177(4) Å] is comparable to those of the B′–Ru2′ connectivities [2.152(4)-2.214(4) Å].

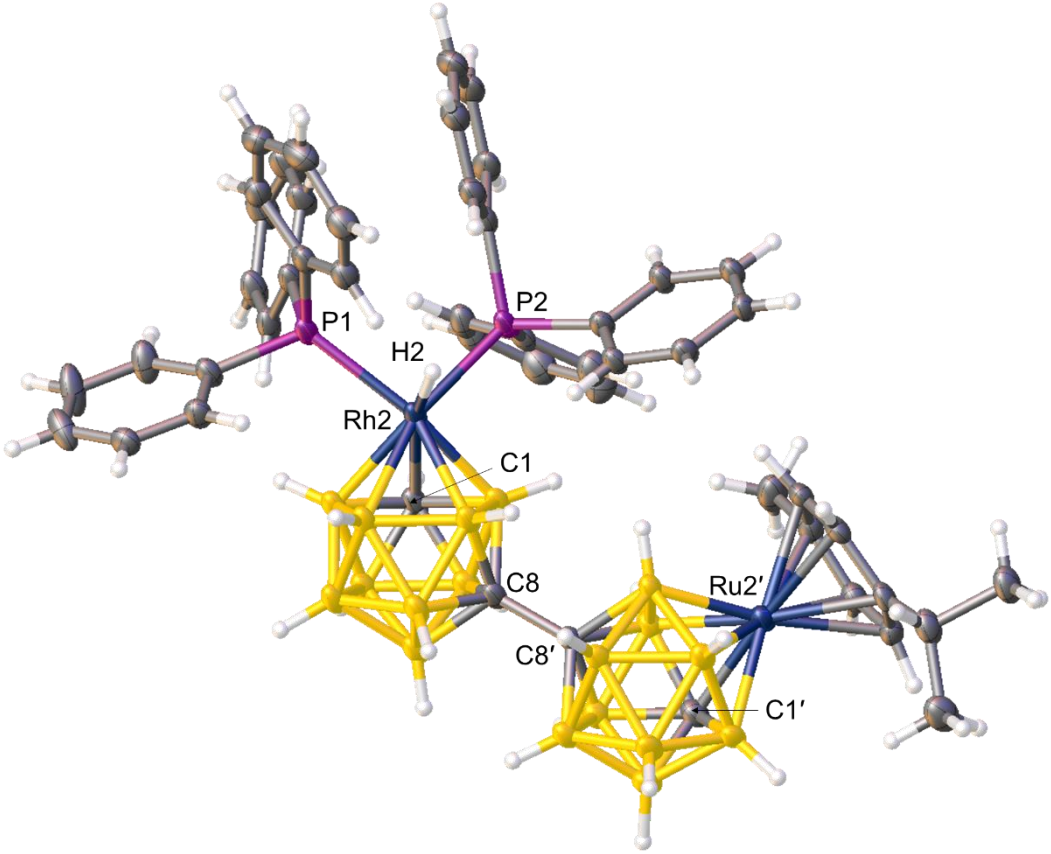

Figure 3.14 Perspective view of *β*-[8-(8′-2′-(*p*-cymene)-*closo*-2′,1′,8′-$RuC_2B_9H_{10}$)-2-H-2,2-$(PPh_3)_2$-*closo*-2,1,8-$RhC_2B_9H_{10}$] (**11*β***).

3.4 Synthesis of *α*-[8-(8′-2′-Cp*-*closo*-2′,1′,8′-$CoC_2B_9H_{10}$)-2-H-2,2-$(PPh_3)_2$-*closo*-2,1,8-$RhC_2B_9H_{10}$] (12*α*) and *β*-[8-(8′-2′-Cp*-*closo*-2′,1′,8′-$CoC_2B_9H_{10}$)-2-H-2,2-$(PPh_3)_2$-*closo*-2,1,8-$RhC_2B_9H_{10}$] (12*β*)

Reaction of **7** with $[Rh(PPh_3)_3Cl]$ following deprotonation affords a dark brown mixture. Stirring overnight and subsequent purification by preparative TLC yields two major mobile yellow bands. These were revealed to be two diastereoisomers of [8-(8′-2′-Cp*-*closo*-2′,1′,8′-$CoC_2B_9H_{10}$)-2-H-2,2-$(PPh_3)_2$-*closo*-2,1,8-$RhC_2B_9H_{10}$] (**12**) determined by microanalysis, mass spectrometry, NMR spectroscopy and ultimately crystallographically.

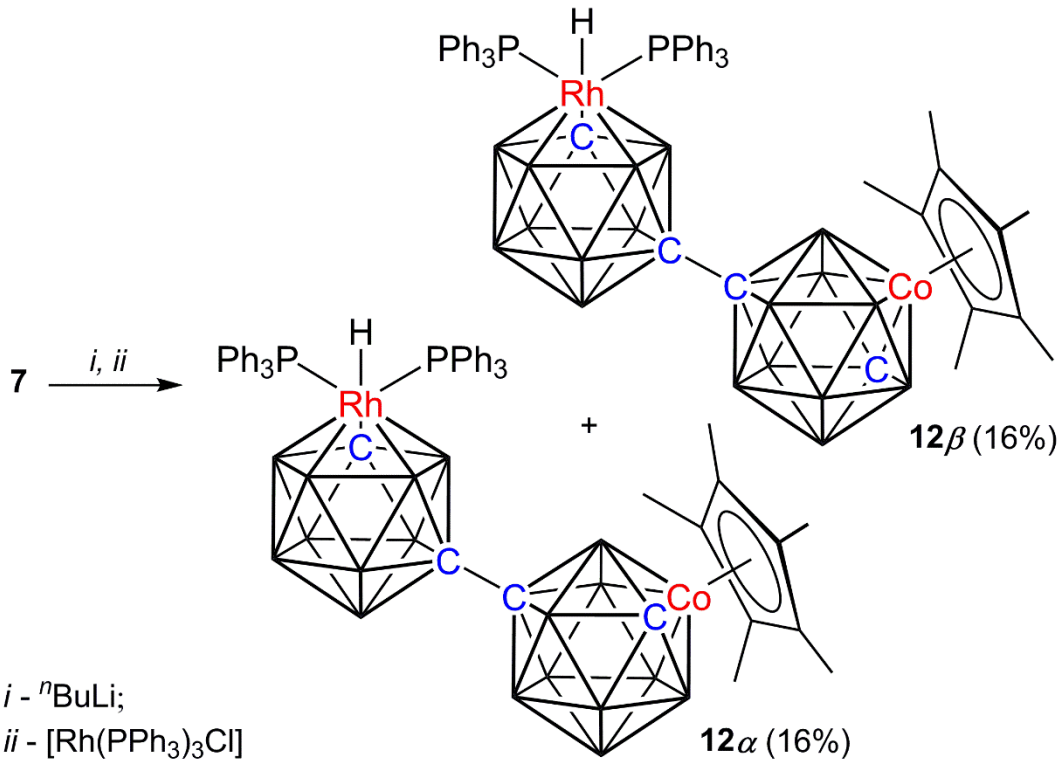

Figure 3.15 Metalation of salt **7** with $[Rh(PPh_3)_3Cl]$ to afford both diastereoisomers of **12**.

Elemental analysis of the lower R_f band **12*α*** is in good agreement with the anticipated product $C_{50}H_{66}B_{18}CoP_2Rh$. No meaningful data were obtained from mass spectrometry

using EI as the ionisation technique. However, using the milder ESI method revealed an envelope centred on *m/z* 822 which corresponds to the expected product after the loss of a PPh_3 ligand.

The ^{1}H NMR spectrum displays the expected multiplet centred at δ 7.26 ppm arising from the phosphine phenyl rings as well as a sharp singlet at δ 1.74 ppm from the Cp* ligand. The $C_{cage}H$ resonances are observed at δ 1.65 and 1.40 ppm, tentatively assigned to the cobaltacarborane and rhodacarborane respectively. The hydride is found at δ -8.57 ppm with the expected doublet of doublet of doublets splitting ($J_{Rh\text{-}H}$ = 30.3 Hz, $J_{P\text{-}H}$ = 24.2 and 15.6 Hz) as seen in Figure 3.16 (left).

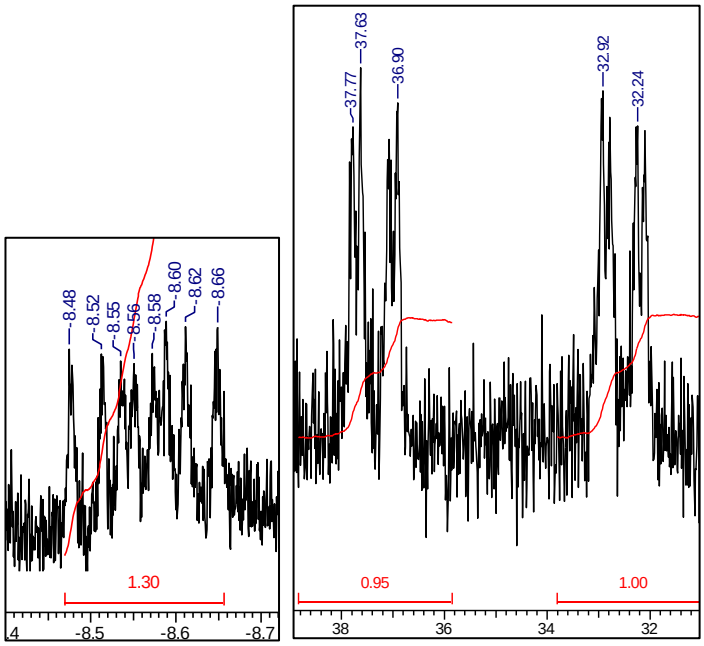

Figure 3.16 The ^{1}H NMR signal of the hydride ligand (left) and the $^{31}P\{^{1}H\}$ NMR spectrum of **12*α***. Units in ppm.

Interestingly, the $^{11}B\{^{1}H\}$ NMR spectrum displays two overlapped regions (δ 0.9 to -8.5 and -14.7 to -22.0 ppm) with relative integrals of 12 and 6 (Figure 3.18, left), analogous to both diastereoisomers of **11**. Two sets of doublet of doublets are noted in the $^{31}P\{^{1}H\}$ NMR spectrum as anticipated (Figure 3.16, right).

A crystallographic study of **12*α*** revealed the species to be *α*-[8-(8′-2′-Cp*-*closo*-2′,1′,8′-$CoC_2B_9H_{10}$)-2-H-2,2-$(PPh_3)_2$-*closo*-2,1,8-$RhC_2B_9H_{10}$]. Two independent molecules are present in the asymmetric unit. Due to relatively poor diffraction data, positional refinement of the cage H atoms was not possible prohibiting the use of the BHD method to locate the cage C atoms. However, application of the VCD method was successful in locating unambiguously the cage C atoms not involved in the intercage linkage in all four cages.

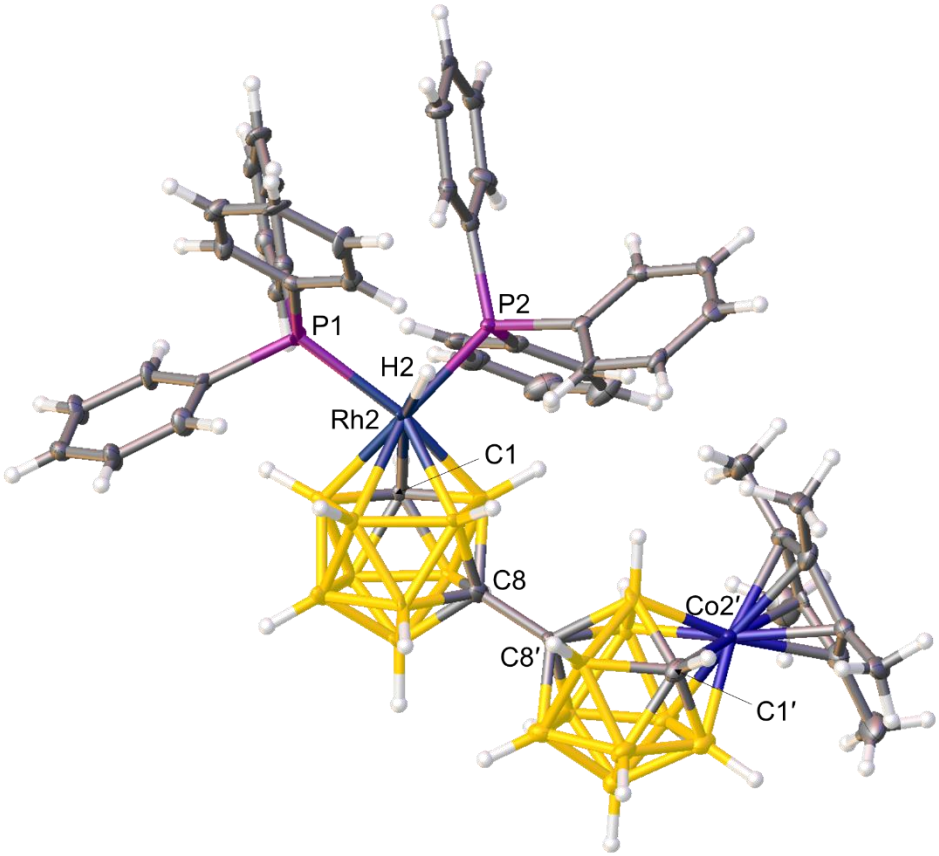

Figure 3.17 Perspective view of one of the independent molecules (rotamer 1) of *α*-[8-(8′-2′-Cp*-*closo*-2′,1′,8′-$CoC_2B_9H_{10}$)-2-H-2,2-$(PPh_3)_2$-*closo*-2,1,8-$RhC_2B_9H_{10}$] (**12*α***).

The two independent molecules differ in the relative orientations of the metallacarborane cages where one (rotamer 1) is analogous to the alignment observed in **11*α*** to give a Co2′C8′C8Rh2 torsion angle of 32.1(19)° (Figure 3.17). The second molecule (rotamer 2) has rotated about the C8–C8′ cage linkage to minimise steric interactions between the two metal fragments, giving a Co2′C8′C8Rh2 torsion angle of 176.7(6)° (Figure 3.18).

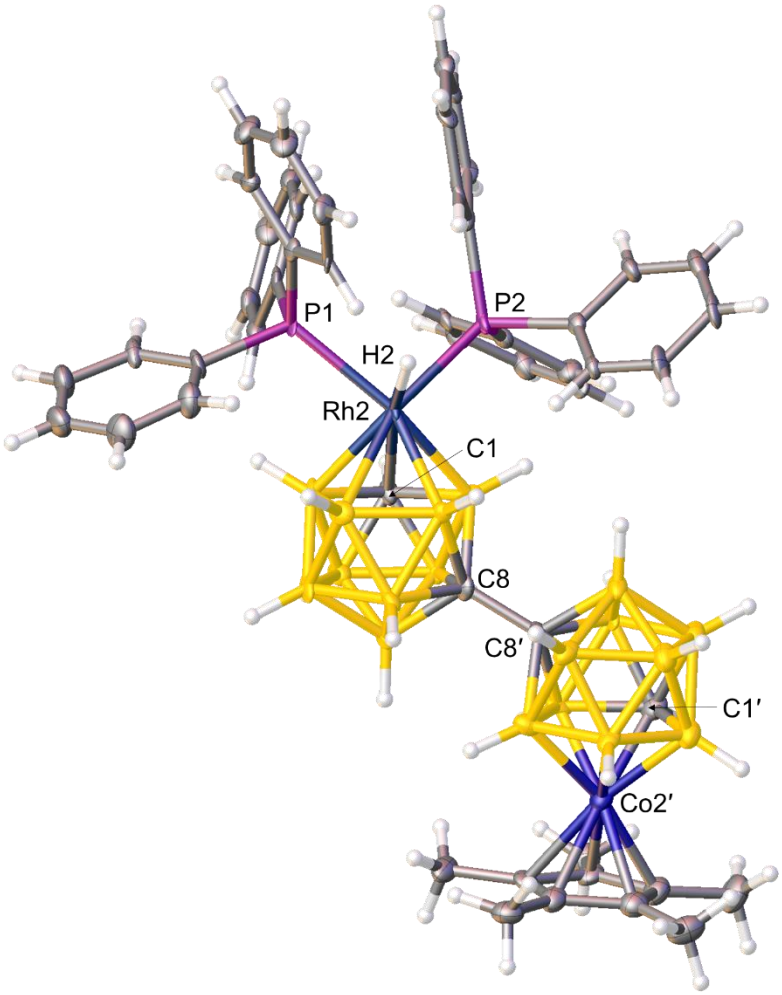

Figure 3.18 Perspective view of one of the independent molecules (rotamer 2) of *α*-[8-(8′-2′-Cp*-*closo*-2′,1′,8′-$CoC_2B_9H_{10}$)-2-H-2,2-$(PPh_3)_2$-*closo*-2,1,8-$RhC_2B_9H_{10}$] (**12*α***).

As expected, the Cp* ligands in both molecules are effectively parallel relative to the lower pentagonal belt of the cage. The hydride ligands are positioned effectively trans to the cage C atom as observed in **10** and **11*α*** resulting in long C1–Rh2 connectivities relative to the B–Rh connectivities. In the cobaltacarborane cages, the C1′–Co2′ connectivities are, in contrast, the second shortest cage C/B–Co lengths (Table 3.1).

	Connectivity	Rotamer 1	Rotamer 2
Rhodacarborane	C1–Rh2	2.252(13) Å	2.288(12) Å
	B3–Rh2	2.203(14) Å	2.193(14) Å
	B6–Rh2	2.247(13) Å	2.227(15) Å
	B7–Rh2	2.243(14) Å	2.214(14) Å
	B11–Rh2	2.251(14) Å	2.255(15) Å
Cobaltacarborane	C1′–Co2′	2.022(13) Å	2.027(14) Å
	B3′–Co2′	2.010(15) Å	1.996(14) Å
	B6′–Co2′	2.041(15) Å	2.049(16) Å
	B7′–Co2′	2.041(14) Å	2.045(16) Å
	B11′–Co2′	2.104(15) Å	2.109(15) Å

Table 3.1 Vertex-to-metal distances of **12*α*** (cage C entries highlighted in blue).

Microanalysis confirms that **12*β*** is a structural isomer of **12*α*** and the same fragment ($M^+ - PPh_3$) is observed in the ESI mass spectrum. Additionally, the ^1H NMR spectrum is remarkably similar where all observed resonances, with the exception of the phenyl protons, have shifted by ~0.01 ppm suggesting **12*β*** to be a diastereoisomer as opposed to a geometrical isomer. The $^{11}B\{^1H\}$ and $^{31}P\{^1H\}$ NMR spectra of **12*β*** again are effectively superimposable on those of **12*α*** (Figure 3.19).

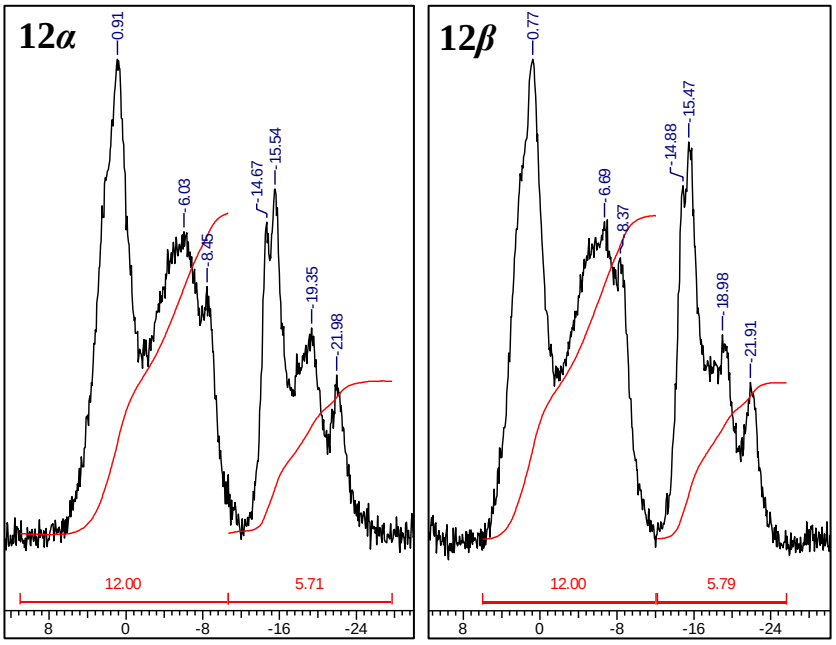

Figure 3.19 The $^{11}B\{^1H\}$ NMR spectra of **12*α*** (left) and **12*β*** (right). Units in ppm.

The definitive structure of **12*β*** was confirmed crystallographically to be the beta form of [8-(8′-2′-Cp*-*closo*-2′,1′,8′-$CoC_2B_9H_{10}$)-2-H-2,2-$(PPh_3)_2$-*closo*-2,1,8-$RhC_2B_9H_{10}$] in which all cage C atoms were identified by the VCD method. Two independent molecules are present in the asymmetric fraction of the unit cell. Relatively poor data again prohibited the use of the BHD method.

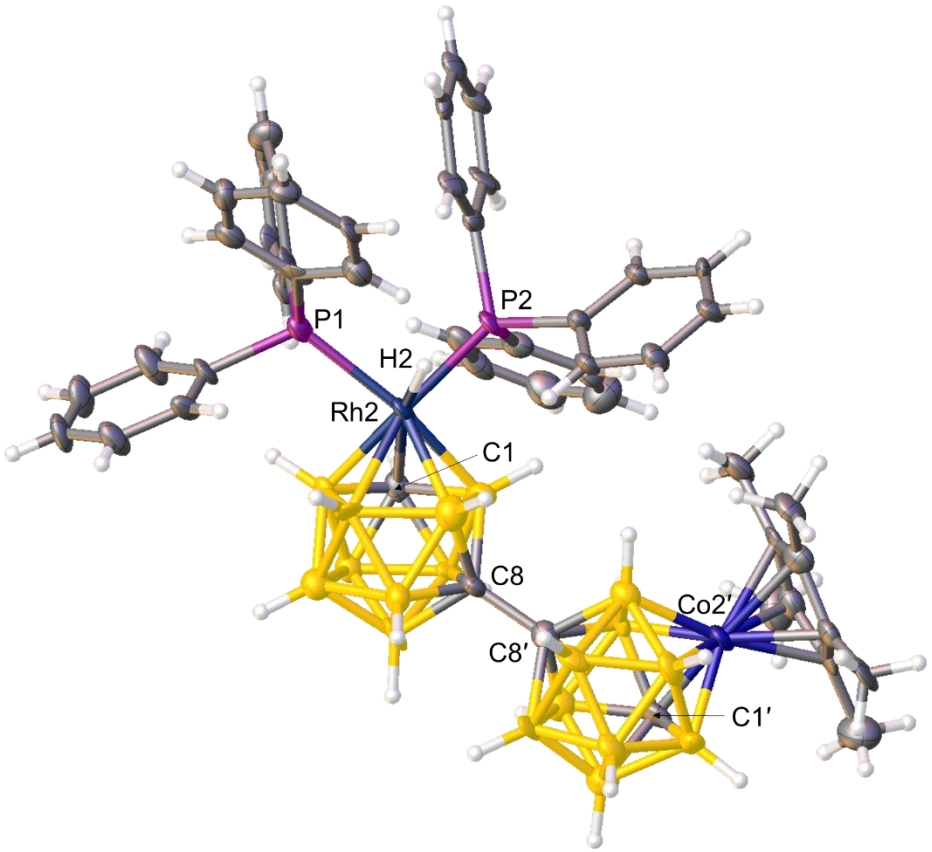

Figure 3.20 Perspective view of one of the independent molecules (rotamer 1) of *β*-[8-(8′-2′-Cp*-*closo*-2′,1′,8′-$CoC_2B_9H_{10}$)-2-H-2,2-$(PPh_3)_2$-*closo*-2,1,8-$RhC_2B_9H_{10}$] (**12*β***).

It is interesting to note that despite the fact that the crystals of **12*α*** and **12*β*** are isomorphous, the two diastereoisomers can be identified unambiguously. As such, the orientation of the two independent molecules are identical to those in **12*α*** with Co2′C8′C8Rh2 torsion angles of 31.0(2)° (rotamer 1, Figure 3.20) and 178.8(6)° (rotamer 2). Similarly, the hydride ligands are positioned trans to the cage C atom of the CB_4 face and a notable lengthening of the C1–Rh2 distances is observed relative to the B–Rh connectivities in both independent molecules (Table 3.2).

	Connectivity	Rotamer 1	Rotamer 2
Rhodacarborane	C1–Rh2	2.293(12) Å	2.276(13) Å
	B3–Rh2	2.218(15) Å	2.193(15) Å
	B6–Rh2	2.193(15) Å	2.239(15) Å
	B7–Rh2	2.246(17) Å	2.225(16) Å
	B11–Rh2	2.256(16) Å	2.306(16) Å
Cobaltacarborane	C1′–Co2′	2.035(14) Å	2.041(14) Å
	B3′–Co2′	2.021(17) Å	2.038(15) Å
	B6′–Co2′	2.053(16) Å	2.076(17) Å
	B7′–Co2′	2.076(16) Å	2.005(18) Å
	B11′–Co2′	2.079(17) Å	2.099(19) Å

Table 3.2 Vertex-to-metal distances of **12*β*** (cage C entries highlighted in blue).

3.5 Discussion

The first report of a catalytically-active metallacarborane[1] was by Hawthorne in 1974, ten years after the establishment of the metallacarborane field. The bis(phosphine)hydrido-rhodacarborane **VIII** was found to catalyse a number of reactions[11-13] and it was established that the {$Rh(PPh_3)_2H$} fragment was key to its catalytic activity. Although the single-cage rhodacarborane has been significantly investigated, this fragment has yet to be successfully inserted into a bis(carborane) framework.

A modified protocol for the insertion of the {$Rh(PPh_3)_2H$} fragment into bis(*o*-carborane) has been developed involving removal of the bridging/endo-H prior to metalation. The enhanced coulombic attraction between the dianionic carborane and the cationic rhodium fragment is postulated to drive the metalation. The insertion of the {$Rh(PPh_3)_2H$} fragment into **XI** has led to the first crystallographically-studied rhodacarborane/ carborane species **10**.

Compound **10** is a candidate for subsequent deboronation and metalation, increasing the range of potential heterometalated bis(carborane) precursors (Figure 3.21). Unfortunately, all reagents for deboronation (KOH/EtOH, KF and acetonitrile) trialled did not afford the desired product and typically resulted in decomposition of the starting material. Therefore, the only viable method for synthesising bis(phosphine)hydrido-rhodium derivatives of heterometalated bis(carboranes) is to insert the rhodium fragment second.

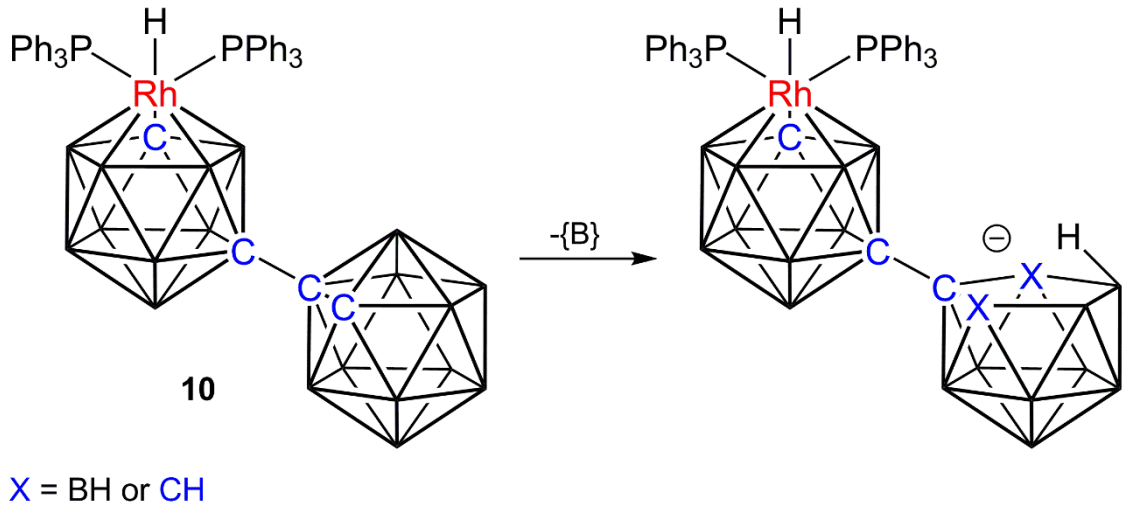

Figure 3.21 Proposed deboronation of **10**.

Using the adapted metalation protocol combined with the previously described salts **1** and **7** led to the preparation of two further examples of heterometalated bis(carboranes), each bearing a rhodacarborane unit (**11** and **12**). Both **11** and **12** were successfully separated into their diastereomeric components (α and β) and studied crystallographically.

In all four cases, all non-H atoms were freely refined and successfully modelled with the exception of disordered solvent molecules that were removed using the BYPASS procedure in OLEX2.[14] Electron density peaks corresponding to the hydride ligand were observed in all five species (**10**, **11*α***, **11*β***, **12*α*** and **12*β***) but only in the rhodacarborane/carborane species **10** were the diffraction data sufficiently good to refine the H ligand positionally. Therefore, the hydride ligands in **11*α***, **11*β***, **12*α*** and **12*β*** were geometrically constrained based on parameters from the successfully refined **10**; Rh–H 1.58(2) Å and P···H 2.55(2) Å. As noted, relatively poor data from **12*α*** and **12*β*** prevented the use of the BHD method in determining the precise diastereoisomer as positional refinement of the cage H atoms produced nonsensical models. Therefore, for these species the cage H atoms were set in idealised positions riding on their respective B or C atom and cage C identification was accomplished by only the VCD method.

All five rhodium derivatives of bis(*o*-carborane) exhibit a 2,1,8-RhC_2B_9 geometry suggesting the additional steric bulk from either the carborane or metallacarborane substituent prevents the isolation of the non-isomerised 3,1,2-RhC_2B_9 species.

The hydride resonance in the ^1H NMR spectra of the four rhodacarborane/metallacarborane complexes (**11*α***, **11*β***, **12*α*** and **12*β***) are remarkably similar (δ -8.56 to -8.58 ppm) indicating that the rhodium fragment is effectively in equivalent environments. This is also mirrored in the similarities between their $^{31}P\{^1H\}$ NMR spectra. This is perhaps unsurprising as the second metal fragment, although substantially different to each other, is located far from the rhodium fragment. In comparison to **10** (δ -8.70 ppm), the hydride resonances are relatively upfield implying the metallacarborane substituent is marginally more electron-withdrawing than the carborane substituent.

By modifying the metalation protocol for the bis(phosphine)hydridorhodium fragment together with application of the previously described heterometalation protocol, five novel bis(carborane) derivatives of **VIII** were successfully prepared. All five species hold the same catalytic potential as **VIII** and this will be explored in the subsequent chapter.

3.6 References

1. T. E. Paxson and M. F. Hawthorne, *J. Am. Chem. Soc.*, 1974, **96**, 4674-4676.

2. J. A. Long, T. B. Marder, P. E. Behnken and M. F. Hawthorne, *J. Am. Chem. Soc.*, 1984, **106**, 2979-2989.

3. C. B. Knobler, T. B. Marder, E. A. Mizusawa, R. G. Teller, J. A. Long, P. E. Behnken and M. F. Hawthorne, *J. Am. Chem. Soc.*, 1984, **106**, 2990-3004.

4. A. McAnaw, G. Scott, L. Elrick, G. M. Rosair and A. J. Welch, *Dalton Trans.*, 2013, **42**, 645-664.

5. P. E. Behnken, C. B. Knobler and M. F. Hawthorne, *Angew. Chem., Int. Ed.*, 1983, **22**, 722-723.

6. P. E. Behnken, T. B. Marder, R. T. Baker, C. B. Knobler, M. R. Thompson and M. F. Hawthorne, *J. Am. Chem. Soc.*, 1985, **107**, 932-940.

7. B. J. Coe and S. J. Glenwright, *Coord. Chem. Rev.*, 2000, **203**, 5-80.

8. G. Thiripuranathar, W. Y. Man, C. Palmero, A. P. Y. Chan, B. T. Leube, D. Ellis, D. McKay, S. A. Macgregor, L. Jourdan, G. M. Rosair and A. J. Welch, *Dalton Trans.*, 2015, **44**, 5628-5637.

9. I. T. Chizhevsky, I. V. Pisareva, E. V. Vorontzov, V. I. Bregadze, F. M. Dolgushin, A. I. Yanovsky, Yu. T. Struchkov, C. B. Knobler and M. F. Hawthorne, *J. Organomet. Chem.*, 1997, **536**, 223-231.

10. I. T. Chizhevsky, I. A. Lobanova, P. V. Petrovskii, V. I. Bregadze, F. M. Dolgushin, A. I. Yanovsky, Yu. T. Struchkov, A. L. Chistyakov, I. V. Stankevich, C. B. Knobler and M. F. Hawthorne, *Organometallics*, 1999, **18**, 726-735.

11. J. A. Belmont, J. Soto, R. E. King III, A. J. Donaldson, J. D. Hewes and M. F. Hawthorne, *J. Am. Chem. Soc.*, 1989, **111**, 7475-7486.

12. H. C. Kang and M. F. Hawthorne, *Organometallics*, 1990, **9**, 2327-2332.

13. V. N. Lebedev, E. V. Balagurova, F. M. Dolgushin, A. I. Yanovskii and L. I. Zakharkin, *Russ. Chem. Bull.*, 1997, **46**, 550-558.

14. P. van der Sluis and A. L. Spek, *Acta. Cryst.*, 1990, **A46**, 194-201.

Chapter 4

Rhodacarboranes in Catalysis

4.1 Introduction

In the pioneering report[1] of the original rhodacarborane [3-H-3,3-$(PPh_3)_2$-*closo*-3,1,2-$RhC_2B_9H_{11}$] (**VIII**), the complex was shown to catalyse the isomerisation and hydrogenation of alkenes. It was also found to catalyse the hydrosilylation of acetophenone, the scope of which was subsequently expanded by Zakharkin.[2] A series of papers was published following the initial synthesis of **VIII** investigating the active catalytic species[3,4] as well as furthering the reaction scope to the hydrogenolysis[4] and hydrosilanolysis[5] of alkenyl acetates.

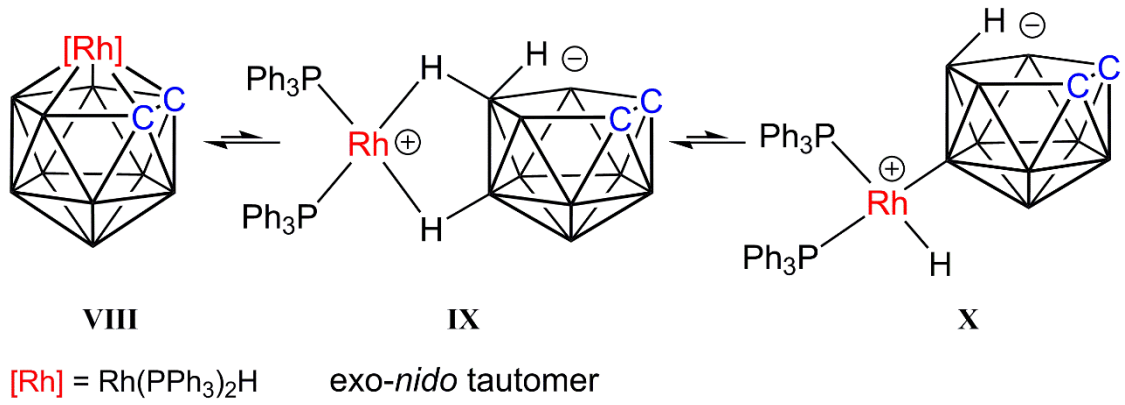

Figure 4.1 The proposed tautomerisation and B–H oxidative addition products, **IX** and **X** respectively, formed from the closo rhodacarborane precursor **VIII**.

As discussed in Chapter 1.4.1, Hawthorne concludes that the active catalyst is the Rh(III) species **X** formed from the reversible oxidative addition of Rh(I) in **IX** into a B–H bond (Figure 4.1). Kinetic studies have shown that the rate of hydrogenation is inversely proportional to the concentration of PPh_3. This suggests that the dissociation of a phosphine ligand is a critical pre-activation step required before the rhodacarborane enters the catalytic cycle.

This was exploited by Hawthorne where a derivative of **VIII** possessing only one phosphine ligand was prepared. In place of the second phosphine, an η^2-alkene which was tethered to a cage C atom was used as a two electron donor (**XXVIII**).[6] In hydrogenation, the coordinated alkene (dubbed as a 'suicide ligand') is irreversibly hydrogenated to generate rhodacarborane **XXIX** which possesses a formal vacant site (Figure 4.2). This species was found to be one of the most active known homogeneous catalysts for alkene hydrogenation.

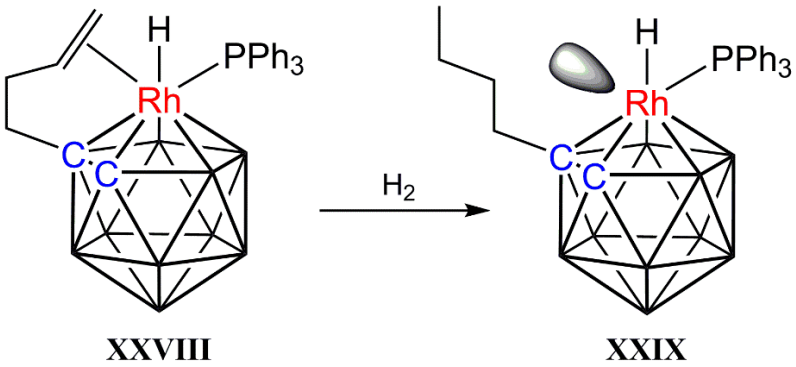

XXVIII **XXIX**

Figure 4.2 The irreversible hydrogenation of the ^{n}butenyl-substituted rhodacarborane (**XXVIII**) to the ^{n}butyl-substituted species (**XXIX**) which possesses a formal vacant site.

The effect of cage substitution on the catalytic properties of **VIII** has not been widely investigated. Bulky *C*-substituted derivatives have been synthesised which allowed the existence of the exo-*nido* tautomer to be demonstrated crystallographically.[7] However, it was shown to have only comparable catalytic activity to its closo precursors and even diminished activity in the hydrosilanolysis of alkenyl acetates. Zakharkin found *B*-polyfluorinated derivatives of **VIII** to be comparable in the hydrosilylation of alkenes and alkynes although with decreased product selectivity.[2]

Within this chapter, the rhodium derivatives of bis(carborane) **10**-**12** will be employed in the isomerisation of 1-hexene and the hydrosilylation of acetophenone.

4.2 Characterisation of [2-H-2,2-$(PPh_3)_2$-*closo*-2,1,12-$RhC_2B_9H_{11}$] (XXX)

Prior to catalytic testing, the single-cage analogues [3-H-3,3-$(PPh_3)_2$-*closo*-3,1,2-$RhC_2B_9H_{11}$] (**VIII**) and [2-H-2,2-$(PPh_3)_2$-*closo*-2,1,12-$RhC_2B_9H_{11}$] (**XXX**) were identified as suitable benchmarks for comparison. The isomerised rhodacarborane **XXX** was selected as in it the carborane ligand binds to the rhodium centre through a CB_4 face, analogous to the situation in compounds **10**-**12**. Ideally, the 2,1,8-$Rh_2C_2B_9$ single-cage analogue would also be employed, allowing for a more direct comparison between the catalyst precursors, but several attempts at preparing this species were unsuccessful. Whilst extensive research has been undertaken on **VIII** and its performance as a catalyst precursor, the isomerised species **XXX** is less well investigated.

Compound **XXX** can be prepared in *ca.* 90% yield from the reaction between the anion [*nido*-2,9-$C_2B_9H_{12}]^-$ and $[Rh(PPh_3)_3Cl]$ in degassed ethanol.[8] Multinuclear NMR studies of the product have been reported but only the ^{1}H NMR chemical shift of the hydride ligand is noted. Additionally, **XXX** has also been shown to catalyse the isomerisation and hydrogenation of simple alkenes with an enhanced rate relative to **VIII**.[3]

Following the literature, **XXX** was successfully prepared and the product was fully characterised spectroscopically. In addition to the previously reported hydride ligand (δ -8.74 ppm) in the ^{1}H NMR spectrum, the phenyl protons of the PPh_3 ligands span from δ 7.68 to 6.94 ppm and the two $C_{cage}H$ protons are found at δ 2.34 and 1.49 ppm. In addition to full spectroscopic characterisation, yellow block crystals of **XXX** were successfully grown and a crystallographic study was undertaken (Figure 4.3).

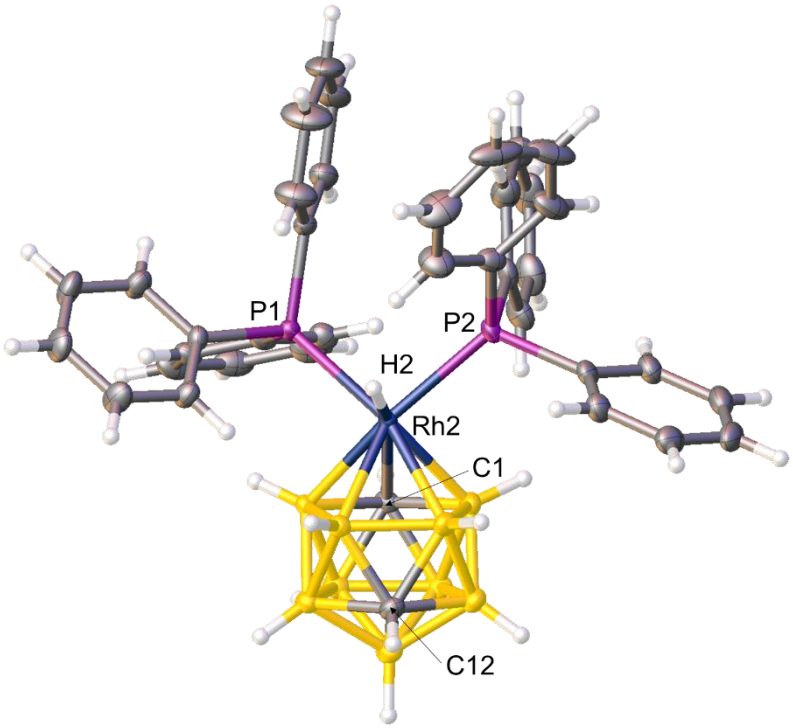

Figure 4.3 Perspective view of [2-H-2,2-$(PPh_3)_2$-*closo*-2,1,12-$RhC_2B_9H_{11}$] (**XXX**).

As expected, the structure of **XXX** is essentially superimposable on its 3,1,2-analogue **VIII** with the exception of the cage C positions. These positions were identified unambiguously using both the VCD and BHD methods independently. Similar to the previously described 2,1,8-isomers (**10**-**12**), the hydride ligand is positioned effectively trans to the cage C atom of the CB_4 face.

4.3 Isomerisation of 1-Hexene

The seven catalyst precursors (**VIII**, **XXX**, **10**, **11*α***, **11*β***, **12*α*** and **12*β***) were employed in the isomerisation of 1-hexene (Figure 4.4) using a 0.2 mol% loading of the appropriate catalyst. The reaction was performed in deuterated chloroform under an inert atmosphere and its progress was monitored by ^{1}H NMR spectroscopy against mesitylene as an internal standard.

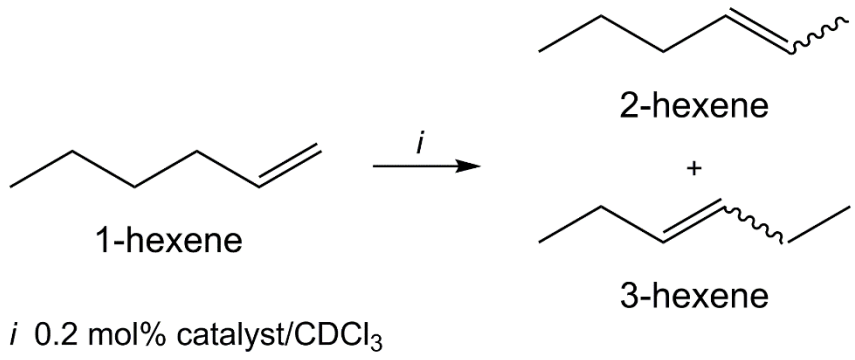

Figure 4.4 General scheme for the isomerisation of 1-hexene.

Alkene isomerisation is a simple transformation and has been thoroughly investigated in the literature. However, that very simplicity allows the rapid testing for catalytic activity of the new complexes (**10**-**12**) as well as affording a swift performance comparison with the single-cage rhodacarboranes **VIII** and **XXX** (Figure 4.5).

Selected entries are tabulated in Table 4.1. Due to overlapped ^{1}H NMR resonances, the two isomers of 3-hexene could not be clearly discerned and thus are reported as a combined yield. Comparison of the two single-cage analogues **VIII** and **XXX** shows that the latter is a vastly superior catalyst precursor for the isomerisation of 1-hexene, as expected.[3] Compound **VIII** achieves a combined yield of 45% after 6 h whereas **XXX** attains a comparable yield (46%) in only 0.5 h and the reaction is effectively complete by 3 h.

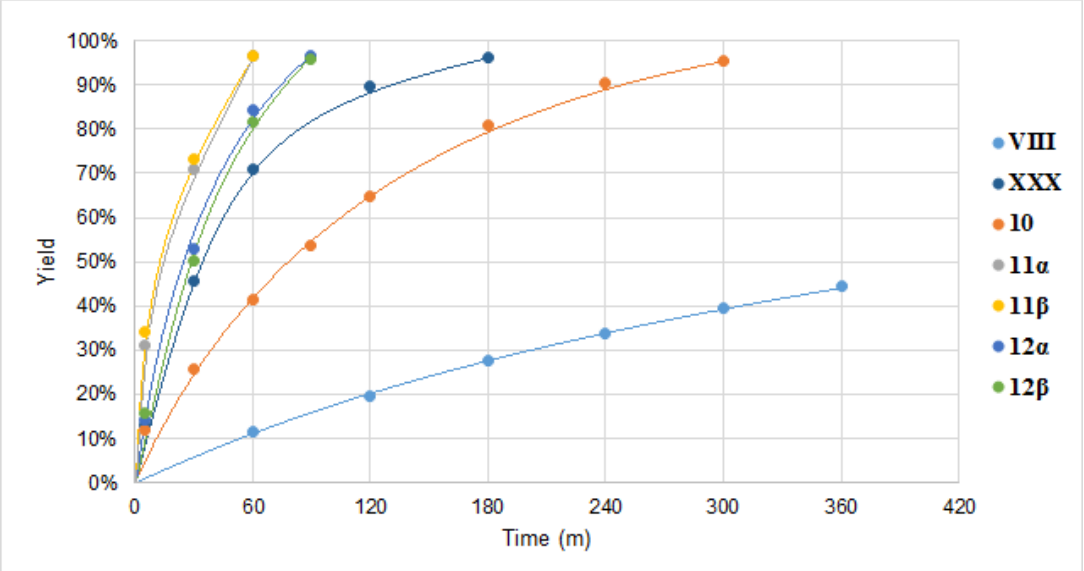

Figure 4.5 Plot of the NMR yield of the isomerisation of 1-hexene against time.

Catalyst Precursor	Time (h)	Trans-2-hexene (%)	Cis-2-hexene (%)	3-Hexenes (%)	Total Yield (%)
VIII	1	7.1	4.4	0	11.5
	3	17.6	10.1	0	27.7
	6	29.2	15.4	0	44.6
XXX	1	46.0	24.9	0	70.9
	3	63.4	26.8	6.2	96.4
10	1	24.2	17.2	0	41.4
	3	51.2	29.6	0	80.8
11*α*	1	61.3	27.9	7.3	96.5
11*β*	1	61.0	27.2	8.5	96.7
12*α*	1	52.3	31.0	1.0	84.3
12*β*	1	47.5	29.9	4.3	81.7

Table 4.1 Isomerisation of 1-hexene catalysed by **VIII**, **XXX**, **10**, **11*α***, **11*β***, **12*α*** and **12*β***. Reactions performed in duplicate and average NMR yields quoted, with yields calculated from the relative integrals of the products in the ^{1}H NMR spectra against the mesitylene internal standard (entries at the same time are highlighted).

These results clearly indicate that isomeric differences play a substantial role in the catalytic activity of the rhodacarborane. The most notable difference between **VIII** and **XXX**, aside from the cage C positions, is the binding face of the carborane ligand, C_2B_3 and CB_4 respectively. The greater binding strength of the CB_4 face, relative to a C_2B_3 face, to the rhodium centre appears to enhance the rate of alkene isomerisation. Therefore, the singly-metalated species **10** should perform better than **VIII** in the same reaction as it also possesses a CB_4 face.

This is indeed observed since **10** achieves a 41% yield after just 1 h and essentially full conversion by 5 h. Given the isomerised 2,1,8-RhC_2B_9 architecture of **10**, steric effects arising from the carboranyl substituent should be minimal and thus the rate enhancement is attributed to electronic factors. However, relative to **XXX**, compound **10** performs somewhat sluggishly. This suggests that either the isomeric difference between 2,1,8-RhC_2B_9 and 2,1,12-RhC_2B_9 or the electron-withdrawing *C*-bound carboranyl substituent is supressing the rate of alkene isomerisation.

Ruthenacarborane-rhodacarborane catalyst precursors **11*α*** and **11*β*** achieve effectively full conversion after 1 h and no notable differences in the product distribution can be observed between the two diastereoisomers. Cobaltacarborane-rhodacarborane compounds **12*α*** and **12*β*** also performed similarly to each other, affording *ca.* 96% conversion in 1.5 h, marginally slower than the ruthenium derivatives **11**. Likewise, minimal variations in the rate and product distribution are noted between the two diastereoisomers. All four heterobimetallic species perform superior to **XXX**, completing the isomerisation in less than half the time. Hence, the order of the most active catalyst precursors is **11** > **12** > **XXX** > **10** >> **VIII**.

Catalyst Precursor	Time (h)	Total Yield (%)	δ($C_{cage}H$) (ppm)
VIII	5	39.4	2.24
10	5	95.6	1.84
XXX	3	96.4	1.49
12*α*	1.5	96.5	1.40
12*β*	1.5	95.9	1.38
11*α*	1	96.5	1.31
11*β*	1	96.7	1.33

Table 4.2 The catalyst precursors ordered in increasing catalytic activity (top to bottom) for the isomerisation of 1-hexene with the ^{1}H NMR resonance of the rhodacarborane $C_{cage}H$ noted. Times for >95% yield selected (if possible) and entries of the same time highlighted.

A *C*-bound metallacarborane substituent is a weaker electron-withdrawing group than a *C*-bound carboranyl substituent, evident from the downfield shift of the rhodacarborane $C_{cage}H$ resonances in the ^{1}H NMR spectra of **11** (δ ~1.3 ppm) and **12** (δ ~1.4 ppm) relative to **10** (δ 1.84 ppm). The ordering of these rhodacarborane $C_{cage}H$ chemical shifts matches the trend observed in the rate of isomerisation (**11** > **12** > **10**), suggesting that a strong electron-withdrawing substituent is detrimental for alkene isomerisation. In fact, a consistent trend between the rate of isomerisation and the ^{1}H NMR chemical shift of the $C_{cage}H$ in the rhodacarborane for all the catalyst precursors can be noted (Table 4.2).

As the ^{1}H NMR resonance of the rhodacarborane $C_{cage}H$ shifts upfield, the time required to achieve essentially total conversion is reduced. Although **VIII** fits the observed trend, the adjacency of the cage C atoms in the carborane ligand face will skew the $C_{cage}H$ chemical shift and, as such, this entry should be considered with caution. Additionally, **XXX** should also be treated with caution as the vertex (C against B in the 2,1,8-RhC_2B_9 species) antipodal to the measured $C_{cage}H$ vertex could have an influence on its chemical shift.

As such, it is not possible to conclude whether a carboranyl substituent is beneficial relative to an H atom for the isomerisation of 1-hexene. However, a metallacarborane substituent is a distinctly superior modification relative to a carboranyl substituent, boosting the catalytic capabilities of the rhodacarborane in alkene isomerisation.

It is interesting to note that the ruthenacarborane substituent is noticeably better than the cobaltacarborane substituent at promoting the reaction rate despite the distance of the Ru/Co fragment from the active rhodium centre. Therefore, the ranking of the substituent for a 2,1,8-RhC_2B_9 cage is ruthenacarborane > cobaltacarborane > carborane for the isomerisation of 1-hexene.

These preliminary results have demonstrated the flexibility of the bis(carborane) framework where five novel catalyst precursors have been shown to catalyse the isomerisation of 1-hexene at varying rates depending on its substituent.

4.4 Hydrosilylation of Acetophenone

The hydrosilylation of acetophenone using diphenylsilane (Figure 4.6) was catalysed by 0.5 mol% loading of the appropriate catalyst. The reaction was performed in a sealed J. Young NMR tube under nitrogen at 55 °C using $CDCl_3$ as the solvent. The reaction was monitored periodically using ^1H NMR spectroscopy and the conversion was calculated from the relative integrals of the products against a mesitylene internal standard.

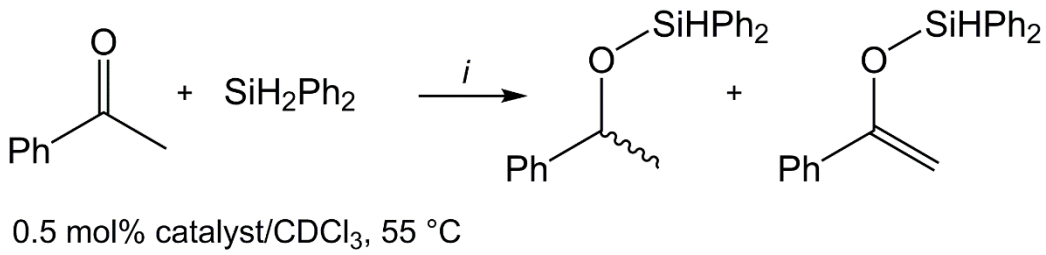

Figure 4.6 General scheme for the hydrosilylation of acetophenone using diphenylsilane to produce the corresponding silyl ether and the silyl enol ether product.

In marked contrast to isomerisation reaction, both single-cage analogues **VIII** and **XXX** show the most rapid reaction rates, achieving 89% in 2 h and 96% in 1 h, respectively (Figure 4.7). The product distribution is *ca*. 3:1 of silyl enol ether:silyl ether in both cases. No reactivity is observed at room temperature.

Using **10** as the catalyst precursor, the same reaction reaches 43% conversion in 2 h and only 82% even after 17 h. A comparable product distribution is observed (*ca*. 2:1) where the silyl enol ether is the major species (Table 4.3).

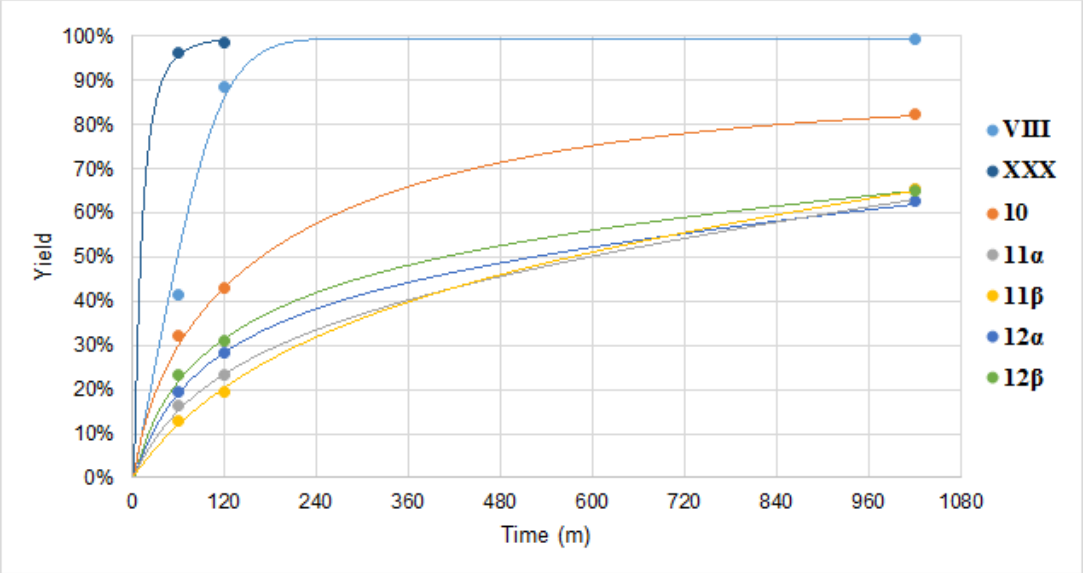

Figure 4.7 Plot of the yield of the hydrosilylation of acetophenone against time.

Catalyst Precursor	Time (h)	Silyl ether (%)	Silyl enol ether (%)	Total Yield (%)
VIII	1	17.7	23.9	41.6
	2	23.2	65.5	88.7
	17	26.1	73.4	99.5
XXX	1	20.0	76.4	96.4
10	2	14.1	29.0	43.1
	17	30.5	51.7	82.2
11*α*	17	35.6	29.8	65.4
11*β*	17	36.0	29.4	65.4
12*α*	17	26.6	36.1	62.7
12*β*	17	25.4	39.6	65.0

Table 4.3 Hydrosilylation of acetophenone using diphenylsilane catalysed by **VIII**, **XXX**, **10**, **11*α***, **11*β***, **12*α*** and **12*β***. Reactions completed in duplicate and average NMR yields are quoted, with yields calculated from the relative integrals of the products in the ^{1}H NMR spectra against the mesitylene internal standard (entries at the same time are highlighted).

Compounds **11*α***, **11*β***, **12*α*** and **12*β*** all perform sluggishly relative to **10** and only *ca*. 65% conversion is achieved after 17 h. Interestingly, using these catalyst precursors the relative ratio of the products (1:1.25) is reversed depending on the metallacarborane substituent on the rhodacarborane. The ruthenacarborane substituents (**11**) promotes the formation of the silyl ether whereas the cobaltacarborane substituents (**12**) favours the silyl enol ether product. Again, no discernible differences can be noted between the two diastereomeric forms of each of the catalyst precursors.

From the initial reaction rates of the four heterometalated species, **11** is slow in comparison to **12**. Thus the trend of the most catalytically-active species is **XXX** > **VIII** >> **10** > **12** > **11**. From the data, it is clear the single-cage analogues are superior catalyst precursors for hydrosilylation. Therefore, we tentatively postulate the diminished activity of the bis(carborane) derivatives is primarily due to the additional bulky substituent.

Interestingly, the trend observed for these bis(carborane) derivatives is reversed to that from the isomerisation of 1-hexene since **10** is now the most active of the five compounds. Thus, the ranking of the substituent for a 2,1,8-RhC_2B_9 cage is carborane > cobaltacarborane > ruthenacarborane. The trend distinguished suggests that the substituent has a reverse effect in the hydrosilylation of acetophenone compared to alkene isomerisation. This is not unexpected as these processes proceed by different mechanisms.

Disappointingly, the additional carborane/metallacarborane substituents bound to the rhodacarborane cage appears to hinder the hydrosilylation of acetophenone. However, the reactivity is not completely lost and an evident trend can be observed between the substituents suggesting further tuning of the catalyst precursor is possible.

4.5 Computational Insights into the Mechanisms

Density Functional Theory (DFT) calculations were performed (by Prof. S. A. Macgregor, Heriot-Watt University) on **VIII** and several key intermediates in attempts to further understand the possible mechanism for the two catalytic reactions described and potentially rationalise the observed rate trends. Since the initial report of **VIII**, kinetic and deuterium labelling studies were performed to elucidate the nature of the active catalyst as well as the potential catalytic mechanisms.[3,4] Ultimately, the isomeric form **X** was concluded to be the active catalyst for the isomerisation of alkenes where the hydride, sourced from the cage, allows the reaction to proceed *via* the typical migratory insertion/*β*-H transfer pathway (Figure 4.8). However, since these reports in the 1980's, further investigation into these catalytic species has been sparse and no additional mechanistic studies have been undertaken.

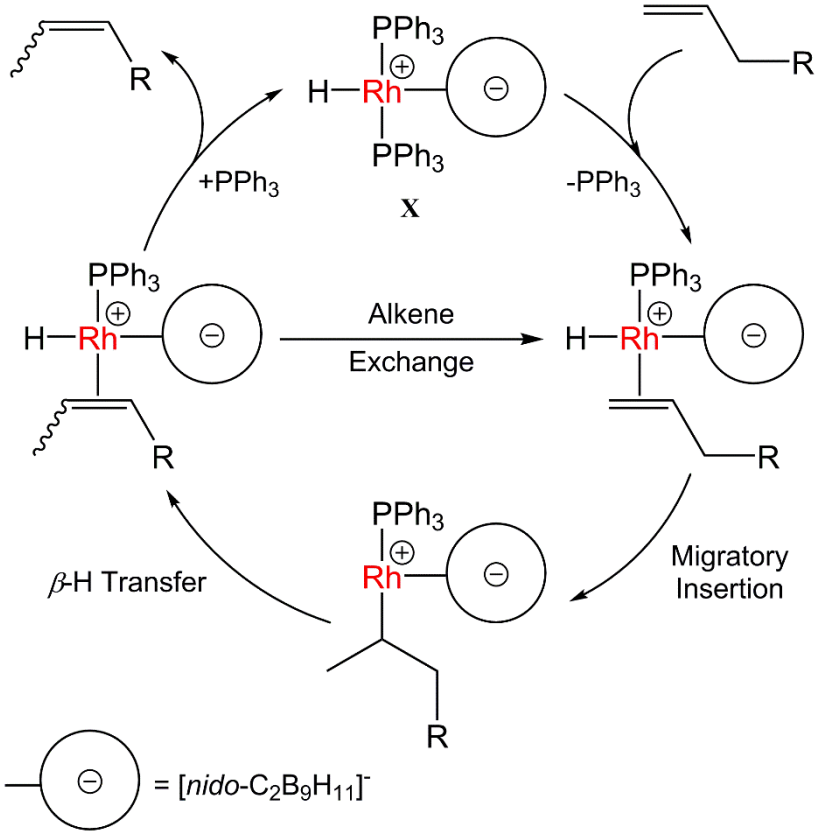

Figure 4.8 Postulated mechanism for the isomerisation of alkenes where **X** is the catalytically-active species.

Prior to investigating the isomerisation mechanism, the relative energies of the precursor **VIII** and its isomeric forms **IX** and **X** must be determined. The optimised structure of **VIII** [using ωB97x-D(DCM/BS2)//BP86(BS1)] was set as the zero point energy at 0.0 kcal/mol (Figure 4.9). The exo-*nido* tautomer **IX** was found to be a local minimum at +2.1 kcal/mol but no discernible pathway for its formation from **VIII** could be established. More importantly, no minimum could be determined for the B–H oxidative addition product **X**. When optimising geometry **X**, the molecule reverts back to **IX** suggesting that **X**, if formed, will likely be an incredibly short-lived species.

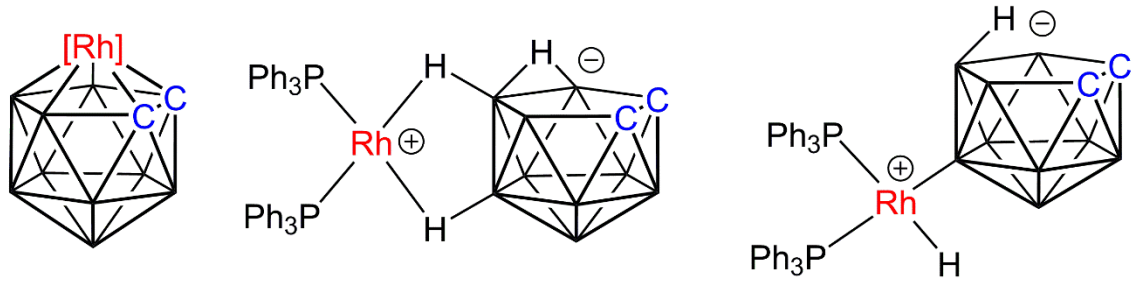

VIII 0.0 **IX** +2.1 **X** No Minimum Found

[Rh] = $Rh(PPh_3)_2H$
Free energies in kcal/mol

Figure 4.9 The proposed exo-*nido* tautomer (**IX**) and B–H oxidative addition product (**X**) formed from the closo rhodacarborane precursor **VIII** and their respective computed free energies.

This is in agreement with the conclusions drawn by Hawthorne where **X** is postulated to be a highly reactive species formed in trace quantities. Although the concentration of **X** is minimal, the subsequently formed Rh(alkene) intermediate is predicted to be a relatively stable species, capable of turning over 50-100 molecules before reverting back to **X** and subsequently **IX** and **VIII**.[4]

The equivalent exo-*nido* tautomer of the 2,1,12-RhC_2B_9 species (**XXXI**) was also optimised and was found to have an energy of +31.6 kcal/mol relative to the optimised structure of **XXX** (Figure 4.10). This suggests the tautomerisation is restricted to the 3,1,2-isomer and the alkene isomerisation catalysed by **XXX** likely proceeds by a different mechanism to that catalysed by **VIII**. The relatively high energy for **XXXI** is expected as the CB_4 face is a stronger donor than the C_2B_3 face. This is reflected in the computed Natural Bond Orbital (NBO) charge of the rhodium atoms where **XXX** (-0.166) is significantly lower than **VIII** (-0.120), thus effectively lowering the zero point energy of **XXX** as opposed to raising the energy of **XXXI**. Again, no minimum could be determined for the B–H oxidative addition product.

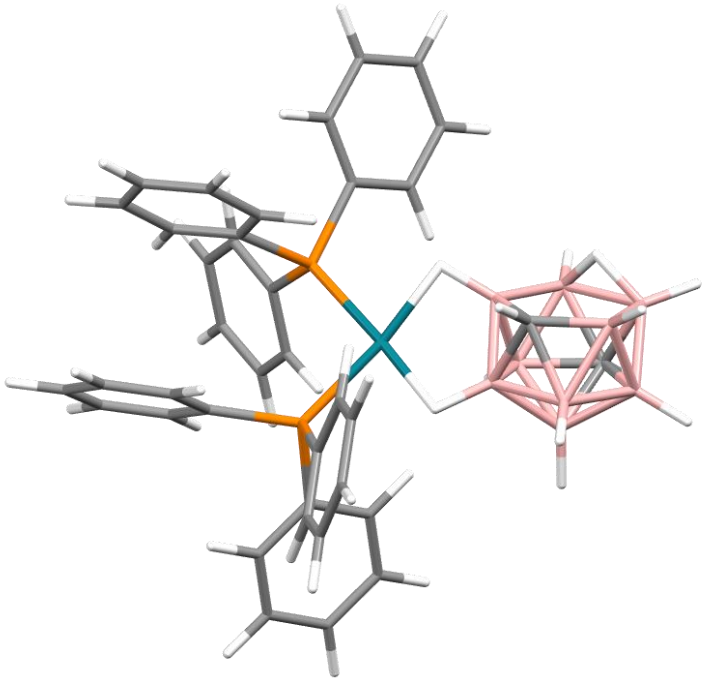

Figure 4.10 Optimised structure of the exo-*nido* tautomer [4,8-{$Rh(PPh_3)_2$}-4,8-μ-$(H)_2$-*nido*-2,9-$C_2B_9H_{12}$] (**XXXI**) with a free energy of +31.6 kcal/mol relative to **XXX**.

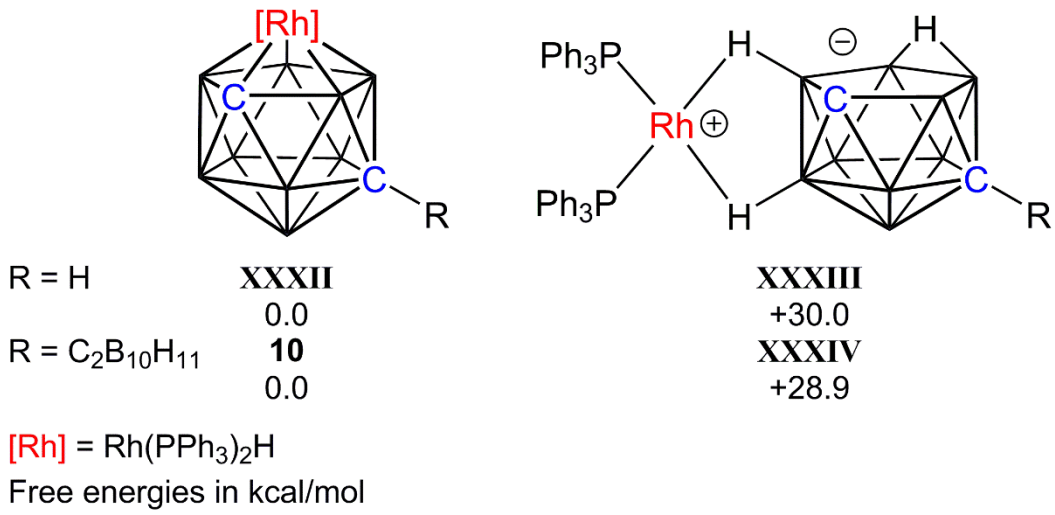

Figure 4.11 The optimised free energies of the 2,1,8-rhodacarboranes and their proposed exo-*nido* tautomers.

Similarly, the optimised exo-*nido* tautomers of both compound **10** and its theoretical 2,1,8-RhC_2B_9 single-cage analogue (**XXXII)** were found to have a relative free energy of *ca.* +30 kcal/mol (Figure 4.11). The slightly lower energy of **XXXIV** relative to **XXXIII** is likely due to stabilisation of the negative charge by the electron-withdrawing *C*-bound carboranyl substituent. This is supported by a subtle difference in the rhodium atom NBO charges of **10** and **XXXII** (-0.161 and -0.164, respectively). Again, the high energies of **XXXIII** and **XXXIV** imply that the catalytic cycles for **10** (and by extension **11** and **12**) likely do not proceed *via* exo-*nido* intermediates.

As the proposed active catalyst **X** could not be calculated, the catalytic cycles involving it could not be explored computationally. However, given the relatively high energy of **XXXI**, **XXXIII** and **XXXIV**, the alkene isomerisation cycle was considered using the closo precursor as a starting point and propene as a substrate to minimise computational demands (Figure 4.12). From **VIII**, loss of a PPh_3 (**A**) followed by coordination of propene affords intermediate **B** with an energy of +15.7 kcal/mol. Migratory insertion of the propene into the Rh–H bond to form the Rh(alkyl) intermediate **C**, which possesses an agostic interaction, affords a product which is slightly higher in energy at +17.6 kcal/mol. The products of subsequent isomerisation/rotation of the alkyl component (**D**) followed by *β*-H transfer (**E**) have not been formally optimised but the relative energies are presumed to be identical to **C** and **B** respectively.

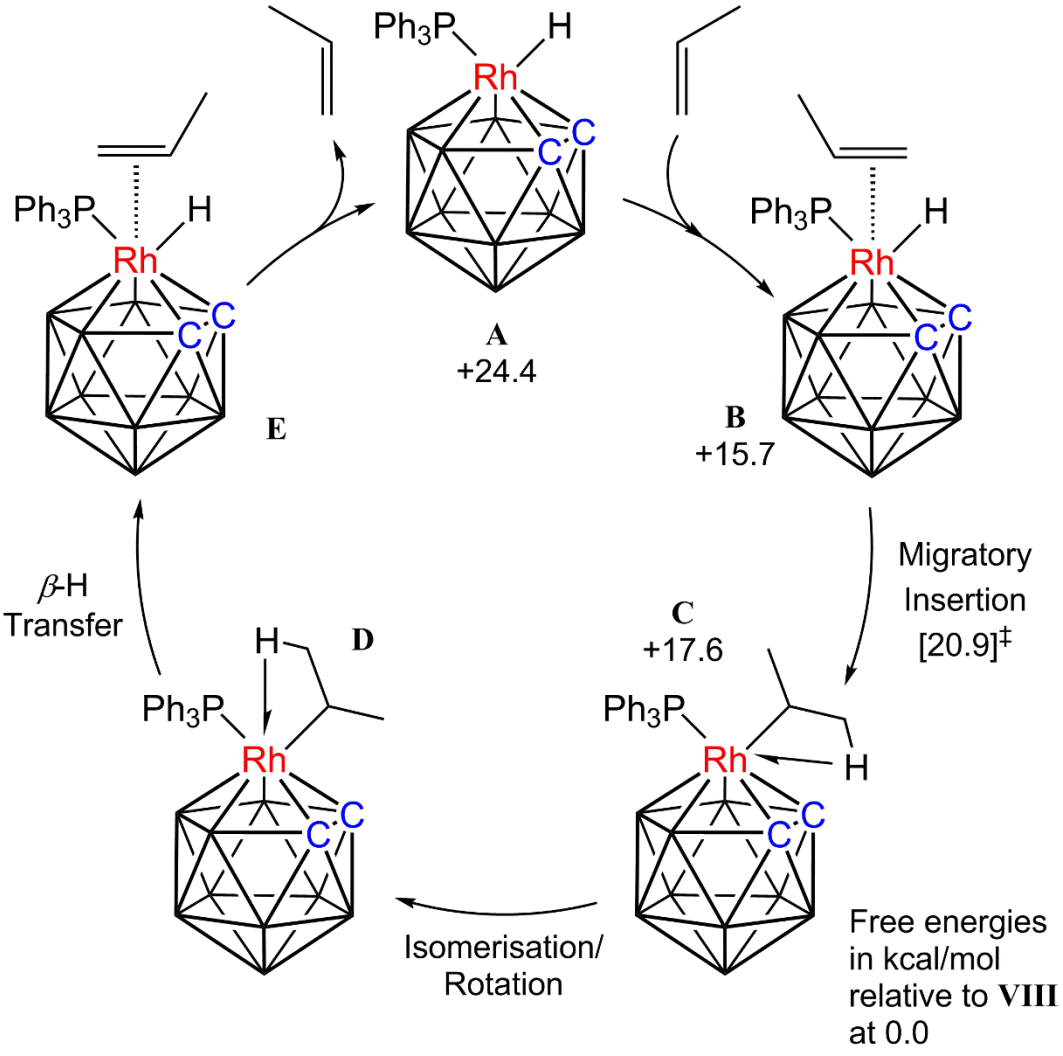

Figure 4.12 Proposed alkene isomerisation mechanisms with free energies of select key intermediates determined.

This pathway describes the conventional alkene isomerisation mechanism when employing a metal-hydride catalyst and the energies of the computed intermediates (**A** and **B**) are within sensible limits. The migratory insertion is typically the rate-limiting step, possessing the highest energy barrier. This transition state **TS(B-C)** (Figure 4.13) was found to have an energy of +20.9 kcal/mol, lower than the optimised intermediate **A**, suggesting that this is an energetically viable pathway.

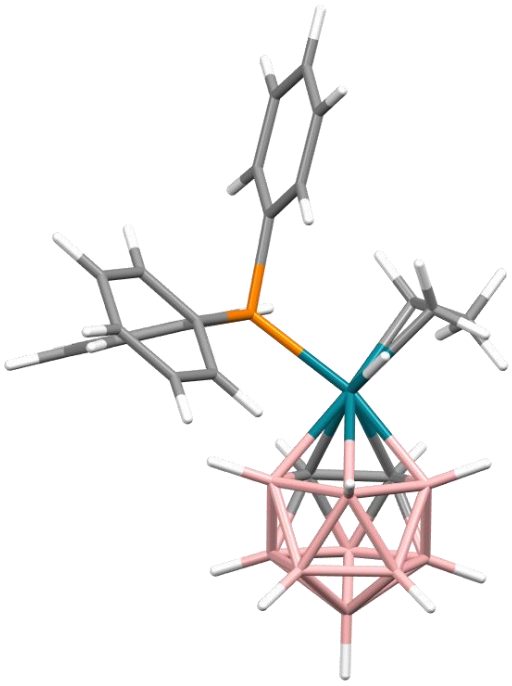

Figure 4.13 The optimised structure of the transition state between intermediates **B** and **C**, **TS(B-C)**, with a free energy of +20.9 kcal/mol.

The equivalent intermediates and transition states were also optimised (where possible) starting from **XXX**, **XXXII** and **10** (Table 4.4). Minimal differences in energies are observed in both intermediates **A** and **B** but the transition states **TS(B-C)** in all three cases are significantly higher in energy than **VIII**–**TS(B-C)**.

Catalyst Precursor	**A (kcal/mol)**	**B (kcal/mol)**	**TS(B-C) (kcal/mol)**	**Exo-*nido* tautomer (kcal/mol)**
VIII	+24.4	+15.7	[20.9]‡	+2.1
XXX	+23.4	+17.8	[25.2]‡	+31.6
XXXII	+21.3	+17.5	[25.4]‡	+30.0
10	+24.3	-	[27.1]‡	+28.9

Table 4.4 Optimised free energies of **A**, **B**, **TS(B-C)** and exo-*nido* tautomer from catalyst precursors **VIII**, **XXX**, **XXXII** and **10**.

Despite the inflated transition state energies, these are still lower than those of the optimised exo-*nido* tautomers. This suggests that catalyst precursors **XXX**, **XXXII** and **10** are more likely to react in their closo forms as opposed to their zwitterionic tautomers.

The lower **TS(B-C)** energy from **XXX** compared to that from **10** is also consistent with the rates observed experimentally where **XXX** is the superior catalyst precursor for the isomerisation of 1-hexene. From the computational results, **VIII** is predicted to be the most effective catalyst as it possesses the lowest **TS(B-C)** energy. However, **VIII** was actually the slowest catalyst precursor tested experimentally. The highest energy in the proposed catalytic cycle for **VIII** is that of intermediate **A** (+24.4 kcal/mol), which is marginally the highest energy found for **A** in all four cases. This suggests that the loss of PPh_3 is likely the rate-determining step for **VIII** when following the proposed catalytic cycle. Due to limited data involving the transition states surrounding **A**, no further comparisons can be drawn but it is likely these barriers exceed the optimised energies of intermediate **A**.

Additionally, compound **VIII** is the only catalyst precursor found to have an accessible exo-*nido* tautomer. Although no minima could be determined for the proposed active catalyst **X**, the exo-*nido* species is still a viable starting point for catalysis. Studies utilising [3-D-3,3-$(PPh_3)_2$-*closo*-3,1,2-$RhC_2B_9H_{11}$] displayed partial loss of the deuterium label in the isomerisation of 1-hexene, recovering 35% of the catalyst precursor unchanged following full conversion to 2-hexenes using a 5.2 mol% catalyst loading.[3] Thus, *ca.* 55 molecules of 1-hexene are isomerised for each deuterium atom lost, from which Hawthorne concludes minimal involvement of the hydride in the isomerisation process. But the fact that partial loss is observed implies the proposed catalytic cycle of Figure 4.12 must be occurring as well as a secondary mechanism which protects the hydride, such as that *via* the exo-*nido* tautomer.

However, in a subsequent publication, Hawthorne states no exchange of the deuterium is noted in the same experiment which led to the postulation of **X** as the sole active catalyst.[4] Given the ambiguity of the deuterium-scrambling experiment, a definitive conclusion cannot be reached but it is plausible that **VIII** could access both possible pathways.

Thus, the relatively slow reaction rate of **VIII** in the isomerisation of 1-hexene is tentatively rationalised by the potentially higher barrier required to access the proposed cycle (Figure 4.12) and the possibility of alternative mechanisms *via* the exo-*nido* intermediate **IX**. Further studies are required to fully elucidate the mechanisms for the isomerisation of 1-hexene and rationalise the observed trend in reaction rates between the seven catalyst precursors.

Preliminary calculations into the hydrosilylation of acetophenone have proven to be far more challenging given the additional complexity of the reaction. The high energy of the exo-*nido* tautomers is consistent with the elevated temperatures required for the reaction to proceed. However, due to the number of possible subsequent steps and their various configurations, a full proposed mechanism is yet to be established.

In summary, DFT studies have shown that the reactivity of the original rhodacarborane **VIII** may not be as simple as previously thought, potentially capable of catalysing the isomerisation the alkenes in both closo and exo-*nido* forms. However, all isomeric forms bearing a CB_4 face bound to the rhodium vertex cannot access their exo-*nido* tautomers under ambient conditions. Thus, these must react in their closo forms, contrary to the accepted assumption that they are analogous to **VIII**.

4.6 References

1. T. E. Paxson and M. F. Hawthorne, *J. Am. Chem. Soc.*, 1974, **96**, 4674-4676.

2. V. N. Lebedev, E. V. Balagurova, F. M. Dolgushin, A. I. Yanovskii and L. I. Zakharkin, *Russ. Chem. Bull.*, 1997, **46**, 550-558.

3. P. E. Behnken, J. A. Belmont, D. C. Busby, M. S. Delaney, R. E. King III, C. W. Kreimendahl, T. B. Marder, J. J. Wilczynski and M. F. Hawthorne, *J. Am. Chem. Soc.*, 1984, **106**, 3011-3025.

4. J. A. Belmont, J. Soto, R. E. King III, A. J. Donaldson, J. D. Hewes and M. F. Hawthorne, *J. Am. Chem. Soc.*, 1989, **111**, 7475-7486.

5. H. C. Kang and M. F. Hawthorne, *Organometallics*, 1990, **9**, 2327-2332.

6. M. S. Delaney, C. B. Knobler and M. F. Hawthorne, *Inorg. Chem.*, 1981, **20**, 1341-1347.

7. C. B. Knobler, T. B. Marder, E. A. Mizusawa, R. G. Teller, J. A. Long, P. E. Behnken and M. F. Hawthorne, *J. Am. Chem. Soc.*, 1984, **106**, 2990-3004.

8. D. C. Busby and M. F. Hawthorne, *Inorg. Chem.*, 1982, **21**, 4101-4103.

Chapter 5

Experimental

5.1 General Experimental

Synthesis

All experiments were performed using standard Schlenk techniques where dry, oxygen-free N_2 was the inert gas source. Subsequent manipulations were occasionally carried out in the open laboratory. Solvents were freshly distilled prior to use from their appropriate drying agents; Na wire (THF, Et_2O and petroleum ether 40-60 °C) or CaH_2 (DCM and MeCN). Deuterated solvents [$CDCl_3$, CD_2Cl_2, $(CD_3)_2CO$ and CD_3CN] and toluene were stored over 4 Å molecular sieves. Reaction solvents were degassed (3 × freeze-pump-thaw cycles) immediately before use.

Chromatography

Column chromatography was performed using 60 Å silica as the stationary phase with the appropriate eluent. Preparative TLC employed 20 × 20 cm Kieselgel F_{254} glass plates where multiple runs were periodically required to achieve complete separation. All appropriate crude reaction mixtures were passed through a 60 Å silica plug prior to chromatography.

Analysis

NMR spectra at 400.1 MHz (^{1}H), 128.4 MHz (^{11}B) or 162.0 MHz (^{31}P) were recorded on a Bruker DPX-400 spectrometer from appropriate deuterated solutions at 298 K. Electron Impact Mass Spectrometry (EIMS) and ElectroSpray Ionisation Mass Spectrometry (ESIMS) were carried out using a Finnigan MAT900XP-Trap spectrometer and Bruker MicroTOF Focus II spectrometer, respectively, at the University of Edinburgh. Elemental analyses were performed using an Exeter CE-440 elemental analyser.

Crystallography

General methodologies for crystal growth employed solvent diffusion, vapour diffusion or slow evaporation. Intensity data from diffraction-quality single crystals were collected at 100 K (unless otherwise specified) on a Bruker X8 APEXII diffractometer (Mo Kα), Rigaku Oxford Diffraction Supernova diffractometer (Mo Kα), Rigaku FR-E+ diffractometer (Mo Kα), Rigaku 007-HF diffractometer (Cu Kα) or Bruker D8 Venture diffractometer (Mo Kα). The specific crystallisation approach and diffractometer used for each compound will be detailed in their experimental section. Using Olex2,[1] structures were solved by direct methods using the SHELXS[2] or SHELXT[3] program and refined by full-matrix least-squares using SHELXL.[4] Refinement was completed with all non-hydrogen atoms assigned anisotropic displacement parameters. Cage C atoms were identified by independent application of VCD and BHD methods with the exception of **12*α*** and **12*β*** where only the VCD approach was applied.[5-7] H atoms bound to cage B or cage C atoms were allowed positional refinement (unless otherwise specified). Electron density corresponding to the hydride ligands in **10**, **11*α***, **11*β***, **12*α***, **12*β*** and **XXX** was observed but only refinement of **10** and **XXX** produced a sensible model. Thus the hydride ligand in the remaining four species were refined with the following restraints adopted from **10**: Rh–H 1.58(2) Å and P···H 2.55(2) Å. All other H atoms were treated as riding on their respective atoms: $C_{primary}$–H 0.98 Å, $C_{secondary}$–H 0.99 Å, $C_{tertiary}$–H 1.00 Å, C_{arene}–H 1.00 Å, C_{Cp}–H 1.00 Å, C_{phenyl}–H 0.95 Å, and B/C_{cage}–H 1.12 Å.

Starting Materials

Literature methods or slight variations thereof were used to prepare 1,1′-bis(*o*-carborane),[8] [Ru(*p*-cymene)Cl_2]$_2$,[9] [8-(1′-*closo*-1′,2′-$C_2B_{10}H_{11}$)-2-(*p*-cymene)-*closo*-2,1,8-$RuC_2B_9H_{10}$] (**XVII**),[10] [8-(1′-*closo*-1′,2′-$C_2B_{10}H_{11}$)-2-Cp-*closo*-2,1,8-$CoC_2B_9H_{10}$],[10] [$HNMe_3$][7-(1′-*closo*-1′,2′-$C_2B_{10}H_{11}$)-*nido*-7,8-$C_2B_9H_{11}$] ([$HNMe_3$][**XI**]),[11] [Rh(PPh_3)$_3$Cl],[12] [3-H-3,3-(PPh_3)$_2$-*closo*-3,1,2-$RhC_2B_9H_{11}$] (**VIII**),[13] and [2-H-2,2-(PPh_3)$_2$-*closo*-2,1,12-$RhC_2B_9H_{11}$] (**XXX**).[14] All other reagents were supplied commercially and used as received.

5.2 Synthesis of [HNMe$_3$][8-(7′-*nido*-7′,8′-$C_2B_9H_{11}$)-2-(*p*-cymene)-*closo*-2,1,8-$RuC_2B_9H_{10}$] (1)

Compound **XVII** (0.200 g, 0.392 mmol) and KF (0.114 g, 1.962 mmol) were dissolved in a mixture of THF (50 mL) and deionised water (5 mL) and the solution was heated to reflux overnight. Following cooling to room temperature, solvents were removed *in vacuo* and the resultant white residue re-dissolved in deionised water (20 mL) and filtered. To the filtrate was added an aqueous solution of excess NMe_3.HCl which immediately resulted in the precipitation of a white solid. This was collected by filtration, washed with water and dried *in vacuo* and subsequently identified as [HNMe$_3$][8-(7′-*nido*-7′,8′-$C_2B_9H_{11}$)-2-(*p*-cymene)-*closo*-2,1,8-$RuC_2B_9H_{10}$] (**1**). The product exists as an equimolar mixture of diastereoisomers.

[HNMe$_3$][8-(7′-*nido*-7′,8′-C$_2$B$_9$H$_{11}$)-2-(*p*-cymene)-*closo*-2,1,8-RuC$_2$B$_9$H$_{10}$] (1)

Yield: 0.188 g, 86%.

CHN: $C_{17}H_{45}B_{18}NRu$ requires C 36.5, H 8.11, N 2.50%.

Found for **1** C 35.6, H 8.23, N 3.06%.

NMR: **^{1}H NMR [(CD$_3$)$_2$CO],** essentially equimolar mixture of diastereoisomers; δ 6.00-5.87 [m, 4H+4H, $CH_3C_6H_4CH(CH_3)_2$], 3.21 [s, 18H, $HN(CH_3)_3$], 2.79 [overlapping app. sept, 1H+1H, $CH_3C_6H_4CH(CH_3)_2$], 2.64 (br. s, 1H+1H, C1*H*), 2.26 [s, 3H+3H, $CH_3C_6H_4CH(CH_3)_2$], 1.93 (br. s, 1H+1H, C8′*H*), 1.30-1.27 [overlapping pairs of d, 6H+6H, $CH_3C_6H_4CH(CH_3)_2$], -2.66 (1H) and -2.81 (1H) (overlapping br. singlets, μ-*H*).

^{11}B{^{1}H} NMR [(CD$_3$)$_2$CO], δ -1.1 (1B), -2.8 (2B), -4.9 (1B), -7.9 (1B), -10.2 (3B), -13.8 (2B), -16.7 (2B), -19.5 (1B), -21.0 (2B), -25.5 (1B), -33.5 (1B), -35.9 (1B).

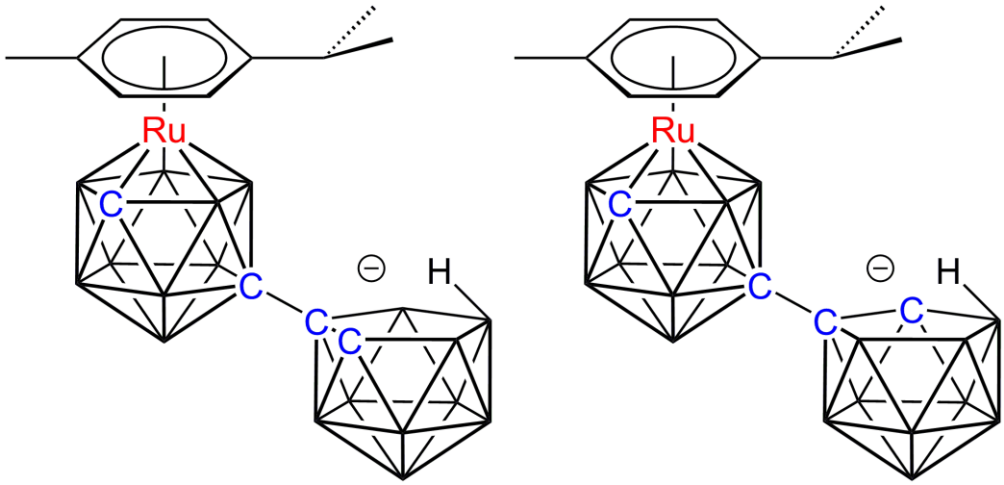

*Cation not shown.

5.3 Synthesis of *α*-[8-(1′-3′-Cp-*closo*-3′,1′,2′-$CoC_2B_9H_{10}$)-2-(*p*-cymene)-*closo*-2,1,8-$RuC_2B_9H_{10}$] (2*α*) and *β*-[8-(1′-3′-Cp-*closo*-3′,1′,2′-$CoC_2B_9H_{10}$)-2-(*p*-cymene)-*closo*-2,1,8-$RuC_2B_9H_{10}$] (2*β*)

^{n}BuLi (0.15 mL of a 2.5 M solution, 0.375 mmol) was added dropwise to a cooled (0 °C) solution of **1** (0.100 g, 0.179 mmol) in THF (20 mL) and the reagents stirred at room temperature for 0.5 h to produce a yellow solution. The mixture was frozen at -196 °C and $CoCl_2$ (0.081 g, 0.624 mmol) and NaCp (0.27 mL of a 2.0 M solution, 0.540 mmol) were added. Upon thawing, the reaction mixture was stirred overnight at room temperature. Following aerial oxidation (0.5 h), solvents were removed *in vacuo* and the residue was purified by column chromatography using a DCM:petrol eluent (1:1) to afford a mobile orange band. The crude product was further purified by preparative TLC using the same eluent system to yield two distinct mobile orange bands subsequently identified as two diastereoisomers of [8-(1′-3′-Cp-*closo*-3′,1′,2′-$CoC_2B_9H_{10}$)-2-(*p*-cymene)-*closo*-2,1,8-$RuC_2B_9H_{10}$] (**2**).

α-[8-(1′-3′-Cp-*closo*-3′,1′,2′-$CoC_2B_9H_{10}$)-2-(*p*-cymene)-*closo*-2,1,8-$RuC_2B_9H_{10}$] (2α)

Yield: 0.024 g, 22%. **R_f:** 0.51

CHN: $C_{19}H_{39}B_{18}CoRu$ requires C 36.7, H 6.32%.

Found for **2α** C 37.3, H 6.77%.

EIMS: Envelope centred on *m/z* 622 (M^+).

[MW = 622.11 g mol^{-1}]

NMR: **^{1}H NMR [$CDCl_3$],** δ 5.93-5.82 [m, 4H, $CH_3C_6H_4CH(CH_3)_2$], 5.80 (s, 5H, C_5H_5), 4.27 (br. s, 1H, C2′*H*), 2.81 [app. sept, 1H, $CH_3C_6H_4CH(CH_3)_2$], 2.63 (br. s, 1H, C1*H*), 2.32 [s, 3H, $CH_3C_6H_4CH(CH_3)_2$], 1.31 [d, 3H, $CH_3C_6H_4CH(CH_3)_2$], 1.29 [d, 3H, $CH_3C_6H_4CH(CH_3)_2$].

^{11}B{^{1}H} NMR [$CDCl_3$], δ 5.2 (1B), 2.3 (1B), -0.9 to -10.0 multiple overlapping resonances with maxima at -0.9, -3.8, -5.2, -6.8, -8.5, -10.0 (total integral 11B), -14.6 (2B), -16.2 (1B), -17.9 (1B), -20.7 (1B).

SC*X*RD: Orange block crystals of **2α** grown by diffusion of a DCM solution and petrol at -20 °C and diffraction data were collected on a Rigaku 007-HF diffractometer (Cu Kα).

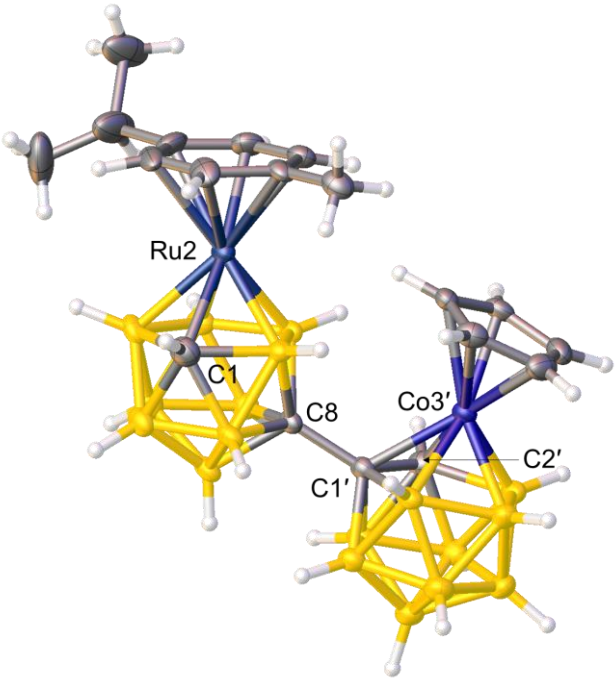
Ru2
C1
C8
Co3′
C2′
C1′

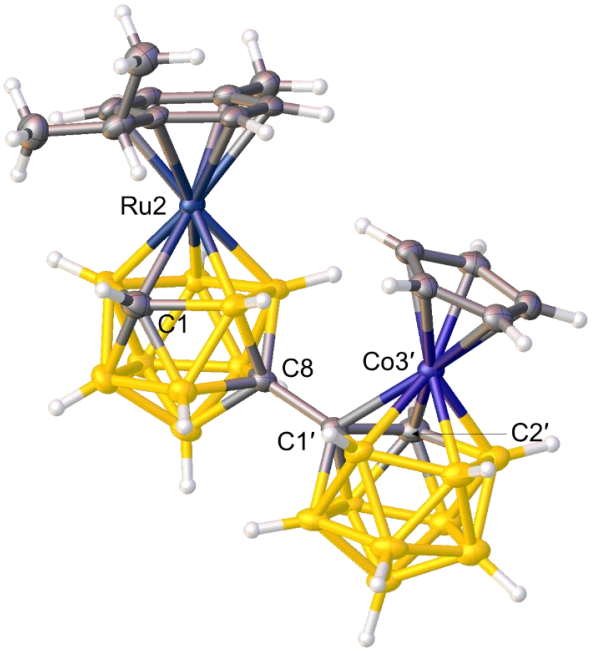
Ru2
C1
C8
Co3′
C2′
C1′

***β*-[8-(1′-3′-Cp-*closo*-3′,1′,2′-$CoC_2B_9H_{10}$)-2-(*p*-cymene)-*closo*-2,1,8-$RuC_2B_9H_{10}$] (2*β*)**

Yield: 0.027 g, 24%. ***R*f:** 0.56

CHN: $C_{19}H_{39}B_{18}CoRu$ requires C 36.7, H 6.32%.

Found for **2*β*** C 35.9, H 6.65%.

EIMS: Envelope centred on *m/z* 622 (M^+).

[MW = 622.11 g mol^{-1}]

NMR: **^{1}H NMR [$CDCl_3$],** δ 5.93-5.80 [m, 4H, $CH_3C_6H_4CH(CH_3)_2$], 5.82 (s, 5H, C_5H_5), 4.12 (br. s, 1H, C2′*H*), 2.79 [app. sept, 1H, $CH_3C_6H_4CH(CH_3)_2$], 2.63 (br. s, 1H, C1*H*), 2.31 [s, 3H, $CH_3C_6H_4CH(CH_3)_2$], 1.30 [d, 3H, $CH_3C_6H_4CH(CH_3)_2$], 1.28 [d, 3H, $CH_3C_6H_4CH(CH_3)_2$].

^{11}B{^{1}H} NMR [$CDCl_3$], δ 5.0 (1B), 2.2 (1B), -0.9 to -10.4 multiple overlapping resonances with maxima at -0.9, -3.9, -5.6, -7.5, -8.7, -10.4 (total integral 11B), -14.6 (2B), -16.5 (1B), -17.4 (1B), -20.7 (1B).

SC*X*RD: Orange block crystals of **2*β***·0.5CH_2Cl_2 grown by diffusion of a DCM solution and petrol at -20 °C and diffraction data were collected on a Bruker X8 APEXII diffractometer (Mo Kα).

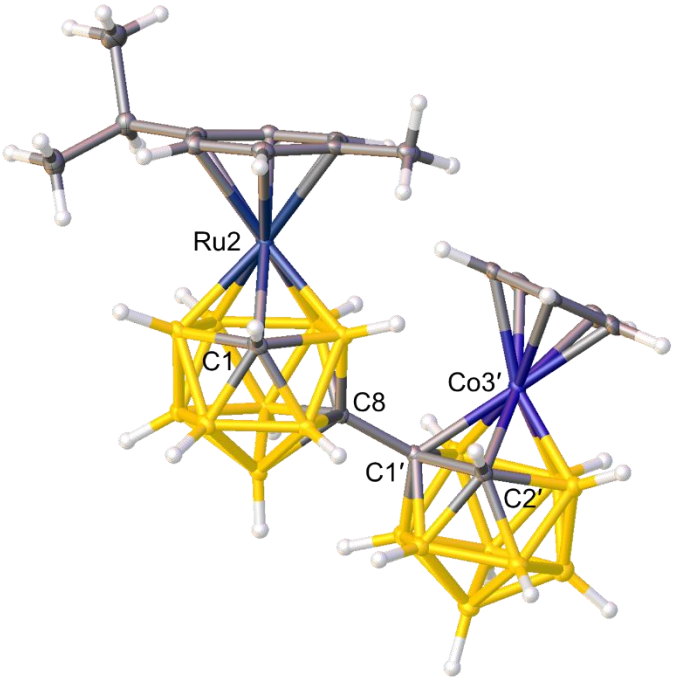
Ru2
C1
C8
Co3′
C1′
C2′

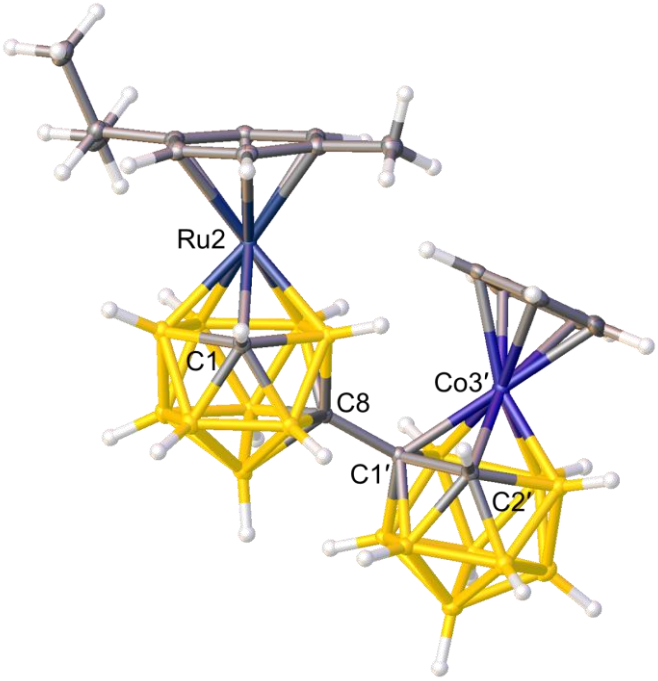
Ru2
C1
C8
Co3′
C1′
C2′

5.4 Synthesis of [HNMe$_3$][8-(7′-*nido*-7′,8′-$C_2B_9H_{11}$)-2-Cp-*closo*-2,1,8-$CoC_2B_9H_{10}$] (3)

Analogous to the preparation of **1**, [8-(1′-*closo*-1′,2′-$C_2B_{10}H_{11}$)-2-Cp-*closo*-2,1,8-$CoC_2B_9H_{10}$] (0.200 g, 0.502 mmol) was deboronated with KF (0.146 g, 2.513 mmol) in THF/water and then methathesised with NMe_3.HCl to afford the product, [HNMe$_3$][8-(7′-*nido*-7′,8′-$C_2B_9H_{11}$)-2-Cp-*closo*-2,1,8-$CoC_2B_9H_{10}$] (**3**), as a yellow solid. Likewise, the product exists as an equimolar mixture of diastereoisomers.

[HNMe$_3$][8-(7′-*nido*-7′,8′-C$_2$B$_9$H$_{11}$)-2-Cp-*closo*-2,1,8-CoC$_2$B$_9$H$_{10}$] (3)

Yield: 0.192 g, 84%

CHN: $C_{12}H_{36}B_{18}CoN$ requires C 32.2, H 8.11, N 3.13%

Found for **3** C 32.3, H 8.18, N 3.01%

NMR: **^{1}H NMR [(CD$_3$)$_2$CO],** essentially equimolar mixture of diastereoisomers; δ 5.50 (s, 5H, C$_5$*H*$_5$), 5.49 (s, 5H, C$_5$*H*$_5$), 3.19 [s, 18H, HN(C*H*$_3$)$_3$], 2.84 (br. s, 1H+1H, C1*H*), 1.88 (br. s, 1H+1H, C8′*H*), -2.70 (1H) and -2.85 (1H) (overlapping br. singlets, μ-*H*).

^{11}B{^{1}H} NMR [(CD$_3$)$_2$CO], δ -0.4 (3B), -1.2 (1B), -5.9 (2B), -9.6 (1B), -10.1 (1B), -12.7 (1B), -14.1 (2B), -17.3 (2B), -18.3 (1B), -20.4 (1B), -24.3 (1B), -33.3 (1B), -35.7 (1B).

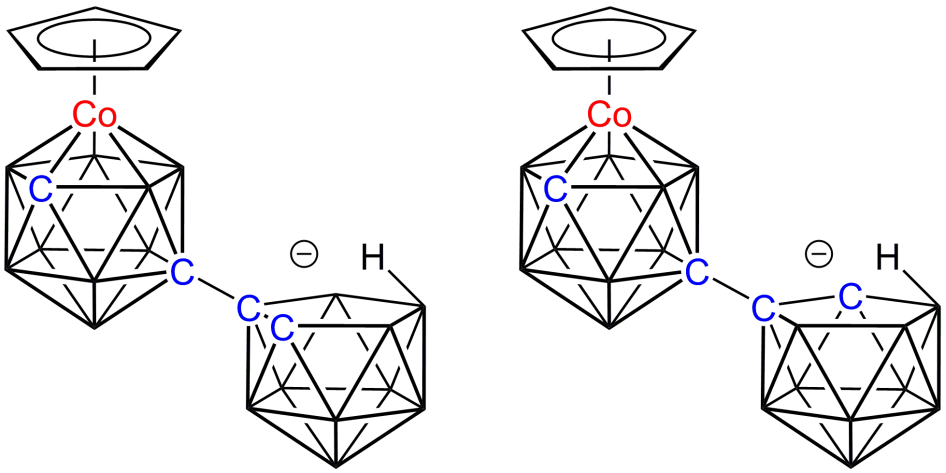

*Cation not shown.

5.5 Synthesis of [1-(1′-*closo*-1′,2′-$C_2B_{10}H_{11}$)-3-Cp*-*closo*-3,1,2-$CoC_2B_9H_{10}$] (4), [8-(1′-*closo*-1′,2′-$C_2B_{10}H_{11}$)-2-Cp*-*closo*-2,1,8-$CoC_2B_9H_{10}$] (5), and [12-(1′-*closo*-1′,2′-$C_2B_{10}H_{11}$)-4,5-Cp^*_2-*closo*-4,5,1,12-$Co_2C_2B_9H_{10}$] (6)

^{n}BuLi (0.60 mL of a 2.5 M solution, 1.500 mmol) was added dropwise to a cooled (0 °C) solution of [$HNMe_3$][**XI**] (0.250 g, 0.745 mmol) in THF (25 mL) and the products stirred for 1 h at room temperature. The pale yellow solution was then frozen at -196 °C, and $CoCl_2$ (0.320 g, 2.465 mmol) and NaCp* (4.2 mL of a 0.5 M solution, 2.100 mmol) were added. Upon thawing, the reaction mixture was stirred overnight at room temperature. Following aerial oxidation (0.5 h), the volatiles were removed *in vacuo* and the residue purified by column chromatography using a DCM:petrol eluent (2:3) to afford red, yellow and green (trace) bands.

[1-(1′-*closo*-1′,2′-$C_2B_{10}H_{11}$)-3-Cp*-*closo*-3,1,2-$CoC_2B_9H_{10}$] (4)

Yield: 0.120 g, 34%. **R_f:** 0.41

CHN: $C_{14}H_{36}B_{19}Co$ requires C 35.9, H 7.74%.

Found for **4** C 35.8, H 7.83%.

EIMS: Envelope centred on *m/z* 469 (M^+).

[MW = 468.78 g mol^{-1}]

NMR: **^{1}H NMR [$CDCl_3$],** δ 4.10 (br. s, 1H, C2′*H*), 3.37 (br. s, 1H, C2*H*), 1.84 [s, 15H, $C_5(CH_3)_5$].

^{11}B{^{1}H} NMR [$CDCl_3$], δ 10.1 (1B), -1.9 (2B), -3.8 (4B), -6.0 (2B), -9.6 (6B), -12.4 (3B), -15.0 (1B).

SC*X*RD: Dark red block crystals of **4** grown by diffusion of a DCM solution and petrol at -20 °C and diffraction data were collected at 120 K on a Rigaku Oxford Diffraction SuperNova diffractometer (Mo Kα).

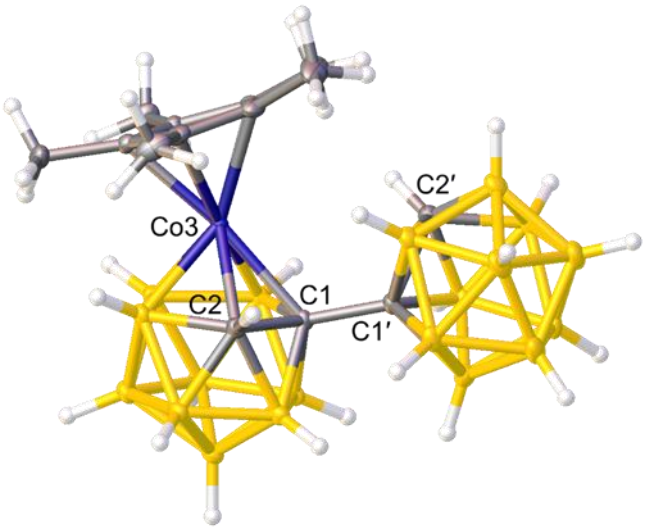

[8-(1′-*closo*-1′,2′-$C_2B_{10}H_{11}$)-2-Cp*-*closo*-2,1,8-$CoC_2B_9H_{10}$] (5)

Yield: 0.033 g, 9%. ***R*f:** 0.68

CHN: $C_{14}H_{36}B_{19}Co$ requires C 35.9, H 7.74%.

Found for **4** C 36.3, H 7.86%.

EIMS: Envelope centred on *m/z* 469 (M^+).

[MW = 468.78 g mol^{-1}]

NMR: **^{1}H NMR [$CHCl_3$:CD_3CN, 1:10],** δ 4.01 (br. s, 1H, C2′*H*), 2.09 (br. s, 1H, C1*H*), 1.84 [s, 15H, $C_5(CH_3)_5$].

^{11}B{^{1}H} NMR [$CDCl_3$], δ 3.2 (1B), 1.1 (2B), -2.6 (1B), -4.1 (2B), -4.9 (1B), -7.2 (1B), -9.9 (6B), -13.3 (2B), -13.9 (1B), -18.0 (1B), -18.6 (1B).

SC*X*RD: Dark yellow block crystals of **5** grown by diffusion of a DCM solution and petrol at -20 °C and diffraction data were collected at 120 K on a Rigaku Oxford Diffraction SuperNova diffractometer (Mo Kα).

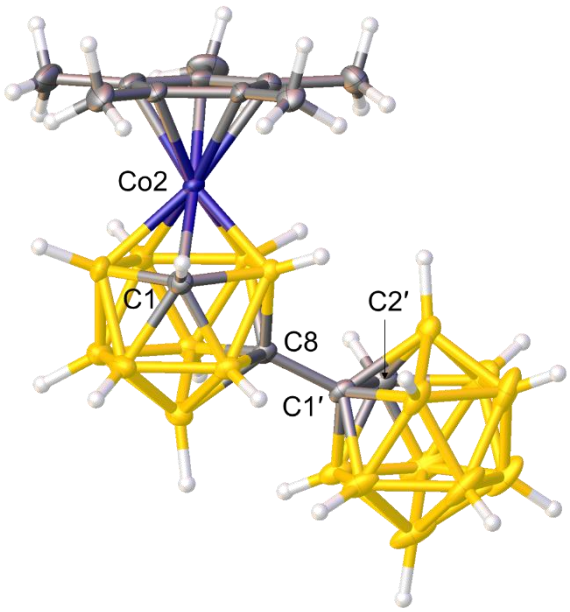

[12-(1′-*closo*-1′,2′-$C_2B_{10}H_{11}$)-4,5-Cp*$_2$-*closo*-4,5,1,12-$Co_2C_2B_9H_{10}$] (6)

Yield: 0.004 g, <1%. **R_f:** 0.31

CHN: Insufficient mass for elemental analyses

EIMS: Envelopes centred on *m/z* 663 (M^+) and 469 (M^+ - {CoCp*}).

[MW = 662.94 g mol^{-1}]

NMR: **^{1}H NMR [$CDCl_3$],** δ 3.80 (br. s, 1H, C2′*H*), 1.68 [s, 30H, $C_5(CH_3)_5$], 1.26 (br. s, 1H, C1*H*).

^{11}B{^{1}H} NMR [$CDCl_3$], δ 7.6 (1B), 3.0 (5B), -3.1 (2B), -4.7 (2B), -5.9 (1B), -10.6 (6B), -13.4 (2B).

SC*X*RD: Green needle crystals of **6**·$CHCl_3$ grown by slow evaporation of a $CHCl_3$ solution at room temperature and diffraction data were collected on a Bruker X8 APEXII diffractometer (Mo Kα).

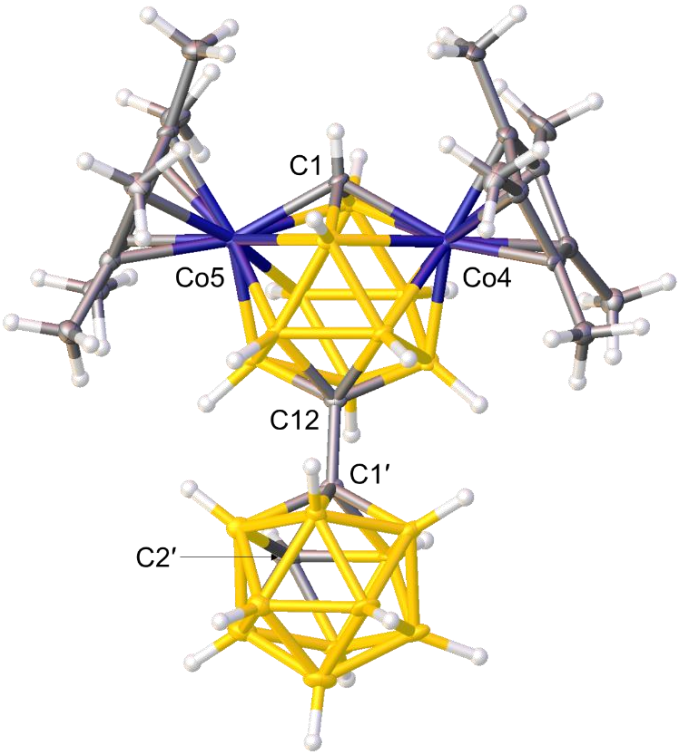

5.6 Isomerisation of 4 to 5

Redox Isomerisation

To a frozen solution of **4** (0.020 g, 0.043 mmol) in THF (10 mL) was added sodium naphthalenide (1 mL of a 0.043 M solution in THF, 0.043 mmol). The reagents were warmed to room temperature and stirred under N_2 for 1 h before being aerially oxidised (0.5 h). Purification by preparative TLC using a DCM:petrol eluent (2:3) afforded the starting material **4** and a yellow product identical to **5** by ^{1}H and $^{11}B\{^{1}H\}$ NMR spectroscopies.

Compound **4**

Yield: 0.008 g, 40%. ***R*f:** 0.40

Compound **5**

Yield: 0.009 g, 45%. ***R*f:** 0.65

Thermal Isomerisation

A solution of **4** (0.020 g, 0.043 mmol) in toluene (20 mL) was heated to reflux overnight to afford a yellow solution. Upon cooling, the volatiles was removed *in vacuo* and the crude product was purified by preparative TLC using a DCM:petrol eluent (2:3) to afford **5**, again confirmed by ^{1}H and $^{11}B\{^{1}H\}$ NMR spectroscopies.

Compound **5**

Yield: 0.018 g, 90%. ***R*f:** 0.67

5.7 Synthesis of [HNMe$_3$][8-(7′-*nido*-7′,8′-$C_2B_9H_{11}$)-2-Cp*-*closo*-2,1,8-$CoC_2B_9H_{10}$] (7)

Compound **5** (0.100 g, 0.213 mmol) and KF (0.062 g, 1.067 mmol) were dissolved in a THF/water mixture (55 mL, 10:1) and the resulting yellow solution was heated to reflux overnight. Following cooling, the volatiles were removed *in vacuo* and the residue re-dissolved in deionised water. The solution was then filtered and excess NMe_3.HCl was added to the filtrate produce a yellow precipitate. The solid was collected by filtration, washed with water and dried *in vacuo*. This was subsequently identified as [$HNMe_3$][8-(7′-*nido*-7′,8′-$C_2B_9H_{11}$)-2-Cp*-*closo*-2,1,8-$CoC_2B_9H_{10}$] (**7**) which exists as an equimolar mixture of diastereoisomers.

[HNMe$_3$][8-(7′-*nido*-7′,8′-C$_2$B$_9$H$_{11}$)-2-Cp*-*closo*-2,1,8-CoC$_2$B$_9$H$_{10}$] (7)

Yield: 0.078 g, 71%

CHN: $C_{17}H_{46}B_{18}CoN$ requires C 39.4, H 8.95, N 2.70%

Found for **7** C 40.2, H 8.81, N 2.75%

NMR: **^{1}H NMR [(CD$_3$)$_2$CO],** essentially equimolar mixture of diastereoisomers; δ 3.18 (s, 18H, HN(C*H*$_3$)$_3$), 1.96 (br. s, 1H+1H, C1*H*), 1.88 (br. s, 1H+1H, C8′*H*), 1.85 [s, 15H, C$_5$(C*H*$_3$)$_5$], 1.84 [s, 15H, C$_5$(C*H*$_3$)$_5$], -2.68 (1H) and -2.84 (1H) (overlapping br. singlets, μ-*H*).

^{11}B{^{1}H} NMR [(CD$_3$)$_2$CO], δ 1.3 (3B), -4.2 (2B), -7.1 (1B), -9.4 (1B), -10.1 (1B), -13.9 (3B), -17.2 (1B), -18.0 (1B), -19.1 (1B), -20.5 (1B), -24.3 (1B), -33.4 (1B), -35.7 (1B).

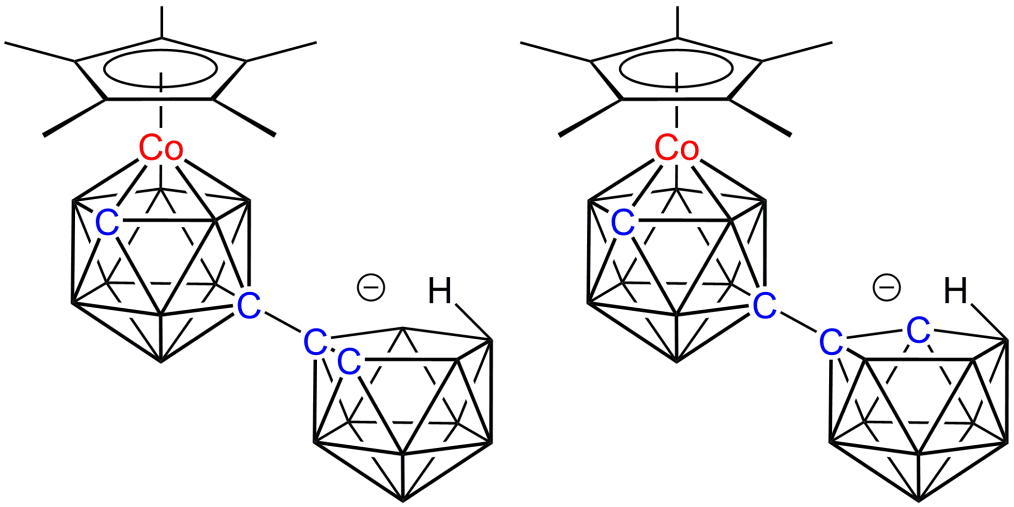

*Cation not shown.

5.8 Synthesis of [8-(1′-3′-(*p*-cymene)-*closo*-3′,1′,2′-$RuC_2B_9H_{10}$)-2-Cp*-*closo*-2,1,8-$CoC_2B_9H_{10}$] (8)

To an ice-cooled solution of **7** (0.100 g, 0.193 mmol) in THF (20 mL) was added ^{n}BuLi (0.17 mL of a 2.5 M solution, 0.425 mmol) dropwise. After warming to room temperature, the dark yellow solution was frozen at -196 °C and [Ru(*p*-cymene)Cl_2]$_2$ (0.059 g, 0.096 mmol) was added. The reaction mixture was thawed and stirred overnight at room temperature. The volatiles were removed *in vacuo* and the residue was purified by column chromatography using a DCM:petrol eluent (3:7) to afford a mobile yellow band subsequently identified as [8-(1′-3′-(*p*-cymene)-*closo*-3′,1′,2′-$RuC_2B_9H_{10}$)-2-Cp*-*closo*-2,1,8-$CoC_2B_9H_{10}$] (**8**). NMR spectroscopy reveals **8** to be a mixture of the two diastereoisomers in an approximate 2:1 ratio which, in spite of exhaustive chromatography, could not be separated.

[8-(1′-3′-(*p*-cymene)-*closo*-3′,1′,2′-RuC$_2$B$_9$H$_{10}$)-2-Cp*-*closo*-2,1,8-CoC$_2$B$_9$H$_{10}$] (8)

Yield: 0.046 g, 24%. ***R*$_f$:** 0.34

CHN: $C_{24}H_{49}B_{18}CoRu$ requires C 41.6, H 7.13%.

Found for **8** C 41.0, H 7.16%.

EIMS: Envelope centred on *m/z* 692 (M^+).

[MW = 692.25 g mol^{-1}]

NMR: **^{1}H NMR [CDCl$_3$],** major diastereoisomer; δ 6.04-5.78 [m, 4H, $CH_3C_6H_4CH(CH_3)_2$], 3.75 (br. s, 1H, C2′*H*), 3.03 [app. sept, 1H, $CH_3C_6H_4CH(CH_3)_2$], 2.46 [s, 3H, $CH_3C_6H_4CH(CH_3)_2$], 1.847 [s, 15H, $C_5(CH_3)_5$], 1.79 (br. s, 1H, C1*H*), 1.35-1.26 [m, 6H, $CH_3C_6H_4CH(CH_3)_2$].

Minor diastereoisomer; δ 6.04-5.78 [m, 4H, $CH_3C_6H_4CH(CH_3)_2$], 3.88 (br. s, 1H, C2′*H*), 3.03 [app. sept, 1H, $CH_3C_6H_4CH(CH_3)_2$], 2.44 [s, 3H, $CH_3C_6H_4CH(CH_3)_2$], 1.852 [s, 15H, $C_5(CH_3)_5$], 1.79 (br. s, 1H, C1*H*), 1.35-1.26 [m, 6H, $CH_3C_6H_4CH(CH_3)_2$].

^{11}B{^{1}H} NMR [CDCl$_3$], δ 2.7 to 0.3 multiple overlapping resonances with maxima at 2.7, 1.9, 0.3 (total 5B), -3.8 to -7.6 multiple overlapping resonances with maxima at -3.8, -6.1, -7.6 (total 7B), -13.1 to -19.6 multiple overlapping resonances with maxima at -13.1, -14.8, -17.2, -19.6 (total 6B).

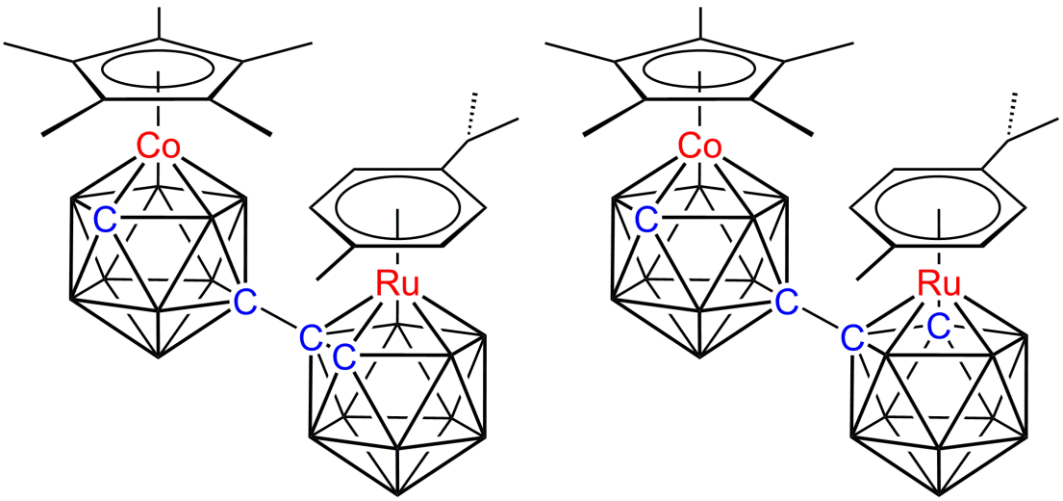

5.9 Thermal isomerisation of 8 to [8-(8′-2′-(*p*-cymene)-*closo*-2′,1′,8′-$RuC_2B_9H_{10}$)-2-Cp*-*closo*-2,1,8-$CoC_2B_9H_{10}$] (9)

Mixture **8** (0.020 g, 0.029 mmol) in DME (10 mL) was heated to reflux overnight. Following cooling, the solvent was removed *in vacuo* and the yellow residue was purified by preparative TLC using a DCM:petrol eluent (2:3) to afford a mobile yellow band. This was identified as [8-(8′-2′-(*p*-cymene)-*closo*-2′,1′,8′-$RuC_2B_9H_{10}$)-2-Cp*-*closo*-2,1,8-$CoC_2B_9H_{10}$] (**9**) which was shown to be a mixture of two diastereoisomers in an approximate 2:1 ratio by ^{1}H NMR spectroscopy. Like previously, exhaustive chromatography failed to separate these components.

[8-(8′-2′-(*p*-cymene)-*closo*-2′,1′,8′-RuC$_2$B$_9$H$_{10}$)-2-Cp*-*closo*-2,1,8-CoC$_2$B$_9$H$_{10}$] (9)

Yield: 0.017 g, 85%. ***R*$_f$:** 0.36

CHN: $C_{24}H_{49}B_{18}CoRu$ requires C 41.6, H 7.13%.

$C_{24}H_{49}B_{18}CoRu\cdot 0.5CH_2Cl_2$ requires C 40.1, H 6.86%.

Found for **8** C 40.1, H 6.98%.

EIMS: Envelope centred on *m/z* 692 (M^+).

[MW = 692.25 g mol^{-1}]

NMR: **^{1}H NMR [CDCl$_3$],** major diastereoisomer; δ 5.86-5.71 [m, 4H, $CH_3C_6H_4CH(CH_3)_2$], 2.81 [app. sept, 1H, $CH_3C_6H_4CH(CH_3)_2$], 2.59 (br. s, 1H, C1′*H*), 2.30 [s, 3H, $CH_3C_6H_4CH(CH_3)_2$], 1.84 [s, 15H, $C_5(CH_3)_5$], 1.74 (br. s, 1H, C1*H*), 1.29-1.26 [m, 6H, $CH_3C_6H_4CH(CH_3)_2$].

Minor diastereoisomer; δ 5.86-5.71 [m, 4H, $CH_3C_6H_4CH(CH_3)_2$], 2.81 [app. sept, 1H, $CH_3C_6H_4CH(CH_3)_2$], 2.62 (br. s, 1H, C1′*H*), 2.30 [s, 3H, $CH_3C_6H_4CH(CH_3)_2$], 1.83 [s, 15H, $C_5(CH_3)_5$], 1.77 (br. s, 1H, C1*H*), 1.29-1.26 [m, 6H, $CH_3C_6H_4CH(CH_3)_2$].

^{11}B{^{1}H} NMR [CDCl$_3$], δ 2.4 to -7.9 multiple overlapping resonances with maxima at 2.4, 1.0, -1.7, -4.9, -6.6, -7.9 (total 12B), -14.3 to -20.5 multiple overlapping resonances with maxima at -14.3, -16.2, -19.1, -20.5 (total 6B).

SC*X*RD: Yellow plate crystals of **9**·CH_2Cl_2 grown by diffusion of a DCM solution and petrol at -20 °C and diffraction data were collected on a Rigaku FR-E+ diffractometer (Mo Kα).

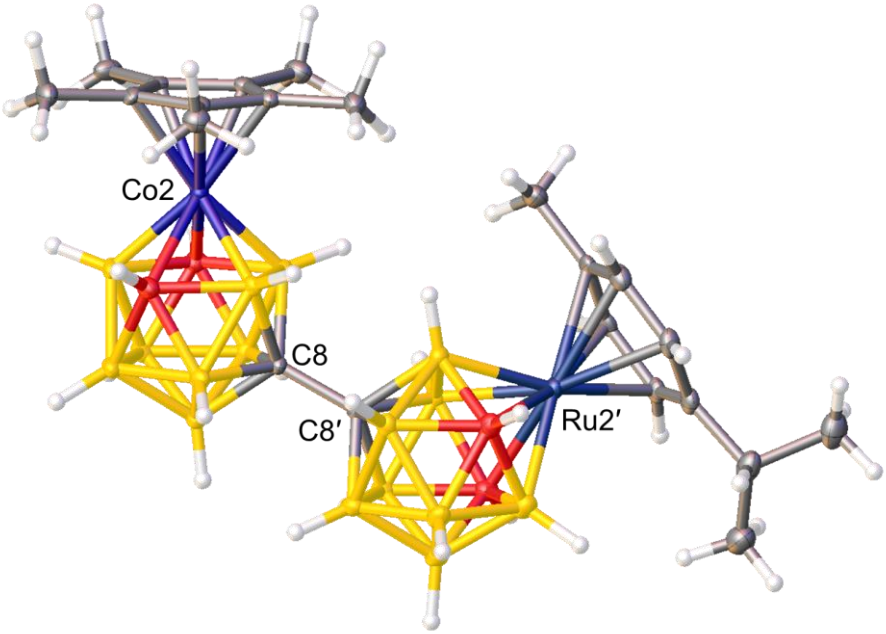

*B/C disorder observed in vertices marked in red.

5.10 Synthesis of [8-(1′-*closo*-1′,2′-$C_2B_{10}H_{11}$)-2-H-2,2-$(PPh_3)_2$-*closo*-2,1,8-$RhC_2B_9H_{10}$] (10)

^{n}BuLi (0.41 mL of a 1.6 M solution, 0.656 mmol) was added dropwise to cooled (0 °C) solution of [$HNMe_3$][**XI**] (0.100 g, 0.298 mmol) in THF (25 mL) and the products stirred for 1 h at room temperature. The pale yellow solution was then frozen at -196 °C, [$Rh(PPh_3)_3Cl$] (0.276 g, 0.298 mmol) was added and the reaction mixture allowed to thaw and stir overnight. The solvents were removed *in vacuo* and the residue was purified by column chromatography using a DCM:petrol eluent (1:1) to afford a yellow band. The yellow solid was subsequently identified as [8-(1′-*closo*-1′,2′-$C_2B_{10}H_{11}$)-2-H-2,2-$(PPh_3)_2$-*closo*-2,1,8-$RhC_2B_9H_{10}$] (**10**).

[8-(1′-*closo*-1′,2′-$C_2B_{10}H_{11}$)-2-H-2,2-$(PPh_3)_2$-*closo*-2,1,8-$RhC_2B_9H_{10}$] (10)

Yield: 0.142 g, 53%. ***R*f:** 0.44

CHN: $C_{40}H_{52}B_{19}P_2Rh$ requires C 53.2, H 5.80%.

Found for **10** C 54.1, H 5.99%.

NMR: **^{1}H NMR [CD_2Cl_2],** δ 7.67-7.13 (m, 30H, C_6H_5), 1.95 (br. s, 1H, C2′*H*), 1.84 (br. s, 1H, C1*H*), -8.70 (ddd, 1H, Rh*H*, J_{Rh-H} = 26.9 Hz, J_{P-H} = 26.9 and 15.4 Hz).

^{11}B{^{1}H} NMR [CD_2Cl_2], δ -0.8 to -13.1 multiple overlapping resonances with maxima at -0.8, -3.3, -4.4, -6.1, - 10.5, -13.1 (total integral 16B), -17.4 to -19.1 multiple overlapping resonances with maxima at -17.4, -19.1 (total integral 3B).

^{31}P{^{1}H} NMR [CD_2Cl_2], δ 35.82 (dd, 1P, J_{Rh-P} = 114.9 Hz, J_{P-P} = 27.7 Hz), 32.93 (dd, 1P, J_{Rh-P} = 107.0 Hz, J_{P-P} = 27.7 Hz).

SC*X*RD: Fine yellow needle crystals of **10**·0.5CH_2Cl_2 grown by diffusion of a DCM solution and petrol at -20 °C and diffraction data were collected on a Rigaku Oxford Diffraction AFC11 diffractometer (Mo Kα).

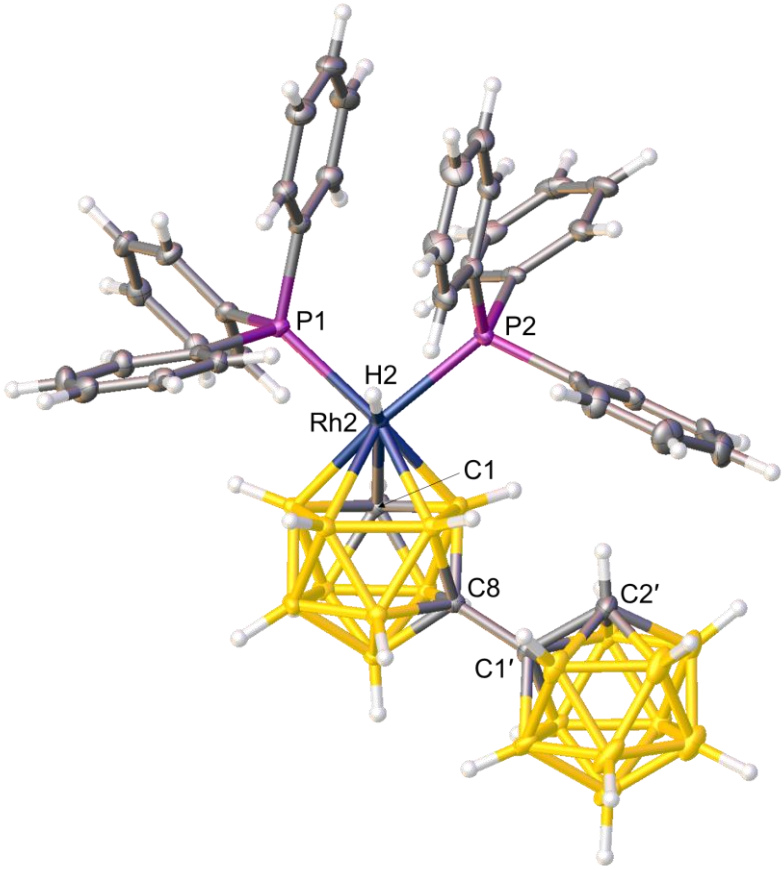
P1
P2
H2
Rh2
C1
C8
C2′
C1′

5.11 Synthesis of *α*-[8-(8′-2′-(*p*-cymene)-*closo*-2′,1′,8′-$RuC_2B_9H_{10}$)-2-H-2,2-$(PPh_3)_2$-*closo*-2,1,8-$RhC_2B_9H_{10}$] (11*α*) and *β*-[8-(8′-2′-(*p*-cymene)-*closo*-2′,1′,8′-$RuC_2B_9H_{10}$)-2-H-2,2-$(PPh_3)_2$-*closo*-2,1,8-$RhC_2B_9H_{10}$] (11*β*)

^{n}BuLi (0.12 mL of a 1.6 M solution, 0.192 mmol) was added dropwise to a cooled (0 °C) solution of **1** (0.050 g, 0.089 mmol) in THF (15 mL). Following warming to room temperature, the yellow solution was frozen at -196 °C and $[Rh(PPh_3)_3Cl]$ (0.083 g, 0.090 mmol) was added. Once thawed, the reaction mixture was heated to reflux overnight. Following cooling and filtration through silica, the solvents were removed *in vacuo* and the residue was purified by preparative TLC using a DCM:petrol eluent (1:1) to afford two major colourless bands.

α-[8-(8′-2′-(*p*-cymene)-*closo*-2′,1′,8′-$RuC_2B_9H_{10}$)-2-H-2,2-$(PPh_3)_2$-*closo*-2,1,8-$RhC_2B_9H_{10}$] (11α)

Yield: 0.021 g, 21%. **R_f:** 0.28

CHN: $C_{50}H_{65}B_{18}P_2RhRu$ requires C 53.3, H 5.82%.

Found for **11α** C 54.5, H 6.08%.

EIMS: Envelope centred on *m/z* 603 ($M^+ - 2 \times PPh_3$).

[MW = 1126.57 g mol^{-1}]

NMR: **^{1}H NMR [CD_2Cl_2],** δ 7.43-7.09 (m, 30H, C_6H_5), 5.74-5.63 [m, 4H, $CH_3C_6H_4CH(CH_3)_2$], 2.70 [app. sept, 1H, $CH_3C_6H_4CH(CH_3)_2$], 2.45 (br. s, 1H, C1′*H*), 2.17 [s, 3H, $CH_3C_6H_4CH(CH_3)_2$], 1.31 (br. s, 1H, C1*H*), 1.23 [d, 3H, $CH_3C_6H_4CH(CH_3)_2$], 1.21 [d, 3H, $CH_3C_6H_4CH(CH_3)_2$], -8.56 (ddd, 1H, Rh*H*, J_{Rh-H} = 29.8 Hz, J_{P-H} = 23.7 and 15.4 Hz).

^{11}B{^{1}H} NMR [CD_2Cl_2], δ 0.2 to -8.6 multiple overlapping resonances with maxima at 0.2, -1.7, -5.2, -8.6 (total integral 12B), -15.7 to -21.0 multiple overlapping resonances with maxima at -15.7, -16.5, -21.0 (total integral 6B).

^{31}P{^{1}H} NMR [CD_2Cl_2], δ 36.95 (dd, 1P, J_{Rh-P} = 114.9 Hz, J_{P-P} = 26.8 Hz), 32.65 (dd, 1P, J_{Rh-P} = 109.0 Hz, J_{P-P} = 26.8 Hz).

SC*X*RD: Pale yellow blade crystals of **11α**·$2CH_2Cl_2$ grown by diffusion of a DCM solution and petrol at -20 °C and diffraction data were collected on a Rigaku Oxford Diffraction AFC11 diffractometer (Cu Kα).

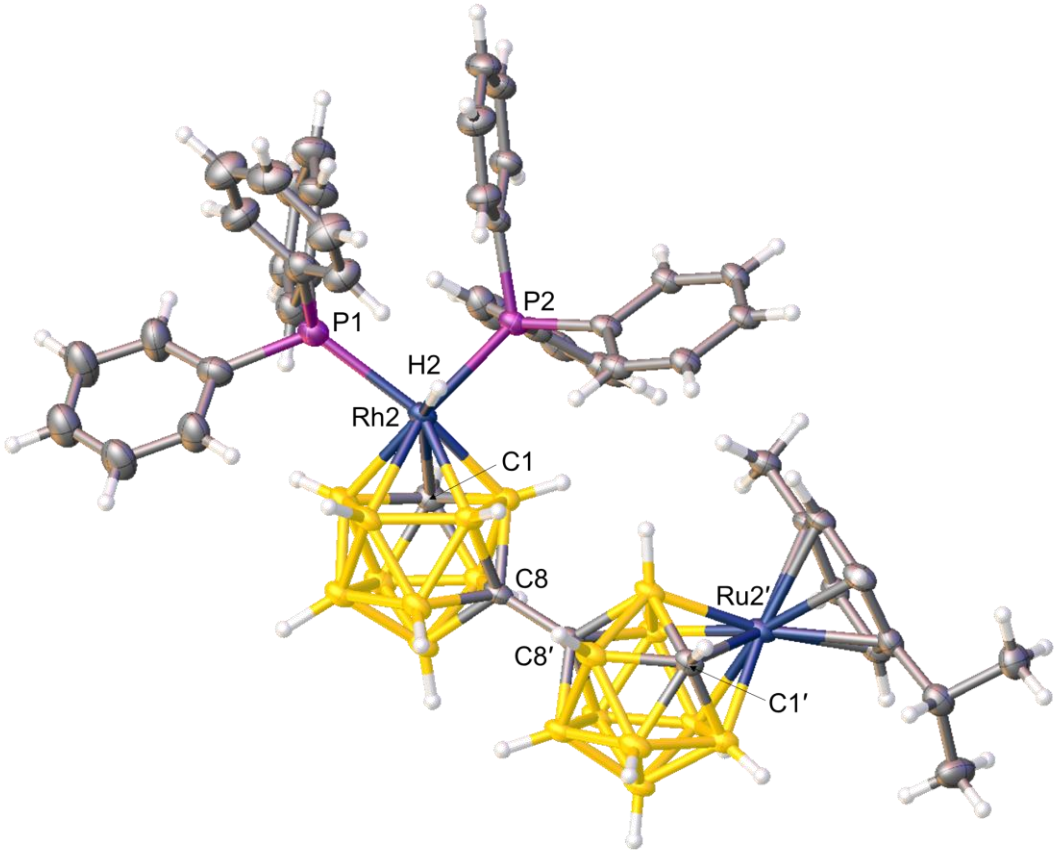
P1
P2
H2
Rh2
C1
C8
C8′
Ru2′
C1′

***β*-[8-(8′-2′-(*p*-cymene)-*closo*-2′,1′,8′-RuC$_2$B$_9$H$_{10}$)-2-H-2,2-(PPh$_3$)$_2$-*closo*-2,1,8-RhC$_2$B$_9$H$_{10}$] (11*β*)**

Yield: 0.033 g, 33%. ***R*$_f$:** 0.35

CHN: $C_{50}H_{65}B_{18}P_2RhRu$ requires C 53.3, H 5.82%.

Found for **11*β*** C 53.4, H 5.86%.

EIMS: Envelope centred on *m/z* 603 ($M^+ - 2 \times PPh_3$).

[MW = 1126.57 g mol^{-1}]

NMR: **^{1}H NMR [CD$_2$Cl$_2$],** δ 7.42-7.09 (m, 30H, C$_6$*H*$_5$), 5.79-5.66 [m, 4H, CH$_3$C$_6$*H*$_4$CH(CH$_3$)$_2$], 2.71 [app. sept, 1H, CH$_3$C$_6$H$_4$C*H*(CH$_3$)$_2$], 2.45 (br. s, 1H, C1′*H*), 2.20 [s, 3H, C*H*$_3$C$_6$H$_4$CH(CH$_3$)$_2$], 1.33 (br. s, 1H, C1*H*), 1.24 [d, 3H, CH$_3$C$_6$H$_4$CH(C*H*$_3$)$_2$], 1.22 [d, 3H, CH$_3$C$_6$H$_4$CH(C*H*$_3$)$_2$], -8.57 (ddd, 1H, Rh*H*, J_{Rh-H} = 30.1 Hz, J_{P-H} = 23.7 and 14.7 Hz).

^{11}B{^{1}H} NMR [CD$_2$Cl$_2$], δ 0.0 to -8.5 multiple overlapping resonances with maxima at 0.0, -5.1, -8.5 (total integral 12B), -15.8 to -21.1 multiple overlapping resonances with maxima at -15.8, -16.6, -21.1 (total integral 6B).

^{31}P{^{1}H} NMR [CD$_2$Cl$_2$], δ 36.99 (dd, 1P, J_{Rh-P} = 113.0 Hz, J_{P-P} = 25.8 Hz), 32.62 (dd, 1P, J_{Rh-P} = 109.0 Hz, J_{P-P} = 25.8 Hz).

SC*X*RD: Colourless plate crystals of **11*β***·1.5CH$_2$Cl$_2$ grown by vapour diffusion of a DCM solution and petrol at -20 °C and diffraction data were collected on a Rigaku Oxford Diffraction AFC11 diffractometer (Cu Kα).

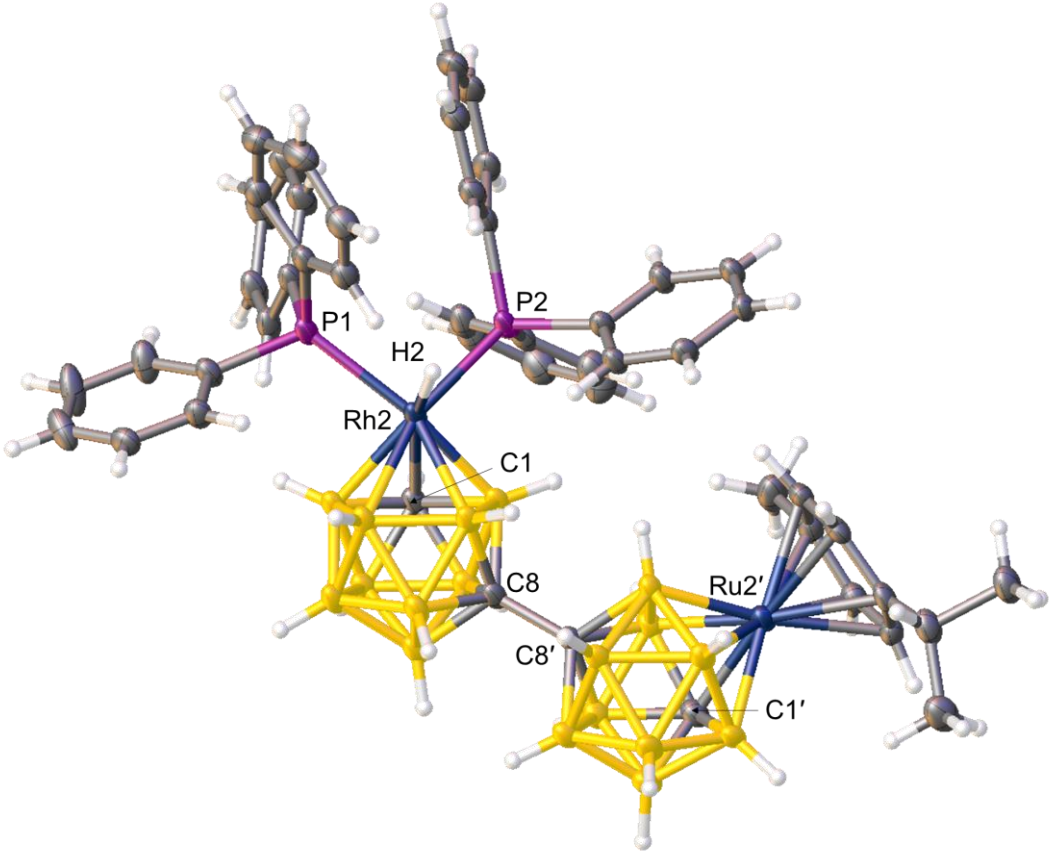
P1
P2
H2
Rh2
C1
C8
C8′
Ru2′
C1′

5.12 Synthesis of *α*-[8-(8′-2′-Cp*-*closo*-2′,1′,8′-$CoC_2B_9H_{10}$)-2-H-2,2-$(PPh_3)_2$-*closo*-2,1,8-$RhC_2B_9H_{10}$] (12*α*) and *β*-[8-(8′-2′-Cp*-*closo*-2′,1′,8′-$CoC_2B_9H_{10}$)-2-H-2,2-$(PPh_3)_2$-*closo*-2,1,8-$RhC_2B_9H_{10}$] (12*β*)

^{n}BuLi (0.13 mL of a 1.6 M solution, 0.208 mmol) was added dropwise to an ice-cooled solution of **7** (0.050 g, 0.097 mmol) in THF (15 mL). Following warming to room temperature, the dark yellow solution was frozen at -196 °C and $[Rh(PPh_3)_3Cl]$ (0.090 g, 0.097 mmol) was added. Upon thawing, the resultant deep red solution was stirred at room temperature overnight. Following filtration through silica, the solvents were removed *in vacuo* and the residue was purified by preparative TLC using a DCM:petrol eluent (1:1) to afford two major pale-yellow bands.

α-[8-(8′-2′-Cp*-*closo*-2′,1′,8′-$CoC_2B_9H_{10}$)-2-H-2,2-$(PPh_3)_2$-*closo*-2,1,8-$RhC_2B_9H_{10}$] (12α)

Yield: 0.017 g, 16%. **R_f:** 0.36

CHN: $C_{50}H_{66}B_{18}CoP_2Rh$ requires C 55.3, H 6.13%.

Found for **12α** C 55.8, H 6.08%.

ESIMS: Envelope centred on *m/z* 822 ($M^+ - PPh_3$).

[MW = 1085.44 g mol^{-1}]

NMR: **^{1}H NMR [CD_2Cl_2],** δ 7.42-7.09 (m, 30H, C_6H_5), 1.74 [s, 15H, $C_5(CH_3)_5$], 1.65 (br. s, 1H, C1′*H*), 1.40 (br. s, 1H, C1*H*), -8.57 (ddd, 1H, Rh*H*, J_{Rh-H} = 30.3 Hz, J_{P-H} = 24.2 and 15.6 Hz).

^{11}B{^{1}H} NMR [CD_2Cl_2], δ 0.9 to -8.5 multiple overlapping resonances with maxima at 0.9, -6.0, -8.5 (total integral 12B), -14.7 to -22.0 multiple overlapping resonances with maxima at -14.7, -15.5, -19.6, -22.0 (total integral 6B).

^{31}P{^{1}H} NMR [CD_2Cl_2], δ 37.35 (dd, 1P, J_{Rh-P} = 113.0 Hz, J_{P-P} = 22.8 Hz), 32.51 (dd,1P, J_{Rh-P} = 109.0 Hz, J_{P-P} = 22.8 Hz).

SC*X*RD: Yellow plate crystals of **12α**·2.5CH_2Cl_2 grown by diffusion of a DCM solution and petrol at -20 °C and diffraction data were collected on a Bruker X8 APEXII diffractometer (Mo Kα).

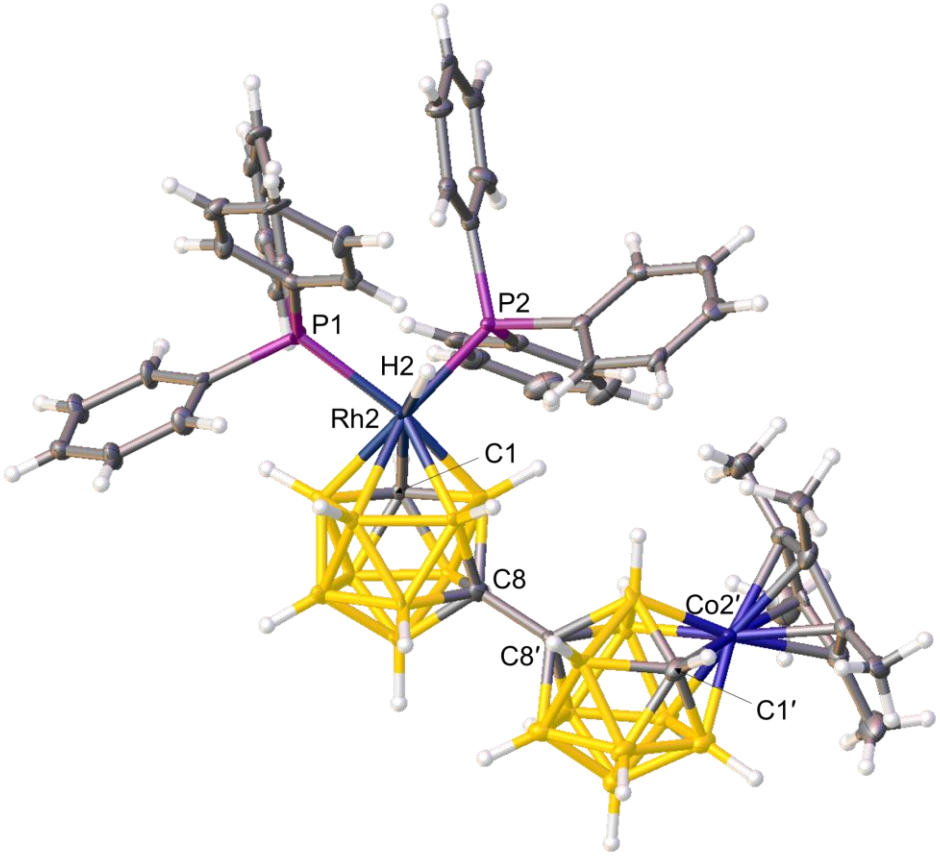
P1
P2
H2
Rh2
C1
C8
C8′
Co2′
C1′

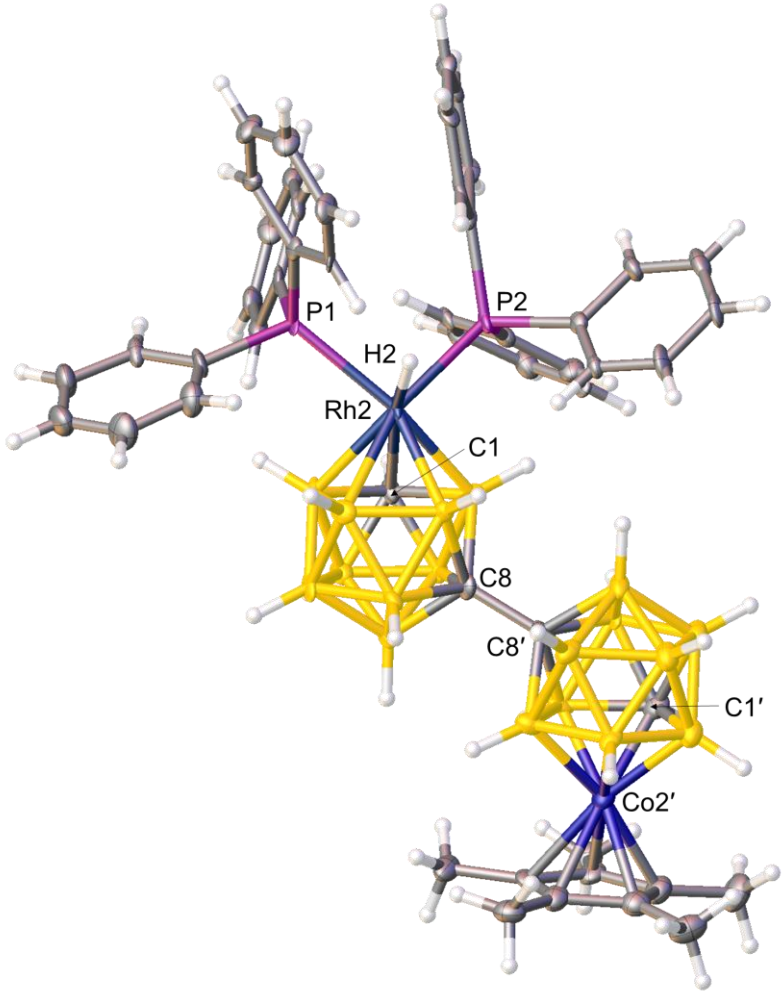
P1
P2
H2
Rh2
C1
C8
C8′
C1′
Co2′

***β*-[8-(8′-2′-Cp*-*closo*-2′,1′,8′-$CoC_2B_9H_{10}$)-2-H-2,2-$(PPh_3)_2$-*closo*-2,1,8-$RhC_2B_9H_{10}$] (12*β*)**

Yield: 0.019 g, 18%. ***R*f:** 0.41

CHN: $C_{50}H_{66}B_{18}CoP_2Rh$ requires C 55.3, H 6.13%.

Found for **12*β*** C 56.2, H 6.11%.

ESIMS: Envelope centred on *m/z* 822 ($M^+ - PPh_3$).

[MW = 1085.44 g mol^{-1}]

NMR: **^{1}H NMR [CD_2Cl_2],** δ 7.42-7.09 (m, 30H, C_6H_5), 1.75 (s, 15H, $C_5(CH_3)_5$), 1.66 (br. s, 1H, C1′*H*), 1.38 (br. s, 1H, C1*H*), -8.58 (ddd, 1H, Rh*H*, J_{Rh-H} = 28.9 Hz, J_{P-H} = 23.0 and 14.2 Hz).

^{11}B{^{1}H} NMR [CD_2Cl_2], δ 0.8 to -8.4 multiple overlapping resonances with maxima at 0.8, -6.7, -8.4 (total integral 12B), -14.9 to -21.9 multiple overlapping resonances with maxima at -14.9, -15.5, -19.0, -21.9 (total integral 6B).

^{31}P{^{1}H} NMR [CD_2Cl_2], δ 37.18 (dd, 1P, J_{Rh-P} = 113.0 Hz, J_{P-P} = 26.8 Hz), 32.54 (dd,1P, J_{Rh-P} = 109.0 Hz, J_{P-P} = 26.8 Hz).

SC*X*RD: Yellow block crystals of **12*β***·2.5CH_2Cl_2 grown by diffusion of a DCM solution and petrol at -20 °C and diffraction data were collected on a Bruker X8 APEXII diffractometer (Mo Kα).

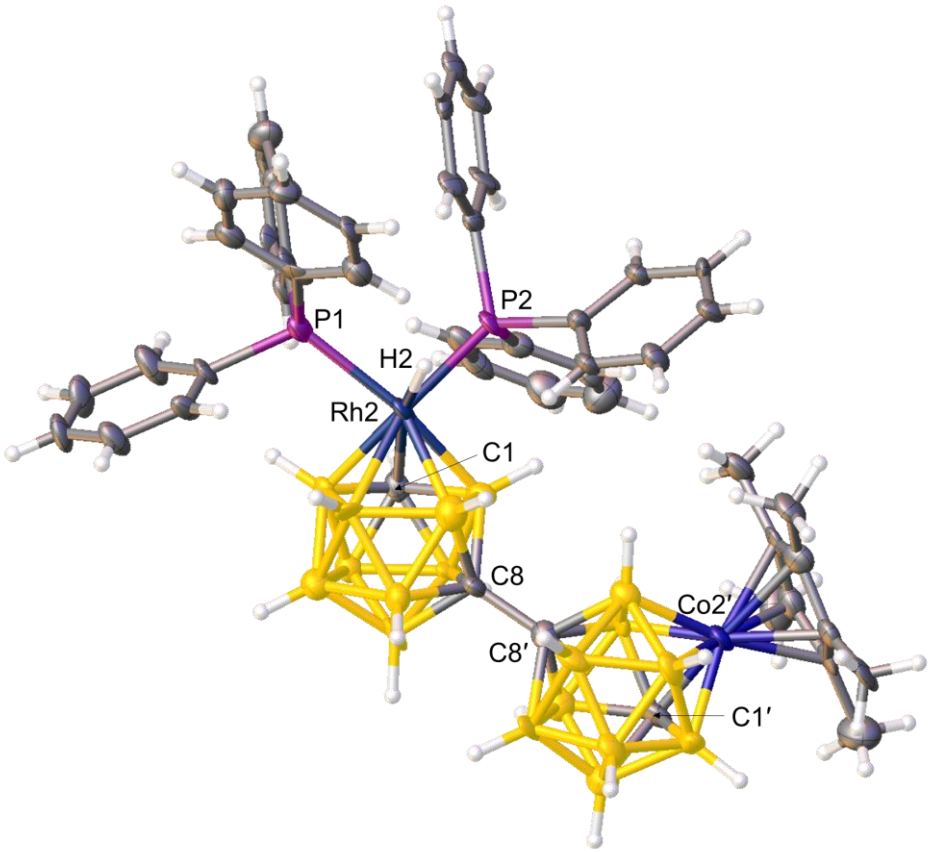
P1
P2
H2
Rh2
C1
C8
Co2′
C8′
C1′

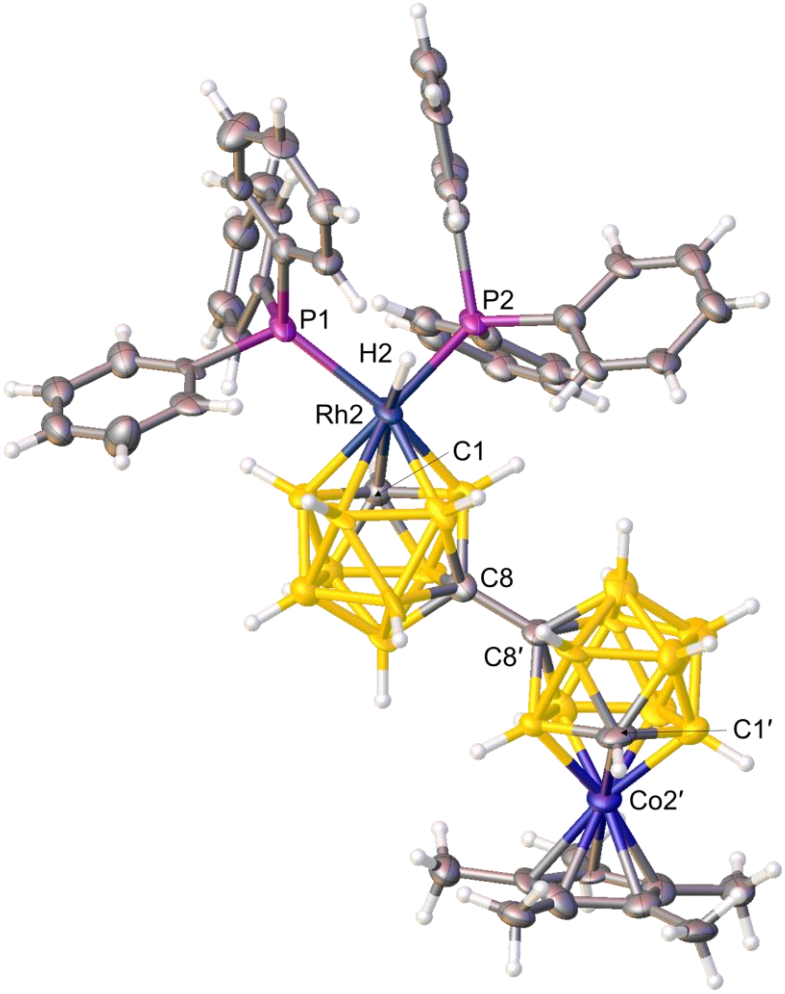
P1
P2
H2
Rh2
C1
C8
C8′
C1′
Co2′

5.13 Characterisation of [2-H-2,2-(PPh$_3$)$_2$-*closo*-2,1,12-RhC$_2$B$_9$H$_{11}$] (XXX)

Yield: 0.313 g, 90%.

NMR: **^{1}H NMR [CD$_2$Cl$_2$],** δ 7.68-6.94 (m, 30H, C$_6$*H*$_5$), 2.34 (br. s, 1H, C12*H*), 1.49 (br. s, 1H, C1*H*), -8.74 (dt, 1H, Rh*H*, J_{Rh-H} = 27.4 Hz, J_{P-H} = 14.9 Hz).

^{11}B{^{1}H} NMR [CD$_2$Cl$_2$], δ -1.4 (1B), -6.5 (2B), -9.2 (2B), -19.7 (4B).

^{31}P{^{1}H} NMR [CD$_2$Cl$_2$], δ 36.12 (d, 2P, J_{Rh-P} = 111.0 Hz).

SC*X*RD: Yellow block crystals of **XXX** grown by diffusion of a DCM solution and petrol at -20 °C and diffraction data were collected at 150 K on a Bruker D8 Venture diffractometer (Mo Kα).

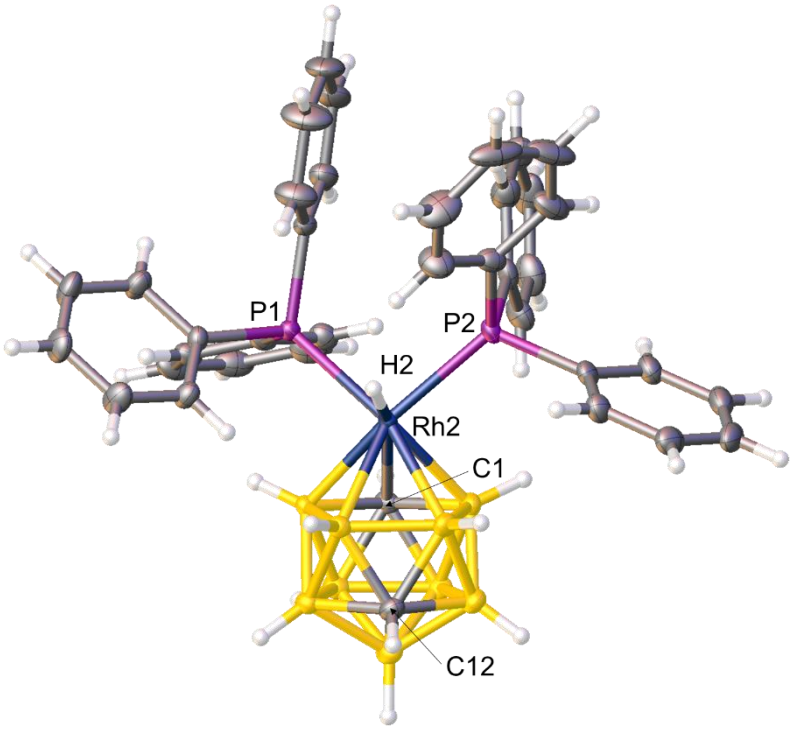

5.14 General Protocol for the Isomerisation of 1-Hexene

A J. Young NMR tube was flushed with N_2 and charged with 1-hexene (188 µL, 1.503 mmol) and mesitylene (104 µL, 0.748 mmol). A $CDCl_3$ (1 mL) solution of the appropriate catalyst precursor (0.003 mmol) was added and the progress of the reaction was monitored by ^{1}H NMR spectroscopy. NMR yields were determined by the relative integrals of the products against the mesitylene internal standard (chemical shifts used underlined, trans-3-hexene and cis-3-hexene could not be distinguished). Reactions performed in duplicate.

1-Hexene

NMR: **^{1}H NMR [$CDCl_3$],** δ 5.79-5.69 (1H, CH_2=C*H*), 5.01-4.93 (2H, CH_2=CH), 1.99-1.94 (2H, CH_2), 1.32-1.21 (4H, 2 × CH_2), 0.86-0.83 (3H, CH_3).

Trans-2-hexene

NMR: **^{1}H NMR [$CDCl_3$],** δ 5.41-5.37 (2H, 2 × CH), 1.95-1.90 (2H, CH_2), <u>1.60-1.59</u> (3H, CH_3), 1.38-1.29 (2H, CH_2), 0.88-0.84 (3H, CH_3).

Cis-2-hexene

NMR: **^{1}H NMR [$CDCl_3$],** δ 5.51-5.38 (2H, 2 × CH), 2.01-1.95 (2H, CH_2), <u>1.54-1.52</u> (3H, CH_3), 1.38-1.28 (2H, CH_2), 0.89-0.85 (3H, CH_3).

Trans-3-hexene

NMR: **^{1}H NMR [$CDCl_3$],** δ <u>5.43</u> (2H, 2 × CH), 2.00 (4H, 2 × CH_2), 0.79 (3H, 2 × CH_3).

Cis-3-hexene

NMR: **^{1}H NMR [$CDCl_3$],** δ <u>5.33</u> (2H, 2 × CH), 2.03 (4H, 2 × CH_2), 0.96 (3H, 2 × CH_3).

Mesitylene

NMR: **^{1}H NMR [$CDCl_3$],** δ 6.91 (3H, C_6H_3), 2.38 (9H, 3 × CH_3).

5.15 General Protocol for the Hydrosilylation of Acetophenone

Acetophenone (37 µL, 0.317 mmol), diphenylsilane (74 µL, 0.399 mmol) and mesitylene (22 µL, 0.158 mmol) was added to a J Young NMR tube flushed with N_2. A $CDCl_3$ (1 mL) solution of the appropriate catalyst precursor (0.0016 mmol) was added to the reaction and the mixture was heated to 55 °C. Yields were monitored by ^{1}H NMR spectroscopy using mesitylene as an internal standard (chemical shifts used underlined). Reactions performed in duplicate.

Acetophenone

NMR: **^{1}H NMR [$CDCl_3$],** δ 7.96-7.94 (2H, C_6H_5), 7.57-7.55 (1H, C_6H_5), 7.47-7.43 (2H, C_6H_5), 2.59 (3H, CH_3).

Diphenylsilane

NMR: **^{1}H NMR [$CDCl_3$],** δ 7.65-7.64 (4H, C_6H_5), 7.43-7.39 (6H, C_6H_5), 4.98 (2H, 2 × Si*H*).

Diphenyl(1-phenylethoxy)silane

NMR: **^{1}H NMR [$CDCl_3$],** δ 7.83-7.32 (15H, C_6H_5), 5.55 (1H, Si*H*), 5.12 (1H, C*H*), 1.62 (3H, CH_3).

Diphenyl{(1-phenylvinyl)oxy}silane

NMR: **^{1}H NMR [$CDCl_3$],** δ 7.83-7.32 (15H, C_6H_5), 5.85 (1H, Si*H*), 5.05 (1H, CH_2), 4.65 (1H, CH_2).

Mesitylene

NMR: **^{1}H NMR [$CDCl_3$],** δ 6.91 (3H, C_6H_3), 2.38 (9H, 3 × CH_3).

5.16 References

1. O. V. Dolomanov, L. J. Bourhis, R. J. Gildea, J. A. K. Howard, H. Puschmann, *J. Appl. Cryst.*, 2009, **42**, 339-341.

2. G. M. Sheldrick, *Acta Cryst.*, 2008, A**64**, 112-122.

3. G. M. Sheldrick, *Acta Cryst.*, 2015, A**71**, 3-8.

4. G. M. Sheldrick, *Acta Cryst.*, 2015, C**71**, 3-8.

5. A. McAnaw, G. Scott, L. Elrick, G. M. Rosair and A. J. Welch, *Dalton Trans*., 2013, **42**, 645-664.

6. A. McAnaw, M. E. Lopez, D. Ellis, G. M. Rosair and A. J. Welch, *Dalton Trans*., 2014, **43**, 5095-5105.

7. A. J. Welch, *Crystals*, 2017, **7**, 234.

8. S. Ren and Z. Xie, *Organometallics*, 2008, **27**, 5167-5168.

9. M. A. Bennett, T.-N. Huang, T. W. Matheson and A. K. Smith, *Inorg. Synth.*, 1982, **21**, 74-78.

10. G. Thiripuranathar, A. P. Y. Chan, D. Mandal, W. Y. Man, M. Argentari, G. M. Rosair and A. J. Welch, *Dalton Trans.*, 2017, **46**, 1811-1821.

11. G. S. Kazakov, I. B. Sivaev, K. Y. Suponitsky, A. D. Kirilin, V. I. Bregadze and A. J. Welch, *J. Organomet. Chem.*, 2016, **805**, 1-5.

12. J. A. Osborn, G. Wilkinson, *Inorg. Synth.*, 1967, **10**, 67-71.

13. T. E. Paxson and M. F. Hawthorne, *J. Am. Chem. Soc.*, 1974, **96**, 4674-4676.

14. D. C. Busby and M. F. Hawthorne, *Inorg. Chem.*, 1982, **21**, 4101-4103.

Appendix A

Rhodacarboranes bearing Phosphite Ligands

Transition metal catalysts bearing phosphine ligands are commonly altered by variations in the PR_3 units. The electronic and steric properties can be fine-tuned using appropriate R substituents and can even be made chiral for enantioselective reactions.[1] Recent studies have shown catalytic enhancement simply by use of mixed phosphine and phosphite ligands in analogues of Wilkinson's catalyst.[2] This prompted a similar study where preparation and investigation of the phosphite analogues of **VIII** and **10** (Figure A.1) would be initially undertaken and, if successful, transitioned on to the mixed ligand systems.

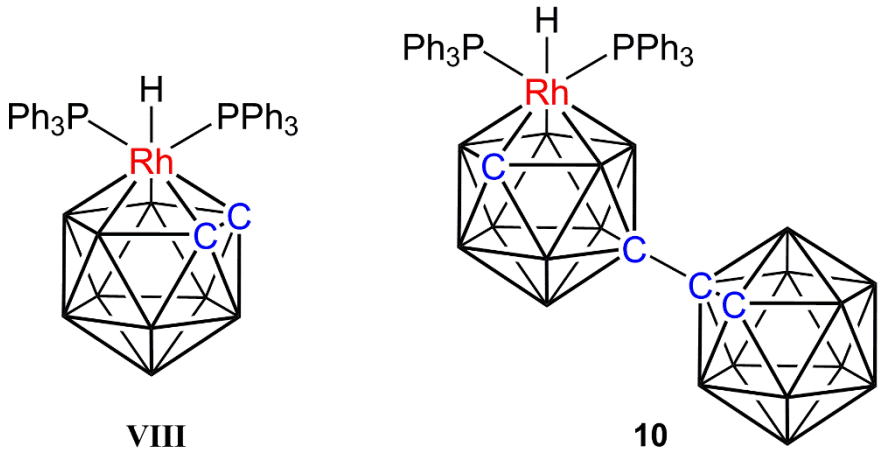

Figure A.1 Structures of the rhodacarboranes **VIII** and **10**.

The phosphite analogue of Wilkinson's catalyst $[Rh\{P(OPh)_3\}_3Cl]$ was prepared by displacement of the cyclooctadiene (COD) ligands in the dimeric species $[Rh(COD)Cl]_2$ (0.200 g, 0.406 mmol) in DCM (10 mL) by the slow addition of triphenylphosphite (0.66 mL, 2.510 mmol). Following a 3 h stir, the solvent was removed *in vacuo* and the crude product was washed with petrol to afford a yellow powder which was subsequently confirmed, by comparison with the literature,[3] to be $[Rh\{P(OPh)_3\}_3Cl]$ (0.852 g, 99%).

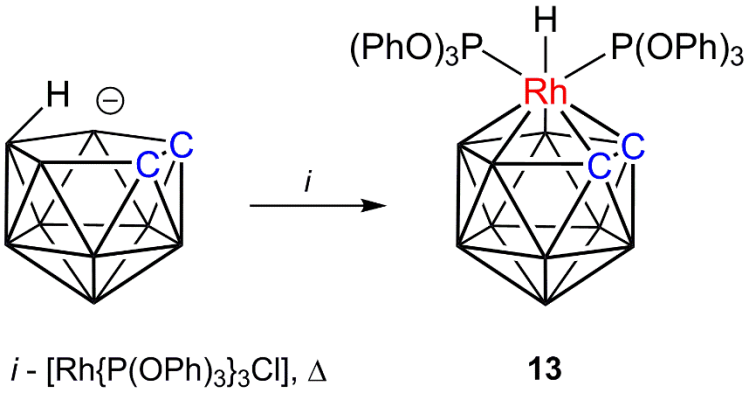

Figure A.2 Metalation of [HNMe$_3$][*nido*-7,8-$C_2B_9H_{12}$] with [Rh{P(OPh)$_3$}$_3$Cl] to afford **13**.

The salt [HNMe$_3$][*nido*-7,8-$C_2B_9H_{12}$] (0.050 g, 0.258 mmol) and [Rh{P(OPh)$_3$}$_3$Cl] (0.276 g, 0.258 mmol) were dissolved in EtOH (40 mL) and heated to reflux for 2 h (Figure A.2). Upon cooling, the yellow precipitate was collected, washed with minimal EtOH and dried *in vacuo*. The product [3-H-3,3-{P(OPh)$_3$}$_2$-*closo*-3,1,2-$RhC_2B_9H_{11}$] (**13**) was analysed by NMR spectroscopy and its structure was confirmed by crystallography (Figure A.3). It is important to note that **13** displays minor decomposition when in solution for extended periods (>24 h) suggesting that the bis(phosphite)hydridorhodium fragment is not as robust as its phosphine analogue.

[3-H-3,3-{P(OPh)$_3$}$_2$-*closo*-3,1,2-RhC$_2$B$_9$H$_{11}$] (13)

Yield: 0.080 g, 36%.

NMR: **^{1}H NMR [CD$_2$Cl$_2$],** δ 7.33-7.02 [m, 30H, C$_6$*H*$_5$], 2.85 (br.s, 2H, C*H*), -7.75 (dt, 1H, Rh*H*, J_{Rh-H} = 28.1 Hz, J_{P-H} = 20.1 Hz).

^{11}B{^{1}H} NMR [CD$_2$Cl$_2$], δ 1.7 (1B), -1.6 (1B), -7.4 (2B), -10.9 (2B), -18.1 (2B), -21.6 (1B).

^{31}P{^{1}H} NMR [CD$_2$Cl$_2$], δ 117.13 (d, 2P, J_{Rh-P} = 208.1 Hz).

SC*X*RD: Yellow block crystals grown by diffusion of a DCM solution and petrol at -20 °C and diffraction data were collected at 120 K on a Rigaku Oxford Diffraction SuperNova diffractometer (Mo Kα).

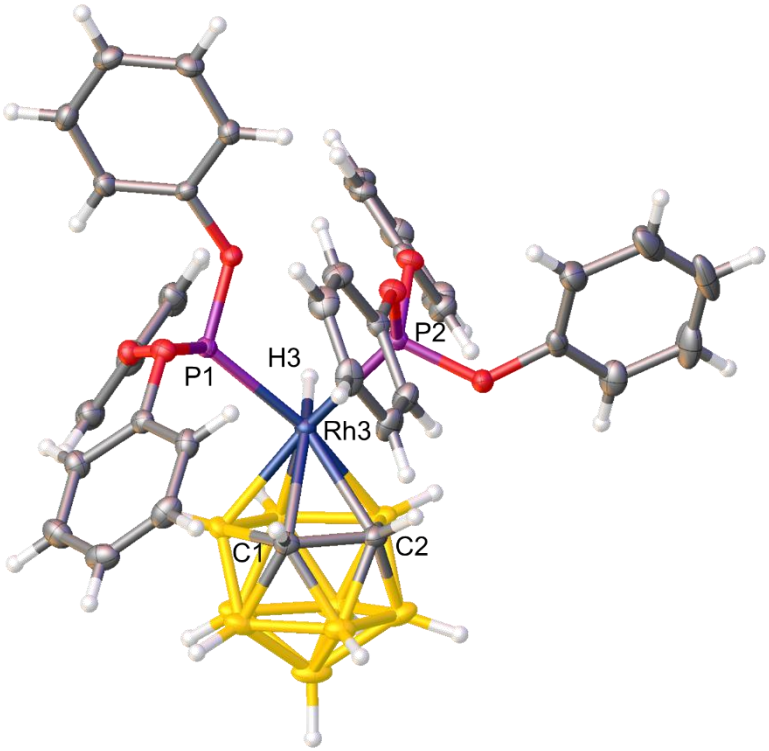

Figure A.3 Perspective view of [3-H-3,3-{P(OPh)$_3$}$_2$-*closo*-3,1,2-RhC$_2$B$_9$H$_{11}$] (**13**).

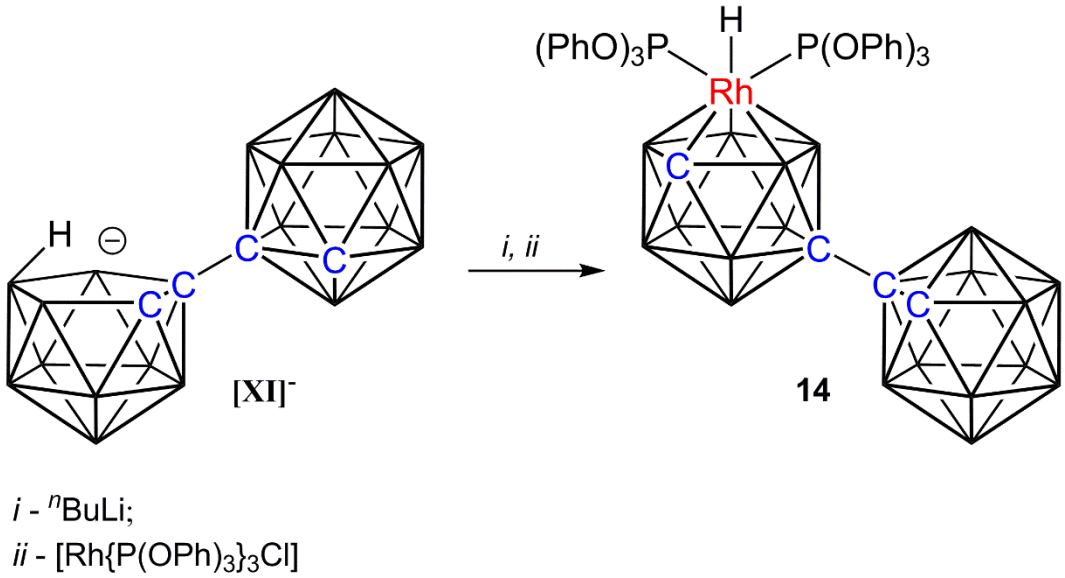

Figure A.4 Metalation of [HNMe$_3$][**XI**] with [Rh{P(OPh)$_3$}$_3$Cl].

The salt [HNMe$_3$][**XI**] (0.100 g, 0.298 mmol) was deprotonated using ^{n}BuLi (0.25 mL of a 2.5 M solution, 0.625 mmol) in THF (10 mL) at 0 °C. Following a 1 h stir at room temperature, the pale yellow solution was frozen at -196 °C and [Rh{P(OPh)$_3$}$_3$Cl] (0.320 g, 0.299 mmol) was added. Upon thawing, the reaction mixture was stirred at room temperature overnight. The resultant brown mixture was purified by preparative TLC (Figure A.5) in which two trace intense purple bands and a yellow band (**14**) were isolated.

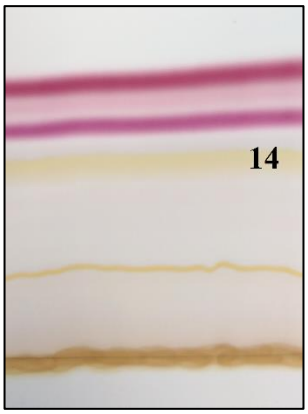

Figure A.5 Preparative TLC plate of the reaction mixture showing two intense purple bands and the yellow product band **14**.

$^{31}P\{^{1}H\}$ NMR spectroscopy of the yellow product **14** reveals two doublets of doublets with a 1:1 ratio of relative integrals (Figure A.6, right); δ 99.85 (dd, 1P, $J_{Rh\text{-}P}$ = 166.5 Hz, $J_{P\text{-}P}$ = 115.9 Hz), 92.35 (dd,1P, $J_{Rh\text{-}P}$ = 200.1 Hz, $J_{P\text{-}P}$ = 115.9 Hz). This is reminiscent of the previously described rhodacarborane **10**, suggesting the targeted fragment has been successfully inserted. The $^{11}B\{^{1}H\}$ NMR spectrum shows a broad overlapped signal ranging from δ 7.6 to -17.7 ppm (Figure A.6, left), confirming **14** to be a closo species but quantification of the relative integrals could not be achieved. Two $C_{cage}H$ resonances are observed (δ 2.50 and 1.65 ppm) as well as a multiplet ranging from δ 7.41 to 7.14 ppm, assigned to the phenyl protons. Therefore, we tentatively assign **14** to be the phosphite analogue [8-(1′-*closo*-1′,2′-$C_2B_{10}H_{11}$)-2-H-2,2-{$P(OPh)_3$}$_2$-*closo*-2,1,8-$RhC_2B_9H_{10}$].

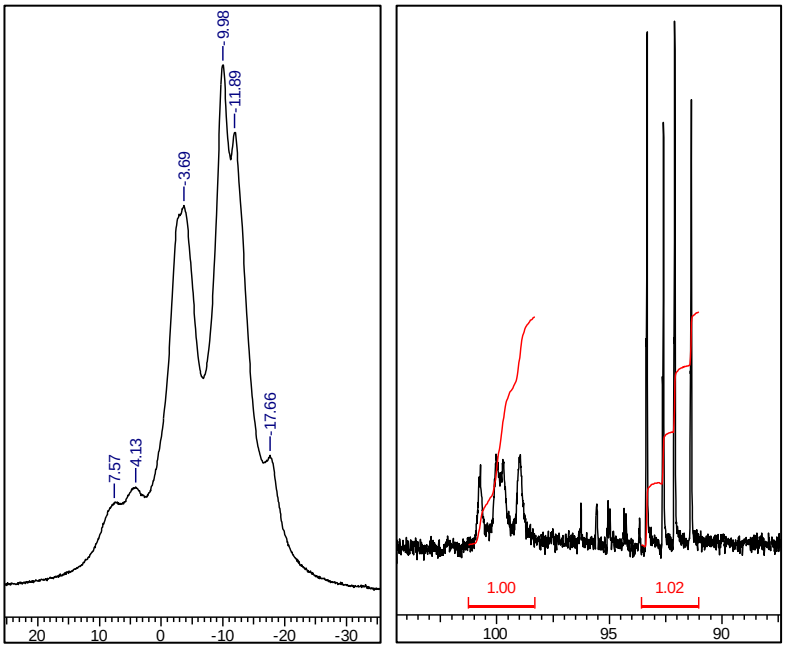

Figure A.6 The $^{11}B\{^{1}H\}$ NMR and $^{31}P\{^{1}H\}$ NMR spectra of **14** (left and right, respectively). Units in ppm.

However, compound **14** is unstable in solution in air and discolouration of the NMR sample was apparent after these NMR experiment, prohibiting the high-field ^{1}H NMR experiment for the hydride ligand. Spot TLC of the sample revealed two additional purple spots with matching R_f values to the purple bands observed from preparative TLC as well

as a significant baseline. The instability of **14** mitigated against its use in catalysis and thus only the phosphine analogues were pursued.

NMR spectroscopy of both purple compounds showed a single broad resonance in the $^{11}B\{^{1}H\}$ NMR spectra, confirming the presence of a carborane cluster but no meaningful analysis could be performed. A minute broad doublet can be barely discerned from the baseline in the $^{31}P\{^{1}H\}$ NMR spectra at δ *ca.* 104 ppm, revealing only a single phosphorus environment is present. As the precursor **14** is asymmetric and possessing two phosphorus environments, these purple decomposition products most likely involves loss of one phosphite ligand. Due to the minimal yield of these products, the ^{1}H NMR spectra is dominated by residual solvent. These two purple compounds are tentatively postulated to be dimeric species as rhodacarboranes are known to form bimetallic clusters, which are typically blue or purple in colour.[4]

The novel $\{Rh(P\{OPh\}_3)_2H\}$ fragment has been successfully incorporated into both carborane and bis(carborane) frameworks to afford new analogues of rhodacarboranes. However, due to their relative instability, catalytic potential is limited to inert conditions and thus left unpursued.

References

1. C. A. Tolman, *Chem. Rev.*, 1977, **77**, 313-348.

2. I. Choinopoulos, I. Papageorgiou, S. Coco, E. Simandiras and S. Koinis, *Polyhedron*, 2012, **45**, 255-261.

3. P. Serp, M. Hernandez, B. Richard and P. Klack, *Eur. J. Inorg. Chem.*, 2001, **2001**, 2327-2336.

4. P. E. Behnken, T. B. Marder, R. T. Baker, C. B. Knobler, M. R. Thompson and M. F. Hawthorne, *J. Am. Chem. Soc.*, 1985, **107**, 932-940.

Appendix B

Deboronation and Metalation of 1,1′-Bis(*meta*-carborane)

The synthesis of 1,1′-bis(*meta*-carborane), commonly known as bis(*m*-carborane), was first reported by Zakharkin in 1973,[1] almost a decade after that of its ortho analogue. The compound is prepared *via* a copper-mediated coupling of the lithiated *m*-carborane (Figure B.1), analogous to the preparation of bis(*o*-carborane).

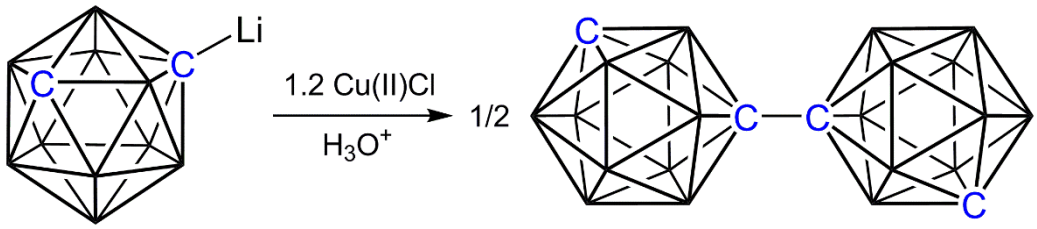

Figure B.1 Copper-mediated coupling of monolithiated *m*-carborane followed by hydrolysis with HCl to afford 1,1′-bis(*m*-carborane).

Spectroscopic characterisation of bis(*m*-carborane) was subsequently reported by Hawthorne[2] and, more recently, the definitive crystal structure was determined by Welch.[3] In addition to bis(*m*-carborane), Hawthorne also reports the formation of tetra(*m*-carborane) where four *m*-carborane units are linked together through the cage C atoms (Figure B.2). The synthesis of bis(*m*-carborane) was subsequently optimised by Hey-Hawkins and in this the tetramer side-product is no longer observed.[4]

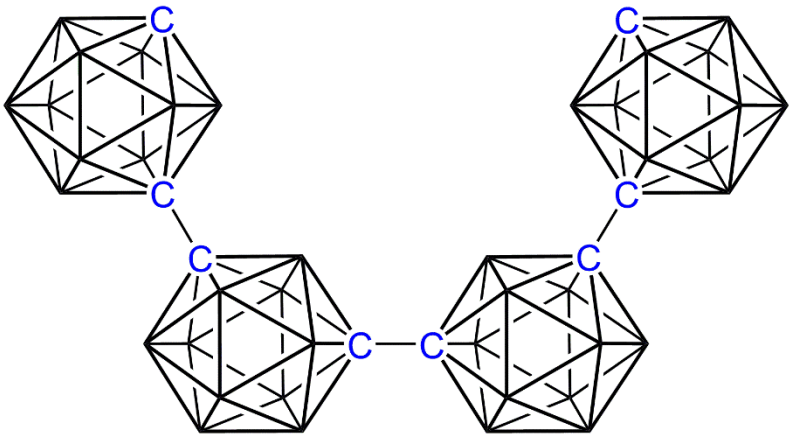

Figure B.2 Tetra(*m*-carborane) side-product isolated by Hawthorne from the synthesis of bis(*m*-carborane).

The chemistry of bis(*m*-carborane) is essentially unexplored. Substitution at the cage C positions has been shown to proceed similarly to the bis(*o*-carborane) analogue whereby deprotonation of the relatively acidic C–H proton followed by addition of an appropriate electrophile affords the *C*-substituted product. Hey-Hawkins reports two di-substituted derivatives, confirmed crystallographically, in which the cage C vertices has been substituted with a $–P(NMe_2)_2$ or $–P(NMe_2)(OMe)$ unit (Figure B.3). Subsequent manipulations of the phosphorus centres were then undertaken to generate potentially biologically-useful species.[4] Currently, no further examples of substitution at a cage vertex have been reported.

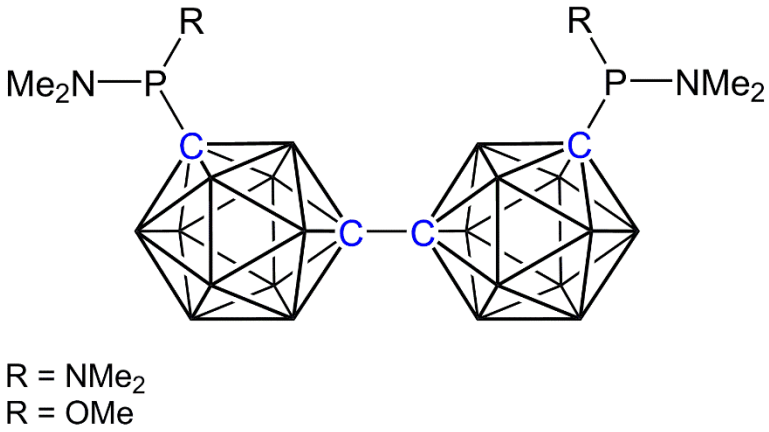

Figure B.3 The two known examples of di-substituted bis(*m*-carborane), where R = OMe, the product exists as an inseparable mixture of diastereoisomers.

Furthermore, polyhedral subrogation and polyhedral expansion of bis(*m*-carborane) have yet to be reported in the literature. Therefore, we set out to pioneer the deboronation and metalation chemistry of 1,1′-bis(*meta*-carborane) to advance the methodologies for synthesising novel metallacarborane/carborane compounds.

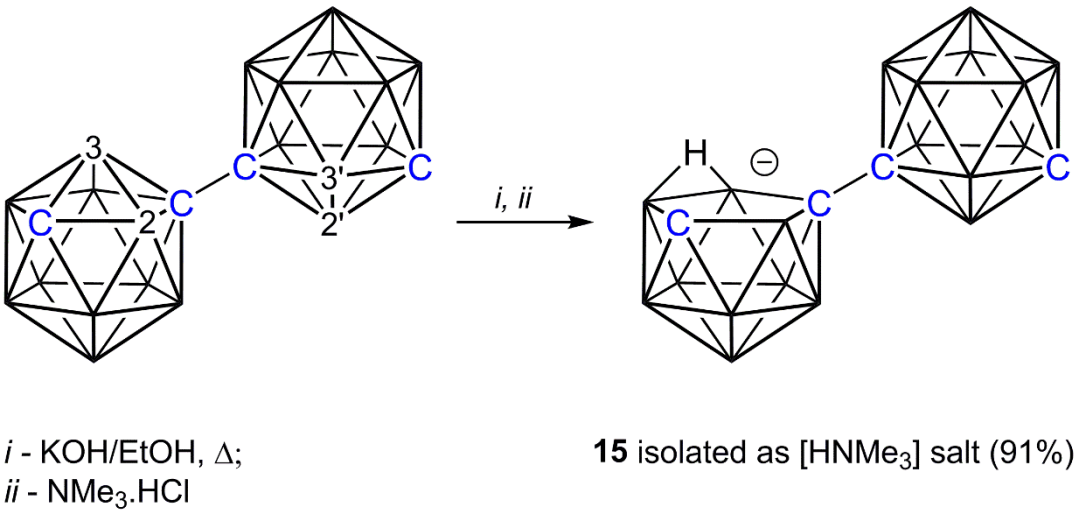

Figure B.4 Deboronation of [1-(1′-*closo*-1′,7′-$C_2B_{10}H_{11}$)-*closo*-1,7-$C_2B_{10}H_{11}$] using KOH/EtOH to afford **15**.

1,1′-Bis(*m*-carborane) (0.200 g, 0.698 mmol) and KOH (0.235 g, 4.188 mmol) were dissolved in EtOH (50 mL) and the resultant clear solution was heated to reflux overnight. Upon cooling, the volatiles was removed *in vacuo* and the white residue was re-dissolved in deionised water (20 mL). The solution was filtered and an aqueous solution of excess NMe_3.HCl was added to the filtrate resulting in the immediate precipitation of a white solid. This was collected by filtration, washed with deionised water and dried *in vacuo* to afford [$HNMe_3$][7-(1′-*closo*-1′,7′-$C_2B_{10}H_{11}$)-*nido*-7,9-$C_2B_9H_{11}$] (**15**). The product was characterised by elemental analysis, NMR spectroscopy and single crystals of the product were grown for a crystallographic study (Figure B.5).

[HNMe$_3$][7-(1′-*closo*-1′,7′-$C_2B_{10}H_{11}$)-*nido*-7,9-$C_2B_9H_{11}$] (15)

Yield: 0.212 g, 91%

CHN: $C_7H_{32}B_{19}N$ requires C 25.0, H 9.61, N 4.17%

Found for **15** C 25.6, H 9.11, N 4.93%

NMR: **^{1}H NMR [(CD$_3$)$_2$CO],** δ 6.53 (br.s, 1H, *H*N(CH$_3$)$_3$), 3.29 (br.s, 1H, C7′*H*), 3.14 (s, 9H, HN(C*H*$_3$)$_3$), 1.19 (br.s, 1H, C9*H*).

^{1}H{^{11}B} NMR [(CD$_3$)$_2$CO], δ -2.07 (t, 1H, μ-*H*).

^{11}B{^{1}H} NMR [(CD$_3$)$_2$CO], δ -0.7 (1B), -3.2 (1B), -4.1 (1B), -4.9 (1B), -9.6 (2B), -10.6 (1B), -12.0 (2B), -14.2 (2B), -14.6 (2B), -17.3 (1B), -21.0 (1B), -21.9 (1B), -22.6 (1B), -32.8 (1B), -35.8 (1B).

SC*X*RD: Colourless block crystals of **15**·CH_2Cl_2 grown by diffusion of a DCM solution and petrol at -20 °C and diffraction data were collected on a Rigaku Oxford Diffraction SuperNova diffractometer (Mo Kα).

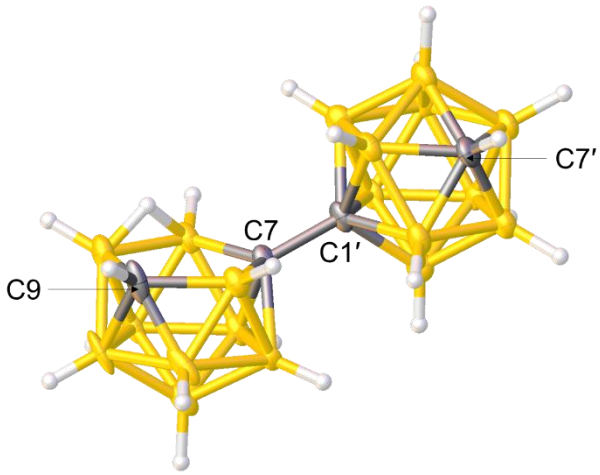

Figure B.5 Perspective view of one arbitrary conformation of [HNMe$_3$][7-(1′-*closo*-1′,7′-$C_2B_{10}H_{11}$)-*nido*-7,9-$C_2B_9H_{11}$] (**15**). Cation omitted for clarity.

Microanalysis of **15** was consistent with the anticipated formula $C_7H_{32}B_{19}N$. Vertices B2 and B3 (and by symmetry B2′ and B3′) are chemically equivalent so either vertices can be deboronated. However, the same product is afforded irrespective of the vertex removed.

The ^1H NMR spectrum displays a sharp singlet at δ 3.14 ppm corresponding to the methyl groups of the $[HNMe_3]^+$ cation. The $C_{cage}H$ shifts were observed at δ 3.29 and 1.19 ppm as broad singlets where the former is assigned to the *closo*-$C_2B_{10}H_{11}$ cage and the latter to the deboronated cage. An additional broad singlet is observed at δ 6.53 ppm with a relative integral of 1H arising from the ammonium proton of the cation. An apparent triplet centred on δ -2.07 ppm is visible in the $^1H\{^{11}B\}$ NMR spectrum and is assigned to the bridging-*H* on the open face of the nido carborane (Figure B.6, left). The resonance is split by the two inequivalent exo-H atoms on vertices B10 and B11 to formally give a splitting pattern of a doublet of doublets.

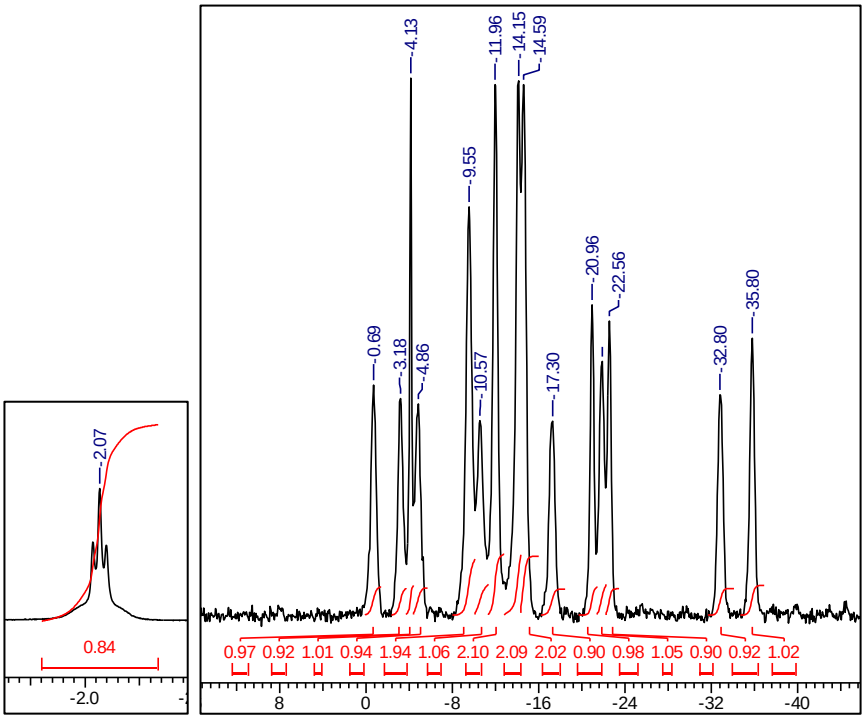

Figure B.6 The $^1H\{^{11}B\}$ NMR signal of the bridging-H on the open face (left) and the $^{11}B\{^1H\}$ NMR spectrum of **15**. Units in ppm.

The $^{11}B\{^{1}H\}$ NMR spectrum displays a 1:1:1:1:2:1:2:2:2:1:1:1:1:1:1 ratio of peaks (Figure B.6, right). Unique 1B signals suggests that the species is asymmetric and, coupled with the total integral of 19B, confirms only one cage has been selectively deboronated. The two upfield resonances (δ -32.8 and -35.8 ppm) are indicative of a nido cage and tentatively assigned to vertices B1 and B6 respectively by comparison with the upfield resonances in its single-cage analogue.[5]

Colourless block crystals were grown from DCM/petrol diffusion and a crystallographic study of **15** was undertaken. The product was confirmed to be $[HNMe_3][7\text{-}(1'\text{-}closo\text{-}1',7'\text{-}C_2B_{10}H_{11})\text{-}nido\text{-}7,9\text{-}C_2B_9H_{11}]$ in which the bridging-H is located between vertices B10 and B11 (Figure B.5). Only half a molecule is present in the asymmetric fraction of the unit cell where the mirror plane bisects the primed cage through the cage C vertices. Thus vertices B4 and C9 in the nido cage are related by symmetry leading to 0.50:0.50 occupancy ratio of the cage C positions between these two vertices. Additionally, B3 is only 0.50 occupancy as it is disordered with the open face.

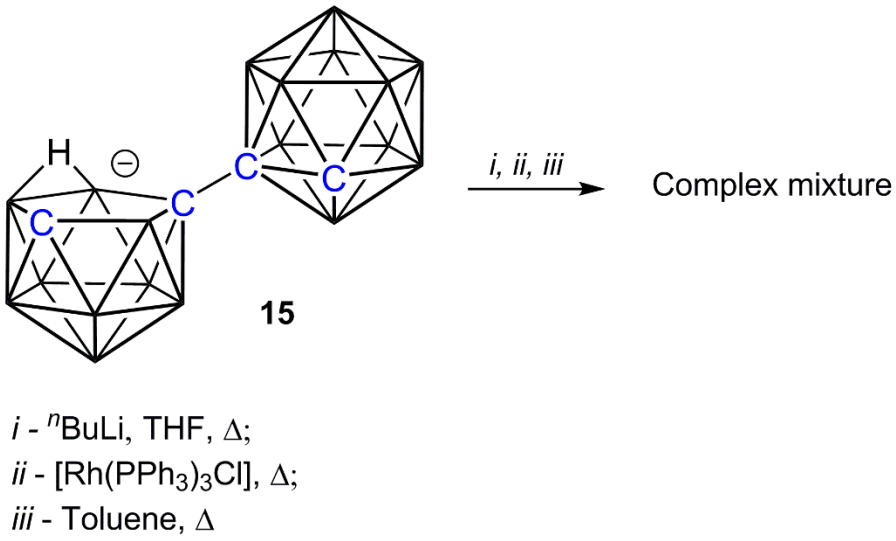

Figure B.7 Attempted metalation of salt **15** using $[Rh(PPh_3)_3Cl]$.

Repeated attempts at the metalation of **15** employing the newly established protocol for inserting $\{Rh(PPh_3)_2H\}$ fragment did not yield the desired product.

Following deprotonation and addition of [$Rh(PPh_3)_3Cl$], no change can be observed in the $^{11}B\{^1H\}$ NMR spectrum even after performing the reaction at reflux temperatures in THF. Subsequently, the solvent was switched to toluene and the reaction mixture was heated to 110 °C for 2 h. The $^{11}B\{^1H\}$ NMR spectrum displayed minimal signals attributed to the nido cage of the starting material indicating metalation has occurred. Spot TLC of the crude mixture shows a large number of close-moving mobile bands (Figure B.8), confirming the formation of neutral, therefore likely metalated, products. Additionally, ^1H NMR spectroscopy displays several, albeit minor, resonances in the hydride region ca. δ -11 ppm.

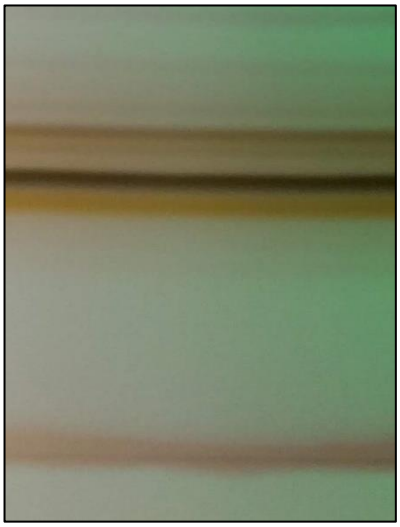

Figure B.8 Preparative TLC of the reaction mixture showing a large number of bands with similar R_f values.

However, upon isolation and analysis of the major components, no hydride signals could be detected in the high-field ^1H NMR experiments suggesting the target compound is likely formed in trace yields. The desired product is likely to have the carboranyl substituent on the lower pentagonal belt of the rhodacarborane to minimise steric congestion, analogous to all known rhodium derivatives of bis(carborane). Therefore, an isomerisation must occur during its formation. Due to already separated nature of the cage C atoms in the precursor **15**, the same thermodynamic driving force is no longer present in comparison to the ortho analogue [**XI**]$^-$. Thus, the isomerisation is likely to require more energy leading to minimum formation of the target compound.

Further investigations within the group have observed the formation of the non-isomerised 2,1,7-MC_2B_9-1′,7′-C_2B_{10} species (where M = {CoCp} and {Ru(*p*-cymene)}) as the sole products.[6] Previous studies[7] have shown the formation of both the non-isomerised and isomerised products upon metalation of [**XI**]$^-$ with the same metal fragments, confirming the additional difficulty of isomerising compounds derived from **15**.

Future attempts of preparing bis(phosphine)hydridorhodium derivatives of bis(*m*-carborane) will require the use temperatures exceeding the trialled 110 °C or potentially variations in the phosphine ligands to adjust the steric factors to promote isomerisation.

References

1. L. I. Zakharkin and A. I. Kovredov, *Bull. Acad. Sci. USSR, Div. Chem. Sci.*, 1973, **22**, 1396.

2. X. Yang, W. Jiang, C. B. Knobler, M. D. Mortimer and M. F. Hawthorne, *Inorg. Chim. Acta*, 1995, **240**, 371-378.

3. L. Elrick, G. M. Rosair and A. J. Welch, *Acta Cryst.*, 2014, **E70**, 376-378.

4. S. Stadlbauer, P. Lönnecke, P. Welzel and E. Hey-Hawkins, *Eur. J. Org. Chem.*, 2010, **2010**, 3129-3139.

5. J. Plešek, B. Štíbr, X. L. R. Fontaine, J. D. Kennedy, S. Heřmánek and T. Jelínek, *Collect. Czech. Chem. Commun.*, 1991, **56**, 1618-1635.

6. R. J. Jeans, A. P. Y. Chan, G. M. Rosair and A. J. Welch, *unpublished*.

7. G. Thiripuranathar, W. Y. Man, C. Palmero, A. P. Y. Chan, B. T. Leube, D. Ellis, D. McKay, S. A. Macgregor, L. Jourdan, G. M. Rosair and A. J. Welch, *Dalton Trans.*, 2015, **44**, 5628-5637.

Appendix C

Crystallographic Tables

Compound	**2*α***	**2*β***	**4**
Empirical Formula	$C_{19}H_{39}B_{18}CoRu$	$C_{19}H_{40}B_{18}CoRu{\cdot}0.5CH_2Cl_2$	$C_{14}H_{36}B_{19}Co$
M/g mol^{-1}	622.08	664.54	468.75
Temperature/K	100	100	120
Crystal System	Triclinic	Triclinic	Orthorhombic
Space Group	$P\bar{1}$	$P\bar{1}$	*Pbca*
a/Å	9.0526(3)	13.0896(9)	14.0429(3)
b/Å	16.0530(5)	15.6050(11)	18.3107(5)
c/Å	19.5784(7)	16.1374(11)	19.0533(4)
α/°	82.385(3)	64.491(3)	90
β/°	87.118(3)	85.635(4)	90
γ/°	78.086(3)	85.818(4)	90
U/Å^3	2758.55(16)	2963.4(4)	4899.27(19)
Z, Z'	4, 2	4, 2	8, 1
F(000)/e	1256	1340	1936
D_{calc}/g cm^{-3}	1.498	1.490	1.271
X-radiation	Cu-K_α	Mo-K_α	Mo-K_α
λ/Å	1.54178	0.71073	0.71073
μ/mm^{-1}	9.190	1.174	0.705
θ_{max}/°	68.24	33.10	29.79
Reflections Collected	39206	77809	51637
Unique Reflections	10028	21546	6532
R_{int}	0.0414	0.0430	0.0479
R, wR_2 (Obs. Data)	0.0430, 0.1172	0.0367, 0.0810	0.0469, 0.1032
S (All Data)	1.086	1.049	1.140
Variables	850	856	375
E_{max}, E_{min}/e Å^{-3}	1.32, -0.80	1.07, -1.32	0.61, -0.41

Compound	**5**	**6**	**9**
Empirical Formula	$C_{14}H_{36}B_{19}Co$	$C_{14}H_{51}B_{19}Co_2 \cdot CHCl_3$	$C_{24}H_{49}B_{18}CoRu \cdot CH_2Cl_2$
M/g mol^{-1}	468.75	782.26	777.13
Temperature/K	120	100	100
Crystal System	Orthorhombic	Triclinic	Triclinic
Space Group	$Pca2_1$	$P\bar{1}$	$P\bar{1}$
a/Å	13.2177(3)	8.3035(5)	9.4177(5)
b/Å	13.9889(4)	15.0776(9)	12.5377(7)
c/Å	27.0886(7)	16.2446(10)	16.5690(10)
α/°	90	72.909(4)	97.298(3)
β/°	90	75.995(4)	98.088(2)
γ/°	90	89.479(4)	111.076(2)
U/Å^3	5008.7(2)	1882.0(2)	1773.66(18)
Z, Z'	8, 2	2, 1	2, 1
F(000)/e	1936	804	792
D_{calc}/g cm^{-3}	1.243	1.380	1.455
X-radiation	Mo-K_α	Mo-K_α	Mo-K_α
λ/Å	0.71073	0.71073	0.71073
μ/mm^{-1}	0.690	1.116	1.065
θ_{max}/°	32.84	27.05	27.48
Reflections Collected	67177	37219	41225
Unique Reflections	14322	8078	10596
R_{int}	0.0488	0.0588	0.0816
R, wR_2 (Obs. Data)	0.0459, 0.1037	0.0512, 0.1145	0.0471, 0.0909
S (All Data)	1.060	1.027	1.012
Variables	750	539	497
E_{max}, E_{min}/e Å^{-3}	0.42, -0.32	0.77, -0.81	0.87, -1.04
Flack Parameter	0.469(19)	-	-

Compound	**10**	**11*α***	**11*β***
Empirical Formula	$C_{40}H_{52}B_{19}P_2Rh \cdot 0.5CH_2Cl_2$	$C_{50}H_{65}B_{18}P_2RhRu \cdot 2CH_2Cl_2$	$C_{50}H_{65}B_{18}P_2RhRu \cdot 1.5CH_2Cl_2$
M/g mol^{-1}	945.52	1296.37	1253.90
Temperature/K	100	100	100
Crystal System	Monoclinic	Monoclinic	Triclinic
Space Group	$P2_1/c$	$P2_1/c$	$P\bar{1}$
a/Å	14.3180(4)	24.3210(5)	10.7800(2)
b/Å	24.5697(6)	14.1399(2)	14.7172(3)
c/Å	13.0131(4)	18.6151(3)	18.7587(4)
α/°	90	90	90.2185(16)
β/°	94.727(3)	107.293(2)	106.5492(18)
γ/°	90	90	101.0331(15)
U/Å^3	4562.3(2)	6112.32(18)	2794.62(10)
Z, Z'	4, 1	4, 1	2, 1
F(000)/e	1932	2632	1274
D_{calc}/g cm^{-3}	1.377	1.409	1.490
X-radiation	Mo-K_α	Cu-K_α	Cu-K_α
λ/Å	0.71073	1.54184	1.54178
μ/mm^{-1}	0.536	6.540	6.706
θ_{max}/°	27.48	68.23	68.24
Reflections Collected	38649	48915	51318
Unique Reflections	10245	11100	10174
R_{int}	0.0725	0.0690	0.0711
R, wR_2 (Obs. Data)	0.0635, 0.1373	0.0605, 0.1651	0.0513, 0.1418
S (All Data)	1.050	1.065	1.039
Variables	625	742	716
E_{max}, E_{min}/e Å^{-3}	2.52, -0.99	1.50, -1.23	2.37, -1.01

Compound	**12*α***	**12*β***	**XXX**
Empirical Formula	$C_{50}H_{66}B_{18}CoP_2Rh \cdot 2.5CH_2Cl_2$	$C_{50}H_{66}B_{18}CoP_2Rh \cdot 2.5CH_2Cl_2$	$C_{38}H_{42}B_9P_2Rh$
M/g mol^{-1}	1297.70	1297.70	760.85
Temperature/K	100	100	150
Crystal System	Monoclinic	Monoclinic	Monoclinic
Space Group	$P2_1/c$	$P2_1/c$	$P2_1/n$
a/Å	20.848(10)	21.082(4)	12.1833(4)
b/Å	29.306(13)	29.554(6)	15.9589(5)
c/Å	20.172(9)	20.354(4)	18.9662(7)
α/°	90	90	90
β/°	97.299(12)	97.60(3)	90.4340(10)
γ/°	90	90	90
U/Å^3	12225(10)	12571(4)	3687.5(2)
Z, Z'	8, 2	8, 2	4, 1
F(000)/e	5304	5304	1560
D_{calc}/g cm^{-3}	1.410	1.371	1.370
X-radiation	Mo-K_α	Mo-K_α	Mo-K_α
λ/Å	0.71073	0.71073	0.71073
μ/mm^{-1}	0.849	0.826	0.578
θ_{max}/°	26.29	24.83	28.30
Reflections Collected	174815	117405	42882
Unique Reflections	24342	20919	9122
R_{int}	0.2373	0.3237[b]	0.0668
R, wR_2 (Obs. Data)	0.1462, 0.3628	0.1091, 0.2503	0.0323, 0.0778
S (All Data)	1.307	0.955	1.052
Variables	1340	1340	487
E_{max}, E_{min}/e Å^{-3}	6.69[a], -2.50	1.54, -2.63	0.52/-0.55

[a]E_{max} peak observed within 1 Å of the rhodium atom.

[b]High R_{int} value due to poor data.

Compound	**13**	**15**
Empirical Formula	$C_{38}H_{42}B_9O_6P_2Rh \cdot 0.5CHCl_3$	$C_8H_{32}B_{19}N \cdot CH_2Cl_2$
M/g mol^{-1}	917.04	420.65
Temperature/K	120	120
Crystal System	Triclinic	Orthorhombic
Space Group	$P\bar{1}$	*Pbcm*
a/Å	10.6882(4)	19.1302(12)
b/Å	14.2317(4)	9.4004(7)
c/Å	14.5349(4)	13.2215(8)
α/°	93.476(2)	90
β/°	91.133(3)	90
γ/°	108.203(3)	90
U/Å^3	2059.28(12)	2377.6(3)
Z, Z'	2, 1	4, 0.5
F(000)/e	935	872
D_{calc}/g cm^{-3}	1.479	1.175
X-radiation	Mo-K_α	Mo-K_α
λ/Å	0.71073	0.71073
μ/mm^{-1}	0.636	0.272
θ_{max}/°	31.21	28.97
Reflections Collected	55290	11042
Unique Reflections	12276	2894
R_{int}	0.0446	0.0590
R, wR_2 (Obs. Data)	0.0325, 0.0660	0.1321, 0.2649
S (All Data)	1.026	1.173
Variables	573	208
E_{max}, E_{min}/e Å^{-3}	0.47, -0.54	0.51/-0.51

Dalton Transactions

PAPER

View Article Online
View Journal | View Issue

Cite this: *Dalton Trans.*, 2015, **44**, 5628

Icosahedral metallacarborane/carborane species derived from 1,1′-bis(*o*-carborane)†‡

Gobika Thiripuranathar, Wing Y. Man, Cesar Palmero, Antony P. Y. Chan, Bernhard T. Leube, David Ellis, David McKay, Stuart A. Macgregor, Laure Jourdan, Georgina M. Rosair and Alan J. Welch*

Received 8th January 2015,
Accepted 9th February 2015

DOI: 10.1039/c5dt00081e

www.rsc.org/dalton

Examples of singly-metallated derivatives of 1,1′-bis(*o*-carborane) have been prepared and spectroscopically and structurally characterised. Metallation of [7-(1′-1′,2′-*closo*-$C_2B_{10}H_{11}$)-7,8-*nido*-$C_2B_9H_{10}$]$^{2-}$ with a {Ru(*p*-cymene)}$^{2+}$ fragment affords both the unisomerised species [1-(1′-1′,2′-*closo*-$C_2B_{10}H_{11}$)-3-(*p*-cymene)-3,1,2-*closo*-$RuC_2B_9H_{10}$] (**2**) and the isomerised [8-(1′-1′,2′-*closo*-$C_2B_{10}H_{11}$)-2-(*p*-cymene)-2,1,8-*closo*-$RuC_2B_9H_{10}$] (**3**), and **2** is easily transformed into **3** with mild heating. Metallation with a preformed {CoCp}$^{2+}$ fragment also affords a 3,1,2-MC_2B_9-1′,2′-C_2B_{10} product [1-(1′-1′,2′-*closo*-$C_2B_{10}H_{11}$)-3-Cp-3,1,2-*closo*-$CoC_2B_9H_{10}$] (**4**), but if $CoCl_2$/NaCp is used followed by oxidation the result is the 2,1,8-CoC_2B_9-1′,2′-C_2B_{10} species [8-(1′-1′,2′-*closo*-$C_2B_{10}H_{11}$)-2-Cp-2,1,8-*closo*-$CoC_2B_9H_{10}$] (**5**). Compound **4** does not convert into **5** in refluxing toluene, but does do so if it is reduced and then reoxidised, perhaps highlighting the importance of the basicity of the metal fragment in the isomerisation of metallacarboranes. A computational study of 1,1′-bis(*o*-carborane) is in excellent agreement with a recently-determined precise crystallographic study and establishes that the {1′,2′-*closo*-$C_2B_{10}H_{11}$} fragment is electron-withdrawing compared to H.

Introduction

1,1′-Bis(*o*-carborane), the trivial name for [1-(1′-1′,2′-*closo*-$C_2B_{10}H_{11}$)-1,2-*closo*-$C_2B_{10}H_{11}$] (Fig. 1), is the simplest bis(carborane) species, comprising two *ortho*-carborane units connected by a C–C bond.[1] It was first synthesised by insertion of diacetylene into B_{10} frameworks[2] but it is also produced from the $CuCl_2$-mediated coupling reactions of mono- or di-lithiated salts of *ortho*-carborane,[3] although yields by this route are somewhat compromised by the additional formation of C–B and B–B linked isomers. $CuCl_2$-coupling was also used to make 1,1′-bis(*m*-carborane)[3,4] and 1,1′-bis(*p*-carborane),[4,5] the latter an important starting point for the construction of "carborods", rigid-rod oligomers of *para*-carborane. Ref. 5(*a*) also notes that 1,1′-bis(*p*-carborane) can be prepared by CuCl-coupling, an idea subsequently used by Xie to afford an improved yield of 1,1′-bis(*o*-carborane).[6]

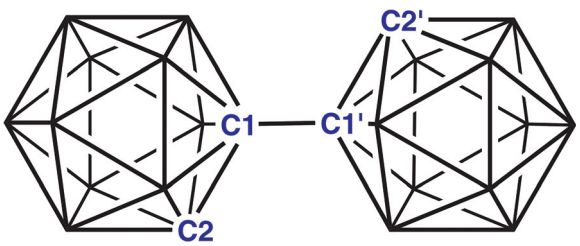

Fig. 1 1,1′-bis(*o*-carborane).

Although 1,1′-bis(*o*-carborane) has been known for many years, its chemistry remains underdeveloped. Double deprotonation forms a dianionic chelating ligand which has been used to complex a variety of transition-metal cations[7] and also an {AsMe} fragment.[8] Mono- and di-deboronation (single and double "decapitation", respectively) of 1,1′-bis(*o*-carborane) has also been reported.[9] In addition, 1,1′-bis(*o*-carborane) has been reduced with both 2e and 4e.[10] In solution, $[PPh_3Me]^+$ and $[(15\text{-crown-}5)_3Na_2]^{2+}$ salts of the 2e reduced species are identical, whilst in the solid state the anion of the $[PPh_3Me]^+$ salt has two partially-open 4-atom CBCB faces[11] and the anion of the $[(15\text{-crown-}5)_3Na_2]^{2+}$ salt has one 4-atom CBCB face which is partially-open and one 5-atom CBCBB face which is rather more open.[10] Double protonation of the 4e reduced form and subsequent work-up caused the linking C atoms to adopt bridging positions on B–B edges above *nido* 11-vertex

Institute of Chemical Sciences, Heriot-Watt University, Edinburgh, UK EH14 4AS. E-mail: a.j.welch@hw.ac.uk; Tel: +44 (0)131 451 3217

† In memory of Professor Kenneth Wade.

‡ Electronic supplementary information (ESI) available: Table S1; ^{11}B NMR chemical shifts for key reference compounds. Tables S2–S5; computational models. CCDC 1042151–1042155 (salt [BTMA][**1**] and compounds **2–5**, respectively). For ESI and crystallographic data in CIF or other electronic format see DOI: 10.1039/c5dt00081e

cages, in a similar manner to the protonation and work-up of [7,9-*nido*-$C_2B_{10}H_{12}$]$^{2-}$ affording [$\mu_{9,10}$-CH_2-7-*nido*-$CB_{10}H_{11}$]$^-$.[12]

Prior to our recent research[13,14] the only metallacarboranes derived from bis(carboranes) of which we are aware are two 2,1,8-MC_2B_9-1′,2′-C_2B_{10} species[15,16] and two bis(metallacarboranes),[17] one of 3,1,2-MC_2B_9-3′,1′,2′-MC_2B_9 geometry and the other of 3,1,2-MC_2B_9-2′,1′,8′-MC_2B_9 geometry.[18]

Recently we explored the consequences of 4e reduction and metallation of bis(*o*-carborane). Reduction and metallation with {Ru(*p*-cymene)}$^{2+}$ fragments (*p*-cymene = η-$C_{10}H_{14}$, 1-^{i}Pr,4-MeC_6H_4) led unexpectedly to a 13-vertex metallacarborane/12-vertex carborane species and cleavage of an aromatic C–C bond under ambient conditions.[13] Reduction and metallation with {CoCp}$^{2+}$ fragments (Cp = η-C_5H_5) afforded racemic and meso diastereoisomers of the 13-vertex metallacarborane/13-vertex metallacarborane species [1-(1′-4′-Cp-4′,1′,6′-*closo*-$CoC_2B_{10}H_{11}$)-4-Cp-4,1,6-*closo*-$CoC_2B_{10}H_{11}$].[14]

In this contribution we report the monodeboronation and subsequent metallation with {ML} fragments (L = η-bonded polyene) of 1,1′-bis(*o*-carborane) leading to 12-vertex metallacarborane/12-vertex carborane products with both non-isomerised [1-(1′-1′,2′-*closo*-$C_2B_{10}H_{11}$)-3-L-3,1,2-*closo*-$MC_2B_9H_{10}$] and isomerised [8-(1′-1′,2′-*closo*-$C_2B_{10}H_{11}$)-2-L-2,1,8-*closo*-$MC_2B_9H_{10}$] architectures. We describe detailed spectroscopic and structural studies of these products and investigate the isomerisation between them.

Results and discussion

Monodeboronation of 1,1′-bis(*o*-carborane) with one equivalent of KOH in refluxing EtOH, according to the procedure outlined by Hawthorne *et al.*,[9] followed by cation metathesis, afforded the anion [7-(1′-1′,2′-*closo*-$C_2B_{10}H_{11}$)-7,8-*nido*-$C_2B_9H_{11}$]$^-$ ([**1**]$^-$), as either the [$HNMe_3$]$^+$ or [BTMA]$^+$ salt (BTMA = benzyltrimethylammonium) in good yields. The ^{1}H NMR spectrum of [**1**]$^-$ shows, in addition to the resonances associated with the appropriate cation, two CH_{cage} resonances of equal integral at δ *ca.* 4.4 and 2.0 ppm. The former is assigned to the {*closo*-C_2B_{10}} component and the latter to the {*nido*-C_2B_9} component with reference to the spectra of 1,1′-bis(*o*-carborane) and [7,8-*nido*-$C_2B_9H_{12}$]$^-$.[19]

The ^{11}B{^{1}H} NMR spectrum of [**1**]$^-$ consists of a 1 : 1 : 1 : 5 : 2 : 3 : 2 : 1 : 1 : 1 : 1 pattern between δ −4 and −36 ppm. A ^{11}B{^{1}H}-^{11}B{^{1}H} COSY spectrum of [$HNMe_3$][**1**] in $(CD_3)_2CO$ was obtained in an attempt to assign these resonances to {*closo*-C_2B_{10}} or {*nido*-C_2B_9} components. By analogy with the spectra of [7,8-*nido*-$C_2B_9H_{12}$]$^-$ [19] and 1,2-*closo*-$C_2B_{10}H_{12}$,[20] it seems reasonable to suggest that the two highest frequency resonances are due to the {*closo*-C_2B_{10}} cage and the four lowest frequency resonances are due to the {*nido*-C_2B_9} cage, but beyond this it was not possible to deconvolute the entire spectrum of [**1**]$^-$ unambiguously.

The salt [$HNMe_3$][**1**] is a convenient starting point for the synthesis of MC_2B_9-C_2B_{10} products by deprotonation then metallation, following the protocol established for the first metallacarborane by Hawthorne *et al.*[21]

Following deprotonation of [$HNMe_3$][**1**] with *n*-BuLi in THF and addition of [$RuCl_2$(*p*-cymene)]$_2$, yellow [1-(1′-1′,2′-*closo*-$C_2B_{10}H_{11}$)-3-(*p*-cymene)-3,1,2-*closo*-$RuC_2B_9H_{10}$] (**2**) and colourless [8-(1′-1′,2′-*closo*-$C_2B_{10}H_{11}$)-2-(*p*-cymene)-2,1,8-*closo*-$RuC_2B_9H_{10}$] (**3**) were isolated in yields of 8 and 19%, respectively. Both compounds were initially characterised by elemental microanalysis and EI mass spectrometry, the latter clearly showing the molecular ion peaks as a characteristic envelope due to the two naturally-occurring boron isotopes.

In the ^{1}H spectrum of a freshly-prepared $CDCl_3$ solution of **2** are CH_{cage} resonances at δ 4.03 and 3.91 but these are too close to each other to speculate which is due to the carborane and which is due to the ruthenacarborane. The ^{1}H NMR spectrum of **2** also confirms overall molecular asymmetry with two integral-3 doublets (and not one integral-6 doublet) for the CH(CH_3)$_2$ protons of the *p*-cymene ligand. The ^{11}B{^{1}H} NMR spectrum of **2** consists of ten resonances between δ 2.8 and −17.2 with relative integrals 1 : 1 : 2 : 1 : 2 : 2 : 4 : 2 : 1 : 3 from high frequency to low frequency.

With time, solutions of **2** show clear evidence for a slow transformation of **2** into an isomer **3**, a compound which was originally isolated along with **2** from the initial reaction. A THF solution of **2** heated to reflux for two hours reveals its complete conversion to **3**, with 58% of the compound being recovered following work-up involving thin layer chromatography (TLC). In **3** there is a significantly greater separation of the CH_{cage} resonances, which now appear at δ 3.64 and 2.63. Since only the ruthenacarborane part of **2** has changed in its isomerisation into **3** we tentatively assign the lower frequency resonance, δ 2.63, as arising from CH_{cage} in the {RuC_2B_9} portion of **3**. Once again the resonances due to the *p*-cymene ligand reveal the overall molecular structure to be asymmetric. In the ^{11}B{^{1}H} NMR spectrum of **3** are ten resonances between δ −1.0 and −20.4 with integrals in the relative ratios 2 : 2 : 1 : 2 : 1 : 6 : 2 : 1 : 1 : 1.

In addition to {Ru(arene)}[22] a common transition-metal fragment in metallacarborane chemistry is {CoCp}. There are two different ways to introduce this fragment to afford a $CpCoC_2B_x$ metallacarborane, (i) reaction of the [C_2B_x]$^{2-}$ dianion with $CoCl_2$/NaCp (*i.e. in situ* generation of the {CoCp} fragment) followed by oxidation ($Co^{II} \rightarrow Co^{III}$)[23] or (ii) reaction of the [C_2B_x]$^{2-}$ dianion with [CpCo(CO)I_2] (*i.e.* using a "preformed" {CoCp} fragment).[24] In reaction with [$C_2B_9H_{11}$]$^{2-}$ both approaches lead to exactly the same product, but we have found that this is *not* the case starting from [**1**]$^-$.

Deprotonation of [$HNMe_3$][**1**] followed by addition of [CpCo(CO)I_2] affords, on work-up, the isomer [1-(1′-1′,2′-*closo*-$C_2B_{10}H_{11}$)-3-Cp-3,1,2-*closo*-$CoC_2B_9H_{10}$] (**4**) as an orange solid. Microanalysis and mass spectrometry confirm the molecular formula. In the ^{1}H NMR spectrum are three singlets at δ 5.86 (5H, Cp), 4.24 (1H) and 4.03 (1H), the last two relatively broad and arising from the cage C*H* atoms. In the ^{11}B NMR spectrum are nine resonances in a 1 : 1 : 5 : 1 : 2 : 5 : 2 : 1 : 1 pattern, lying between δ 6.5 and −15.9 ppm.

To our surprise, treatment of deprotonated $[HNMe_3][\mathbf{1}]$ with $CoCl_2$/NaCp followed by aerial oxidation yielded an isomer of **4**, the 2,1,8-1′,2′ species [8-(1′-1′,2′-*closo*-$C_2B_{10}H_{11}$)-2-Cp-2,1,8-*closo*-$CoC_2B_9H_{10}$] (**5**). This yellow product has, as well as the expected singlet for the Cp protons, cage C*H* resonances at lower frequency than in **4**, δ 3.59 and 2.73. In **4** the $\{CoC_2B_9\}$ part of the molecule has a 3,1,2-CoC_2 heteroatom pattern whilst in **5** it is 2,1,8-CoC_2. In the corresponding reference compound [3-Cp-3,1,2-*closo*-$CoC_2B_9H_{11}$] the cage C*H* atoms resonate at δ 4.08 ($CDCl_3$) and in [2-Cp-2,1,8-*closo*-$CoC_2B_9H_{11}$] they resonate at δ 2.73 and 2.47,[25] on the basis of which we tentatively assign the signal at δ 2.73 in **5** to the $\{2,1,8\text{-}CoC_2B_9\}$ fragment. The ^{11}B NMR spectrum of **5** reveals eleven resonances between δ 1.7 and −17.7 in a 1 : 2 : 1 : 1 : 1 : 2 : 6 : 1 : 2 : 1 : 1 pattern of integrals. Note that in the synthesis of **4** a trace amount of **5** is also detected (see Experimental) and that in the synthesis of **5** a trace amount of **4** is observed.

Given that the 3,1,2-RuC_2B_9-1′,2′-C_2B_{10} species **2** easily transforms to its isomer 2,1,8-RuC_2B_9-1′,2′-C_2B_{10} **3** on heating to reflux in THF we attempted to thermally isomerise the 3,1,2-CoC_2B_9-1′,2′-C_2B_{10} species **4**, expecting it to convert into 2,1,8-CoC_2B_9-1′,2′-C_2B_{10} **5**. However, even in refluxing toluene for five hours there is no evidence that **4** converts into **5** by thermolysis. We later show from crystallographic studies that, at least as far as we can tell, compounds **2** and **4** suffer similar degrees of intramolecular steric crowding, implying that the different isomerisation characteristics of **2** and **4** cannot be explained by steric factors.

When $[\mathbf{1}]^{2-}$ is treated with $[CpCo(CO)I_2]$ a $\{Co^{III}Cp\}^{2+}$ fragment is introduced to the dianion, affording the non-isomerised **4**. However, when $[\mathbf{1}]^{2-}$ is treated with $CoCl_2$/NaCp the reacting fragment is $\{Co^{II}Cp\}^{+}$. This generates the 19e monoanion $[CpCo^{II}(C_2B_9H_{10})(C_2B_{10}H_{11})]^{-}$, which is then oxidised to the 18e, isomerised, Co^{III} species **5**. We therefore added one equivalent of electrons to **4** at room temperature and, after stirring for one hour, oxidised the product aerially. Only **5** was detected by ^{1}H and ^{11}B NMR spectroscopies. This strongly implies that in the bulk synthesis of **5**, a $[3,1,2\text{-}CoC_2B_9\text{-}1',2'\text{-}C_2B_{10}]^{-}$ species is formed first (as would be expected from the reaction between a $\{CoCp\}^{+}$ cation and a $[7,8\text{-}C_2B_9\text{-}1',2'\text{-}C_2B_{10}]^{2-}$ anion) and that this 19e anionic intermediate then isomerises before it is oxidised. Taken together with the facile isomerisation of the 3,1,2-RuC_2B_9-1′,2′-C_2B_{10} *p*-cymene species **2** these observations highlight that the basicity of the metal fragment, and not just its steric bulk, might be important in effecting a 3,1,2-MC_2B_9 to 2,1,8-MC_2B_9 isomerisation.

For compounds **2**, **4** and **5** we attempted to identify which ^{11}B resonances were due to which part of the molecule ($\{MC_2B_9\}$ or $\{C_2B_{10}\}$) from $^{11}B\{^1H\}$–$^{11}B\{^1H\}$ COSY spectra but, as was the case with $[\mathbf{1}]^{-}$, it proved impossible to do this unambiguously. In Table 1 we list the weighted average ^{11}B chemical shifts, $\langle\delta(^{11}B)\rangle$, of the conjoined species 1,1′-bis(*o*-carborane), **2**, **4** and **5** along with those of their "components", [1,2-*closo*-$C_2B_{10}H_{12}$],[20] [3-(*p*-cymene)-3,1,2-*closo*-$RuC_2B_9H_{11}$],[26] [3-Cp-3,1,2-*closo*-$CoC_2B_9H_{11}$][23] and [2-Cp-2,1,8-*closo*-$CoC_2B_9H_{11}$].[25]

Table 1 Weighted average ^{11}B NMR chemical shifts, $\langle\delta(^{11}B)\rangle$, for conjoined cage compounds and their "components".[a] All spectra recorded in $CDCl_3$ at room temperature

Compound	$\langle\delta(^{11}B)\rangle$
1,1′-bis(*o*-carborane)	−8.9
[1-(1′-1′,2′-*closo*-$C_2B_{10}H_{11}$)-3-(*p*-cymene)-3,1,2-*closo*-$RuC_2B_9H_{10}$] (**2**)	−9.1
[1-(1′-1′,2′-*closo*-$C_2B_{10}H_{11}$)-3-Cp-3,1,2-*closo*-$CoC_2B_9H_{10}$] (**4**)	−6.7
[8-(1′-1′,2′-*closo*-$C_2B_{10}H_{11}$)-2-Cp-2,1,8-*closo*-$CoC_2B_9H_{10}$] (**5**)	−7.9
1,2-*closo*-$C_2B_{10}H_{12}$	−10.7
3-(*p*-cymene)-3,1,2-*closo*-$RuC_2B_9H_{11}$	−10.5
3-Cp-3,1,2-*closo*-$CoC_2B_9H_{11}$	−7.3
2-Cp-2,1,8-*closo*-$CoC_2B_9H_{11}$	−7.7

[a] For 1,1′-bis(*o*-carborane), 1,2-*closo*-$C_2B_{10}H_{12}$, 3-(*p*-cymene)-3,1,2-*closo*-$RuC_2B_9H_{11}$, 3-Cp-3,1,2-*closo*-$CoC_2B_9H_{11}$ and 2-Cp-2,1,8-*closo*-$CoC_2B_9H_{11}$ individual ^{11}B chemical shifts are given in Table S1 (ESI).

Although the spectra of 1,1′-bis(*o*-carborane)[3,6] and all these "components" have been reported previously we have re-measured some of them here in $CDCl_3$ for internal consistency. Note that we have not included compound **3** in this Table since its $\{MC_2B_9\}$ component, [2-(*p*-cymene)-2,1,8-*closo*-$RuC_2B_9H_{11}$], is not currently known.

These data show that when 1,1′-bis(*o*-carborane) and the metallacarborane-carborane species **2**, **4** and **5** are "constructed" from their constituent parts the $\langle\delta(^{11}B)\rangle$ value for the "product" lies to high frequency of the (weighted) average of that of the two "components". For **5** the $\langle\delta(^{11}B)\rangle$ value is very close (and slightly to low frequency of) to that for the metallacarborane component, whilst for 1,1′-bis(*o*-carborane), **2** and **4** the $\langle\delta(^{11}B)\rangle$ value is actually to high frequency of that of both components.

A shift to higher frequency of the average ^{11}B resonance implies, overall, that the B nuclei in these last two conjoined cages are deshielded, and therefore δ+, relative to those in the individual components. A comparative computational study of [1,2-*closo*-$C_2B_{10}H_{12}$] and 1,1′-bis(*o*-carborane) supports this conclusion. By DFT calculation we find effectively no preference in 1,1′-bis(*o*-carborane) between conformations with C2–C1–C1′–C2′ torsion angles of 108° and 180° (Fig. 2). In terms

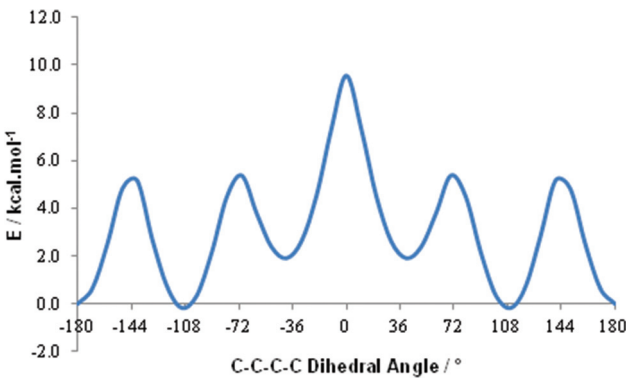

Fig. 2 Plot of energy *vs.* dihedral angle for 1,1′-bis(*o*-carborane) from DFT calculation where the C2–C1–C1′–C2′ torsion angle was subjected to a relaxed scan from –180° to 0° and the resulting data points mirrored to illustrate full 360° rotation.

of only the electronic energy the 108° conformation is favoured by 0.2 kcal mol^{-1}, whereas if zero point energy is included the 180° conformation is preferred by 0.5 kcal mol^{-1}. The barrier to free rotation about the C1–C1′ bond is only *ca.* 10 kcal mol^{-1}, corresponding to a transition state at a C2–C1–C1′–C2′ torsion angle of 0°. Computational models are listed in the ESI.‡ It is very satisfying to note that our recent definitive crystallographic study of 1,1′-bis(*o*-carborane) found that the non-linking C atom is equally disordered between vertices 2 and 3 (and, by symmetry, 2′ and 3′).[1] This means that in the crystal any one molecule of 1,1′-bis(*o*-carborane) is equally likely to have a C–C–C–C torsion angle of 180° (C2–C1–C1′–C2′) or 108° (C3–C1–C1′–C2′), in perfect agreement with the results of the DFT study. The computed C1–C1′ distance in the 180° conformation is 1.542 Å, and in the 108° conformation it is 1.540 Å. Experimentally C1–C1′ is 1.5339(11) Å.[1]

Table 2 Natural atomic charges in 1,2-*closo*-$C_2B_{10}H_{12}$ and 1,1′-bis(*o*-carborane) (180° conformation) by DFT calculation. H atoms carry the same number as the B or C to which they are bonded

Atom	Charge
(a) 1,2-*closo*-$C_2B_{10}H_{12}$	
C1, C2	−0.56
B3, B6	+0.13
B4, B5, B7, B11	−0.03
B8, B10	−0.19
B9, B12	−0.17
H1, H2	+0.36
H3, H6	+0.08
H4, H5, H7, H11	+0.10
H8, H10	+0.11
H9, H12	+0.10
(b) 1,1′-bis(*o*-carborane)	
C1	−0.31
C2	−0.51
B3, B6	+0.15
B4, B5	−0.01
B7, B11	−0.01
B8, B10	−0.18
B9	−0.16
B12	−0.14
H2	+0.32
H3, H6	+0.08
H4, H5	+0.08
H7, H11	+0.09
H8, H10	+0.10
H9	+0.10
H12	+0.09

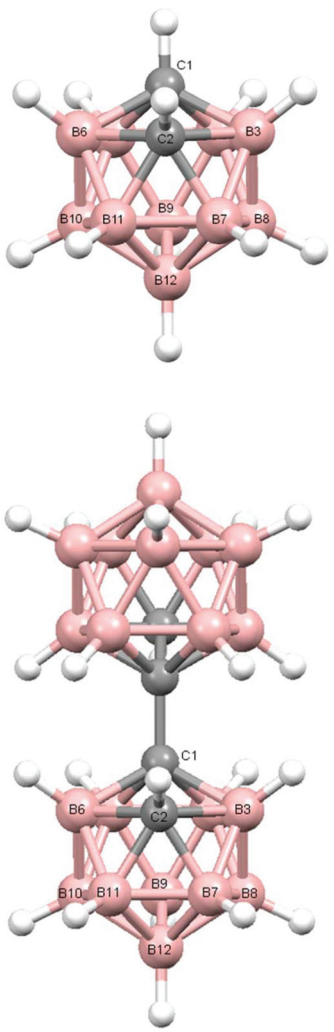

In Table 2 we list the natural charges for atoms in [1,2-*closo*-$C_2B_{10}H_{12}$] and 1,1′-bis(*o*-carborane), the latter in the 180° conformation. In [1,2-*closo*-$C_2B_{10}H_{12}$] the C atoms carry a charge of −0.56 and the B atoms an average charge of −0.06. H bonded to C is +0.36 whilst the average charge of H bonded to B is +0.10. In 1,1′-bis(*o*-carborane) the negative charge on both C atoms decreases (C1, the substituted atom, −0.31; C2, −0.51) and the B atoms are also less negative (average charge −0.04). The remaining C-bonded H atom carries a charge of +0.32 and the average charge on H bound to B is +0.09. Thus substitution of one of the C-bound H atoms in [1,2-*closo*-$C_2B_{10}H_{12}$] by a {1′,2′-*closo*-$C_2B_{10}H_{11}$} unit causes all the polyhedral atoms (both C and B) in the original cage to become less negatively charged. At the same time there is an opposite, but smaller, change in the charges on the H atoms bonded to the polyhedral atoms, which become slightly less positively charged. The overall charge on the {$C_2B_{10}H_{11}$} fragment changes from −0.36 in [1,2-*closo*-$C_2B_{10}H_{12}$] to precisely zero in 1,1′-bis(*o*-carborane).[27] In brief the {1′,2′-*closo*-$C_2B_{10}H_{11}$} substituent is electron-withdrawing compared to H. This conclusion is consistent with our analysis of the $<\delta(^{11}B)>$ values for 1,1′-bis(*o*-carborane) and for **2**.

Salt [BTMA][**1**] and compounds **2**–**5** were also studied crystallographically. In [BTMA][**1**] (Fig. 3) the C_2B_{10} cage is ordered but the C_2B_9 cage is disordered with positions 3 and 12 partially occupied by boron. The second C atom of the *nido* cage is ordered, however, and the C8–C7–C1′–C2′ torsion angle is 177.2(6)°. The linking C7–C1′ bond length is 1.514(9) Å.

Perspective views of single molecules of the 3,1,2-RuC_2B_9-1′,2′-C_2B_{10} species **2**, its 2,1,8-RuC_2B_9-1′,2′-C_2B_{10} analogue **3**, and the equivalent cobalt species **4** and **5** are presented in

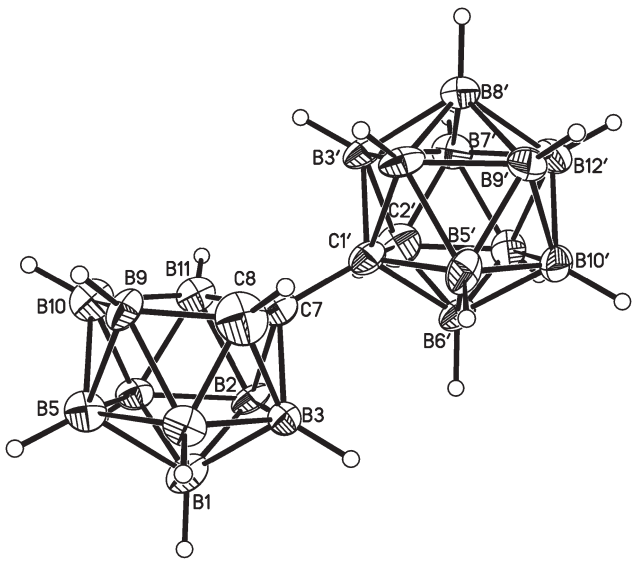

Fig. 3 Perspective view of the anion in the salt [BTMA][**1**] and atom numbering scheme. In the unprimed cage there is partial disorder of B3, part of which appears as the 12th atom of an icosahedron (not shown for clarity); partial occupancies are B3 0.548(10) and B12 0.452(10). The H atom bridging on the open face of the unprimed cage was not located. Displacement ellipsoids are drawn at the 40% probability level except for H atoms.

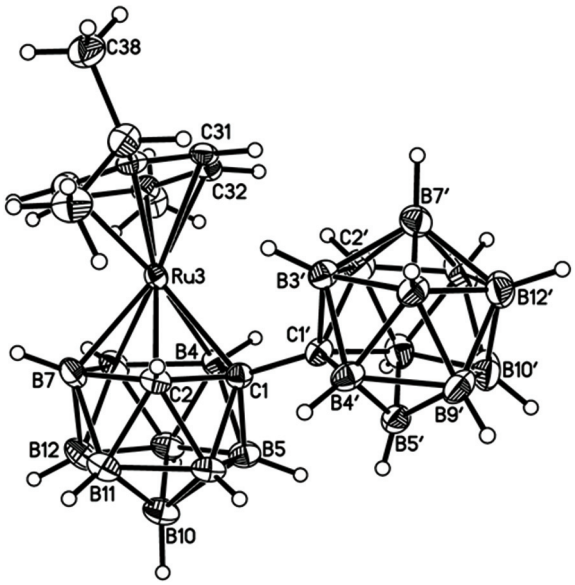

Fig. 4 Perspective view of compound **2** and atom numbering scheme. Displacement ellipsoids are drawn at the 50% probability level except for H atoms.

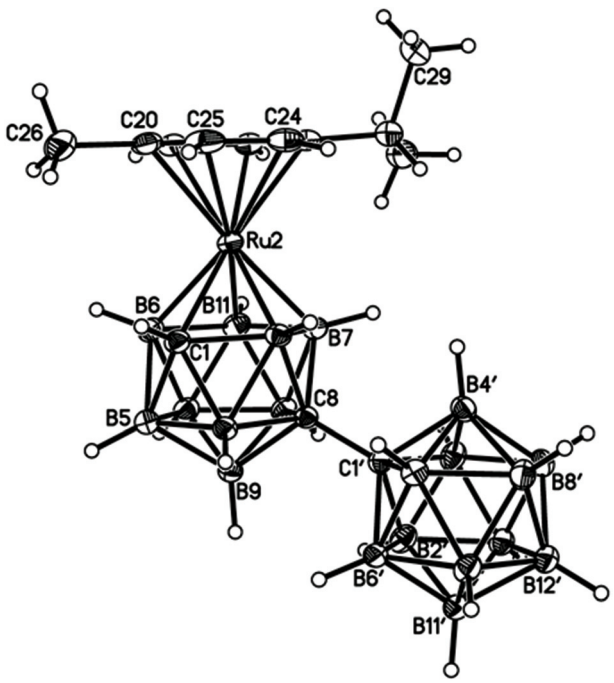

Fig. 5 Perspective view of compound **3** and atom numbering scheme. Position 2′ is 0.446(19)B + 0.554(19)C, with complementary occupations at position 3′. Displacement ellipsoids as for Fig. 4.

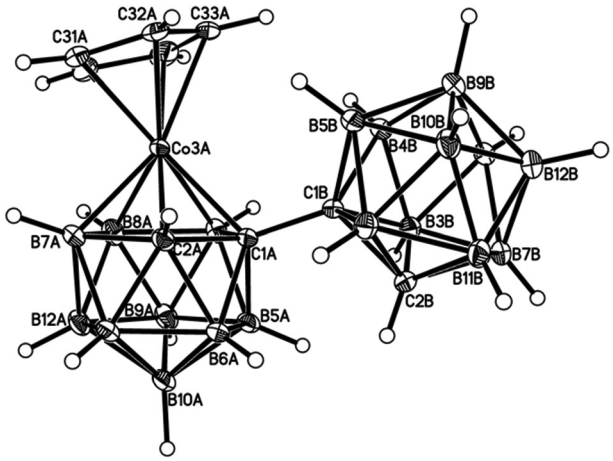

Fig. 6 Perspective view of one of two crystallographically-independent molecules (molecule AB) of compound **4** and atom numbering scheme. Displacement ellipsoids as for Fig. 4.

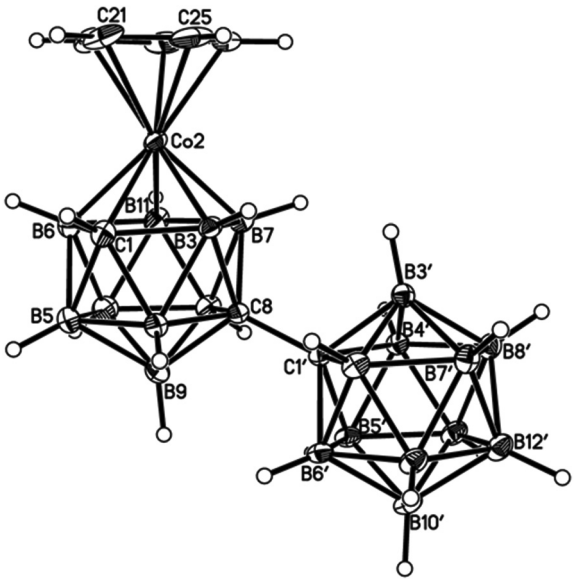

Fig. 7 Perspective view of compound **5** and atom numbering scheme. Displacement ellipsoids as for Fig. 4.

Fig. 4–7, respectively. Since compounds **2**, **4** and **5** are composed of {3,1,2-*closo*-RuC_2B_9} (compound **2**), {3,1,2-*closo*-CoC_2B_9} (compound **4**) and {2,1,8-*closo*-CoC_2B_9} (compound **5**) icosahedra conjoined to {1,2-*closo*-C_2B_{10}} icosahedra, and all these individual components have previously been studied crystallographically, we have used the *Structure Overlay* tool in Mercury[28] to calculate individual atom and overall fragment root-mean-square (rms) misfits between the components of **2**, **4** and **5** and the corresponding literature molecules (there is currently no structural study of a 2-(arene)-2,1,8-*closo*-$RuC_2B_9H_{11}$ species in the literature and so a similar exercise cannot be undertaken for compound **3**). The results, summarised in Table 3, clearly show that for the {3,1,2-MC_2B_9} fragments the greatest misfit is at the metal vertex, *ca.* 0.08–0.09 Å, and that the misfit at C1 (the position of substitution) is also relatively large, *ca.* 0.06–0.08 Å. The overall misfit for {3,1,2-MC_2B_9} is typically 0.038–0.040 Å. In contrast the misfit for the {2,1,8-MC_2B_9} fragment is considerably less with an overall misfit of only 0.012 Å, the greatest individual misfit, 0.025 Å, occurring at C8 (the position of substitution) and no other

Table 3 Rms deviations (Å) between the $\{MC_2B_9\}$ and $\{C_2B_{10}\}$ "components" of compounds **2**, **4** and **5** and these fragments in reference single cage compounds

Compound **2**[a]				Compound **4** (**C–D**)[b]				Compound **4** (**C–D**)[b]				Compound **5**[c]			
$\{RuC_2B_9\}$	Dev.	$\{C_2B_{10}\}$	Dev.	$\{CoC_2B_9\}$	Dev.	$\{C_2B_{10}\}$	Dev.	$\{CoC_2B_9\}$	Dev.	$\{C_2B_{10}\}$	Dev.	$\{CoC_2B_9\}$	Dev.	$\{C_2B_{10}\}$	Dev.
C1	0.066	C1′	0.054	C1	0.074	C1′	0.059	C1	0.076	C1′	0.054	C1	0.004	C1′	0.032
C2	0.036	C2′	0.056	C2	0.039	C2′	0.020	C2	0.037	C2′	0.017	Co2	0.012	C2′	0.056
Ru3	0.083	B3′	0.039	Co3	0.081	B3′	0.009	Co3	0.091	B3′	0.009	B3	0.006	B3′	0.013
B4	0.033	B4′	0.012	B4	0.024	B4′	0.016	B4	0.025	B4′	0.016	B4	0.006	B4′	0.014
B5	0.025	B5′	0.047	B5	0.028	B5′	0.013	B5	0.020	B5′	0.014	B5	0.008	B5′	0.024
B6	0.038	B6′	0.017	B6	0.025	B6′	0.008	B6	0.037	B6′	0.008	B6	0.010	B6′	0.044
B7	0.008	B7′	0.008	B7	0.016	B7′	0.022	B7	0.012	B7′	0.015	B7	0.018	B7′	0.011
B8	0.016	B8′	0.009	B8	0.010	B8′	0.005	B8	0.006	B8′	0.010	C8	0.025	B8′	0.007
B9	0.009	B9′	0.009	B9	0.008	B9′	0.010	B9	0.011	B9′	0.006	B9	0.000	B9′	0.010
B10	0.025	B10′	0.005	B10	0.013	B10′	0.009	B10	0.019	B10′	0.009	B10	0.005	B10′	0.006
B11	0.013	B11′	0.017	B11	0.011	B11′	0.011	B11	0.009	B11′	0.017	B11	0.016	B11′	0.009
B12	0.006	B12′	0.013	B12	0.014	B12′	0.017	B12	0.015	B12′	0.016	B12	0.005	B12′	0.013
Overall	0.038	Overall	0.030	Overall	0.037	Overall	0.021	Overall	0.039	Overall	0.020	Overall	0.012	Overall	0.025

[a] The reference $\{RuC_2B_9\}$ compound is 3-(*p*-cymene)-3,1,2-*closo*-$RuC_2B_9H_{11}$ (ref. 26). CCDC refcode ODOGAQ. [b] The reference $\{CoC_2B_9\}$ compound is 3-Cp-3,1,2-*closo*-$CoC_2B_9H_{11}$ (ref. 45). CCDC refcode DUBDIN. [c] The reference $\{CoC_2B_9\}$ compound is 2-Cp-2,1,8-*closo*-$CoC_2B_9H_{11}$ (ref. 25). CCDC refcode NOWMIX00. [a–c] In all cases the reference $\{C_2B_{10}\}$ compound is 1,2-*closo*-$C_2B_{10}H_{12}$ (ref. 46). CCDC refcode TOKGIJ. We arbitrarily used the molecule containing C13 and C14 (CCDC numbering) matching C13 with C1′.

atom having a misfit >0.018 Å. The $\{C_2B_{10}\}$ fragments fit better with their reference molecule, the overall misfit here being 0.02–0.03 Å, and it is always C1′ or C2′ that has the largest individual misfit, typically 0.05–0.06 Å.

It is clear from Fig. 4 and 6 that a consistent feature of the 3,1,2-MC_2B_9-1′,2′-C_2B_{10} structures is a pronounced bend-back of the arene or Cp ligand in a direction away from the C_2B_{10} substituent on C1. This structural feature is undoubtedly the result of intramolecular steric crowding, which also likely contributes to the relatively large misfit values of the metal atoms in **2** and **4**. The ligand bend-back is conveniently quantified by θ, the dihedral angle between the plane of the ligand C atoms (arene or Cp) and the plane defined by B5B6B11B12B9 (the lower pentagonal belt usually taken as the reference plane in 3,1,2-MC_2B_9 icosahedra).[29] For **2** θ is 16.08(9)° whilst for **4** θ is 15.83(8)° (molecule **A–B**) and 16.34(8)° (molecule **C–D**; in **4** there are two crystallographically-independent molecules **A–B** and **C–D** where the first letter refers to the CoC_2B_9 cage and second letter to the C_2B_{10} cage). C1–C1′ distances in **2** and **4** are 1.545(3), 1.549(2) (**A–B**) and 1.550(2) Å (**C–D**), respectively. All these are significantly longer that the C1–C1′ distance in 1,1′-bis(*o*-carborane), 1.5339(11) Å,[1] again a reflection of the steric crowding in **2** and **4**.

In the 2,1,8-MC_2B_9-1′,2′-C_2B_{10} compounds **3** and **5** significant intramolecular steric crowding is removed since the C_2B_{10} substituent to the MC_2B_9 cage is now at position 8 and so not adjacent to the metal atom. Consequently the arene or Cp ring plane lies effectively parallel to the lower pentagonal belt, now the C8B4B5B10B12 plane [θ is only 0.27(5)° in **3** and 2.19(7)° in **5**], and the C8–C1′ distances are 1.5294(17) and 1.5329(16)Å, respectively, slightly shorter than or identical to the intercage C–C distance in 1,1′-bis(*o*-carborane).[1]

The gross similarities between the structures of **2** and **4** (similar ligand bend-back angles, similar C–C1′ distances) imply that, to a first approximation, they are equally sterically crowded. However, whilst **2** is relatively easily isomerised to **3** by gentle heating, even prolonged heating to reflux of **4** in toluene does not convert it into **5**; rather **4** has to be reduced to the anion $[\mathbf{4}]^-$ which then isomerises (presumably to $[\mathbf{5}]^-$) at room temperature, affording **5** on aerial oxidation. This reduction-induced isomerisation of metallacarboranes has precedent in the literature.[30] Thus, as already has been noted, it appears that the basicity of the metal fragment, and not simply the steric crowding it affords, is important in determining the ease of 3,1,2-MC_2B_9 to 2,1,8-MC_2B_9 isomerisation in these species. Given that it is generally accepted that cobaltacarboranes are more susceptible to isomerisation than ruthenacarboranes, at least for 13-vertex species,[31] this is an interesting observation and one that we will address more fully in future contributions.[32]

Conclusions

Examples of 12-vertex metallacarborane/carborane compounds, MC_2B_9-C_2B_{10}, derived from single deboronation and

then metallation of 1,1′-bis(*o*-carborane), have been prepared and characterised. Both non-isomerised 3,1,2-MC_2B_9-1′,2′-C_2B_{10} and isomerised 2,1,8-MC_2B_9-1′,2′-C_2B_{10} isomers have been isolated. For M = {Ru(*p*-cymene)} the isomerisation of the former to the latter is effected by gentle heating. In contrast, the non-isomerised form with M = {CoCp} does not isomerise in refluxing toluene but readily isomerises as the result of 1e reduction followed by reoxidation.

Experimental

Synthesis

Experiments were performed under dry, oxygen free N_2, using standard Schlenk techniques, although subsequent manipulations were sometimes performed in the open laboratory. All solvents were freshly distilled under nitrogen from the appropriate drying agents immediately before use (CH_2Cl_2 [DCM], CaH_2: THF and 40–60 petroleum ether; sodium wire) or were stored over 4 Å molecular sieves and were degassed (3 × freeze–pump–thaw cycles) before use. Preparative TLC employed 20 × 20 cm Kieselgel F_{254} glass plates. NMR spectra at 400.1 MHz (^{1}H) or 128.4 MHz (^{11}B) were recorded on a Bruker DPX-400 spectrometer from $CDCl_3$ or $(CD_3)_2CO$ solutions at room temperature. Electron impact mass spectrometry (EIMS) was carried out using a Finnigan (Thermo) LCQ Classic ion trap mass spectrometer at the University of Edinburgh. Elemental analyses were conducted using an Exeter CE-440 elemental analyser at Heriot-Watt University. The starting materials 1,1′-bis(*o*-carborane),[6] $[Ru(p\text{-cymene})Cl_2]_2$,[33] $[Ru(\eta\text{-}C_6H_6)Cl_2]_2$ [34] and $CpCo(CO)I_2$ [35] were prepared by literature methods or slight variations thereof. All other reagents were supplied commercially.

[$HNMe_3$][7-(1′-1′,2′-*closo*-$C_2B_{10}H_{11}$)-7,8-*nido*-$C_2B_9H_{11}$] ([$HNMe_3$][1]) and [BTMA][7-(1′-1′,2′-*closo*-$C_2B_{10}H_{11}$)-7,8-*nido*-$C_2B_9H_{11}$] ([BTMA][1]). 1,1′-bis(*o*-carborane (0.50 g, 1.75 mmol) and KOH (0.09 g, 1.75 mmol) were heated to reflux in EtOH (30 mL) for 4 h. The solution was allowed to cool and the solvent removed to give a white oily residue. Deionised water (20 mL) was added, and the suspension filtered to give a slightly cloudy solution. To this was added an aqueous solution of either $[HNMe_3]Cl$ (0.17 g, 1.8 mmol) or [BTMA]Cl (0.32 g, 1.8 mmol) resulting in the immediate precipitation of [$HNMe_3$][7-(1′-1′,2′-*closo*-$C_2B_{10}H_{11}$)-7,8-*nido*-$C_2B_9H_{11}$] ([$HNMe_3$][**1**]) or [BTMA][7-(1′-1′,2′-*closo*-$C_2B_{10}H_{11}$)-7,8-*nido*-$C_2B_9H_{11}$] ([BTMA][**1**]) as white solids. These were isolated by filtration, washed with H_2O (3 × 20 mL) and dried *in vacuo*.

[$HNMe_3$][**1**]: Yield 0.37 g, 64%. $C_7H_{32}B_{19}N$ requires C 25.0, H 9.60, N 4.17. Found for [$HNMe_3$]**1**: C 24.7, H 9.71, N 4.04%. $^{11}B\{^1H\}$ NMR [$(CD_3)_2CO$], δ −3.9 (1B), −6.0 (1B), −8.8 (1B), −10.4 (5B), −11.2 (sh., 2B), −13.5 (3B), −16.8 (2B), −19.0 (1B), −22.7 (1B), −33.9 (1B), −35.3 (1B). ^{1}H NMR [$(CD_3)_2CO$], δ 4.36 (s, 1H, CH_{cage}), 3.22 (s, 9H, $N(CH_3)_3$), 1.99 (s, 1H, CH_{cage}).

[BTMA][**1**]: Yield 0.55 g, 74%. $C_{14}H_{38}B_{19}N$ requires C 39.5, H 8.99, N 3.29. Found for [BTMA]**1**: C 41.5, H 9.15, N 3.25%. $^{11}B\{^1H\}$ NMR [$(CD_3)_2CO$], δ −4.2 (1B), −6.2 (1B), −9.0 (1B), −10.6 (5B), −11.5 (sh., 2B), −13.8 (3B), −17.0 (2B), −19.2 (1B), −22.8 (1B), −33.2 (1B), −35.5 (1B). ^{1}H NMR [$(CD_3)_2CO$], δ 7.75–7.45 (m, 5H, C_6H_5), 4.75 (s, 2H, CH_2), 4.35 (s, 1H, CH_{cage}), 3.35 (s, 9H, $N(CH_3)_3$), 1.95 (s, 1H, CH_{cage}).

[1-(1′-1′,2′-*closo*-$C_2B_{10}H_{11}$)-3-(*p*-cymene)-3,1,2-*closo*-$RuC_2B_9H_{10}$] (2) and [8-(1′-1′,2′-*closo*-$C_2B_{10}H_{11}$)-8-(*p*-cymene)-2,1,8-*closo*-$RuC_2B_9H_{10}$] (3). *n*-BuLi (0.48 mL of 2.5M solution, 1.2 mmol) was added dropwise to a cooled (0 °C) solution of [$HNMe_3$][**1**] (0.20 g, 0.60 mmol) in THF (20 mL) and the products stirred for 1 h. The pale yellow solution was frozen at −196 °C, $[RuCl_2(p\text{-cymene})]_2$ (0.18 g, 0.30 mmol) added and the reaction mixture stirred overnight at room temperature. THF was removed *in vacuo* and the crude mixture dissolved in DCM and filtered through Celite®. Preparative TLC using an eluent system of DCM and petroleum ether in a ratio of 30 : 70 afforded a yellow band (R_f = 0.47) subsequently identified as [1-(1′-1′,2′-*closo*-$C_2B_{10}H_{11}$)-3-(*p*-cymene)-3,1,2-*closo*-$RuC_2B_9H_{10}$] (**2**) (0.024 g, 8%) and a colourless band (R_f = 0.51) identified as [8-(1′-1′,2′-*closo*-$C_2B_{10}H_{11}$)-2-(*p*-cymene)-2,1,8-*closo*-$RuC_2B_9H_{10}$] (**3**) (0.057 g, 19%).

2: $C_{14}H_{35}B_{19}Ru$ requires C 33.0, H 6.92. Found for **2**: C 32.5, H 7.17%. $^{11}B\{^1H\}$ NMR [$CDCl_3$], δ 2.8 (1B), 0.5 (1B), −2.8 (2B), −3.9 (sh., 1B), −7.2 (2B), −8.8 (2B), −10.7 (4B), −12.6 (2B), −14.4 (1B), −17.2 (3B). ^{1}H NMR [$CDCl_3$], δ 6.11–5.96 (m, 4H, C_6H_4), 4.03 (s, 1H, CH_{cage}), 3.91 (s, 1H, CH_{cage}), 3.04 (app. septet, 1H, $CH(CH_3)_2$), 2.49 (s, 3H, CH_3), 1.37 (d, 3H, $CH(CH_3)_2$), 1.35 (d, 3H, $CH(CH_3)_2$). EIMS: envelope centred on *m*/*z* 510 (M^+).

3: $C_{14}H_{35}B_{19}Ru$ requires C 33.0, H 6.92. Found for **3**: C 33.0, H 6.82%. $^{11}B\{^1H\}$ NMR [$CDCl_3$], δ −1.0 (2B), −2.8 (2B), −4.1 (1B), −4.9 (2B), −8.0 (1B), −10.1 (6B), −13.4 (2B), −16.2 (1B), −19.2 (1B), −20.4 (1B). ^{1}H NMR [$CDCl_3$], δ 5.94–5.84 (m, 4H, C_6H_4), 3.64 (s, 1H, CH_{cage}), 2.81 (app. septet, 1H, $CH(CH_3)_2$), 2.63 (s, 1H, CH_{cage}), 2.31 (s, 3H, CH_3), 1.30 (d, 3H, $CH(CH_3)_2$), 1.28 (d, 3H, $CH(CH_3)_2$). EIMS: envelope centred on *m*/*z* 510 (M^+).

Thermal isomerisation of 2. Compound **2** (0.024 g, 0.05 mmol) was dissolved in THF (20 mL) and the solution heated at reflux for 2 h. The solvent was removed and the product purified by preparative TLC using an eluent system of DCM–petroleum ether, 30 : 70, to afford a colourless band at R_f = 0.51 identified as **3** (0.014 g, 58%) by ^{1}H and ^{11}B NMR spectroscopies.

[1-(1′-1′,2′-*closo*-$C_2B_{10}H_{11}$)-3-Cp-3,1,2-*closo*-$CoC_2B_9H_{10}$] (4). [$HNMe_3$][**1**] (0.25 g, 0.74 mmol) was deprotonated with *n*-BuLi (0.60 mL of 2.5 M solution, 1.48 mmol) as above then frozen at −196 °C. To this was added $CpCo(CO)I_2$ (0.30 g, 0.74 mmol) and the reaction mixture was allowed to warm to room temperature and stirred overnight. Following spot TLC* (DCM–petroleum ether, 30 : 70, R_f = 0.28) purification by column chromatography using the same eluent gave, on removal of solvent, an orange powder (0.038 g, 13%), subsequently identified as [1-(1′-1′,2′-*closo*-$C_2B_{10}H_{11}$)-3-Cp-3,1,2-*closo*-$CoC_2B_9H_{10}$] (**4**). $C_9H_{26}B_{19}Co$ requires C 27.1, H 6.57. Found for **4**: C 26.5, H 6.67%. $^{11}B\{^1H\}$ NMR [$CDCl_3$], δ 6.5 (1B), 2.5 (1B), −2.6 (5B), −4.4 (1B), −8.0 (2B), −9.7 (5B), −12.3 (2B), −14.2 (1B), −15.9 (1B). ^{1}H

NMR [$CDCl_3$], δ 5.86 (s, 5H, C_5H_5), 4.24 (s, 1H, CH_{cage}), 4.03 (s, 1H, CH_{cage}). EIMS: envelope centred on m/z 399 (M^+).

*A trace amount of a yellow spot (R_f = 0.34) identified as [8-(1′-1′,2′-*closo*-$C_2B_{10}H_{11}$)-2-Cp-2,1,8-*closo*-$CoC_2B_9H_{10}$] (**5**) was also observed and its identity confirmed *via* ^{1}H NMR spectroscopy.

[8-(1′-1′,2′-*closo*-$C_2B_{10}H_{11}$)-2-Cp-2,1,8-*closo*-$CoC_2B_9H_{10}$] (5). [$HNMe_3$][**1**] (0.20 g, 0.60 mmol) was deprotonated with *n*-BuLi (0.48 mL of 2.5 M solution, 1.20 mmol) as above and frozen at −196 °C. To this were added NaCp (0. 89 mL of 2.0 M solution, 1.79 mmol) and $CoCl_2$ (0.28 g, 2.20 mmol) and the mixture stirred overnight at room temperature. Following aerial oxidation (0.5 h) and filtration through silica THF was replaced by DCM and the product again filtered, through Celite®. Following spot TLC** (DCM–petroleum ether, 50 : 50, R_f = 0.69) purification by column chromatography using the same eluent gave, on removal of solvent, a yellow powder (0.117 g, 49%), subsequently identified as [8-(1′-1′,2′-*closo*-$C_2B_{10}H_{11}$)-2-Cp-2,1,8-*closo*-$CoC_2B_9H_{10}$] (**5**). $C_9H_{26}B_{19}Co$ requires C 27.1, H 6.57. Found for **6**: C 27.1, H 6.75%. $^{11}B\{^1H\}$ NMR [$CDCl_3$], δ 1.7 (1B), 0.0 (2B), −0.9 (1B), −2.5 (1B), −3.8 (1B), −6.1 (2B), −9.9 (6B), −11.8 (1B), −13.2 (2B), −16.8 (1B), −17.7 (1B). ^{1}H NMR [$CDCl_3$], δ 5.50 (s, 5H, C_5H_5), 3.59 (s, 1H, CH_{cage}), 2.73 (s, 1H, CH_{cage}). EIMS: envelope centred on m/z 399 (M^+).

A trace amount of an orange spot (R_f = 0.60) identified as **4 was also observed and its identity confirmed *via* ^{1}H NMR spectroscopy.

Attempted thermal isomerisation of 4. Compound **4** (0.038 g, 0.10 mmol) was dissolved in toluene (20 mL) and the solution heated at reflux for 5 h. The solvent was removed and the crude residue was submitted for ^{1}H and ^{11}B NMR spectroscopies, however there was no evidence that **4** had converted to **5**. Preparative TLC using an eluent of DCM–petroleum ether, 30 : 70, led to the recovery of **4** (0.020 g, 53%).

Redox isomerisation of 4. To a solution of **4** (0.012 g, 0.030 mmol) in dry degassed THF (10 mL) was added a solution of sodium naphthalenide (1 mL of a 0.031 M solution in THF, 0.031 mmol). The reaction was allowed to stir under nitrogen for 1 h, oxidised using a water aspirator for 30 min, and solvent was removed *in vacuo*. Only compound **5** was identified by ^{1}H and ^{11}B NMR spectroscopies.

Crystallography

Diffraction-quality crystals of salt [BTMA][**1**] and compounds **2**, **3**, **4** and **5** were afforded by slow diffusion of a CH_2Cl_2 solution of the appropriate species and 40–60 petroleum ether at −30 °C. Intensity data for all except **4** were collected on a Bruker X8 APEXII diffractometer using Mo-K_α X-radiation, with crystals mounted in inert oil on a cryoloop and cooled to 100 K by an Oxford Cryosystems Cryostream. Compound **4** afforded crystals too small for our in-house system and consequently data were collected at the National Crystallographic Service at the University of Southampton at 100 K on a Rigaku AFC12 diffractometer operating with Mo-K_α X-radiation. Indexing, data collection and absorption correction were performed using the APEXII suite of programs.[36] Structures were solved by direct methods (SHELXS[37] or OLEX2[38]) and refined by full-matrix least-squares (SHELXL).[37]

Cage C atoms not involved in the intercage link were identified by a combination of (i) the examination of refined (as B) isotropic thermal parameters, (ii) the lengths of cage connectivities, (iii) the *Vertex-Centroid Distance Method*[39] and (iv) the *Boron-H Distance Method*,[40] with all four methods affording excellent mutual agreement.

Table 4 Crystallographic data

	[BTMA][**1**]	**2**	**3**	**4**	**5**
Formula	$C_{14}H_{38}B_{19}N$	$C_{14}H_{35}B_{19}Ru$	$C_{14}H_{35}B_{19}Ru$	$C_9H_{26}B_{19}Co$	$C_9H_{26}B_{19}Co$
M	425.84	509.88	509.88	398.62	398.62
Crystal system	Monoclinic	Monoclinic	Monoclinic	Triclinic	Monoclinic
Space group	$P2_1/c$	$P2_1/n$	$P2_1/n$	$P\bar{1}$	$P2_1/c$
a/Å	18.851(9)	11.5653(7)	10.9051(9)	6.7993(5)	12.6472(6)(4)
b/Å	10.072(4)	14.1222(9)	16.9528(14)	14.4533(10)	6.6422(3)
c/Å	13.477(6)	15.1116(10)	13.8437(11)	20.3575(14)	23.8175(10)
α (°)	90	90	90	89.609(3)	90
β (°)	97.068(13)	91.611(4)	105.039(4)	85.554(3)	95.642(2)
γ (°)	90	90	90	89.158(3)	90
U/Å^3	2540(2)	2467.2(3)	2471.7(4)	1994.3(2)	1991.10(16)
Z, Z'	4, 1	4, 1	4, 1	4, 2	4, 1
F(000)/e	896	1032	1032	808	808
D_{calc}/Mg m^{-3}	1.114	1.373	1.370	1.328	1.330
μ(Mo-K_α)/mm^{-1}	0.052	0.640	0.639	0.853	0.855
θ_{max} (°)	20.84	27.47	33.53	27.48	29.57
Data measured	14 879	34 686	52 456	26 471	37 451
Unique data, n	2651	5604	9614	9102	5581
R_{int}	0.2172	0.0431	0.0388	0.0378	0.0368
R, wR_2 (obs. data)	0.0867, 0.1912	0.0309, 0.0689	0.0288, 0.0639	0.0334, 0.0821	0.0325, 0.0732
S	1.005	1.029	1.031	1.070	1.086
Variables	308	373	374	649	325
E_{max}, E_{min}/e Å^{-3}	0.27, −0.26	0.68, −0.71	0.96, −1.37	0.66, −0.34	0.36, −0.24

The anion in [BTMA][**1**] is partially disordered. The C_2B_{10} cage is fully ordered but the C_2B_9 cage has one B atom disordered between two sites, B3 and B12, with SOFs 0.548(10) and 0.452(10) respectively. Atoms B3 and B12 were refined with an isotropic thermal parameter fixed at 0.03 Å^2. There is also partial disorder in **3** between atoms C2′ and B3′ (C_2B_{10} cage), successfully modelled with vertex 2 being 0.446(19)C + 0.554(19)B, with complementary SOFs at vertex 3.

In [BTMA][**1**] it was not possible to locate the (disordered) bridging H atom associated with the open face of the *nido* cage and final refinement with constrained BH and $C_{cage}H$ atoms (B–H = C_{cage}–H = 1.12 Å) afforded better agreement than that with these H atoms allowed to refine. In the BTMA cation the H atoms were constrained to C_{phenyl}–H = 0.95 Å, $C_{secondary}$–H = 0.99 Å, C_{methyl}–H = 0.98 Å. For all other structures BH and $C_{cage}H$ atoms were allowed to refine positionally whilst other H atoms were constrained to idealised geometries; $C_{aromatic}$–H = 1.00 Å, C_{Cp}–H = 1.00 Å, $C_{tertiary}$–H = 1.00 Å, C_{methyl}–H = 0.98 Å. All H displacement parameters, U_{iso}, were constrained to be 1.2 × U_{eq} (bound B or C) except Me H atoms [U_{iso}(H) = 1.5 × U_{eq} C(Me)]. Table 4 contains further experimental details.

Calculations

All geometries were optimised without constraints using Gaussian 03, Revision D.01[41] employing the BP86 functional[42] and 6-31G** basis sets for B, C and H atoms.[43] Analytical frequency calculations were used to confirm geometries as minima or transition states. The transition state was further characterised through IRC calculations.[44]

Acknowledgements

We thank ORSAS (GS) and the EPSRC (DE and DMcK supported by project EP/E02971X/1, WYM supported by project EP/I031545/1) for funding. We also thank the UK National Crystallography Service (University of Southampton) for collecting intensity data on compound **4**, and Dr Dmitry Perekalin (INEOS-RAS, Moscow, Russia) for useful discussion. CP is an Erasmus exchange student from the Universidad de Zaragoza, Spain, BTL is an Erasmus exchange student from the Philipps-Universität Marburg, Germany, and LJ is a *Stagier* exchange student from the IUT de Rouen, France.

References

1 W. Y. Man, G. M. Rosair and A. J. Welch, *Acta Crystallogr., Sect. E: Struct. Rep. Online*, 2014, **70**, 462.
2 (*a*) J. A. Dupont and M. F. Hawthorne, *J. Am. Chem. Soc.*, 1964, **86**, 1643; (*b*) T. E. Paxon, K. P. Callahan and M. F. Hawthorne, *Inorg. Chem.*, 1973, **12**, 708.
3 X. Yang, W. Jiang, C. B. Knobler, M. D. Mortimer and M. F. Hawthorne, *Inorg. Chim. Acta*, 1995, **240**, 371.
4 L. I. Zakharkin and A. I. Kovredov, *Izv. Akad. Nauk SSSR, Ser. Khim.*, 1973, 1428.
5 (*a*) X. Yang, W. Jiang, C. B. Knobler and M. F. Hawthorne, *J. Am. Chem. Soc.*, 1992, **114**, 9719; (*b*) J. Müller, K. Baše, T. F. Magnera and J. Michl, *J. Am. Chem. Soc.*, 1992, **114**, 9721.
6 S. Ren and Z. Xie, *Organometallics*, 2008, **27**, 5167.
7 (*a*) D. A. Owen and M. F. Hawthorne, *J. Am. Chem. Soc.*, 1970, **92**, 3194; (*b*) D. A. Owen and M. F. Hawthorne, *J. Am. Chem. Soc.*, 1971, **93**, 873; (*c*) D. E. Harwell, J. McMillan, C. B. Knobler and M. F. Hawthorne, *Inorg. Chem.*, 1997, **36**, 5951.
8 A. I. Yanovsky, N. G. Furmanova, Y. T. Struchkov, N. F. Shemyakin and L. I. Zakharkin, *Izv. Akad. Nauk SSSR, Ser. Khim.*, 1979, 1523.
9 M. F. Hawthorne, D. A. Owen and J. W. Wiggins, *Inorg. Chem.*, 1971, **10**, 1304.
10 T. D. Getman, C. B. Knobler and M. F. Hawthorne, *Inorg. Chem.*, 1992, **31**, 101.
11 T. D. Getman, C. B. Knobler and M. F. Hawthorne, *J. Am. Chem. Soc.*, 1990, **112**, 4594.
12 (*a*) G. B. Dunks, R. J. Wiersema and M. F. Hawthorne, *J. Chem. Soc., Chem. Commun.*, 1972, 899; (*b*) G. B. Dunks, R. J. Wiersema and M. F. Hawthorne, *J. Am. Chem. Soc.*, 1973, **95**, 3174.
13 D. Ellis, D. McKay, S. A. Macgregor, G. M. Rosair and A. J. Welch, *Angew. Chem., Int. Ed.*, 2010, **49**, 4943.
14 D. Ellis, G. M. Rosair and A. J. Welch, *Chem. Commun.*, 2010, **46**, 7394.
15 J. A. Doi, E. A. Mizusawa, C. B. Knobler and M. F. Hawthorne, *Inorg. Chem.*, 1984, **23**, 1482.
16 J. A. Long, T. B. Marder, P. E. Behnken and M. F. Hawthorne, *J. Am. Chem. Soc.*, 1984, **106**, 2979.
17 P. E. Behnken, T. B. Marder, R. T. Baker, C. B. Knobler, M. R. Thompson and M. F. Hawthorne, *J. Am. Chem. Soc.*, 1985, **107**, 932.
18 A B8–B9′ linked species, [8-(9′-3′-Cp-3′,1′,2′-*closo*-$CoC_2B_9H_{10}$)-3-Cp-3,1,2-*closo*-$CoC_2B_9H_{10}$] has been reported but was prepared from the reaction between [3-Cp-3,1,2-*closo*-$CoC_2B_9H_{11}$] and S_8/$AlCl_3$, not from a bis(carborane); J. G. Planas, C. Viñas, F. Teixidor, M. E. Light and M. B. Hursthouse, *J. Organomet. Chem.*, 2006, **691**, 3472.
19 J. Buchanan, E. J. M. Hamilton, D. Reed and A. J. Welch, *J. Chem. Soc., Dalton Trans.*, 1990, 677.
20 M. A. Fox, J. A. K. Howard, A. K. Hughes, J. M. Malget and D. S. Yufit, *J. Chem. Soc., Dalton Trans.*, 2001, 2263.
21 M. F. Hawthorne, D. C. Young and P. A. Wegner, *J. Am. Chem. Soc.*, 1965, **87**, 1818.
22 M. P. Garcia, M. Green, F. G. A. Stone, R. G. Somerville, A. J. Welch, C. E. Briant, D. N. Cox and D. M. P. Mingos, *J. Chem. Soc., Dalton Trans.*, 1985, 2343.
23 C. J. Jones and M. F. Hawthorne, *Inorg. Chem.*, 1973, **12**, 606.
24 A. Burke, R. McIntosh, D. Ellis, G. M. Rosair and A. J. Welch, *Collect. Czech. Chem. Commun.*, 2002, **67**, 991.
25 W. Y. Man, S. Zlatogorsky, H. Tricas, D. Ellis, G. M. Rosair and A. J. Welch, *Angew. Chem., Int. Ed.*, 2014, **53**, 12222.

26 M. E. Lopez, M. J. Edie, D. Ellis, A. Horneber, S. A. Macgregor, G. M. Rosair and A. J. Welch, *Chem. Commun.*, 2007, 2243.
27 Since 1,1′-bis(*o*-carborane) is neutral overall and symmetric about the C1–C1′ mid-point, the two halves individually must be neutral.
28 F. Macrae, P. R. Edgington, P. McCabe, E. Pidcock, G. P. Shields, R. Taylor, M. Towler and J. van de Streek, *J. Appl. Crystallogr.*, 2006, **39**, 453. A free download of Mercury is available from the Cambridge Crystallographic Data Centre, http://www.ccdc.cam.ac.uk/.
29 D. M. P. Mingos, M. I. Forsyth and A. J. Welch, *J. Chem. Soc., Dalton Trans.*, 1978, 1363.
30 *e.g.* (*a*) T. E. Paxson, M. K. Kaloustian, G. M. Tom, R. J. Wiersema and M. F. Hawthorne, *J. Am. Chem. Soc.*, 1972, **94**, 4882; (*b*) T. P. Hanusa and L. J. Todd, *Polyhedron*, 1985, **4**, 2063.
31 *e.g.* (*a*) D. Ellis, M. E. Lopez, R. McIntosh, G. M. Rosair, A. J. Welch and R. Quenardelle, *Chem. Commun.*, 2005, 1348; (*b*) S. Zlatogorsky, D. Ellis, G. M. Rosair and A. J. Welch, *Chem. Commun.*, 2007, 2178.
32 D. Mandal, G. Thiripuranathar, W. Y. Man, G. M. Rosair and A. J. Welch, work in progress.
33 M. A. Bennett, T.-N. Huang, T. W. Matheson and A. K. Smith, *Inorg. Synth.*, 1982, **21**, 74.
34 M. A. Bennett and A. K. Smith, *J. Chem. Soc., Dalton Trans.*, 1974, 233.
35 S. A. Frith and J. L. Spencer, *Inorg. Synth.*, 1990, **28**, 273.
36 *Bruker AXS APEX2, version 2009-5*, Bruker AXS Inc., Madison, Wisconsin, USA, 2009.
37 G. M. Sheldrick, *Acta Crystallogr., Sect. A: Found. Crystallogr.*, 2008, **64**, 112.
38 O. V. Dolomanov, L. J. Bourhis, R. J. Gildea, J. A. K. Howard and H. Puschmann, *J. Appl. Crystallogr.*, 2009, **42**, 339.
39 A. McAnaw, G. Scott, L. Elrick, G. M. Rosair and A. J. Welch, *Dalton Trans.*, 2013, **42**, 645.
40 A. McAnaw, M. E. Lopez, D. Ellis, G. M. Rosair and A. J. Welch, *Dalton Trans.*, 2014, **43**, 5095.
41 M. J. Frisch, G. W. Trucks, H. B. Schlegel, G. E. Scuseria, M. A. Robb, J. R. Cheeseman, J. A. Montgomery, Jr., T. Vreven, K. N. Kudin, J. C. Burant, J. M. Millam, S. S. Iyengar, J. Tomasi, V. Barone, B. Mennucci, M. Cossi, G. Scalmani, N. Rega, G. A. Petersson, H. Nakatsuji, M. Hada, M. Ehara, K. Toyota, R. Fukuda, J. Hasegawa, M. Ishida, T. Nakajima, Y. Honda, O. Kitao, H. Nakai, M. Klene, X. Li, J. E. Knox, H. P. Hratchian, J. B. Cross, V. Bakken, C. Adamo, J. Jaramillo, R. Gomperts, R. E. Stratmann, O. Yazyev, A. J. Austin, R. Cammi, C. Pomelli, J. W. Ochterski, P. Y. Ayala, K. Morokuma, G. A. Voth, P. Salvador, J. J. Dannenberg, V. G. Zakrzewski, S. Dapprich, A. D. Daniels, M. C. Strain, O. Farkas, D. K. Malick, A. D. Rabuck, K. Raghavachari, J. B. Foresman, J. V. Ortiz, Q. Cui, A. G. Baboul, S. Clifford, J. Cioslowski, B. B. Stefanov, G. Liu, A. Liashenko, P. Piskorz, I. Komaromi, R. L. Martin, D. J. Fox, T. Keith, M. A. Al-Laham, C. Y. Peng, A. Nanayakkara, M. Challacombe, P. M. W. Gill, B. Johnson, W. Chen, M. W. Wong, C. Gonzalez and J. A. Pople, Gaussian Inc., Wallingford, CT, USA, 2004.
42 (*a*) H. L. Schmider and A. D. Becke, *J. Chem. Phys.*, 1998, **108**, 9624; (*b*) J. P. Perdew, *Phys. Rev. B: Condens. Matter*, 1986, **33**, 8822.
43 (*a*) W. J. Hehre, R. Ditchfield and J. A. Pople, *J. Chem. Phys.*, 1972, **56**, 2257; (*b*) P. Hariharan and J. A. Pople, *Theor. Chim. Acta*, 1973, **28**, 213.
44 (*a*) C. Gonzalez and H. B. Schlegel, *J. Phys. Chem.*, 1990, **94**, 5523; (*b*) C. Gonzalez and H. B. Schlegel, *J. Chem. Phys.*, 1989, **90**, 2154.
45 D. E. Smith and A. J. Welch, *Organometallics*, 1986, **5**, 760.
46 M. G. Davidson, T. G. Hibbert, J. A. K. Howard, A. Mackinnon and K. Wade, *Chem. Commun.*, 1996, 2285.

Dalton Transactions

PAPER

View Article Online
View Journal | View Issue

Cite this: *Dalton Trans.*, 2016, **45**, 1127

Unprecedented flexibility of the 1,1′-bis(*o*-carborane) ligand: catalytically-active species stabilised by B-agostic B–H⇀Ru interactions†‡

Laura E. Riley,[a] Antony P. Y. Chan,[a] James Taylor,[a] Wing Y. Man,[a] David Ellis,[a] Georgina M. Rosair,[a] Alan J. Welch*[a] and Igor B. Sivaev[b]

Doubly-deprotonated 1,1′-bis(*o*-carborane) reacts with $[RuCl_2(p\text{-cymene})]_2$ to afford $[Ru(\kappa^3\text{-}2,2',3'\text{-}\{1\text{-}(1'\text{-}1',2'\text{-}closo\text{-}C_2B_{10}H_{10})\text{-}1,2\text{-}closo\text{-}C_2B_{10}H_{10}\})(p\text{-cymene})]$ (**1**) in which 1,1′-bis(*o*-carborane) acts as an $X_2(C,C')$L ligand where "L" is a B3′–H3′⇀Ru B-agostic interaction, fluctional over four BH units (3′, 6′, 3 and 6) at 298 K but partially arrested at 203 K (B3′ and B6′). This interaction is readily cleaved by CO affording $[Ru(\kappa^2\text{-}2,2'\text{-}\{1\text{-}(1'\text{-}1',2'\text{-}closo\text{-}C_2B_{10}H_{10})\text{-}1,2\text{-}closo\text{-}C_2B_{10}H_{10}\})(p\text{-cymene})(CO)]$ (**2**) with the 1,1′-bis(*o*-carborane) simply an $X_2(C,C')$ ligand. With PPh_3 or dppe **1** yields $[Ru(\kappa^3\text{-}2,3',3\text{-}\{1\text{-}(1'\text{-}1',2'\text{-}closo\text{-}C_2B_{10}H_{10})\text{-}1,2\text{-}closo\text{-}C_2B_{10}H_{10}\})(PPh_3)_2]$ (**3**) or $[Ru(\kappa^3\text{-}2,3',3\text{-}\{1\text{-}(1'\text{-}1',2'\text{-}closo\text{-}C_2B_{10}H_{10})\text{-}1,2\text{-}closo\text{-}C_2B_{10}H_{10}\})(dppe)]$ (**4**) *via* unusually facile loss of the η-(*p*-cymene) ligand. In **3** and **4** the 1,1′-bis(*o*-carborane) has unexpectedly transformed into an $X_2(C,B')$L ligand with "L" now a B3–H3⇀Ru B-agostic bond. Unlike in **1** the B-agostic bonding in **3** and **4** appears non-fluctional at 298 K. With CO the B-agostic interaction of **3** is cleaved and a PPh_3 ligand is lost to afford $[Ru(\kappa^2\text{-}2,3'\text{-}\{1\text{-}(1'\text{-}1',2'\text{-}closo\text{-}C_2B_{10}H_{10})\text{-}1,2\text{-}closo\text{-}C_2B_{10}H_{10}\})(CO)_3(PPh_3)]$ (**5**), which exists as a 1 : 1 mixture of isomers, one having PPh_3 *trans* to C2, the other *trans* to B3′. With MeCN the analogous product $[Ru(\kappa^2\text{-}2,3'\text{-}\{1\text{-}(1'\text{-}1',2'\text{-}closo\text{-}C_2B_{10}H_{10})\text{-}1,2\text{-}closo\text{-}C_2B_{10}H_{10}\})(MeCN)_3(PPh_3)]$ (**6**) is formed as only the former isomer. With CO **4** affords $[Ru(\kappa^2\text{-}2,3'\text{-}\{1\text{-}(1'\text{-}1',2'\text{-}closo\text{-}C_2B_{10}H_{10})\text{-}1,2\text{-}closo\text{-}C_2B_{10}H_{10}\})(CO)_2(dppe)]$ (**7**), whilst with MeCN **4** yields $[Ru(\kappa^2\text{-}2,3'\text{-}\{1\text{-}(1'\text{-}1',2'\text{-}closo\text{-}C_2B_{10}H_{10})\text{-}1,2\text{-}closo\text{-}C_2B_{10}H_{10}\})(MeCN)_2(dppe)]$ (**8**). In **5** and **6** the three common ligands (CO or MeCN) are meridional, whilst in **7** and **8** the two monodentate ligands are mutually *trans*. Compound **1** is an 18-e, 6-co-ordinate, species but with a labile B-agostic interaction and **3** and **4** are 16-e, formally 5-co-ordinate, species also including a B-agostic interaction, and thus all three have the potential to act as Lewis acid catalysts. A 1% loading of **1** catalyses the Diels–Alder cycloaddition of cyclopentadiene and methacrolein in CH_2Cl_2 with full conversion after 6 h at 298 K, affording the product with *exo* diastereoselectivity (de >77%). Compounds **1–8** are fully characterised spectroscopically and crystallographically.

Received 2nd September 2015,
Accepted 13th November 2015

DOI: 10.1039/c5dt03417e

www.rsc.org/dalton

Introduction

Carboranes are a little over 50 years old,[1] and over those five decades a substantial amount of research has been devoted to them to the point where they are now regarded as an established part of inorganic, bordering on organic, chemistry.[2] It is particularly pleasing to note that, especially in the last 10–15 years, in parallel with the growing maturity of carborane chemistry there has been an increasing appreciation of the applications of carboranes and their derivatives in a truly diverse range of fields,[3] in large measure due to the unique nature and structure of these compounds.

1,1′-Bis(*o*-carborane) is the trivial name for $[1\text{-}(1'\text{-}1',2'\text{-}closo\text{-}C_2B_{10}H_{11})\text{-}1,2\text{-}closo\text{-}C_2B_{10}H_{11}]$ (Fig. 1), the simplest bis(carborane) species comprising two *ortho*-carborane units connected by a C–C bond.[4] It was first prepared by insertion of diacetylene into B_{10} frameworks[5] but it is now most conveniently synthesised from two C_2B_{10} units by copper-coupling reactions.[6,7] Compared to the extensive chemistry of *ortho*-carborane, 1,2-*closo*-$C_2B_{10}H_{12}$,[2] that of 1,1′-bis(*o*-carborane) remains considerably underdeveloped. Early studies reported both 2-e and 4-e

[a]*Institute of Chemical Sciences, Heriot-Watt University, Edinburgh, EH14 4AS UK. E-mail: a.j.welch@hw.ac.uk; Tel: +44 (0)131 451 3217*
[b]*A. N. Nesmeyanov Institute of Organoelement Compounds, Russian Academy of Sciences, 28 Vavilov Str., 119991 Moscow, Russia*

†In part, first reported at IMEBoron-XV, Prague, Czech Republic, August 2014 (presentation FP17).

‡Electronic supplementary information (ESI) available: Details of 3-channel NMR experiments on compound **4**. Perspective views of single molecules of compounds **3**, **6** and **8**. Line diagrams of both structural isomers of compound **5**. CCDC 1418090–1418096 and 1431560. For ESI and crystallographic data in CIF or other electronic format see DOI: 10.1039/c5dt03417e

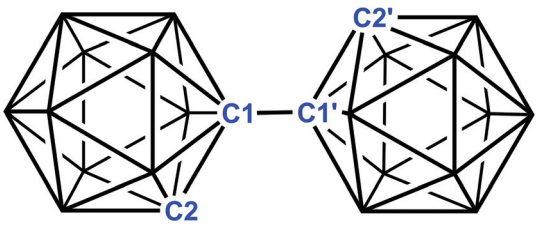

Fig. 1 1,1′-bis(*o*-carborane).

reduction[8,9] and a limited amount of deboronation[8] and deboronation–metallation chemistry.[10–13] More recently we have expanded the deboronation–metallation chemistry[14] and exploited the 4-e reduction and metallation of 1,1′-bis(*o*-carborane), the latter leading in one case to racemic and meso diastereoisomers of 13-vertex metallacarborane/13-vertex metallacarborane species[15] and in another to a unique 13-vertex metallacarborane/12-vertex carborane species whose formation involves cleavage of an aromatic C–C bond under ambient conditions.[16]

Of particular relevance to the present work is the fact that double deprotonation of 1,1′-bis(*o*-carborane) affords a chelating (*C*,*C*′), dianionic, ligand which has been used to complex a variety of transition-metal[17–19] and main-group[20] fragments. In the majority of these cases the 1,1′-bis(*o*-carborane) unit functions simply as a $X_2(C,C')$ ligand with the metal or main-group element bound to it *via* two σ-bonds to C2 and C2′.

In this contribution we report the interaction of doubly-deprotonated 1,1′-bis(*o*-carborane) with the {Ru(*p*-cymene)} fragment (*p*-cymene = η-$C_{10}H_{14}$, 1-^{i}Pr,4-MeC_6H_4) to afford an 18-e complex in which 1,1′-bis(*o*-carborane) displays its co-ordinative flexibility, acting as an $X_2(C,C')$L ligand with, in addition to σ-bonds from C2 and C2′, a B–H→Ru B-agostic interaction providing an additional pair of electrons to the metal centre. This B-agostic bond is readily cleaved by CO with the 1,1′-bis(*o*-carborane) reverting to a simple $X_2(C,C')$ ligand. With PPh_3 and dppe [dppe = 1,2-bis(diphenylphosphino)-ethane] however, it is the η-(*p*-cymene) ligand which is surprisingly displaced affording 5-co-ordinate 16-e bis(phosphine) species in which the 1,1′-bis(*o*-carborane) has undergone a remarkable transformation into an $X_2(C,B')$L ligand. With either CO or MeCN these 5-co-ordinate compounds are converted into fully electronically and co-ordinatively saturated species with the 1,1′-bis(*o*-carborane) an $X_2(C,B')$ ligand. Finally, we demonstrate the potential of some of these compounds to act as homogeneous Lewis acid catalysts or catalyst precursors for the cycloaddition of cyclopentadiene and methacrolein.

Results and discussion

The reaction between doubly-deprotonated 1,1′-bis(*o*-carborane) and $[RuCl_2(p\text{-cymene})]_2$ affords, after work-up involving column chromatography, an orange product **1** in modest yield, identified by microanalysis and mass spectrometry as $C_{14}H_{34}B_{20}Ru$. See Scheme 1. The room temperature $^{11}B\{^{1}H\}$ NMR spectrum of **1** reveals five resonances with relative integrals 2 : 2 : 4 : 8 : 4 from high frequency to low frequency and in the ^{1}H NMR spectrum are two integral-2 doublets assigned to aromatic protons, an integral-3 singlet at δ 2.35 ppm assigned to the 4-Me group, and a linked 1-H septet at δ 2.81 and 6-H doublet at δ 1.39 ppm arising from the 1-^{i}Pr group. Both spectra are consistent with the molecule [Ru($C_2B_{10}H_{10}$–$C_2B_{10}H_{10}$)(*p*-cymene)] having time-averaged C_s molecular symmetry.

A crystallographic study of **1** (Fig. 2) revealed that, unlike in the recently-reported[18] 16-e species [M(κ^2-2,2′-{1-(1′-1′,2′-*closo*-$C_2B_{10}H_{10}$)-1,2-*closo*-$C_2B_{10}H_{10}$})Cp*] (Cp* = η-C_5Me_5, M = Rh, Ir) the 1,1′-bis(*o*-carborane) ligand in 1 is κ^3-bonded to the Ru atom *via* not only the expected σ-bonds from C2 and C2′ but also an additional interaction involving the {B3′H3′} fragment, Ru1–B3′ 2.430(3) Å, Ru1–H3′ 1.89(3) Å. This last interaction could be alternatively described as a 3c-2e Ru–H–B bridge or as a B–H→Ru agostic interaction.[21] To fully emphasise the organometallic nature of **1**, we prefer the latter although we shall refer to it as B-agostic to differentiate it from the classic C–H→M for which the term agostic was formally intended.[22] Thus the deprotonated 1,1′-bis(*o*-carborane) is now an $X_2(C,C')$ L ligand and the metal centre has an 18-e configuration. Compound **1** is therefore formulated as [Ru(κ^3-2,2′,3′-{1-(1′-1′,2′-*closo*-$C_2B_{10}H_{10}$)-1,2-*closo*-$C_2B_{10}H_{10}$})(*p*-cymene)].[23] Note that whilst B–H→M agostic interactions are well-known (and generally involve *nido* heteroboranes),[24] those involving B3 are relatively rare,[25] particulary when the heteroborane is *closo*.[23]

Seeking to establish if this B-agostic bonding is retained in solution we recorded the $^{1}H\{^{11}B\}$ NMR spectrum of **1**. At room temperature, in addition to the resonances due to the *p*-cymene ligand, are observed five resonances between δ 2.58 and 2.11 ppm, integrating for 16H, and a low frequency resonance at δ −0.02 ppm integrating for 4H. This implies that at room temperature there is a fluctional process operating by which four {BH} units (presumably BH3, BH3′, BH6 and BH6′) alternatively act as the B-agostic BH in rapid exchange with each other. Cooling the sample causes the signal at δ −0.02 to slowly collapse into the baseline at 233 K, re-emerging as two integral-2 resonances at lower temperatures, δ 0.78 and −1.03 ppm at the lowest temperature achieved, 203 K. Assuming that the lower frequency resonance arises from the B-agostic BH[22,26] we conclude that even at 203 K the fluctional nature of the B-agostic interaction is only partially arrested. At 203 K the resonances arising from the *p*-cymene ligand still show time-averaged C_s symmetry. However, the BH resonances which were never involved in B-agostic bonding now appear as a 2 : 2 : 3 : 3 : 3 : 3 pattern (between δ 2.52 and 1.96 ppm, from high frequency to low frequency). The presence of odd-numbered integrals suggests that at 203 K the *p*-cymene ligand is no longer rapidly rotating about the Ru-arene axis, but is aligned such that its mirror plane is aligned with that containing C2C1C1′C2′, *i.e.* the low-temperature C_s conformation of the molecule is that shown in Fig. 3a rather than Fig. 3b. The

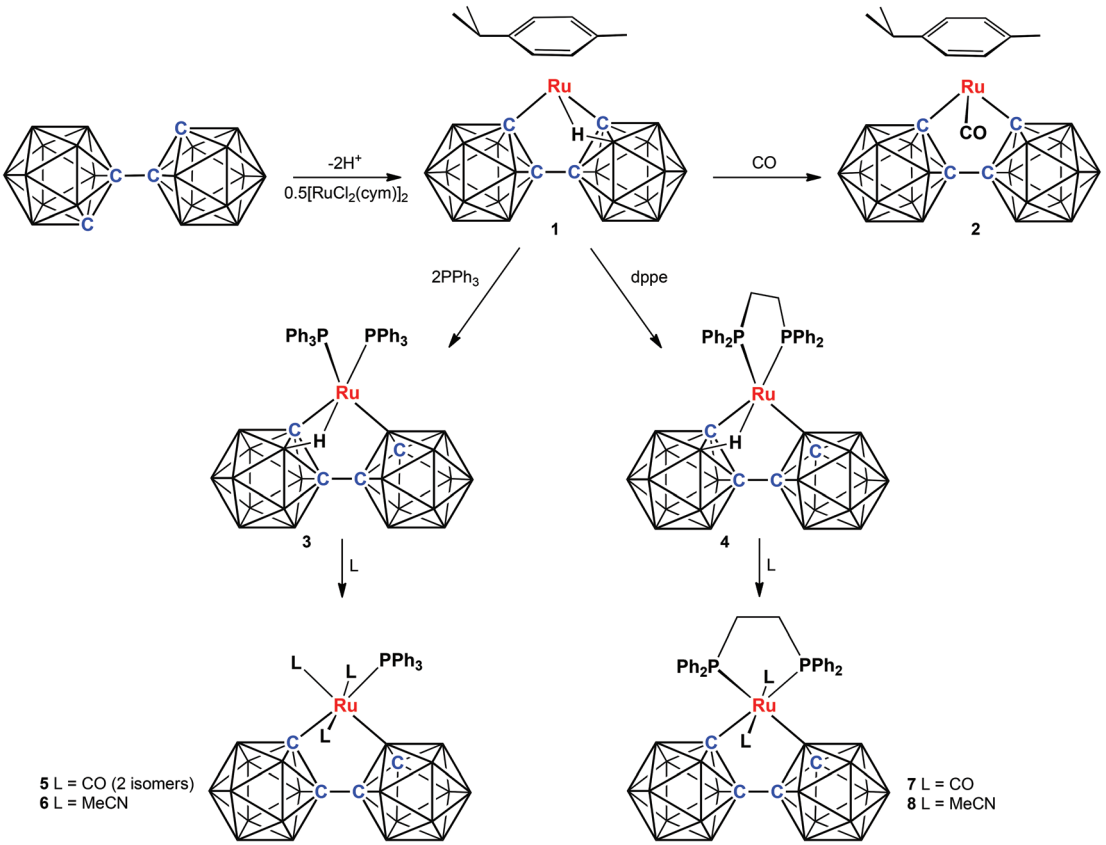

Scheme 1 General reaction scheme for compounds **1**–**8**.

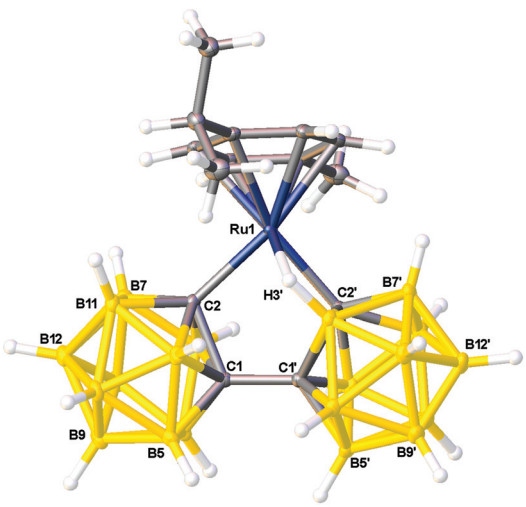

Fig. 2 Perspective view of compound **1** and part of the atom numbering scheme. Selected interatomic distances (Å): Ru1–C2 2.103(2), Ru1–C2′ 2.124(2), Ru1–H3′ 1.89(3), Ru1–B3′ 2.430(3), B3′–H3′ 1.18(3), Ru1–arene 2.163(2)-2.250(2), C1–C1′ 1.514(3).

B-agostic bonding is still fluctional between two sites on the same cage, *i.e.* B3′ and B6′ (numbering as in Fig. 2) or alternatively B3 and B6.

Compound **1** reacts readily with CO to afford [Ru(κ^2-2,2′-{1-(1′-1′,2′-*closo*-$C_2B_{10}H_{10}$)-1,2-*closo*-$C_2B_{10}H_{10}$})(*p*-cymene)(CO)] (**2**), isolated as a yellow crystalline material in modest yield. Microanalysis, mass spectrometry and IR spectroscopy (ν_{CO} at 2007 cm^{-1}) all support carbonyl bonding. The $^{11}B\{^1H\}$ and ^1H NMR spectra of **2** are relatively uninformative (but are consistent with time-averaged C_s molecular symmetry), however crucially the $^1H\{^{11}B\}$ spectrum yields no evidence of B-agostic bonding with resonances from all 20 BH units appearing between δ 2.88 and 2.12 ppm. A crystallographic study (Fig. 4) confirms that the CO ligand has displaced the B-agostic interaction and thus demonstrates the flexibility of the 1,1′-bis(*o*-carborane) ligand, now a simple $X_2(C,C')$ ligand. There are slight increases in the Ru–C2, Ru–C2′ and Ru–arene distances on moving from **1** to **2**, but essentially the two structures are very similar except for replacement of the B-agostic link by the CO ligand.

A much more profound change happens on reaction of **1** with PPh_3. Initially this reaction was performed with one equivalent of phosphine yielding a small amount of a yellow-orange product, **3**, after chromatography. Microanalysis and

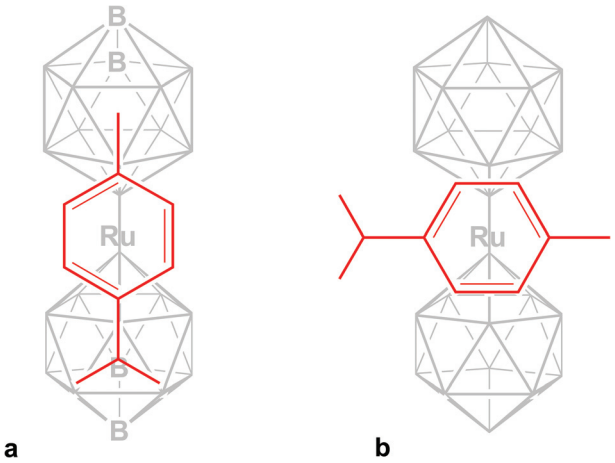

Fig. 3 Possible orientations of the *p*-cymene ligand above the Ru(κ^2-2,2′-{1-(1′-1′,2′-*closo*-$C_2B_{10}H_{10}$)-1,2-*closo*-$C_2B_{10}H_{10}$}) unit in compound **1** such that the molecular symmetry is C_s. The observation of four BH resonances of integral 3 in the $^1H\{^{11}B\}$ NMR spectrum is only consistent with conformation **a**, not conformation **b**.

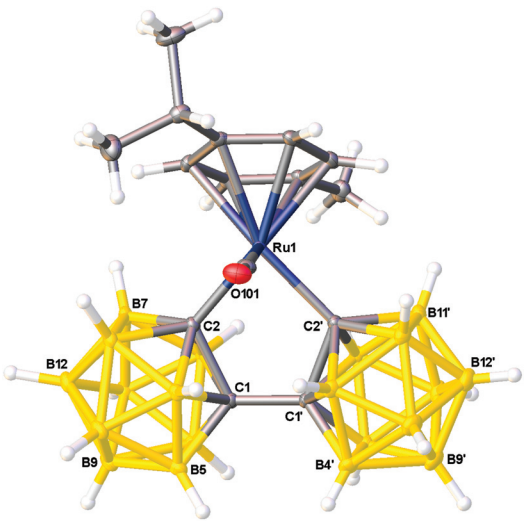

Fig. 4 Perspective view of compound **2** and part of the atom numbering scheme. Selected interatomic distances (Å) and angles (°): Ru1–C2 2.115(2), Ru1–C2′ 2.134(3), Ru1–C101 1.861(3), Ru1–arene 2.271(2)–2.398(2), C1–C1′ 1.526(2), Ru1–C101–O101 174.26(15).

mass spectrometry suggested a product of formula $C_{40}H_{50}B_{20}P_2Ru$, *i.e.* containing two PPh_3 ligands but no *p*-cymene, a conclusion also supported by ^1H NMR spectroscopy. Accordingly the reaction was repeated using two equivalents of phosphine affording **3** in somewhat better yield.

Similarly compound **4** is afforded when **1** is treated with dppe, and spectroscopically compounds **3** and **4** are fully analogous. Their $^{11}B\{^1H\}$ NMR spectra are relatively uninformative with multiple overlapping resonances between δ 3 and −20 ppm (compound **3**) and δ 1 and −17 ppm (compound **4**). The ^{31}P spectra consist of two doublets, one broad at higher frequency and the other sharp at lower frequency. In the ^1H NMR spectra is one broad resonance characteristic of a $C_{cage}H$ signal (δ 1.94 ppm in **3** and 2.17 ppm in **4**) which integrates for 1 H atom assuming there are 30 aromatic protons (compound **3**) or 20 aromatic protons (compound **4**). On ^{11}B decoupling there appears, in addition to a set of resonances assigned to BH_{exo} nuclei, a low-frequency doublet resonance in the B-agostic region, δ −4.23 ppm in **3** and δ −2.25 ppm in **4**. That this doublet arises from coupling to a P atom was only established by a $^1H\{^{11}B, ^{31}P\}$ NMR experiment on compound **4** (see ESI‡).

The structures of **3** and **4** were established by diffraction studies. Unfortunately that of **3** suffers from disorder modelled in terms of major and minor components of the Ru atom, with site occupancy factors of 0.803(2) and 0.197(2) respectively, and although it must be the case that more of the molecule than simply the Ru atom is disordered it was not possible to account for this. Because of this disorder the crystallographic determination is relatively imprecise but nevertheless accurately defines the molecular structure (see ESI‡). Fortunately the structure of **4** (Fig. 5) suffers no such disorder and is of high precision so the following discussion focuses on this structure. The *p*-cymene ligand of **1** has indeed been lost and the Ru atom is coordinated by dppe and the 1,1′-bis(*o*-carborane). The primed cage is now bound to the Ru atom by a 2c-2e B–Ru σ bond and not a C–Ru σ bond. The unprimed cage is still connected to the metal by a C–Ru σ bond but this is now complemented by a B–H⇀Ru B-agostic bond from the {B3H3} unit. Overall, the 1,1′-bis(*o*-carborane) has changed from

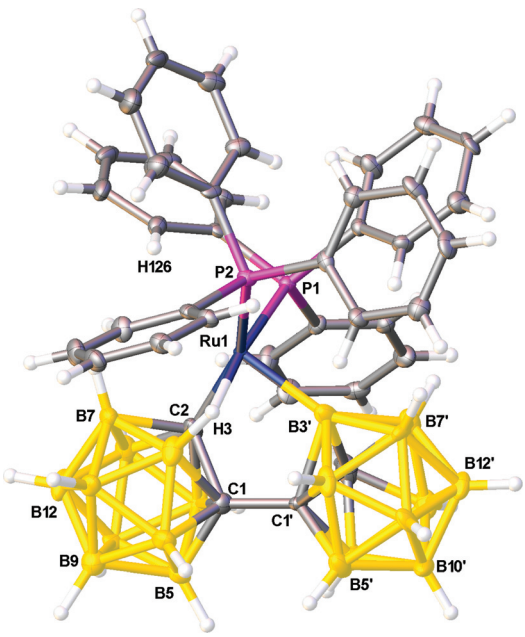

Fig. 5 Perspective view of compound **4** and part of the atom numbering scheme. Selected interatomic distances (Å): Ru1–C2 2.1479(19), Ru1–B3′ 2.034(2), Ru1–H3 1.955(19), Ru1–B3 2.413(2), B3–H3 1.15(2), Ru1–P1 2.2952(6), Ru1–P2 2.2423(6), C1–C1′ 1.520(3).

an $X_2(C,C')L$ ligand in **1** to an $X_2(C,B')L$ ligand in **3** and **4**, now established as [Ru(κ^3-2,3′,3-{1-(1′-1′,2′-*closo*-$C_2B_{10}H_{10}$)-1,2-*closo*-$C_2B_{10}H_{10}$})(PPh_3)$_2$] and [Ru(κ^3-2,3′,3-{1-(1′-1′,2′-*closo*-$C_2B_{10}H_{10}$)-1,2-*closo*-$C_2B_{10}H_{10}$})(dppe)], respectively, 16-e, 5-coordinate Ru^{II} species formally related to classic co-ordination compounds such as [$RuCl_2(PPh_3)_3$].[27] The metal geometry is approximately square-pyramidal (B3′ apical) and, as was also the case in the structure of [$RuCl_2(PPh_3)_3$],[28] there is a long Ru···H anagostic[29] interaction to a phenyl α-H atom [H212 in **4**, Ru1···H212 2.724(5) Å, Ru1···H212–C126 122.6(2)°] blocking the sixth octahedral site.

Having identified the nature of **3** a more obvious route to its synthesis was apparent; the reaction of doubly-deprotonated 1,1′-bis(*o*-carborane) with either [$RuCl_2(PPh_3)_4$] or [$RuCl_2(PPh_3)_3$] affords **3** in somewhat better yield than going *via* the *p*-cymene compound **1**.

The formation of compounds **3** and **4** by the room-temperature arene displacement from **1** was unexpected. Although not unknown under ambient conditions,[30] arene substitution in Ru^{II} species usually involves either heating or UV irradiation.[31] Indeed, the kinetic stability of the {(η-arene)Ru} moiety is one of the key factors in the use of arene-Ru species in both medicine[32] and catalysis.[33]

Compound **2** does not react with triphenylphosphine suggesting that in the reaction between **1** and PPh_3 the initial stage is displacement of the weak B-agostic interaction in **1** by phosphine. This would afford a presumably very sterically-crowded species which might then facilitate slippage of the *p*-cymene ligand from η^6- to η^4- to η^2-bonding and eventually complete dissociation, accompanied by bonding of the second PPh_3 to Ru at some point. An analogous process for the reaction between **1** and dppe would involve initial κ^1-co-ordination by dppe.

In forming **3** and **4**, either from the reaction between **1** and the appropriate phosphine or (for **3**) by the reaction between doubly-deprotonated 1,1′-bis(*o*-carborane) and either [$RuCl_2(PPh_3)_4$] or [$RuCl_2(PPh_3)_3$], 1,1′-bis(*o*-carborane) further displays its flexibility by becoming an $X_2(C,B')L$ ligand. Transition-metal metallacarboranes with B–M σ bonds are comparatively rare[34] and cases in which a carborane previously bound to metal through C is converted to B-bound are even rarer.[34c] In the present case it is likely that the initial products of these reactions are the species [Ru(κ^3-2,2′,3′-{1-(1′-1′,2′-*closo*-$C_2B_{10}H_{10}$)-1,2-*closo*-$C_2B_{10}H_{10}$})P_2], in which the 1,1′-bis(*o*-carborane) acts as an $X_2(C,C')L$ ligand with a B-agostic bond from the {B3′H3′} fragment to Ru. However, even with this B-agostic interaction the metal centre is only in a 16-e configuration. Since a carborane is expected to be a stronger σ-donor when bonded to metal through B as opposed to C (clear evidence for this is presented subsequently) and the B3′–H3′ bond is already activated by the agostic bonding, we suggest that the B3′–H3′ bond is cleaved and the primed cage changes from C2′–Ru σ-bonded to B3′–Ru σ-bonded by a *ca.* 72° rotation about the C1–C1′ axis. Whether the H atom lost by B3′ is transferred to C2′ or whether C2′ picks up H from solvent during work-up is unknown at this stage. The final stage in the process is the formation of a B-agostic bond from the {B3H3} unit to Ru to restore the 16-e configurations in **3** and **4**.

Since compounds **3** and **4** are both electronically and co-ordinatively unsaturated their reactions with 2-e donor ligands were explored. A freshly-prepared (not isolated) sample of **3** in THF was allowed to react with CO to afford the colourless product **5**. Microanalysis of crystals of **5** corresponds to [Ru($C_2B_{10}H_{10}$–$C_2B_{10}H_{10}$)(CO)$_3$(PPh_3)] plus one molecule of DCM of crystallisation. Although there is only one triphenylphosphine ligand, two singlets are observed in the ^{31}P NMR spectrum (the lower-frequency one being very broad) and in the ^1H spectrum are two broad singlets in the region associated with carborane C*H* resonances, each of which integrates for 0.5 protons against an assumed total of 15 aromatic protons.

Collectively, these data suggest that **5** is afforded as a mixture of isomers, and this is fully supported by the crystallographic structure (Fig. 6). One PPh_3 ligand from **3** has been replaced by three CO ligands and the B-agostic interaction has been broken. Thus compound **5** is [Ru(κ^2-2,3′-{1-(1′-1′,2′-*closo*-$C_2B_{10}H_{10}$)-1,2-*closo*-$C_2B_{10}H_{10}$})(CO)$_3$(PPh_3)]. The geometry of the Ru centre is octahedral and the three CO ligands are in a meridional arrangement. However, crystallographically there is 1 : 1 disorder between C2 and B3′, meaning that the compound exists as two isomers, one with PPh_3 *trans* to C2 (shown in Fig. 6) and the other with PPh_3 *trans* to B3′ (see ESI‡). We attribute the broad ^{31}P resonance to this latter phosphine.

A fully analogous reaction occurs upon dissolving **3** in MeCN, resulting in immediate decolourisation and the iso-

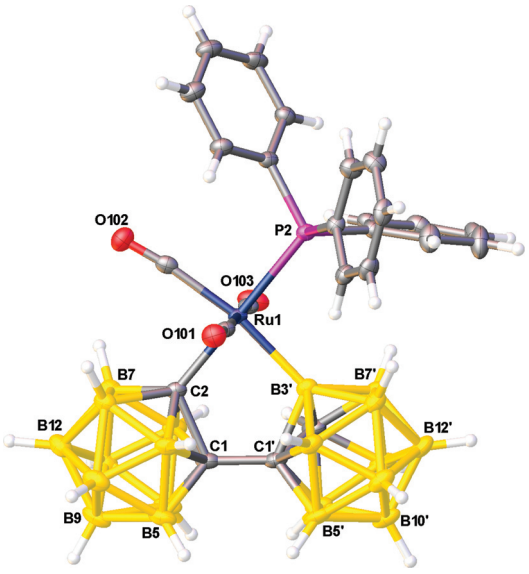

Fig. 6 Perspective view of compound **5** and part of the atom numbering scheme. Note that compound **5** is a mixture of two isomers only one of which is shown, and that crystallographically there is a 1 : 1 disorder between atoms C2 and B3′. Selected interatomic distances (Å) and angles (°): Ru1–C/B2 2.188(2), Ru1–B/C3′ 2.243(2), Ru1–P2 2.4623(7), Ru1–C101 1.960(2), Ru1–C102 1.963(2), Ru1–C103 1.957(2), C1–C1′ 1.534(3), Ru1–C101–O101 174.67(19), Ru1–C102–O102 173.74(19), Ru1–C103–O103 178.28(19).

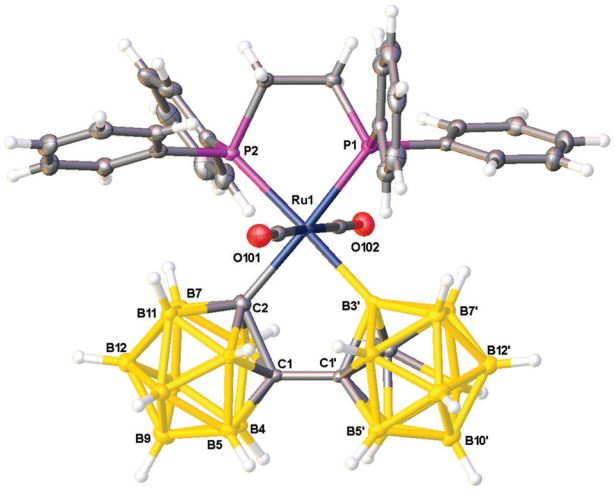

Fig. 7 Perspective view of compound **7** and part of the atom numbering scheme. Selected interatomic distances (Å) and angles (°): Ru1–C2 2.2078(19), Ru1–B3′ 2.242(2), Ru1–P1 2.3964(6), Ru1–P2 2.4328(6), Ru1–C101 1.9737(19), Ru1–C102 1.9615(19), C1–C1′ 1.537(3), Ru1–C101–O101 177.46(16), Ru1–C102–O102 173.76(15).

lation, following work-up, of a new compound [Ru(κ^2-2,3′-{1-(1′-1′,2′-*closo*-$C_2B_{10}H_{10}$)-1,2-*closo*-$C_2B_{10}H_{10}$})$(MeCN)_3(PPh_3)$] (**6**). In **6** there is only one (narrow) signal in the ^{31}P NMR spectrum and in the ^{1}H spectrum are observed a single C*H* resonance and three resonances assigned to MeCN. The ^{11}B{^{1}H} spectrum features a high-frequency (δ 12.8 ppm), integral-1, resonance that does not show ^{1}H coupling in the ^{11}B spectrum. These spectroscopic data are fully consistent with the structure established for **6** by a crystallographic study (see ESI‡). Relative to the precursor compound **3** a PPh_3 ligand has been lost and the B-agostic interaction broken, to be replaced by three meridional MeCN ligands. Compound **6** exists in a single isomeric form, with no disorder between C2 and B3′ and with the PPh_3 ligand *trans* to C and an MeCN ligand *trans* to B. This arrangement is fully consistent with the concept of a carborane being a stronger σ-donor ligand when bonded to metal through B rather than through C and the stronger *trans* influence of triphenylphosphine compared to MeCN.[35] Thus in existing as a single isomer compound **6** differs from compound **5**, where the broadly similar *trans* influences of PPh_3 and CO result in two isomers and partial crystallographic disorder.

The reaction of compound **4** with CO affords a pale-yellow product, **7**, which features a broad, high-frequency, resonance in its ^{11}B{^{1}H} NMR spectrum (δ 8.5 ppm) which integrates for 1 B out of a total of 20 and remains a singlet in the ^{11}B spectrum. In the ^{31}P NMR spectrum are two resonances indicating inequivalent P environments with the lower-frequency one being very broad, and in the ^{1}H spectrum is a single resonance typical of carborane C*H* of integral 1. Collectively these data suggest that **7** is [Ru(κ^2-2,3′-{1-(1′-1′,2′-*closo*-$C_2B_{10}H_{10}$)-1,2-*closo*-$C_2B_{10}H_{10}$})$(CO)_2$(dppe)], a conclusion confirmed by a crystallographic study (Fig. 7). In the octahedral geometry at the metal centre the carbonyl ligands are mutually *trans* and the Ru–P distance *trans* to B3′, 2.4328(6) Å, is significantly longer than that *trans* to C2, 2.3964(6) Å, confirming that carborane is a stronger σ-donor when bound to a metal through B compared to through C.

Finally, treating compound **4** with MeCN also results in partial decolourisation and the isolation of compound **8**, [Ru(κ^2-2,3′-{1-(1′-1′,2′-*closo*-$C_2B_{10}H_{10}$)-1,2-*closo*-$C_2B_{10}H_{10}$})$(MeCN)_2$-(dppe)], which spectroscopically is closely related to **7**. A crystallographic study (as the tri-MeCN solvate, see ESI‡) confirms the structural analogy between **8** and **7**. In compound **8** the Ru–P bond *trans* to B3′, 2.4256(5) Å, is again significantly longer than that *trans* to C2, 2.3473(5) Å.

In compounds **5–8** the 1,1′-bis(*o*-carborane) is now an $X_2(C,B')$ ligand, the fourth different ligating mode observed in this series of compounds. It is important to note that although the nature of the B- or C-ligation of 1,1′-bis(*o*-carborane) was inferred from NMR spectroscopic studies, the positions of the cage C atoms in the crystallographic structures were independently and unambiguously established by both the Vertex-to-Centroid Distance (VCD)[36] and Boron-Hydrogen Distance (BHD)[37] methods in every case.

Compounds **3** and **4** contain electronically and co-ordinatively unsaturated metal centres and in compound **1** the metal atom is only electronically and co-ordinatively saturated by virtue of the B-agostic interaction which is easily broken. Hence compounds **1**, **3** and **4** all have the potential to act as Lewis acid catalysts or catalyst precursors. In a preliminary sighting study, a 1 mol% loading of compound **1** was found to catalyse the cycloaddition reaction between methacrolein and cyclopentadiene to afford 2-methyl-bicyclo[2.2.1]hept-5-ene-2-carboxaldehyde, according to Scheme 2. The product was obtained with *exo* diastereoselectivity (de = 77%) with full conversion after 6 h at room temperature in CH_2Cl_2. Without catalyst the reaction still favours the *exo* diastereoisomer[38] (de = 67%) but proceeds with only 19% conversion after 6 h under the same conditions.

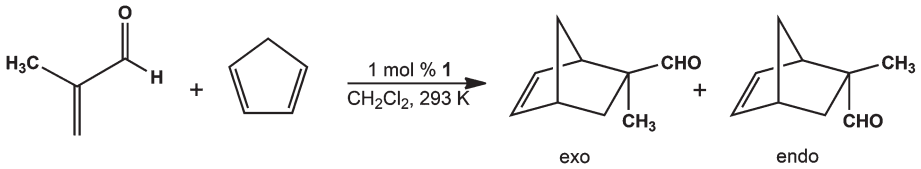

Scheme 2 The cycloaddition of methacrolein and cyclopentadiene catalysed by compound **1**.

Conclusions

This work has demonstrated the remarkable (and previously unrecognised) ligating flexibility of 1,1′-bis(*o*-carborane). In compound **1** 1,1′-bis(*o*-carborane) acts as a $X_2(C,C')$L ligand (where L here refers to a B–H→Ru agostic interaction which affords the otherwise co-ordinatively and electronically unsaturated metal centre an additional pair of electrons) but this is easily modified to $X_2(C,C')$ in compound **2**. In compounds **3** and **4** we see a switch to $X_2(C,B')$L ligation accompanying a most unusual displacement of the *p*-cymene ligand of compound **1** by PPh_3 or dppe under ambient conditions. Compounds **3** and **4** react with either CO or MeCN to co-ordinatively and electronically saturate the metal centre, with the 1,1′-bis(*o*-carborane) becoming an $X_2(C,B')$ ligand in compounds **5–8**. The $X_2(C,C')$L ligating mode for 1,1′-bis(*o*-carborane) has only been reported once previously and the $X_2(C,B')$L and $X_2(C,B')$ ligating modes are reported for the first time here. Compounds **1**, **3** and **4** have the potential to act as Lewis acid catalysts or catalyst precursors, and this is demonstrated for **1** by its catalysis of the Diels–Alder cycloaddition of cyclopentadiene and methacrolein.

Experimental

Synthetic and spectroscopic details

Experiments were performed under dry, oxygen free N_2, using standard Schlenk techniques, although subsequent manipulations were sometimes performed in the open laboratory. Solvents were freshly distilled under nitrogen from the appropriate drying agent immediately before use (THF and 40–60 petroleum ether; sodium wire) or were purified in an MBRAUN SPS-800 [CH_2Cl_2 (DCM), MeCN] and were degassed (3 × freeze–pump–thaw cycles) before use. Deuterated solvents ($CDCl_3$, CD_2Cl_2) were stored over 4 Å molecular sieves. Preparative TLC employed 20 × 20 cm Kieselgel F_{254} glass plates and for column chromatography we used 60 Å silica as the stationary phase. IR spectra were obtained from DCM solutions using a PerkinElmer Spectrum 100 FT-IR spectrometer. NMR spectra at 400.1 MHz (^{1}H), 128.4 MHz (^{11}B) or 162.0 MHz (^{31}P) were recorded on a Bruker AVIII-400 spectrometer from $CDCl_3$ solutions at 298 K unless otherwise stated. Electron impact mass spectrometry (EIMS) was carried out using a Finnigan (Thermo) LCQ Classic ion trap mass spectrometer (at the University of Edinburgh). Elemental analyses were conducted using an Exeter CE-440 elemental analyser. The starting materials 1,1′-bis(*o*-carborane),[7] $[RuCl_2(p\text{-cymene})]_2$,[39] $[RuCl_2(PPh_3)_3]$[40] and $[RuCl_2(PPh_3)_4]$[40] were prepared by literature methods or slight variations thereof. All other reagents were supplied commercially.

[Ru(κ^3-2,2′,3′-{1-(1′-1′,2′-*closo*-$C_2B_{10}H_{10}$)-1,2-*closo*-$C_2B_{10}H_{10}$})(*p*-cymene)] (1). *n*-BuLi (2.80 mL of 2.5 M solution, 6.982 mmol) was added dropwise to a cooled (0 °C) solution of 1,1′-bis(*o*-carborane) (1.000 g, 3.491 mmol) in THF (20 mL) and the products stirred for 1 h. The pale yellow solution was frozen at −196 °C then $[RuCl_2(p\text{-cymene})]_2$ (1.069 g, 1.746 mmol) was added and the reaction mixture stirred overnight at room temperature to give a green solution. The THF was removed *in vacuo* and the crude mixture dissolved in DCM and filtered. Following spot TLC (DCM : petroleum ether, 50 : 50, R_f = 0.71) purification by column chromatography using the same eluent gave, on removal of solvent, an orange solid (0.678 g, 37%), subsequently identified as [Ru(κ^3-2,2′,3′-{1-(1′-1′,2′-*closo*-$C_2B_{10}H_{10}$)-1,2-*closo*-$C_2B_{10}H_{10}$})(*p*-cymene)] (**1**). $C_{14}H_{34}B_{20}Ru$ requires C 32.3, H 6.59. Found for **1**: C 32.6, H 6.76%. ^{11}B{^{1}H} NMR (CD_2Cl_2), δ −1.4 (2B), −4.8 (2B), −7.1 (4B), −9.5 plus shoulder (8B), −10.6 (4B). ^{1}H NMR (CD_2Cl_2), δ 5.48 [d, *J* = 6.0 Hz, 2H, $CH_3C_6H_4CH(CH_3)_2$], 5.30 [d, *J* = 6.0 Hz, 2H, $CH_3C_6H_4CH(CH_3)_2$], 2.81 [sept, *J* = 6.8 Hz, 1H, $CH_3C_6H_4CH(CH_3)_2$], 2.35 [s, 3H, $CH_3C_6H_4CH(CH_3)_2$], 1.39 [d, *J* = 6.8 Hz, 6H, $CH_3C_6H_4CH(CH_3)_2$]. ^{1}H{^{11}B} NMR (CD_2Cl_2), δ 5.48 [d, *J* = 6.0 Hz, 2H, $CH_3C_6H_4CH(CH_3)_2$], 5.31[d, *J* = 6.0 Hz, 2H, $CH_3C_6H_4CH(CH_3)_2$], 2.81 [sept, *J* = 6.8 Hz, 1H, $CH_3C_6H_4CH(CH_3)_2$], 2.58 [s, 4B*H*, 2.36 (s, 3H, $CH_3C_6H_4CH(CH_3)_2$], 2.25 (s, 4B*H*), 2.21 (s, 2B*H*), 2.15 (s, 4B*H*), 2.11 (s, 2B*H*), 1.40 [d, *J* = 6.8 Hz, 6H, $CH_3C_6H_4CH(CH_3)_2$], −0.02 (s, 4H, B$H_{agostic}$). ^{1}H{^{11}B} NMR (CD_2Cl_2, 203 K), δ 5.44 [d, *J* = 6.0 Hz, 2H, $CH_3C_6H_4CH(CH_3)_2$], 5.24 [d, *J* = 6.0 Hz, 2H, $CH_3C_6H_4CH(CH_3)_2$], 2.74 [sept, *J* = 6.8 Hz, 1H, $CH_3C_6H_4CH(CH_3)_2$], 2.52 (s, 2B*H*), 2.47 (s, 2B*H*), 2.29 [s, 3H, $CH_3C_6H_4CH(CH_3)_2$], 2.12 (s, 3B*H*), 2.06 (s, 3B*H*), 2.02 (s, 3B*H*), 1.96 (s, 3B*H*), 1.30 [d, *J* = 6.8 Hz, 6H, $CH_3C_6H_4CH(CH_3)_2$], 0.78 (s, 2B*H*), −1.03 (s, 2H, B$H_{agostic}$). EIMS: *m*/*z* 520.4 (M^+).

[Ru(κ^2-2,2′-{1-(1′-1′,2′-*closo*-$C_2B_{10}H_{10}$)-1,2-*closo*-$C_2B_{10}H_{10}$})(*p*-cymene)(CO)] (2). Compound **1** (0.100 g, 0.192 mmol) was dissolved in THF (10 mL), frozen at −196 °C and the Schlenk tube was then charged with carbon monoxide (0.3 bar). The orange solution was left to warm to room temperature and stirred vigorously overnight to yield a yellow-green solution. The THF was removed *in vacuo* and the product isolated by preparative TLC (DCM : petroleum ether, 50 : 50), affording a yellow band (R_f = 0.34) subsequently identified as [Ru(κ^2-2,2′-{1-(1′-1′,2′-*closo*-$C_2B_{10}H_{10}$)-1,2-*closo*-$C_2B_{10}H_{10}$})(*p*-cymene)(CO)] (**2**) (0.037 g, 35%). $C_{15}H_{34}B_{20}ORu$ requires C 32.9, H 6.26. Found for **2**: C 32.4, H 6.27%. IR: ν_{max} 2570 (BH), 2007 (CO) cm^{-1}. ^{11}B{^{1}H} NMR, δ −2.6 (4B), −5 to −11 (overlapping resonances with maxima at −6.6, −7.8, −8.5, 16B). ^{1}H NMR, δ 6.02 [d, *J* = 6.6 Hz, 2H, $CH_3C_6H_4CH(CH_3)_2$], 5.92 [d, *J* = 6.6 Hz, 2H, $CH_3C_6H_4CH(CH_3)_2$], 2.89 [sept, *J* = 6.8 Hz, 1H, $CH_3C_6H_4CH(CH_3)_2$], 2.40 [s, 3H, $CH_3C_6H_4CH(CH_3)_2$], 1.35 [d, *J* = 6.8 Hz, 6H, $CH_3C_6H_4CH(CH_3)_2$]. ^{1}H{^{11}B} NMR, δ 6.03 [d, *J* = 6.6 Hz, 2H, $CH_3C_6H_4CH(CH_3)_2$], 5.94 [d, *J* = 6.6 Hz, 2H, $CH_3C_6H_4CH(CH_3)_2$], 2.88 (s, 2B*H*), 2.87 [sept, *J* = 6.8 Hz, 1H, $CH_3C_6H_4CH(CH_3)_2$], 2.72 (s, 2B*H*), 2.41–2.12 (multiple overlapping resonances, 16B*H*), 2.36 [s, 3H, $CH_3C_6H_4CH(CH_3)_2$], 1.31 [d, *J* = 6.8 Hz, 6H, $CH_3C_6H_4CH(CH_3)_2$]. EIMS: *m*/*z* 520.4 (M^+-CO), 548.4 (M^+).

[Ru(κ^3-2,3′,3-{1-(1′-1′,2′-*closo*-$C_2B_{10}H_{10}$)-1,2-*closo*-$C_2B_{10}H_{10}$})(PPh_3)$_2$] (3)

Method A: displacement of (p-cymene). Compound **1** (0.100 g, 0.192 mmol) was dissolved in THF (10 mL), frozen at −196 °C

then triphenylphosphine (0.111 g, 0.423 mmol) was added. The orange solution was allowed to warm to room temperature and stirred for 2 h to yield a dark red solution. The THF was removed *in vacuo* and the product purified by preparative TLC (DCM : petroleum ether, 20 : 80) affording a yellow-orange band (R_f = 0.19) subsequently identified as [Ru(κ^3-2,3′,3-{1-(1′-1′,2′-*closo*-$C_2B_{10}H_{10}$)-1,2-*closo*-$C_2B_{10}H_{10}$})$(PPh_3)_2$] (**3**) (0.027 g, 15%).

Method B1: reaction between [$RuCl_2(PPh_3)_4$] and dilithiated 1,1′-bis(o-carborane). *n*-BuLi (0.30 mL of 2.3 M solution, 0.698 mmol) was added dropwise to a cooled (0 °C) solution of 1,1′-bis(*o*-carborane) (0.100 g, 0.349 mmol) in THF (10 mL) and the products stirred for 1 h. The pale yellow solution was frozen at −196 °C then [$RuCl_2(PPh_3)_4$] (0.426 g, 0.349 mmol) was added and the reaction mixture was stirred for 4 h at room temperature to give a dark red solution. The THF was removed *in vacuo* and the crude mixture dissolved in DCM and filtered. The product was purified using preparative TLC (DCM : petroleum ether, 30 : 70) affording an orange band (R_f = 0.24, trace) and a yellow band (R_f = 0.42) subsequently identified as **3** (0.073 g, 23%).

Method B2: reaction between [$RuCl_2(PPh_3)_3$] and dilithiated bis-(o-carborane). *n*-BuLi (0.30 mL of 2.3 M solution, 0.698 mmol) was added dropwise to a cooled (0 °C) solution of 1,1′-bis(*o*-carborane) (0.100 g, 0.349 mmol) in THF (10 mL) and the products stirred for 1 h. The pale yellow solution was frozen at −196 °C, [$RuCl_2(PPh_3)_3$] (0.335 g, 0.349 mmol) was added and the reaction mixture was stirred for 4 h at room temperature to give a dark red solution. THF was removed *in vacuo* and the crude mixture dissolved in DCM. Purification by preparative TLC (DCM : petroleum ether, 30 : 70) yielded a yellow-orange band (R_f = 0.51) subsequently identified as **3** (0.078 g, 25%).

$C_{40}H_{50}B_{20}P_2Ru$ requires C 52.8, H 5.54. Found for **3**: C 52.5, H 5.53%. $^{11}B\{^1H\}$ NMR, δ 3 to −20 (overlapping resonances with maxima at 0.1, −4.8, −7.9, −9.2, −10.1, −12.5, −14.6, −17.4, assume 20B). ^1H NMR, δ 7.47–7.12 (m, 30H, C_6H_5), 1.94 (br. s, 1H, $C_{cage}H$). $^1H\{^{11}B\}$ NMR, δ 7.47–7.12 (m, 30H, C_6H_5), 1.94 (br. s, 1H, $C_{cage}H$), [2.56, 2.47, 2.34, 2.30, 2.24, 2.19, 2.14, 2.10, 2.04, 1.87, 1.79, 1.58, 1.47 (total 19 H, B*H*)], −4.23 (d, 32.0 Hz, 1H, $BH_{agostic}$). $^{31}P\{^1H\}$ NMR, δ 57.98 (br. d, 25.1 Hz, 1P), 40.25 (d, 25.1 Hz, 1P). EIMS: *m*/*z* 910.5 (M^+).

[Ru(κ^3-2,3′,3-{1-(1′-1′,2′-*closo*-$C_2B_{10}H_{10}$)-1,2-*closo*-$C_2B_{10}H_{10}$})(dppe)] (4). Compound **1** (0.140 g, 0.269 mmol) was dissolved in THF (10 mL), frozen at −196 °C then 1,2-bis(diphenylphosphino)ethane (0.107 g, 0.269 mmol) was added. The orange solution was allowed to warm to room temperature and stirred for 2 h to yield a dark red solution. The THF was removed *in vacuo* and the product was purified by preparative TLC (DCM : petroleum ether, 50 : 50) affording a yellow band (R_f = 0.69) subsequently identified as [Ru(κ^3-2,3′,3-{1-(1′-1′,2′-*closo*-$C_2B_{10}H_{10}$)-1,2-*closo*-$C_2B_{10}H_{10}$})(dppe)] (**4**) (0.085 g, 28%). $C_{30}H_{44}B_{20}P_2Ru$ requires C 46.0, H 5.66. Found for **4**: C 44.8, H 6.25%. $^{11}B\{^1H\}$ NMR, δ 3 to −19 (overlapping resonances with maxima at 0.5, −4.3, −7.0, −7.9, −9.2, −10.4, −14.5, −16.1, assume 20 B). ^1H NMR, δ 7.92–7.01 (m, 20H, C_6H_5), 3.08–2.75 (m, 4H, CH_2), 2.17 (br. s, 1H, $C_{cage}H$). $^1H\{^{11}B\}$ NMR, δ 7.90–7.01 (m, 20H, C_6H_5), 3.07–2.75 (m, 4H, CH_2), 2.17 (br. s, 1H, $C_{cage}H$), [2.74, 2.63, 2.57, 2.42, 2.23, 2.13, 2.09, 1.78, 1.75, 1.70, 1.30, 0.66 (total 19H, B*H*)], −2.25 (d, 28.0 Hz, 1H, $BH_{agostic}$). $^{31}P\{^1H\}$ NMR, δ 90.74 (br. unresolved d, 1P), 78.70 (d, 11.3 Hz, 1P). EIMS: *m*/*z* 286.3 [M^+–Ru(dppe)], 510.3, 783.3 (M^+).

[Ru(κ^2-2,3′-{1-(1′-1′,2′-*closo*-$C_2B_{10}H_{10}$)-1,2-*closo*-$C_2B_{10}H_{10}$})$(CO)_3(PPh_3)$] (5). Compound **3** was synthesised using Method **B1** (0.200 g, 0.698 mmol of 1,1′-bis(*o*-carborane)) and the compound was removed from the silica using THF (30 mL). The THF solution was reduced in volume to 10 mL, frozen at −196 °C and the Schlenk tube was then charged with carbon monoxide (0.3 bar). The orange solution was left to warm to room temperature and stirred vigorously overnight to yield a pale yellow solution. The THF was removed *in vacuo* and the product was purified by preparative TLC (DCM : petroleum ether, 50 : 50) affording a colourless band (R_f = 0.76) subsequently identified as [Ru(κ^2-2,3′-{1-(1′-1′,2′-*closo*-$C_2B_{10}H_{10}$)-1,2-*closo*-$C_2B_{10}H_{10}$})$(CO)_3(PPh_3)$] (**5**) (0.036 g, 7% based on 1,1′-bis(*o*-carborane)). $C_{25}H_{35}B_{20}O_3PRu$ requires C 41.0, H 4.82. $C_{25}H_{35}B_{20}O_3PRu{\cdot}CH_2Cl_2$ requires C 38.2, H 4.57. Found for **5**·CH_2Cl_2 (crystals submitted): C 38.5, H 4.62%. IR: ν_{max} 2570 (BH), 2042 (CO), 2034 (CO), 2028 (CO) cm^{-1}. NMR spectra consistent with a 1 : 1 mixture of two isomers. $^{11}B\{^1H\}$ NMR, δ 4.2 (br. 2B, B3′?), 1 to −14 (overlapping resonances with maxima at −2.2, −6.8, −8.9, 38B). ^1H NMR, δ 7.58–7.47 (m, 30H, C_6H_5), 4.18 (br. s, 1H, $C_{cage}H$), 3.94 (br. s, 1H, $C_{cage}H$). $^{31}P\{^1H\}$ NMR, δ 27.74 (s, 1P), 17.12 (v. br s, 1P). EIMS: *m*/*z* 647.1 ($M^+ - 3 \times CO$), 675.1 ($M^+ - 2 \times CO$), 703.1 ($M^+ - CO$), 731.8 (M^+).

[Ru(κ^2-2,3′-{1-(1′-1′,2′-*closo*-$C_2B_{10}H_{10}$)-1,2-*closo*-$C_2B_{10}H_{10}$})$(MeCN)_3(PPh_3)$] (6). Compound **3** was synthesised using Method **B1** (0.200 g, 0.698 mmol of 1,1′-bis(*o*-carborane)) and the compound was removed from the silica using MeCN (30 mL). The orange compound instantly became colourless on contact with MeCN. The solution was left to stir for 2 h then the MeCN was removed *in vacuo*. The compound was separated by preparative TLC (DCM : petroleum ether, 50 : 50) affording an unidentified yellow band (R_f = 0.60, trace) and a colourless band (R_f = 0.14) which was subsequently identified as [Ru(κ^2-2,3′-{1-(1′-1′,2′-*closo*-$C_2B_{10}H_{10}$)-1,2-*closo*-$C_2B_{10}H_{10}$})$(MeCN)_3(PPh_3)$] (**6**) (0.035 g, 7% based on 1,1′-bis(*o*-carborane)). $C_{28}H_{44}B_{20}N_3PRu$ requires C 43.6, H 5.75. N 5.45. Found for **6**: C 44.3, H 5.81, N 4.32%. $^{11}B\{^1H\}$ NMR, δ 12.8 (1B, B3′), 0 to −17 (overlapping resonances with maxima at −3.8, −8.4, −13.9, 19B). ^1H NMR, δ 7.48–7.38 (m, 15H, C_6H_5), 3.43 (br. s, 1H, $C_{cage}H$), 2.11 (d, 1 Hz, 3H, CH_3CN), 2.04 (d, 1 Hz, 3H, CH_3CN), 2.00 (br. s, 3H, CH_3CN). $^{31}P\{^1H\}$ NMR, δ 40.44 (s, 1P). EIMS: *m*/*z* 647.2 ($M^+ - 3 \times MeCN$), 688.1 ($M^+ - 2 \times MeCN$).

[Ru(κ^2-2,3′-{1-(1′-1′,2′-*closo*-$C_2B_{10}H_{10}$)-1,2-*closo*-$C_2B_{10}H_{10}$})$(CO)_2$(dppe)] (7). Compound **4** (0.037 g, 0.047 mmol) was dissolved in THF (10 mL), frozen at −196 °C and the Schlenk tube was then charged with carbon monoxide (0.3 bar). The yellow solution was left to warm to room temperature and stirred vigorously overnight to yield a pale yellow solution. The THF was removed *in vacuo* and the product was purified by preparative TLC (DCM : petroleum ether, 50 : 50) affording a yellow band

(R_f = 0.50) subsequently identified as [Ru(κ^2-2,3′-{1-(1′-1′,2′-*closo*-$C_2B_{10}H_{10}$)-1,2-*closo*-$C_2B_{10}H_{10}$})$(CO)_2$(dppe)] (**7**) (0.020 g, 50%). Microanalysis unreliable due to air-instability of compound. IR: ν_{max} 2566 (BH), 1983 (CO) cm^{-1}. $^{11}B\{^1H\}$ NMR, δ 8.5 (1B, B3′), 0 to −15 (overlapping resonances with maxima at −2.7, −7.1, −9.8, 19B). ^1H NMR, δ 7.98–6.99 (m, 20H, C_6H_5), 3.90 (br. s, 1H, $C_{cage}H$), 3.06–2.86 (m, 4H, CH_2). $^{31}P\{^1H\}$ NMR, δ 49.15 (s, 1P), 40.56 (v. br. s, 1P). EIMS: *m*/*z* 510.3, 783.3 ($M^+ - 2 \times CO$), 811.3 ($M^+ - CO$).

[Ru(κ^2-2,3′-{1-(1′-1′,2′-*closo*-$C_2B_{10}H_{10}$)-1,2-*closo*-$C_2B_{10}H_{10}$})-$(MeCN)_2$(dppe)] (8). Compound **4** (0.052 g, 0.066 mmol) was dissolved in MeCN (10 mL) and stirred for 2 h to give a pale yellow solution. The solvent was removed *in vacuo* and the product was purified by preparative TLC (DCM : petroleum ether, 50 : 50) affording a pale yellow band (R_f = 0.32) subsequently identified as [Ru(κ^2-2,3′-{1-(1′-1′,2′-*closo*-$C_2B_{10}H_{10}$)-1,2-*closo*-$C_2B_{10}H_{10}$})$(MeCN)_2$(dppe)] (**8**) (0.004 g, 7%). $C_{34}H_{50}B_{20}P_2N_2P_2Ru$ requires C 47.2, H 5.82, N 3.23. Found for **8**: C 46.1, H 5.97, N 3.47%. $^{11}B\{^1H\}$ NMR (CD_2Cl_2), δ 19.4 (1B, B3′), −1 to −15 (overlapping resonances with maxima at −2.9, −3.6, −6.0, −8.5, −12.4, 19B). ^1H NMR (CD_2Cl_2), δ 7.97–6.91 (m, 20H, C_6H_5), 3.47 (br. s, 1H, $C_{cage}H$), 3.00–2.75 (m, 4H, CH_2), 2.07 (dd, 3 Hz, 1 Hz, 3H, CH_3CN), 2.04 (app. t, 3H, CH_3CN). $^{31}P\{^1H\}$ NMR (CD_2Cl_2), δ 55.89 (s, 1P), 30.49 (v. br. s, 1P). EIMS: *m*/*z* 783.3 ($M^+ - 2 \times MeCN$).

Lewis acid catalysed Diels–Alder cycloaddition[41]

A solution of **1** (0.011 g, 0.021 mmol) in DCM (2 mL) was added to a solution of methacrolein (0.18 mL, 2.175 mmol) in DCM (1 mL) to produce a yellow solution. An aliquot of freshly cracked CpH (2.17 mL, 25.719 mmol) was added to the reaction mixture and the resultant yellow solution stirred under N_2. Samples of the reaction mixture (0.20 mL) were taken at regular intervals for solution NMR study to determine conversion. Integration of the *exo* and *endo* aldehyde ^1H NMR resonances [($CDCl_3$, 298 K) δ 9.69 *exo*-C*H*O; 9.39 *endo*-C*H*O][37] was used to calculate diastereomeric excess.

Crystallographic details

Single crystals of compound **1** were obtained by the slow evaporation of a DCM solution at room temperature, and crystals of **6** and **8** were similarly obtained by evaporation of MeCN solutions. Crystals of all other compounds (**2**, **3**, **4**, **5** and **7**) were afforded by diffusion of a DCM solution of the compound and a 5-fold excess of petroleum ether at −30 °C. Note that **4** and **5** crystallise with one molecule of DCM of solvation and **8** crystallises with three molecules of MeCN of solvation.

Intensity data from single crystal were collected on a Bruker X8 APEXII diffractometer using Mo-K_α X-radiation, with crystals mounted in inert oil on a cryoloop and cooled to 100 K by an Oxford Cryosystems Cryostream. Indexing, data collection and absorption correction were performed using the APEXII suite of programs.[42] Structures were solved by direct methods (SHELXS[43] or OLEX2[44]) and refined by full-matrix least-squares (SHELXL).[43]

Table 1 Crystallographic data

	1	2	3	4	5	6	7	8
Formula	$C_{14}H_{34}B_{20}Ru$	$C_{15}H_{34}B_{20}ORu$	$C_{40}H_{50}B_{20}P_2Ru$	$C_{30}H_{44}B_{20}P_2Ru{\cdot}CH_2Cl_2$	$C_{25}H_{35}B_{20}O_3PRu{\cdot}CH_2Cl_2$	$C_{28}H_{44}B_{20}N_3PRu$	$C_{32}H_{44}B_{20}O_2P_2Ru$	$C_{34}H_{50}B_{20}N_2P_2Ru{\cdot}3CH_4N$
M	519.68	547.69	910.01	868.79	816.67	770.90	839.88	989.13
Crystal system	Triclinic	Orthorhombic	Triclinic	Triclinic	Triclinic	Triclinic	Triclinic	Monoclinic
Space group	*P*1	$Pna2_1$	*P*1	*P*1	*P*1	*P*1	*P*1	*C*2/*c*
a/Å	9.9651(8)	17.7285(10)	11.2062(9)	10.6783(14)	10.774(2)	10.4838(14)	11.704(3)	21.5530(9)
b/Å	10.4007(8)	15.1002(8)	11.5418(10)	12.1648(17)	14.223(3)	10.6487(16)	12.184(3)	19.6096(8)
c/Å	13.6240(11)	9.8309(5)	17.9159(17)	17.624(2)	14.245(3)	18.114(3)	16.339(4)	23.5945(10)
α (°)	85.831(4)	90	81.178(5)	79.065(7)	63.017(11)	87.152(8)	104.475(7)	90
β (°)	70.460(4)	90	80.736(5)	74.204(7)	79.932(10)	75.088(7)	106.328(6)	94.465(2)
γ (°)	72.262(4)	90	85.546(5)	71.267(7)	80.026(10)	82.148(7)	98.443(7)	90
U/Å^3	1266.79(18)	2631.8(2)	2256.6(3)	2073.0(5)	1904.4(7)	1935.6(5)	2105.1(9)	9941.8(7)
Z, *Z*′	2, 1	4, 1	2, 1	2, 1	2, 1	2, 1	2, 1	8, 1
F(000)/e	524	1104	928	880	820	784	852	4064
D_{calc}/Mg m^{-3}	1.362	1.382	1.339	1.392	1.424	1.323	1.325	1.322
μ(Mo-K_α)/mm^{-1}	0.624	0.608	0.451	0.611	0.626	0.474	0.480	0.417
θ_{max} (°)	27.28	36.13	27.78	30.93	31.36	34.18	30.63	30.20
Data measured	19 182	70 842	39 226	46 792	46 419	40 047	47 883	107 261
Unique data, *n*	5545	11 988	10 414	12 793	12 119	15 552	12 386	14 488
R_{int}	0.0320	0.0370	0.0753	0.0661	0.0609	0.0399	0.0448	0.0429
Data with $I > 2\sigma(I)$	5204	10 594	8961	10 032	8834	13 111	9985	11 576
R (obs. data)	0.0338	0.0250	0.0927	0.0382	0.0427	0.0368	0.0346	0.0351
wR_2 (obs. data)	0.0720	0.0513	0.1532	0.0771	0.0825	0.0740	0.0770	0.0917
S (all data)	1.085	1.014	1.229	1.059	1.052	1.022	1.031	1.057
Variables	379	397	639	562	567	541	574	714
E_{max}, E_{min}/e Å^{-3}	1.78, −0.82	0.74, −0.52	1.75, −1.31	0.62, −0.68	0.71, −0.71	0.56, −0.69	0.49, −0.79	0.53, −0.95
Flack parameter		−0.032(9)						

In all cases cage C or B atoms were initially all treated as B and the structures refined with cage H atoms allowed positional variation, leading to a Prostructure which was then analysed by both the VCD[36] and BHD[37] methods to identify the cage C atoms.

The structures of compounds **1**, **2**, **4** and **6–8** are free of disorder, except that in **8** there are three molecules of MeCN of solvation per asymmetric unit, two of which are disordered. In **3** there is evidence of considerable disorder, but the only part that could be modelled was a fractional Ru atom [Ru1A, SOF 0.197(2)] located 0.884(3) Å from Ru1 [SOF 0.803(2)]. In **5** atoms at cage vertices 2 and 3′ are each 0.5C+0.5B and there is one disordered molecule of CH_2Cl_2 of solvation per asymmetric unit.

Non-cage atoms were constrained to idealised geometries with $C_{aromatic}$–H (*p*-cymene ring) = 1.00 Å, C_{phenyl}–H = 0.95 Å, C_{methyl}–H = 0.98 Å, $C_{secondary}$–H = 0.99 Å, $C_{tertiary}$–H = 1.00 Å. All H displacement parameters, U_{iso}, were constrained to be 1.2 × U_{eq} (bound B or C) except Me H atoms [U_{iso}(H) = 1.5 × U_{eq} C(Me)]. Table 1 contains further experimental details.

Acknowledgements

We thank the Engineering and Physical Sciences Research Council (EPSRC) for support of LER and WYM (grant code: EP/I031545/1). We also thank the EPSRC and the CRITICAT Centre for Doctoral Training for financial support (PhD studentship to APYC; grant code: EP/L016419/1). We are very grateful to Dr Peter Grice (University of Cambridge) for the three-channel NMR experiments on compound **4** using a spectrometer purchased as part of an EPSRC Core Capability grant (code: EP/K039520/1). Finally we thank one of the referees for their critical reading of our original manuscript and their very helpful comments.

References

1 T. P. Onak, R. E. Williams and H. G. Weiss, *J. Am. Chem. Soc.*, 1962, **84**, 2830.
2 R. N. Grimes, *Carboranes*, Academic Press, Oxford, UK, 2nd edn, 2011.
3 R. N. Grimes, *Dalton Trans.*, 2015, **44**, 5939.
4 W. Y. Man, G. M. Rosair and A. J. Welch, *Acta Crystallogr., Sect. E: Struct. Rep. Online*, 2014, **70**, 462.
5 (*a*) J. A. Dupont and M. F. Hawthorne, *J. Am. Chem. Soc.*, 1964, **86**, 1643; (*b*) T. E. Paxson, K. P. Callahan and M. F. Hawthorne, *Inorg. Chem.*, 1973, **12**, 708.
6 X. Yang, W. Jiang, C. B. Knobler, M. D. Mortimer and M. F. Hawthorne, *Inorg. Chim. Acta*, 1995, **240**, 371.
7 S. Ren and Z. Xie, *Organometallics*, 2008, **27**, 5167.
8 T. D. Getman, C. B. Knobler and M. F. Hawthorne, *J. Am. Chem. Soc.*, 1990, **112**, 4594.
9 T. D. Getman, C. B. Knobler and M. F. Hawthorne, *Inorg. Chem.*, 1992, **31**, 101.
10 M. F. Hawthorne, D. A. Owen and J. W. Wiggins, *Inorg. Chem.*, 1971, **10**, 1304.
11 J. A. Doi, E. A. Mizusawa, C. B. Knobler and M. F. Hawthorne, *Inorg. Chem.*, 1984, **23**, 1482.
12 J. A. Long, T. B. Marder, P. E. Behnken and M. F. Hawthorne, *J. Am. Chem. Soc.*, 1984, **106**, 2979.
13 P. E. Behnken, T. B. Marder, R. T. Baker, C. B. Knobler, M. R. Thompson and M. F. Hawthorne, *J. Am. Chem. Soc.*, 1985, **107**, 932.
14 G. Thiripuranathar, W. Y. Man, C. Palmero, A. P. Y. Chan, B. T. Leube, D. Ellis, D. McKay, S. A. Macgregor, L. Jourdan, G. M. Rosair and A. J. Welch, *Dalton Trans.*, 2015, **44**, 5628.
15 D. Ellis, G. M. Rosair and A. J. Welch, *Chem. Commun.*, 2010, **46**, 7394.
16 D. Ellis, D. McKay, S. A. Macgregor, G. M. Rosair and A. J. Welch, *Angew. Chem., Int. Ed.*, 2010, **49**, 4943.
17 (*a*) D. A. Owen and M. F. Hawthorne, *J. Am. Chem. Soc.*, 1970, **92**, 3194; (*b*) D. A. Owen and M. F. Hawthorne, *J. Am. Chem. Soc.*, 1971, **93**, 873; (*c*) D. E. Harwell, J. McMillan, C. B. Knobler and M. F. Hawthorne, *Inorg. Chem.*, 1997, **36**, 5951.
18 Z.-J. Yao, Y.-Y. Zhang and G.-X. Jin, *J. Organomet. Chem.*, 2015, **798**, 274.
19 M. J. Martin, W. Y. Man, G. M. Rosair and A. J. Welch, *J. Organomet. Chem.*, 2015, **798**, 36.
20 A. I. Yanovsky, N. G. Furmanova, Yu. T. Struchkov, N. F. Shemyakin and L. I. Zakharkin, *Izv. Akad. Nauk Gruz. SSR, Ser. Khim.*, 1979, 1523.
21 M. Brookhart, M. L. H. Green and G. Parkin, *Proc. Nat. Acad. Sci. U. S. A.*, 2007, **104**, 6908.
22 M. Brookhart and M. L. H. Green, *J. Organomet. Chem.*, 1983, **250**, 395.
23 Only one example of 1,1′-bis(*o*-carborane) acting as a $X_2(C,C')L$ igand has been previously reported. See: R. A. Love and R. Bau, *J. Am. Chem. Soc.*, 1972, **94**, 8274.
24 *E.g.* F. Teixidor, R. Núñez, M. A. Flores, A. Demonceau and C. Viñas, *J. Organomet. Chem.*, 2000, **614–615**, 48, and references therein.
25 *E.g.* (*a*) F. Teixidor, J. A. Ayllón, C. Viñas, R. Kivekäs, R. Sillanpää and J. Casabó, *J. Chem. Soc., Chem. Commun.*, 1992, 1281; (*b*) G. Barberà, C. Viñas, F. Teixidor, G. M. Rosair and A. J. Welch, *J. Organomet. Chem.*, 2002, **663**, 221.
26 M. Brookhart, M. L. H. Green and L.-L. Wong, *Prog. Inorg. Chem.*, 1988, **36**, 1.
27 T. A. Stephenson and G. Wilkinson, *J. Inorg. Nucl. Chem.*, 1966, **28**, 945.
28 S. J. La Placa and J. A. Ibers, *Inorg. Chem.*, 1965, **4**, 778.
29 W. I. Sundquist, D. P. Bancroft and S. J. Lippard, *J. Am. Chem. Soc.*, 1990, **112**, 1590.
30 For a rare example of arene displacement from Ru^{II} under ambient conditions see R. Castarlenas, C. Vovard, C. Fischmeister and P. H. Dixneuf, *J. Am. Chem. Soc.*, 2006, **128**, 4079 (arene displacement assumed). See also ref. 18 in

S. C. Serron and S. P. Nolan, *Organometallics*, 1995, **14**, 4611.

31 *E.g.* (*a*) M. A. Bennett and A. K. Smith, *J. Chem. Soc., Dalton Trans.*, 1974, 233; (*b*) M. A. Bennett, T.-N. Huang, T. W. Matheson and A. K. Smith, *Inorg. Synth.*, 1982, **21**, 74; (*c*) C. Albrecht, S. Gauthier, J. Wolf, R. Scopelliti and K. Severin, *Eur. J. Inorg. Chem.*, 2009, 1003; (*d*) D. S. Perekalin, E. E. Karslyan, E. A. Trifonova, A. I. Konovalov, N. L. Loskutova, Y. V. Nelyubina and A. R. Kudinov, *Eur. J. Inorg. Chem.*, 2013, 481.

32 *E.g.* (*a*) P. J. Dyson, *Chimia*, 2007, **61**, 698; (*b*) S. J. Dougan and P. J. Sadler, *Chimia*, 2007, **61**, 704; (*c*) G. Süss-Fink, *Dalton Trans.*, 2010, **39**, 1673; (*d*) A. A. Nazarov, C. G. Hartinger and P. J. Dyson, *J. Organomet. Chem.*, 2014, **751**, 251.

33 *E.g.* P. Kumar, R. K. Gupta and D. S. Pandey, *Chem. Soc. Rev.*, 2014, **43**, 707.

34 First reference; E. L. Hoel and M. F. Hawthorne, *J. Am. Chem. Soc.*, 1973, **95**, 2712; E. L. Hoel and M. F. Hawthorne, *J. Am. Chem. Soc.*, 1975, **97**, 6388. Recent references: (*a*) M. Herberhold, H. Yan, W. Milius and B. Wrackmeyer, *Chem. – Eur. J.*, 2002, **8**, 388; (*b*) A. V. Usatov, E. V. Martynova, F. M. Dolgushin, A. S. Peregudov, M. Yu. Antipin and Yu. N. Novikov, *Eur. J. Inorg. Chem.*, 2003, 29; (*c*) D. Liu, L. Dang, Y. Sun, H.-S. Chan, Z. Lin and Z. Xie, *J. Am. Chem. Soc.*, 2008, **130**, 16103; (*d*) A. M. Spokoyny, M. G. Reuter, C. L. Stern, M. A. Ratner, T. Seideman and C. A. Mirkin, *J. Am. Chem. Soc.*, 2009, **131**, 9482; (*e*) A. M. Prokhorov, P. A. Slepukhin, V. L. Rusinov, V. N. Kalinin and D. N. Kozhevnikov, *Chem. Commun.*, 2011, **47**, 7713; (*f*) N. Fey, M. F. Haddow, R. Mistry, N. C. Norman, A. G. Orpen, T. J. Reynolds and P. G. Pringle, *Organometallics*, 2012, **31**, 2907; (*g*) J. Estrada, S. E. Lee, S. G. McArthur, A. El-Hellani, F. S. Tham and V. Lavallo, *J. Organomet. Chem.*, 2015, **798**, 214.

35 B. J. Coe and S. Glenwright, *Coord. Chem. Rev.*, 2000, **5**, 203.

36 A. McAnaw, G. Scott, L. Elrick, G. M. Rosair and A. J. Welch, *Dalton Trans.*, 2013, **42**, 645.

37 A. McAnaw, M. E. Lopez, D. Ellis, G. M. Rosair and A. J. Welch, *Dalton Trans.*, 2014, **43**, 5095.

38 D. F. Schreiber, Y. Ortin, H. Müller-Bunz and A. D. Phillips, *Organometallics*, 2011, **30**, 5381.

39 M. A. Bennett, T.-N. Huang, T. W. Matheson and A. K. Smith, *Inorg. Synth.*, 1982, **21**, 74.

40 P. S. Hallman, T. A. Stephenson and G. Wilkinson, *Inorg. Synth.*, 1970, **12**, 237.

41 J. W. Faller, B. J. Grimmond and D. G. D'Alliessi, *J. Am. Chem. Soc.*, 2001, **123**, 2525.

42 *Bruker AXS APEX2, version 2009-5*, Bruker AXS Inc., Madison, Wisconsin, USA, 2009.

43 G. M. Sheldrick, *Acta Crystallogr., Sect. A: Found. Crystallogr.*, 2008, 64, 112.

44 O. V. Dolomanov, L. J. Bourhis, R. J. Gildea, J. A. K. Howard and H. Puschmann, *J. Appl. Crystallogr.*, 2009, **42**, 339.

Dalton Transactions

PAPER

View Article Online
View Journal | View Issue

Cite this: *Dalton Trans.*, 2017, **46**, 1811

Double deboronation and homometalation of 1,1′-bis(*ortho*-carborane)†‡

Gobika Thiripuranathar, Antony P. Y. Chan, Dipendu Mandal, Wing Y. Man, Mario Argentari, Georgina M. Rosair and Alan J. Welch*

Received 24th November 2016,
Accepted 16th December 2016

DOI: 10.1039/c6dt04457c

rsc.li/dalton

Double deboronation of 1,1′-bis(*ortho*-carborane) results in a mixture of racemic and meso diastereoisomers which are sources of the [7-(7′-7′,8′-*nido*-$C_2B_9H_{10}$)-7,8-*nido*-$C_2B_9H_{10}$]$^{4-}$ tetraanion. Consistent with this, metalation of the mixture with {Ru(*p*-cymene)} affords the diastereoisomers α-[1-(8′-2′-(*p*-cymene)-2′,1′,8′-*closo*-$RuC_2B_9H_{10}$)-3-(*p*-cymene)-3,1,2-*closo*-$RuC_2B_9H_{10}$] (**3**α) and β-[1-(8′-2′-(*p*-cymene)-2′,1′,8′-*closo*-$RuC_2B_9H_{10}$)-3-(*p*-cymene)-3,1,2-*closo*-$RuC_2B_9H_{10}$] (**3**β) in which the primed cage has undergone a spontaneous 3′,1′,2′ to 2′,1′,8′-RuC_2B_9 isomerisation. Analogous cobaltacarboranes α-[1-(8′-2′-Cp-2′,1′,8′-*closo*-$CoC_2B_9H_{10}$)-3-Cp-3,1,2-*closo*-$CoC_2B_9H_{10}$] (**4**α) and β-[1-(8′-2′-Cp-2′,1′,8′-*closo*-$CoC_2B_9H_{10}$)-3-Cp-3,1,2-*closo*-$CoC_2B_9H_{10}$] (**4**β) are formed by metalation with $CoCl_2$/NaCp followed by oxidation, along with a small amount of the unique species [8-(8′-2′-Cp-2′,1′,8′-*closo*-$CoC_2B_9H_{10}$)-2-Cp-2,1,8-*closo*-$CoC_2B_9H_{10}$] (**5**) if the source of the tetraanion is $[HNMe_3]_2$[7-(7′-7′,8′-*nido*-$C_2B_9H_{11}$)-7,8-*nido*-$C_2B_9H_{11}$]. Two-electron reduction and subsequent reoxidation of **4**α and **4**β afford species indistinguishable from **5**. The reaction between $[Tl]_2$[1-(1′-3′,1′,2′-*closo*-$TlC_2B_9H_{10}$)-3,1,2-*closo*-$TlC_2B_9H_{10}$] and $[CoCpI_2(CO)]$ leads to the isolation of a further isomer of $(CpCoC_2B_9H_{11})_2$, *rac*-[1-(1′-3′-Cp-3′,1′,2′-*closo*-$CoC_2B_9H_{10}$)-3-Cp-3,1,2-*closo*-$CoC_2B_9H_{10}$] (**6**), which displays intramolecular dihydrogen bonding. Thermolysis of **6** yields **4**α, allowing a link to be established between the α and β forms of **3** and **4** and racemic and meso forms of the [7-(7′-7′,8′-*nido*-$C_2B_9H_{10}$)-7,8-*nido*-$C_2B_9H_{10}$]$^{4-}$ tetraanion, whilst reduction–oxidation of **6** again results in a product indistinguishable from **5**.

Introduction

The compound [1-(1′-1′,2′-*closo*-$C_2B_{10}H_{11}$)-1,2-*closo*-$C_2B_{10}H_{11}$], two *ortho*-carborane units connected by a C–C bond,[1] is commonly referred to as 1,1′-bis(*ortho*-carborane) (Fig. 1). First prepared in 1964,[2] the chemistry of 1,1′-bis(*o*-carborane) remained underdeveloped for long periods, in large part because of the lack of a reliable and high-yielding synthesis. This problem has now been overcome,[3] and recent years have witnessed an impressive blossoming of the chemistry of 1,1′-bis(*o*-carborane) in a number of diverse areas broadly classified as derivatisation,[4–8] cage expansion,[9–11] metalation,[12–14] bond activation[15–18] and the synthesis of luminescent complexes.[19]

In 2015 we reported the metalation of singly-deboronated 1,1′-bis(*o*-carborane) with both {Ru(*p*-cymene)} and {CoCp} fragments.[13] In both cases non-isomerised 3,1,2-MC_2B_9-1′,2′-C_2B_{10} and isomerised 2,1,8-MC_2B_9-1′,2′-C_2B_{10} products were isolated, and we explored the conversion of the former to the latter by both thermolytic and chemical means. In this contribution we extend this initial work to the homometalation of doubly-deboronated 1,1′-bis(*o*-carborane) which adds two interesting dimensions to the study: (i) double deboronation of 1,1′-bis(*o*-carborane) introduces the possibility of metallacarborane products which are diastereoisomers, and (ii) the presence of two metallacarborane clusters in the same molecule allows for products in which neither of the cages has isomerised, one cage has isomerised or both cages have isomerised.

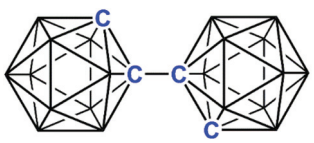

Fig. 1 1,1′-Bis(*ortho*-carborane).

Prior to the present study the only reported examples of metalation of doubly-deboronated 1,1′-bis(*o*-carborane), of

Institute of Chemical Sciences, Heriot-Watt University, Edinburgh, EH14 4AS UK. E-mail: a.j.welch@hw.ac.uk; Tel: +44 (0)131 451 3217

† In memory of Professor Igor T. Chishevsky.

‡ Electronic supplementary information (ESI) available: NMR spectra of all new compounds reported. Details of the disorder in $[BTMA]_2$[**1**]. CCDC 1516771–1516778. For ESI and crystallographic data in CIF or other electronic format see DOI: 10.1039/c6dt04457c

which we are aware, are two bis-rhodacarboranes, one of the 3,1,2-RhC_2B_9-3′,1′,2′-RhC_2B_9 form and the other of the 3,1,2-RhC_2B_9-2′,1′,8′-RhC_2B_9 form, afforded by the reaction between $[Cs]_2$[7-(7′-7′,8′-*nido*-$C_2B_9H_{11}$)-7,8-*nido*-$C_2B_9H_{11}$] and [Rh(COD)(PEt_3)Cl].[20]

Results and discussion

Double deboronation of 1,1′-bis(*o*-carborane)

The single and double deboronations of 1,1′-bis(*o*-carborane) were first reported by Hawthorne *et al.* in 1971.[21] Double deboronation was achieved by heating to reflux 1,1′-bis(*o*-carborane) and five equivalents of KOH in EtOH for 120 h, isolating the product as both $[Cs]^+$ and $[HNMe_3]^+$ salts. We have found that acceptable yields of products are achieved in a considerably less time (18–48 h) by using larger amounts of KOH (typically 25–30 equivalents). The doubly-deboronated product has been isolated as $[HNMe_3]^+$, $[BTMA]^+$ and $[Tl]^+$ salts ($[BTMA]^+$ = benzyltrimethylammonium, $[C_6H_5CH_2NMe_3]^+$). Note, however, that these are described in different ways because in the $[HNMe_3]^+$ and $[BTMA]^+$ salts each cage is protonated to afford a double nido dianion whilst for the $[Tl]^+$ salt the cages are *not* protonated and we assume that one Tl atom is weakly associated with each carborane cage (now formally closo) in the same way as has been confirmed for $[Tl][TlC_2B_9H_{11}]$.[22] Thus the $[HNMe_3]^+$ and $[BTMA]^+$ salts are salts of [7-(7′-7′,8′-*nido*-$C_2B_9H_{11}$)-7,8-*nido*-$C_2B_9H_{11}$]$^{2-}$, $[HNMe_3]_2$[**1**] and $[BTMA]_2$[**1**], respectively, whilst the $[Tl]^+$ salt is $[Tl]_2$[1-(1′-3′,1′,2′-*closo*-$TlC_2B_9H_{10}$)-3,1,2-*closo*-$TlC_2B_9H_{10}$] ($[Tl]_2$[**2**]). In metalation reactions all the three salts are potential sources of the [7-(7′-7′,8′-*nido*-$C_2B_9H_{10}$)-7,8-*nido*-$C_2B_9H_{10}$]$^{4-}$ tetraanion, but for practical purposes $[HNMe_3]_2$[**1**] and $[Tl]_2$[**2**] are the most useful.

The insolubility of $[Tl]_2$[**2**] in common solvents meant that it was characterised only by elemental analysis, whilst the more soluble species $[HNMe_3]_2$[**1**] and $[BTMA]_2$[**1**] were also characterised by ^{11}B and ^1H NMR spectroscopies.

Double deboronation of 1,1′-bis(*o*-carborane) potentially affords both racemic and meso diastereoisomers (Fig. 2). Although Hawthorne and co-workers recognised this possibility they suggested that the meso form would be more stable and hence more likely to form.[21] No evidence for diastereoisomers was afforded by the 80 MHz ^{11}B NMR spectrum of the $[Cs]^+$ salt but, in contrast, we see a clear indication of two such isomers from the 128.4 MHz $^{11}B\{^1H\}$ spectra of $[HNMe_3]_2$[**1**] and $[BTMA]_2$[**1**] (Fig. 3), with minor resonances at δ −17.6, −21.3 and −24.4 close to major resonances at δ −18.5, −20.4 and −23.8, respectively. Approximately, the ratio of major : minor isomers is *ca.* 2 : 1 (this is supported by the relative integrals of two resonances assigned to $C_{cage}H$ in the ^1H NMR spectra), but it is not possible to determine which diastereoisomer is major and which is minor.

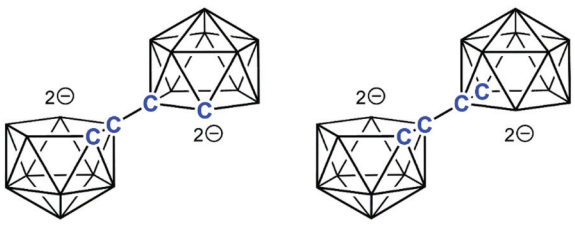

Fig. 2 Racemic (left) and meso (right) forms of doubly-deboronated 1,1′-bis(*ortho*-carborane).

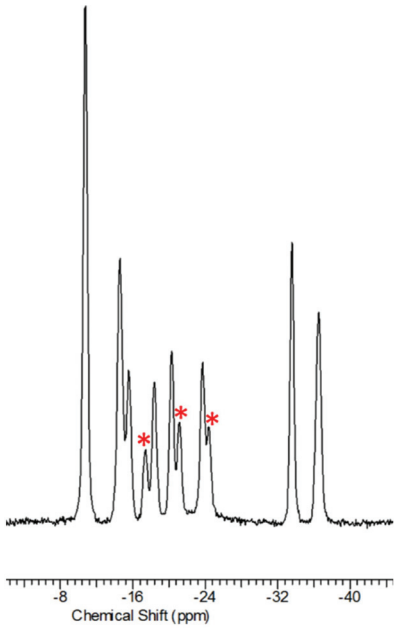

Fig. 3 The 128.4 MHz $^{11}B\{^1H\}$ NMR spectrum of $[HNMe_3]_2$[**1**] in $(CD_3)_2SO$ (that of $[BTMA]_2$[**1**] is identical) showing (asterisks) minor resonances consistent with the sample being a mixture of diastereoisomers.

Frustratingly, a single-crystal diffraction study of $[BTMA]_2$[**1**] did not resolve this question because of disorder. The anion is located on a crystallographic inversion centre at the mid-point of the C7–C7′ bond. Within each cage there is disorder between vertices 8 and 11 (meaning that the ion cannot be described as simply racemic or meso; almost certainly both forms crystallise together) and there is further disorder with both vertices 8 and 11 not fully occupied and a partial ghost vertex, vertex 12, lying over the 7-8-9-10-11 face. The best crystallographic model of the disorder is that vertex 8 is 51%C + 15%B, vertex 11 is 29%C + 65%B and vertex 12 is 20%C + 20%B. This implies that in the solid state more of the anion is in the meso form, and that is what is shown in the simplified representation in Fig. 4.

Thus the combined spectroscopic and crystallographic evidence implies that double deboronation of 1,1′-bis(*o*-carborane) results in a mixture of diastereoisomers, and this is supported by the results of metalation reactions described in the following sections.

Ruthenacarboranes

Deprotonation of $[HNMe_3]_2$[**1**] with *n*-BuLi in THF followed by the addition of $[RuCl_2(p\text{-cymene})]_2$ or, alternatively, direct reac-

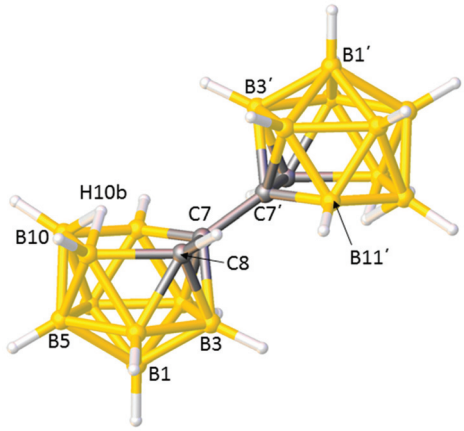

Fig. 4 View of the major (meso) component of the disordered anion in $[BTMA]_2$[**1**]. There is a crystallographic inversion centre at the mid-pint of the C7–C7′ bond. C7–C7′ 1.517(3) Å.

tion between $[Tl]_2$[**2**] and $[RuCl_2(p\text{-cymene})]_2$ in THF affords the isomeric ruthenacarborane compounds α-[1-(8′-2′-(*p*-cymene)-2′,1′,8′-*closo*-$RuC_2B_9H_{10}$)-3-(*p*-cymene)-3,1,2-*closo*-$RuC_2B_9H_{10}$] (**3α**) and β-[1-(8′-2′-(*p*-cymene)-2′,1′,8′-*closo*-$RuC_2B_9H_{10}$)-3-(*p*-cymene)-3,1,2-*closo*-$RuC_2B_9H_{10}$] (**3β**) following isolation by both column and thin-layer chromatography (Scheme 1). Isolated yields by both methods are relatively poor but those obtained by using $[Tl]_2$[**2**] are somewhat better, 11% and 5% respectively.

The isomeric nature of **3α** and **3β** was confirmed by elemental analysis and mass spectrometry, and the close relationship between their molecular structures was implied by the similarity of their NMR spectra. In terms of detailed information the $^{11}B\{^1H\}$ NMR spectra of both are relatively uninformative

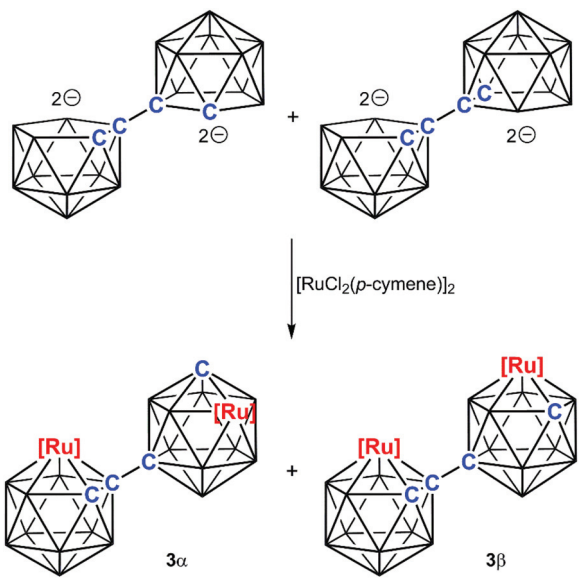

Scheme 1 Synthesis of ruthenacarboranes **3α** and **3β** from either $[HNMe_3]_2$[**1**] or $[Tl]_2$[**2**]. [Ru] = {Ru(*p*-cymene)}.

with multiple overlapping resonances which are impossible to integrate with confidence. In contrast the ^1H NMR spectra of both **3α** and **3β** clearly show two sets of resonances assigned to *p*-cymene and two $C_{cage}H$ resonances, implying that within each species the two ruthenacarborane cages are in different isomeric forms.

The precise natures of **3α** and **3β** were established by crystallographic studies, and perspective views of single molecules are presented in Fig. 5 and 6, respectively. Compounds **3** are diruthenacarboranes in which one cage (unprimed) has a 3,1,2-RuC_2B_9 architecture whilst the other (primed) is 2,1,8-RuC_2B_9. Since compounds **3** result from the metalation of $[HNMe_3]_2$[**1**] or $[Tl]_2$[**2**] in which the C atoms in each cage are adjacent, the 2′,1′,8′-RuC_2B_9 cage must arise from isomerisation following metalation. Importantly, **3α** and **3β** are related as diastereoisomers – with the chiralities of the unprimed cages being the same (as in Fig. 5 and 6) and the chiralities of the primed cages being the opposite. Clearly this arises from the fact that the bis-*nido* precursors $[HNMe_3]_2$[**1**] and $[Tl]_2$[**2**] exist as diastereoisomeric mixtures, and indeed it establishes that this must be so – whilst the anionic diastereomeric precursors could not easily be separated, the neutral metallacarborane products are amenable to separation by chromatography. Note, however, that the terms racemic and meso cannot strictly be applied to the diastereoisomers of **3** since the two metallacarborane components are different (one 3,1,2-MC_2B_9 the other 2′,1′,8′-MC_2B_9). Moreover we cannot easily associate either **3α** or **3β** with a particular racemic or meso precursor (however, see later) since the mechanism of isomerisation that affords the 2′,1′,8′-RuC_2B_9 cage remains unknown, so we use the descriptors α and β to distinguish them.

Presumably the initial product, when doubly-deboronated 1,1′-bis(*o*-carborane) is metalated with {Ru(*p*-cymene)} fragments, is the 3,1,2-RuC_2B_9-3′,1′,2′-RuC_2B_9 compound (as a diastereoisomeric mixture) which then undergoes spontaneous isomerisation of one cage from 3,1,2-RuC_2B_9 to 2,1,8-RuC_2B_9. We recently showed that the singly-metalated species [1-(1′-1′,2′-*closo*-$C_2B_{10}H_{11}$)-3-(*p*-cymene)-3,1,2-*closo*-$RuC_2B_9H_{10}$] (**I**) isomerises to [8-(1′-1′,2′-*closo*-$C_2B_{10}H_{11}$)-2-(*p*-cymene)-2,1,8-*closo*-$RuC_2B_9H_{10}$] with mild heating (THF reflux),[13] and therefore it was of interest to discover if similar thermolysis of compounds **3** would effect the isomerisation of the 3,1,2-RuC_2B_9 cage. It does not. Both **3α** and **3β** are recovered unchanged (save for some decomposition) on heating to reflux in THF for 2.5 h.

Compound **I** was found to be sterically-crowded, with a pronounced bend-back of the *p*-cymene ligand away from the carborane cage attached to C1. Similar steric crowding is discernible in the 3,1,2-RuC_2B_9 cages of **3α** and **3β**, not surprising since they are related to **I** by nominal replacement of the {$C_2B_{10}H_{11}$} substituent of **I** with {(*p*-cymene)$RuC_2B_9H_{10}$}. In **3α** and **3β** the bend-back of the *p*-cymene ligand on Ru3 with respect to the least-squares plane through the metal-bonded cage atoms C1C2B7B8B4 [by 17.6(2) and 17.7(3)° respectively] is clearly visible in Fig. 5 and 6. Further evidence of this intramolecular crowding is the observation that Ru–C1 is *ca.* 0.1 Å longer than Ru–C2. In contrast, in the 2′,1′,8′-RuC_2B_9 cages of

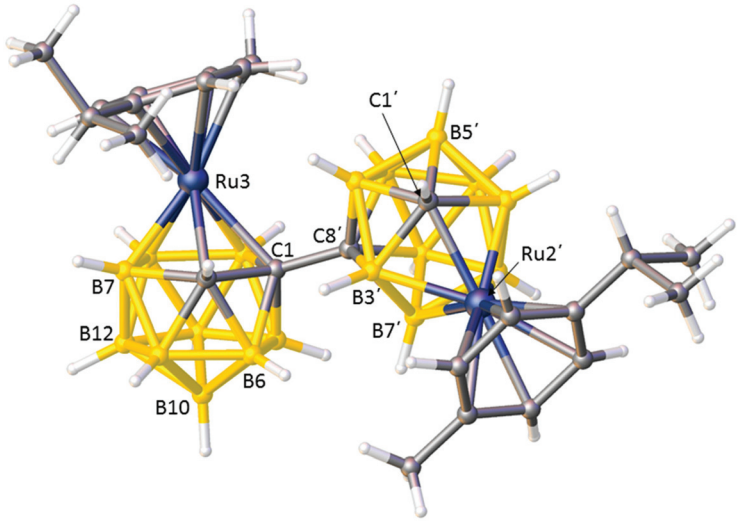

Fig. 5 Perspective view of compound **3**α with atomic numbering scheme. Only the major component of the disordered *p*-cymene ligand on Ru2′ is shown for clarity. Selected interatomic distances (Å): Ru3–C1 2.302(6), Ru3–C2 2.199(6), C1–C2 1.650(9), Ru2′–C1′ 2.176(7), and C1–C8′ 1.546(8).

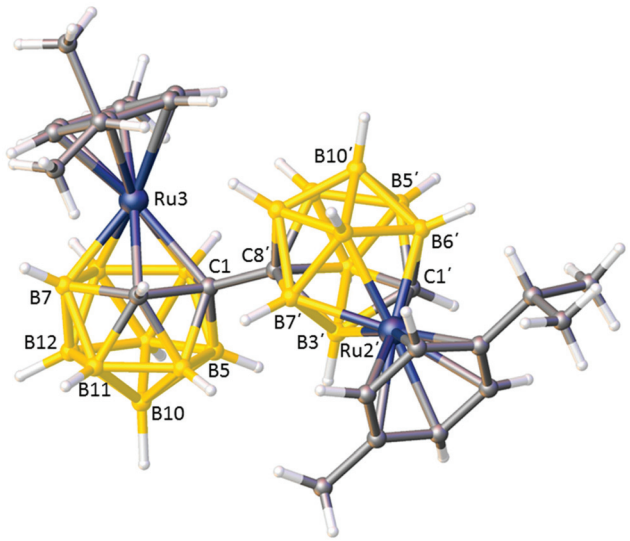

Fig. 6 Perspective view of compound **3**β with atomic numbering scheme. Only the major component of the disordered *p*-cymene ligand on Ru3 is shown for clarity. Selected interatomic distances (Å): Ru3–C1 2.292(7), Ru3–C2 2.200(8), C1–C2 1.634(10), Ru2′–C1′ 2.177(7), and C1–C8′ 1.555(9).

3α and **3**β there is no significant bend-back of the *p*-cymene ligand, which makes dihedral angles of only 3.1(2) and 2.7(3)°, respectively, with the least-squares plane through atoms C1′B6′B11′B7′B3′. We presume that in the 3,1,2-RuC_2B_9-3′,1′,2′-RuC_2B_9 precursors of **3**α and **3**β, both cages suffer steric congestion and that gaining partial relief from this is a contributory factor in the observed isomerisation.

Cobaltacarboranes

Double deprotonation of $[HNMe_3]_2$[**1**] with *n*-BuLi followed by treatment with $CoCl_2$/NaCp and finally aerial oxidation yields, on work-up involving preparative TLC, two mobile orange bands and a trace amount of a mobile yellow band (Scheme 2). The reaction between $[Tl]_2$[**2**] and $CoCl_2$/NaCp affords the same two orange products, in somewhat better yields, but there is no evidence for the yellow species. Elemental analysis and mass spectrometry imply that all three compounds are isomers of $(CpCoC_2B_9H_{10})_2$, *i.e.* both carborane cages have been metalated with {CoCp} fragments. Spectroscopically the two orange products are clearly very similar whereas the yellow species is quite different.

In the ^{1}H NMR spectrum of each of the orange products are two resonances assigned to Cp–*H* atoms (*ca.* 5.8 and 5.5 ppm) and two resonances assigned to $C_{cage}H$ atoms (*ca.* 4.1 and 2.8 ppm), the last pair suggesting that one cobaltacarborane cage is of 3,1,2-CoC_2B_9 architecture and the other is of 2,1,8-CoC_2B_9 architecture, by comparison with the $C_{cage}H$ resonances in [3-Cp-3,1,2-*closo*-$CoC_2B_9H_{11}$][23] and [2-Cp-2,1,8-*closo*-$CoC_2B_9H_{11}$].[12] The fact that the two cages are of different isomeric form is also supported by the relative complexities of the $^{11}B\{^1H\}$ NMR spectra.

Single-crystal X-ray diffraction studies established that the orange products are, indeed, 3,1,2-CoC_2B_9-2′,1′,8′-CoC_2B_9 species and that, as was the case with **3**α and **3**β, they are related as diastereoisomers. In Fig. 7 and 8 the unprimed 3,1,2-CoC_2B_9 cages of α-[1-(8′-2′-Cp-2′,1′,8′-*closo*-$CoC_2B_9H_{10}$)-3-Cp-3,1,2-*closo*-$CoC_2B_9H_{10}$] (**4**α) and β-[1-(8′-2′-Cp-2′,1′,8′-*closo*-$CoC_2B_9H_{10}$)-3-Cp-3,1,2-*closo*-$CoC_2B_9H_{10}$] (**4**β) are drawn with the same chirality whilst in the primed 2′,1′,8′-CoC_2B_9 cages the chiralities are different between α and β forms.[24] Note that the structure of **4**β was determined from two different crystals, one solvent-free and the other containing MeCN of solvation. The two structures are related by a simple twist of *ca.* 72° about the C1–C8′ bond.

Similar to **3**α and **3**β the 3,1,2-CoC_2B_9 cages in **4**α and **4**β suffer from intramolecular steric crowding, manifested by pro-

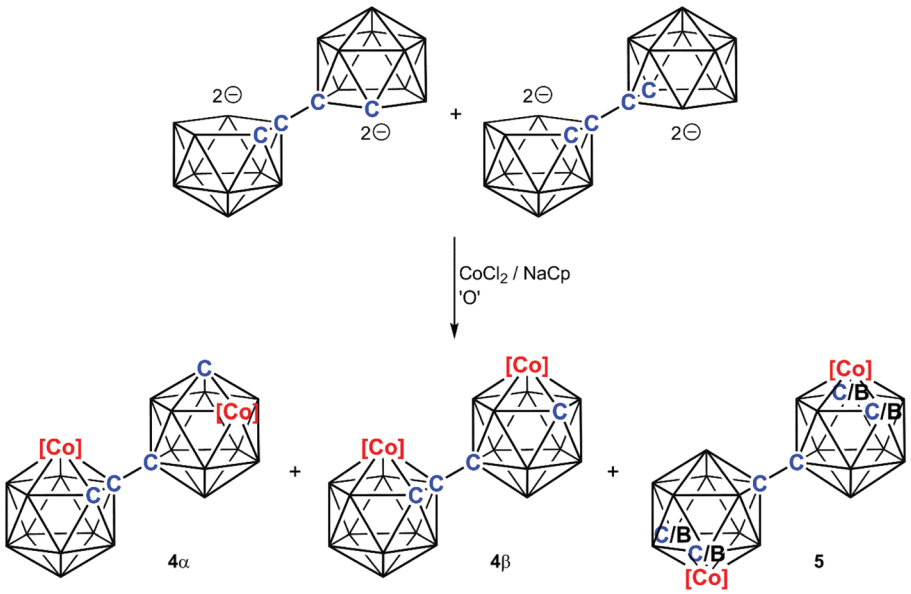

Scheme 2 Synthesis of cobaltacarboranes **4**α, **4**β and **5** from $[HNMe_3]_2$[**1**]. Using $[Tl]_2$[**2**] as the source of the carborane leads to the isolation of only **4**α and **4**β. [Co] = {CoCp}.

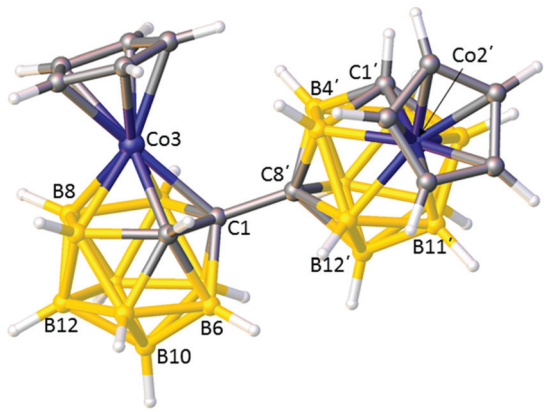

Fig. 7 Perspective view of compound **4**α with atomic numbering scheme. Selected interatomic distances (Å): Co3–C1 2.141(3), Co3–C2 2.051(3), C1–C2 1.640(4), Co2′–C1′ 2.020(3), and C1–C8′ 1.551(4).

nounced bend-back of the Cp ligand relative to the C1C2B7B8B4 plane [15.37(11)° in **4**α, 13.98(12)° in **4**β and 14.5(3)° in **4**β·MeCN] and Co–C1 connectivities *ca.* 0.1 Å longer than Co–C2 connectivities. In contrast there is no discernible bend-back of the Cp ligands in the 2′,1′,8′-CoC_2B_9 cages [dihedral angles between Cp and C1′B6′B11′B7′B3′ planes 2.81(11), 2.29(13) and 2.5(4)°, respectively].

In the ^{1}H NMR spectrum of **5**, the yellow co-product of **4**α and **4**β when $[HNMe_3]_2$[**1**] is the source of double deboronated 1,1′-bis(*ortho*-carborane), is a single Cp–*H* resonance and a single $C_{cage}H$ resonance, the chemical shift of the latter, δ 2.66 ppm, suggestive of a 2,1,8-CoC_2B_9 isomer.[12] The $^{11}B\{^1H\}$ NMR spectrum of **5** is surprisingly simple with only six resonances resolved at 128.4 MHz, 1.1/−0.9 (total 8B), −5.7 (4B), −12.0 (2B) and −16.8/−18.0 (total 4B).

A crystallographic study (Fig. 9) confirmed that **5** is the symmetric species [8-(8′-2′-Cp-2′,1′,8′-*closo*-$CoC_2B_9H_{10}$)-2-Cp-2,1,8-*closo*-$CoC_2B_9H_{10}$], the first example of a 2,1,8-MC_2B_9-2′,1′,8′-MC_2B_9 derivative of 1,1′-bis(*ortho*-carborane) to be reported. The molecule has crystallographically-required C_{2h} symmetry with vertices 1 and 11 (and 1′ and 11′) equally disordered between C and B. Consequently it is impossible to establish from crystallography if **5** is the racemic or meso diastereoisomer or a mixture of both.

Given that the $[HNMe_3]_2$[**1**] starting material is a mixture of racemic and meso forms, it is reasonable to suggest that **5** should also be formed as a racemic–meso mixture, but only one yellow band is isolated by preparative TLC. In the racemic form of **5** the two cages would be both chemically and magnetically equivalent, giving rise to only one Cp–*H* and one $C_{cage}H$ resonance, as observed. In the meso form the cages are chemically equivalent but magnetically inequivalent, potentially giving rise to two Cp–*H* and two $C_{cage}H$ resonances. However, what distinguishes racemic from meso $C_{cage}H$ arrangements (whether vertices 1 and 11 in the other cage are C or B) is six connectivities away whilst what distinguishes racemic from meso Cp–*H* is seven connectivities away, so it is certainly conceivable that the effective distinction could be lost and single resonances observed for the two Cp–*H* atoms and the two $C_{cage}H$ atoms in the meso isomer at the same chemical shifts as those in the racemic isomer.

This suggestion is supported by the results of redox experiments on **4**α and **4**β. We have previously shown that the reduction of [1-(1′-1′,2′-*closo*-$C_2B_{10}H_{11}$)-3-Cp-3,1,2-*closo*-$CoC_2B_9H_{10}$] (**II**) causes a 3,1,2- to 2,1,8-isomerisation of the CoC_2B_9 cobaltacarborane cage.[13] Consequently compounds **4**α

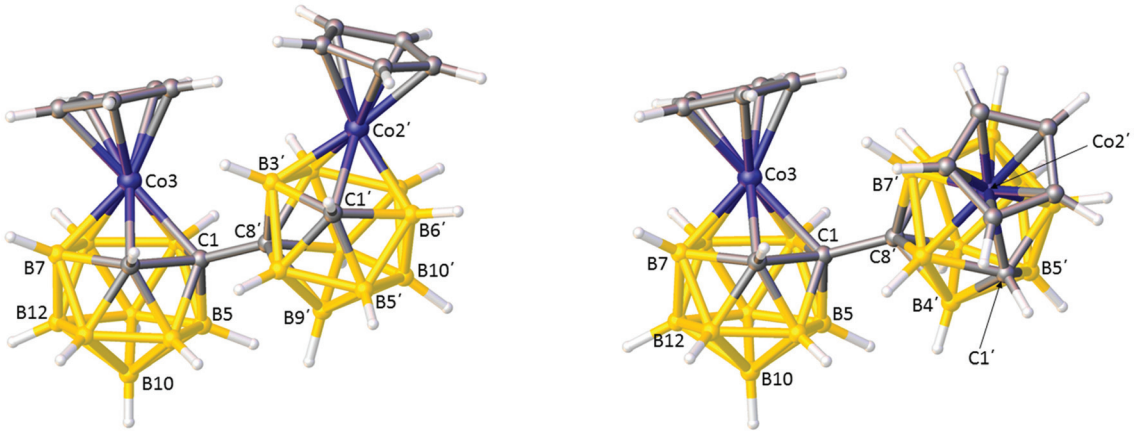

Fig. 8 Two views of compound **4**β. Left is the structure determined from crystals afforded from DCM : petrol and right that afforded from MeCN : Et_2O (MeCN of solvation not shown). The two structures are related by a rotation of *ca*. 72° about the C1–C8′ bond. Selected interatomic distances (Å; left structure in normal text, right structure in italics): Co3–C1 2.127(3), *2.134*(*8*); Co3–C2 2.039(3), *2.050*(*8*); C1–C2 1.651(5), *1.670*(*10*); Co2′–C1′ 2.022(3), *2.005*(*8*); C1–C8′ 1.552(4), and *1.549*(*10*).

and **4**β were each separately reduced (two equivalents of sodium naphthalenide in THF) and then aerially oxidised. In both cases single yellow products with identical (within error) R_f values were obtained which are spectroscopically identical not only to each other but also to **5**. These species must be related as diastereoisomers (one racemic, the other meso) but they are indistinguishable. Crystallisations of the two yellow products yielded crystals with the same unit cell dimensions within experimental error as those recorded for **5**.

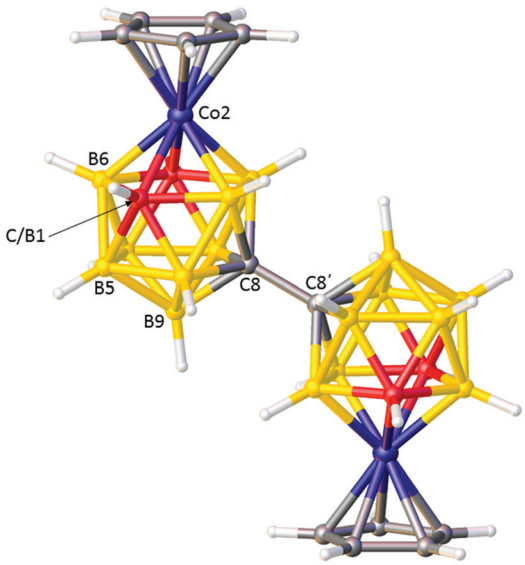

Fig. 9 Perspective view of compound **5** with atomic numbering scheme. The molecule has crystallographically-imposed C_{2h} (2/*m*) symmetry with the C_2 axis bisecting the C8–C8′ bond and the mirror plane in the plane of the paper. Atoms shown in red are disordered, 50%C + 50%B. Selected interatomic distances (Å): Co2–C/B1 2.0423(13), Co2–B3 2.0329(13), Co2–B6 2.0440(19), and C8–C8′ 1.534(3).

The reaction between $[Tl]_2$[**2**] and $[CoCpI_2(CO)]$ affords a single isolated species, *rac*-[1-(1′-3′-Cp-3′,1′,2′-*closo*-$CoC_2B_9H_{10}$)-3-Cp-3,1,2-*closo*-$CoC_2B_9H_{10}$] (**6**) (Scheme 3). Mass spectrometry and elemental analysis were consistent with both carborane cages having been metalated with {CoCp} fragments. In the ^{1}H NMR spectrum of **6** is a single resonance for the Cp–*H* atoms and a single resonance assigned to $C_{cage}H$, the relatively high frequency of the latter (4.25 ppm) consistent with a 3,1,2-CoC_2B_9 architecture.[23] The $^{11}B\{^1H\}$ NMR spectrum is also in accord with a product in which both cages are chemically and magnetically equivalent, with eight discernible resonances from 5.2 to −14.3 ppm.

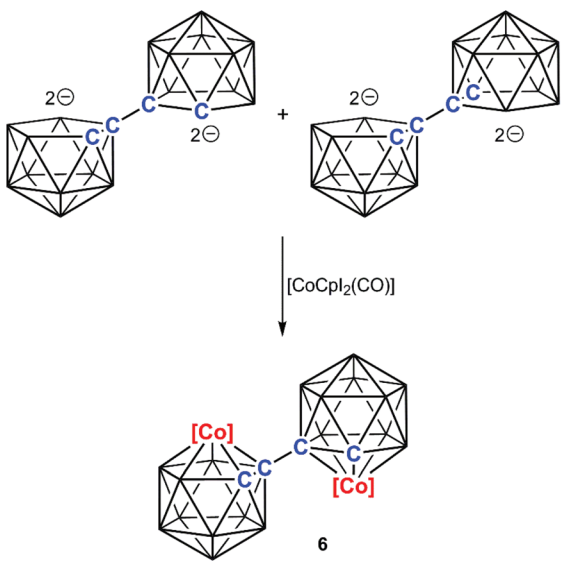

Scheme 3 Synthesis of the racemic cobaltacarborane **6** from the reaction between $[Tl]_2$[**2**] and $[CoCpI_2(CO)]$. [Co] = {CoCp}.

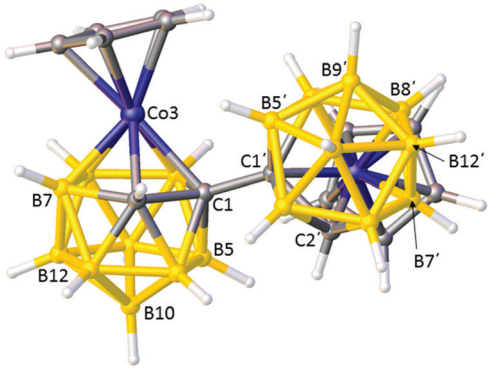

Fig. 10 Perspective view of compound **6** with atomic numbering scheme. Note that only the racemic diastereoisomers of this species were isolated. Selected interatomic distances (Å): Co3–C1 2.140(3), Co3–C2 2.049(3), C1–C2 1.668(4), Co3′–C1′ 2.135(3), Co3′–C2′ 2.043(3), C1′–C2′ 1.664(5), and C1–C1′ 1.563(5).

The structural identity of **6** was confirmed crystallographically (Fig. 10). Both cobaltacarborane cages are present as the 3,1,2-CoC_2B_9 isomer, with bend-back angles of the Cp rings relative to the cages of 16.61(15) and 15.84(14)° for the unprimed and primed cages, respectively, and significantly longer connectivities from the metal atoms to the cage C atoms bearing the metallacarborane substituents. An approximate (non-crystallographically-imposed) C_2 axis bisects the C1–C1′ bond and thus the chirality of both cages is the same, meaning that **6** is the racemic form of [1-(1′-3′-Cp-3′,1′,2′-*closo*-$CoC_2B_9H_{10}$)-3-Cp-3,1,2-*closo*-$CoC_2B_9H_{10}$]. Although both racemic and meso forms of this species might be anticipated, given that $[Tl]_2$[**2**] exists as a diastereoisomeric mixture, we were only able to isolate *rac*-**6**.

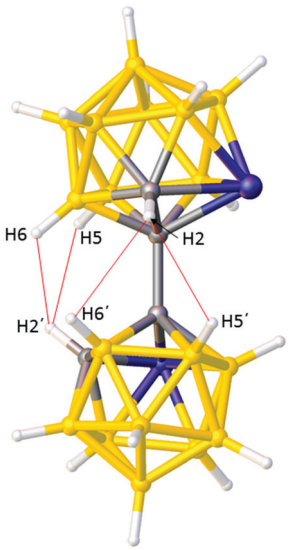

Fig. 11 View of compound **6** demonstrating intramolecular dihydrogen bonding (red lines). Cp ligands have been omitted for clarity. Distances (Å): C*H*2···B*H*5′ 2.43(5), C*H*2···B*H*6′ 2.54(5), C*H*2′···B*H*5 2.44(5), and C*H*2′···B*H*6 2.37(5).

An interesting feature of *rac*-**6** is intramolecular dihydrogen bonding. It is well established that in (hetero)carboranes the C*H* atoms are relatively protonic and the B*H* atoms are relatively hydridic. Moreover, in 3,1,2-$MC_2B_9H_{11}$ compounds whose NMR spectra have been fully assigned,[25] the most shielded (most hydridic) B*H* atoms are H5 (H11) and H6. The racemic arrangement of the two CoC_2B_9 cages in **6** allows for four intramolecular intercage dihydrogen bonds, C*H*2···B*H*5′ 2.43(5) Å, C*H*2···B*H*6′ 2.54(5) Å, C*H*2′···B*H*5 2.44(5) Å and C*H*2′···B*H*6 2.37(5) Å (ref. 26) (Fig. 11). We note that in the analogous meso isomer (not isolated) the maximum number of such interactions would be two, whatever the rotamer (assuming a staggered arrangement of the two opposing 5-atom faces).

Thermolysis of **II** at toluene reflux yielded no evidence for the formation of an isomerised cobaltacarborane,[13] but, in contrast, heating **6** to reflux in dimethoxyethane for 1 h affords compound **4**α (Scheme 4). In this process the primed cage isomerises from 3′,1′,2′-CoC_2B_9 to 2′,1′,8′-CoC_2B_9, an isomerisation most easily visualised by a 120° rotation of either the C1′B4′B5′ or C1′B5′B6′ triangular faces. We recall that a 3,1,2-MC_2B_9 to 2,1,8-MC_2B_9 isomerisation is implicated in the formation of ruthenacarboranes **3** and cobaltacarboranes **4** from their presumed 3,1,2-MC_2B_9-3′,1′,2′-MC_2B_9 precursors. The isolation of **4**α from isomerisation of racemic **6** implies that the α forms of compounds **3** and **4** arise from the metalation of the racemic diastereoisomers of $[HNMe_3]_2$[**1**] and $[Tl]_2$[**2**] and, conversely, the β forms of **3** and **4** arise from the meso precursors.

The singly-metalated species **II** was, however, successfully isomerised by reduction and subsequent oxidation.[13] Addition of two equivalents of sodium naphthalenide to **6** in THF, followed by aerial oxidation, yields a single yellow product identical to the 2,1,8-CoC_2B_9-2′,1′,8′-CoC_2B_9 species **5** by both ^1H and $^{11}B\{^1H\}$ NMR spectroscopies. Based on the above argu-

Scheme 4 Thermal isomerisation of **6** to afford **4**α. [Co] = {CoCp}.

ments it would be reasonable to suggest that this should be the racemic form of **5** but, as has already been discussed, it appears that racemic **5** and meso **5** are indistinguishable spectroscopically. We crystallised the species afforded by redox of **6** but unit cell dimensions are again identical to those of **5** within experimental error.

Conclusions

Metalation of doubly-deboronated 1,1′-bis(*ortho*-carborane) with {Ru(*p*-cymene)} affords diastereoisomeric 3,1,2-RuC_2B_9-2′,1′,8′-RuC_2B_9 bis(ruthenacarboranes) derived from racemic and meso forms of the doubly-deboronated precursor. Metalation with {CoCp} fragments generated *in situ* ($CoCl_2$/NaCp) yields analogous species but also a small amount of the unique 2,1,8-CoC_2B_9-2′,1′,8′-CoC_2B_9 isomer. Due to crystallographic disorder of the non-linking cage C atoms it is impossible to know whether this is the racemic or meso diastereoisomer or a mixture of both forms. Redox of the 3,1,2-CoC_2B_9-2′,1′,8′-CoC_2B_9 species converts each to 2,1,8-CoC_2B_9-2′,1′,8′-CoC_2B_9 isomers which cannot be distinguished. Metalation of doubly-deboronated 1,1′-bis(*ortho*-carborane) with preformed {CoCp} (using [$CoCpI_2$(CO)]) yields the racemic form of the 3,1,2-CoC_2B_9-3′,1′,2′-CoC_2B_9 isomer, a compound showing intramolecular dihydrogen bonding. Thermolysis of the 3,1,2-3′,1′,2′ compound affords only one diastereoisomer of 3,1,2-CoC_2B_9-2′,1′,8′-CoC_2B_9 as expected, whilst redox results in complete isomerisation to the 2,1,8-CoC_2B_9-2′,1′,8′-CoC_2B_9 form.

Experimental

Synthesis

Experiments were performed under dry, oxygen-free, N_2 using standard Schlenk techniques, although subsequent manipulations were sometimes performed in the open laboratory. Solvents for synthesis and work-up were freshly distilled under nitrogen from the appropriate drying agent [THF and 40–60 petroleum ether (petrol), sodium wire: CH_2Cl_2 (DCM), calcium hydride] and were degassed (3 × freeze–pump–thaw cycles) before use. Deuterated solvents for NMR spectroscopy [$CDCl_3$, $(CD_3)_2SO$] were stored over 4 Å molecular sieves. Preparative TLC employed 20 × 20 cm Kieselgel F_{254} glass plates and column chromatography used 60 Å silica as the stationary phase. Elemental analyses were conducted using an Exeter CE-440 elemental analyser. NMR spectra at 400.1 MHz (^{1}H) or 128.4 MHz (^{11}B) were recorded on a Bruker DPX-400 spectrometer at room temperature. Electron impact mass spectrometry (EIMS) was carried out using a Finnigan (Thermo) LCQ Classic ion trap mass spectrometer at the University of Edinburgh. The starting materials 1,1′-bis(*o*-carborane),[3] $[RuCl_2(p\text{-cymene})]_2$ [27] and [$CoCpI_2$(CO)][28] were prepared by literature methods or slight variations thereof. All other reagents were supplied commercially.

[$HNMe_3$]$_2$[7-(7′-7′,8′-*nido*-$C_2B_9H_{11}$)-7,8-*nido*-$C_2B_9H_{11}$] ([$HNMe_3$]$_2$[1]) and [BTMA]$_2$[7-(7′-7′,8′-*nido*-$C_2B_9H_{11}$)-7,8-*nido*-$C_2B_9H_{11}$] ([BTMA]$_2$[1])

1,1′-Bis(*o*-carborane) (0.50 g, 1.75 mmol) and KOH (2.94 g, 52.4 mmol) were dissolved in EtOH (50 mL) and heated to reflux for 48 h. Following cooling to room temperature CO_2(g) was passed through the mixture for 10 min. The mixture was filtered and the filtrate evaporated under reduced pressure to afford an oil. This was dissolved in deionised water (30 mL) to yield a clear solution which was split into two equal parts. To one was added an aqueous solution of excess [$HNMe_3$][Cl] and to the other an aqueous solution of excess [BTMA][Cl]. Both additions immediately resulted in precipitation of white solids which were collected by filtration, washed with water and dried *in vacuo*.

[$HNMe_3$]$_2$[7-(7′-7′,8′-*nido*-$C_2B_9H_{11}$)-7,8-*nido*-$C_2B_9H_{11}$] ([$HNMe_3$]$_2$-[1]). Yield 0.24 g, 0.62 mmol, 71%. $C_{10}H_{42}B_{18}N_2$ requires: C 31.2, H 10.99, N 7.28. Found: C 31.0, H 11.08, N 7.37%. ^{1}H NMR [$(CD_3)_2SO$, 400.1 MHz] δ 9.28 (s, 2H, *H*NMe_3), 2.78 [s, 18H, HN(CH_3)$_3$], 1.83 (s, $C_{cage}H$), 1.79 (s, $C_{cage}H$). ^{11}B{^{1}H} NMR [$(CD_3)_2SO$, 128.4 MHz] δ −10.9, −14.8, −15.7, −17.6, −18.5, −20.4, −21.3, −23.8, −24.4, −33.6, −36.6.

[BTMA]$_2$[7-(7′-7′,8′-*nido*-$C_2B_9H_{11}$)-7,8-*nido*-$C_2B_9H_{11}$] ([BTMA]$_2$[1]). Yield 0.37 g, 0.65 mmol, 75%. $C_{24}H_{54}B_{18}N_2$ requires: C 51.0, H 9.63, N 4.96. Found: C 49.8, H 9.60, N 4.43%. ^{1}H NMR [$(CD_3)_2SO$, 400.1 MHz] δ 7.53 (br. app. s, 10H, C_6H_5), 4.51 (s, 4H, CH_2), 3.02 (s, 18H, CH_3), 1.82 (s, $C_{cage}H$), 1.79 (s, $C_{cage}H$). ^{11}B{^{1}H} NMR [$(CD_3)_2SO$, 128.4 MHz] identical to that of [$HNMe_3$]$_2$**1**.

[Tl]$_2$[1-(1′-3′,1′,2′-*closo*-$TlC_2B_9H_{10}$)-3,1,2-*closo*-$TlC_2B_9H_{10}$] ([Tl]$_2$[2])

Excess KOH (4.81 g, 85.7 mmol) and 1,1′-bis(*o*-carborane) (1.00 g, 3.49 mmol) were dissolved in EtOH (30 mL) and heated to reflux for 18 h. The mixture was cooled and the solvent was removed under reduced pressure. The resulting solid was dissolved in deionised water (30 mL) and filtered. To the filtrate was added a solution of thallous acetate (5.72 g, 21.7 mmol) in deionised water, resulting in the immediate precipitation of a yellow solid. This was collected by filtration, washed with EtOH (30 mL) then Et_2O (30 mL) and dried *in vacuo* to afford a fine yellow powder subsequently stored in a foil-covered Schlenk tube. [Tl]$_2$[1-(1′-3′,1′,2′-*closo*-$TlC_2B_9H_{10}$)-3,1,2-*closo*-$TlC_2B_9H_{10}$] ([Tl]$_2$[**2**]). Yield 3.56 g, 3.29 mmol, 94%. $C_4H_{20}B_{18}Tl_4$ requires: C 4.45, H 1.87. Found: C 4.25, H 1.92%.

α-[1-(8′-2′-(*p*-Cymene)-2′,1′,8′-*closo*-$RuC_2B_9H_{10}$)-3-(*p*-cymene)-3,1,2-*closo*-$RuC_2B_9H_{10}$] (3α) and β-[1-(8′-2′-(*p*-cymene)-2′,1′,8′-*closo*-$RuC_2B_9H_{10}$)-3-(*p*-cymene)-3,1,2-*closo*-$RuC_2B_9H_{10}$] (3β)

$[RuCl_2(p\text{-cymene})]_2$ (0.57 g, 0.93 mmol) was added to a frozen suspension of [Tl]$_2$[**2**] (1.00 g, 0.93 mmol) in THF (20 mL) and the reaction mixture was allowed to thaw and stir for 24 h. The resulting light-brown suspension was filtered and the filtrate was concentrated and purified, first by column chromato-

graphy on silica (DCM : petrol, 1 : 1) and subsequently by TLC (ethyl acetate : petrol, 3 : 7) to afford two mobile yellow bands.

α-[1-(8′-2′-(*p*-Cymene)-2′,1′,8′-*closo*-$RuC_2B_9H_{10}$)-3-(*p*-cymene)-3,1,2-*closo*-$RuC_2B_9H_{10}$] (3α). R_f 0.40. Yield 0.075 g, 0.102 mmol, 11%. $C_{24}H_{48}B_{18}Ru_2$ requires: C 39.3, H 6.60. Found: C 39.0, H 6.89%. ^{1}H NMR [$CDCl_3$, 400.1 MHz] δ 6.06–5.77 (m, 8H, $CH_3C_6H_4CH(CH_3)_2$), 3.96 (br s, 1H, $C_{cage}H$), 3.06 (sept, 1H, $CH_3C_6H_4CH(CH_3)_2$), 2.80 (sept, 1H, $CH_3C_6H_4CH(CH_3)_2$), 2.61 (br s, 1H, $C_{cage}H$), 2.44 (s, 3H, $CH_3C_6H_4CH(CH_3)_2$), 2.31 (s, 3H, $CH_3C_6H_4CH(CH_3)_2$), 1.35–1.26 (m, 12H, $CH_3C_6H_4CH(CH_3)_2$). ^{11}B{^{1}H} NMR [$CDCl_3$, 128.4 MHz] δ 1.7, 0.1, −1.3, −7.7, −8.2, −12.9, −16.8, −21.5. EIMS: envelope centred on *m*/*z* 733 (M^+).

β-[1-(8′-2′-(*p*-Cymene)-2′,1′,8′-*closo*-$RuC_2B_9H_{10}$)-3-(*p*-cymene)-3,1,2-*closo*-$RuC_2B_9H_{10}$] (3β). R_f 0.42. Yield 0.032 g, 0.044 mmol, 5%. $C_{24}H_{48}B_{18}Ru_2$ requires: C 39.3, H 6.60. Found: C 38.8, H 6.51%. ^{1}H NMR [$CDCl_3$, 400.1 MHz] δ 6.08–5.78 (m, 8H, $CH_3C_6H_4CH(CH_3)_2$), 3.79 (br s, 1H, $C_{cage}H$), 3.04 (sept, 1H, $CH_3C_6H_4CH(CH_3)_2$), 2.79 (sept, 1H, $CH_3C_6H_4CH(CH_3)_2$), 2.58 (br s, 1H, $C_{cage}H$), 2.47 (s, 3H, $CH_3C_6H_4CH(CH_3)_2$), 2.30 (s, 3H, $CH_3C_6H_4CH(CH_3)_2$), 1.34–1.27 (m, 12H, $CH_3C_6H_4CH(CH_3)_2$). ^{11}B{^{1}H} NMR [$CDCl_3$, 128.4 MHz] δ 1.7, 0.0, −1.2, −3.8, −4.9, −7.9, −13.1, −16.9, −21.1. EIMS: envelope centred on *m*/*z* 733 (M^+).

NB. In this and the following metalation reactions isolated yields of products (following purification involving both column and preparative thin-layer chromatography) are relatively low. Following chromatography, non-mobile components removed from silica with MeCN have ^{11}B NMR spectra which typically include resonances between −30 and −40 ppm characteristic of 7,8-*nido*-C_2B_9 fragments, so we ascribe the low yields of metallacarborane products to poor conversion as opposed to decomposition.

α-[1-(8′-2′-Cp-2′,1′,8′-*closo*-$CoC_2B_9H_{10}$)-3-Cp-3,1,2-*closo*-$CoC_2B_9H_{10}$] (4α), β-[1-(8′-2′-Cp-2′,1′,8′-*closo*-$CoC_2B_9H_{10}$)-3-Cp-3,1,2-*closo*-$CoC_2B_9H_{10}$] (4β) and [8-(8′-2′-Cp-2′,1′,8′-*closo*-$CoC_2B_9H_{10}$)-2-Cp-2,1,8-*closo*-$CoC_2B_9H_{10}$] (5)

From $[HNMe_3]_2$[1]. To $[HNMe_3]_2$[**1**] (0.20 g, 0.52 mmol) suspended in THF (20 mL) 0 °C was added *n*-BuLi (0.92 mL of 2.5 M solution in hexanes, 2.29 mmol) and the cloudy white product was heated to reflux for 2 h. This was then frozen and NaCp (1.65 mL of a 2 M solution in hexanes, 3.30 mmol) and $CoCl_2$ (0.47 g, 3.62 mmol) were added. Following warming to room temperature and stirring for 18 h the mixture was aerially oxidised for 0.5 h. THF was removed *in vacuo* and the crude mixture was dissolved in DCM and filtered through silica. Preparative TLC yielded orange (R_f 0.24), orange (R_f 0.45) and yellow (R_f 0.61) bands subsequently identified as **4α**, **4β** and **5**, in yields of 0.016 g (0.03 mmol, 6%), 0.010 g (0.02 mmol, 4%) and 0.007 g (0.01 mmol, 3%), respectively.

From $[Tl]_2$[2]. To a frozen suspension of $[Tl]_2$[**2**] (1.40 g, 1.30 mmol) in THF (20 mL) was added $CoCl_2$ (1.18 g, 9.09 mmol) and NaCp (3.95 mL of a 2 M solution in hexanes, 7.90 mmol). The mixture was allowed to warm to room temperature and stirred for 24 h, following which it was aerially oxidised for 1 h. The reagents were filtered and the filtrate was concentrated and purified by column chromatography on silica (DCM : petrol, 1 : 1) affording a mobile orange band which was further purified by preparative TLC (ethyl acetate : petrol, 3 : 7) to afford two orange bands subsequently identified as **4α** (R_f 0.24) and **4β** (R_f 0.43) in yields of 0.090 g (0.18 mmol, 14%) and 0.077 g (0.15 mmol, 12%), respectively.

α-[1-(8′-2′-Cp-2′,1′,8′-*closo*-$CoC_2B_9H_{10}$)-3-Cp-3,1,2-*closo*-$CoC_2B_9H_{10}$] (4α). $C_{14}H_{30}B_{18}Co_2$ requires: C 32.9, H 5.92. Found: C 32.8, H 5.96%. ^{1}H NMR [$CDCl_3$, 400.1 MHz] δ 5.79 (s, 5H, C_5H_5), 5.48 (s, 5H, C_5H_5), 4.20 (br s, 1H, $C_{cage}H$), 2.76 (br s, 1H, $C_{cage}H$). ^{11}B{^{1}H} NMR [$CDCl_3$, 128.4 MHz] δ 5.5, 2.5, 1.7, −1.4, −3.7, −8.5, −10.2, −12.0, −14.6, −15.8, −18.2. EIMS: envelope centred on *m*/*z* 511 (M^+).

β-[1-(8′-2′-Cp-2′,1′,8′-*closo*-$CoC_2B_9H_{10}$)-3-Cp-3,1,2-*closo*-$CoC_2B_9H_{10}$] (4β). $C_{14}H_{30}B_{18}Co_2$ requires: C 32.9, H 5.92. Found: C 33.1, H 6.01%. ^{1}H NMR [$CDCl_3$, 400.1 MHz] δ 5.80 (s, 5H, C_5H_5), 5.47 (s, 5H, C_5H_5), 4.06 (br s, 1H, $C_{cage}H$), 2.76 (br s, 1H, $C_{cage}H$). ^{11}B{^{1}H} NMR [$CDCl_3$, 128.4 MHz] δ 5.4, 2.4, 1.7, −1.7, −3.8, −8.5, −10.4, −12.3, −14.6, −18.2. EIMS: envelope centred on *m*/*z* 511 (M^+).

[8-(8′-2′-Cp-2′,1′,8′-*closo*-$CoC_2B_9H_{10}$)-2-Cp-2,1,8-*closo*-$CoC_2B_9H_{10}$] (5). $C_{14}H_{30}B_{18}Co_2$ requires: C 32.9, H 5.92. Found: C 32.2, H 5.86%. ^{1}H NMR [$CDCl_3$, 400.1 MHz] δ 5.41 (s, 10H, C_5H_5), 2.66 (br s, 2H, $C_{cage}H$). ^{11}B{^{1}H} NMR [$CDCl_3$, 128.4 MHz] δ 1.1, −0.9 (combined integral 8B), −5.7 (4B), −12.0 (2B), −16.8, −18.0 (combined integral 4B). EIMS: envelope centred on *m*/*z* 511 (M^+).

Redox isomerisations of 4α and 4β

To a frozen solution of **4α** (0.02 g, 0.04 mmol) in THF (10 mL) was added a solution of sodium naphthalenide (1 mL of a 0.078 M solution in THF, 0.078 mmol). The reaction was allowed to warm and stir under nitrogen for 16 h and was then aerially oxidised for 0.5 h. Purification by preparative TLC (ethyl acetate : petrol, 3 : 7) afforded orange **4α** (R_f 0.24, 0.014 g, 0.03 mmol, 69%) and a yellow product (R_f 0.59, 0.004 g, 0.01 mmol, 20%) identical to **5** by ^{1}H and ^{11}B{^{1}H} NMR spectroscopies and mass spectrometry. Similarly, from **4β** (0.010 g, 0.020 mmol) in THF (10 mL) and sodium naphthalenide (0.5 mL of a 0.078 M solution in THF, 0.039 mmol) were recovered orange **4β** (R_f 0.43, 0.006 g, 0.01 mmol, 58%) and a yellow product (R_f 0.57, 0.003 g, 0.01 mmol, 29%) which was again identical to **5** by ^{1}H and ^{11}B{^{1}H} NMR spectroscopies and mass spectrometry.

rac-[1-(1′-3′-Cp-3′,1′,2′-*closo*-$CoC_2B_9H_{10}$)-3-Cp-3,1,2-*closo*-$CoC_2B_9H_{10}$] (6)

To a frozen suspension of $[Tl]_2$[**2**] (1.00 g, 0.93 mmol) in THF (20 mL) was added [$CoCpI_2(CO)$] (0.76 g, 1.87 mmol) and the reaction mixture was allowed to thaw and stir for 24 h. The resulting dark suspension was filtered through Celite® and the solvent was removed *in vacuo*. Purification by preparative TLC (ethyl acetate : petrol, 3 : 7) afforded *rac*-[1-(1′-3′-Cp-3′,1′,2′-*closo*-$CoC_2B_9H_{10}$)-3-Cp-3,1,2-*closo*-$CoC_2B_9H_{10}$] (**6**) as an orange solid (R_f 0.48, 0.068 g, 0.13 mmol, 14%). $C_{14}H_{30}B_{18}Co_2$ requires: C 32.9, H 5.92. Found: C 32.2, H 5.73%. ^{1}H NMR

Table 1 Crystallographic data

	[BTMA]$_2$[**1**]	**3α**	**3β**	**4α**	**4β**	**4β**·MeCN	**5**	**6**·MeCN
CCDC	1516771	1516772	1516773	1516774	1516775	1516776	1516777	1516778
Formula	$C_{24}H_{54}B_{18}N_2$	$C_{24}H_{48}B_{18}Ru_2$	$C_{24}H_{48}B_{18}Ru_2$	$C_{14}H_{30}B_{18}Co_2$	$C_{14}H_{30}B_{18}Co_2$	$C_{16}H_{33}B_{18}Co_2N$	$C_{14}H_{30}B_{18}Co_2$	$C_{16}H_{33}B_{18}Co_2N$
M	565.27	733.34	733.34	510.82	510.82	551.87	510.82	551.87
Crystal system	Triclinic	Monoclinic	Monoclinic	Monoclinic	Monoclinic	Orthorhombic	Orthorhombic	Monoclinic
Space group	$P\bar{1}$	$P2_1/n$	$P2_1/c$	$P2_1/c$	$P2_1/c$	$P2_12_12_1$	$Cmce$	Cc
a/Å	8.8436(12)	9.3011(6)	19.190(2)	7.5433(8)	11.6962(13)	8.9085(6)	11.694 3(5)	10.5603(5)
b/Å	10.5897(11)	41.899(3)	10.7869(11)	14.3480(12)	15.9743(17)	13.5333(10)	13.8151(5)	26.9574(12)
c/Å	11.103(2)	9.3950(6)	17.9357(17)	21.5040(17)	12.9143(13)	20.8343(16)	14.4745(6)	9.0101(4)
α/°	116.225(6)	90	90	90	90	90	90	90
β/°	101.483(7)	113.751(2)	116.289(4)	96.906(4)	109.935(4)	90	90	97.611(3)
γ/°	104.113(5)	90	90	90	90	90	90	90
U/Å^3	846.5(2)	3351.2(4)	3328.8(6)	2310.5(4)	2268.3(4)	2511.8(3)	2338.47(17)	2542.4(2)
Z, Z'	1, 0.5	4, 1	4, 1	4, 1	4, 1	4, 1	4, 0.25	4, 1
F(000)/e	302	1480	1480	1032	1032	1120	1032	1120
D_{calc}/Mg m^{-3}	1.109	1.454	1.463	1.448	1.496	1.459	1.451	1.442
μ(Mo-K$_\alpha$)/mm^{-1}	0.055	0.920	0.926	1.440	1.467	1.332	1.423	1.316
θ_{max}/°	28.34	25.69	26.15	27.08	25.99	25.76	27.57	30.03
Data measured	11 069	18 710	42 726	35 422	19 160	26 419	13 750	25 633
Unique data, n	4082	6370	6592	5094	4434	2873	1399	7256
R_{int}	0.0332	0.0647	0.1180	0.0540	0.0757	0.0860	0.0274	0.0483
R, wR_2 (obs. data)	0.0495, 0.1184	0.0657, 0.1228	0.0613, 0.1431	0.0371, 0.0748	0.0457, 0.1105	0.0571, 0.0866	0.0216, 0.0585	0.0352, 0.0633
S	1.026	1.276	1.011	1.046	1.014	1.032	1.087	0.984
Variables	247	475	488	368	367	396	101	395
E_{max}, E_{min}/e Å^{-3}	0.29, −0.23	1.21, −1.17	1.52, −1.89	0.40, −0.45	1.03, −1.04	0.58, −0.56	0.37, −0.26	0.68, −0.36
Abs. str. parameter						0.34(3)		0.022(8)

[$CDCl_3$, 400.1 MHz] δ 5.84 (s, 10H, C_5H_5), 4.24 (br s, 2H, $C_{cage}H$). $^{11}B\{^1H\}$ NMR [$CDCl_3$, 128.4 MHz] δ 5.2 (2B), 1.2 (2B), −2.5, −3.3 (combined integral 6B), −7.6 (2B), −11.7, −13.2, −14.2 (combined integral 6B). EIMS: envelope centred on m/z 511 (M^+).

Thermal isomerisation of 6

Compound **6** (0.02 g, 0.04 mmol) was dissolved in dimethoxyethane (15 mL) and the orange solution was heated at reflux for 1 h. The solvent was removed and the crude residue was subjected to preparative TLC (ethyl acetate : petrol, 3 : 7) affording two orange bands at R_f 0.51 and R_f 0.25, identified as **6** (0.003 g, 0.01 mmol, 15%) and **4α** (0.012 g, 0.02 mmol, 60%), respectively, by ^1H and $^{11}B\{^1H\}$ NMR spectroscopies.

Redox isomerisation of 6

To a frozen solution of **6** (0.025 g, 0.05 mmol) in THF (10 mL) was added sodium naphthalenide (2 mL of a 0.049 M solution in THF, 0.098 mmol). The reaction was allowed to warm and stir under nitrogen for 16 h and was then aerially oxidised for 0.5 h. Purification by preparative TLC (ethyl acetate : petrol, 3 : 7) afforded a yellow product (R_f 0.58, 0.007 g, 0.01 mmol, 28%) identical to **5** by ^1H and $^{11}B\{^1H\}$ NMR spectroscopies.

Crystallography

Diffraction-quality crystals of [BTMA]$_2$[**1**], **3β** and **4β** were grown by slow diffusion of petrol and a DCM solution of the appropriate compound. Crystals of **4β**·MeCN and **6**·MeCN were also grown by solvent diffusion, this time using MeCN as a solvent and diethylether as an antisolvent. Compound **4α** afforded crystals by vapour diffusion between a THF solution of the compound and petrol. Finally, crystals of **3α** and **5** were grown by slow evaporation of a d_6-acetone solution and a DCM solution, respectively. Except for **3α** and **5**, intensity data were collected on a Bruker X8 APEXII diffractometer using Mo-K$_\alpha$ X-radiation, with crystals mounted in inert oil on a cryoloop and cooled to 100 K by using an Oxford Cryosystems Cryostream. Data from **3α** were obtained at 120 K and data from **5** at 100 K by the National Crystallography Service at the University of Southampton. Indexing, data collection and absorption correction were performed using the APEXII suite of programs.[29] Using OLEX2[30] structures were solved by direct methods using the SHELXS[31] or SHELXT[32] programme and refined by full-matrix least-squares (SHELXL).[31]

All crystals were single except those of **3α**, **4α** and **4β**·MeCN, each of which was treated as a two-component twin. All crystals were also fully ordered except those of [BTMA]$_2$[**1**], **3α**, **3β** and **5**. In [BTMA]$_2$[**1**] there is C : B disorder between vertices 8 and 11 of the *nido* carborane cages (arising from the presence of two diastereoisomers) and also a partial disorder of both vertices into the 12th vertex of a *closo* icosahedron affording a 'ghost' vertex. **3α** and **3β** each suffer from a partial disorder of one *p*-cymene ligand, but in all three disordered structures the disorder was satisfactorily modelled. In **5** vertices 1 and 11

(and 1′ and 11′) are required to be 50%C + 50%B by space group symmetry.

Cage C atoms bearing only H substituents were distinguished from B atoms by the VCD[33] and BHD[34] methods (in the case of $[BTMA]_2[\mathbf{1}]$ the VCD method helped to identify the disorder between vertices 8 and 11). For all structures H atoms bound to cage B or cage C atoms were allowed to refine positionally whilst H atoms bound to other C atoms were constrained to idealised geometries, C_{phenyl}–H = 0.95 Å, $C_{primary}$–H = 0.98 Å, $C_{secondary}$–H = 0.99 Å, $C_{tertiary}$–H = 1.00 Å, and $C_{\pi\text{-bonded}}$–H = 1.00 Å. All H displacement parameters, U_{iso}, were constrained to be 1.2 × $U_{eq.}$ (bound B or C) except for Me H atoms [U_{iso}(H) = 1.5 × $U_{eq.}$ C(Me)]. Table 1 contains further experimental details.

Acknowledgements

We thank ORSAS (GT), Heriot-Watt University (DM, James Watt Studentship) and the EPSRC (WYM, grant EP/I031545/1) for support, and the National Crystallography Service (University of Southampton) for data collection from compounds **3**α and **5**. MA is an Erasmus exchange student from the Phillips-Universität Marburg, Germany.

References

1 W. Y. Man, G. M. Rosair and A. J. Welch, *Acta Crystallogr., Sect. E: Struct. Rep. Online*, 2014, **70**, 462.
2 J. A. Dupont and M. F. Hawthorne, *J. Am. Chem. Soc.*, 1964, **86**, 1643.
3 S. Ren and Z. Xie, *Organometallics*, 2008, **27**, 5167.
4 M. J. Martin, W. Y. Man, G. M. Rosair and A. J. Welch, *J. Organomet. Chem.*, 2015, **798**, 36.
5 Z.-J. Yao, Y.-Y. Zhang and G.-X. Jin, *J. Organomet. Chem.*, 2015, **798**, 274.
6 G. S. Kazakov, I. B. Sivaev, K. Yu. Suponitsky, D. D. Kirilin, V. I. Bregadze and A. J. Welch, *J. Organomet. Chem.*, 2016, **806**, 1.
7 S. L. Powley, L. Schaefer, W. Y. Man, D. Ellis, G. M. Rosair and A. J. Welch, *Dalton Trans.*, 2016, **45**, 3635.
8 D. Zhao, J. Zhang, Z. Lin and Z. Xie, *Chem. Commun.*, 2016, **52**, 9992.
9 D. Ellis, G. M. Rosair and A. J. Welch, *Chem. Commun.*, 2010, **46**, 7394.
10 D. Mandal, W. Y. Man, G. M. Rosair and A. J. Welch, *Acta Crystallogr., Sect. C: Cryst. Struct. Commun.*, 2015, **C71**, 793.
11 W. Y. Man, D. Ellis, G. M. Rosair and A. J. Welch, *Angew. Chem., Int. Ed.*, 2016, **55**, 4596.
12 W. Y. Man, S. Zlatogorsky, H. Tricas, D. Ellis, G. M. Rosair and A. J. Welch, *Angew. Chem., Int. Ed.*, 2014, **53**, 12222.
13 G. Thiripuranathar, W. Y. Man, C. Palmero, A. P. Y. Chan, B. T. Leube, D. Ellis, D. McKay, S. A. Macgregor, L. Jourdan, G. M. Rosair and A. J. Welch, *Dalton Trans.*, 2015, **44**, 5628.
14 D. Mandal, W. Y. Man, G. M. Rosair and A. J. Welch, *Dalton Trans.*, 2016, **45**, 15013.
15 D. Ellis, D. McKay, S. A. Macgregor, G. M. Rosair and A. J. Welch, *Angew. Chem., Int. Ed.*, 2010, **49**, 4943.
16 L. E. Riley, A. P. Y. Chan, J. Taylor, W. Y. Man, D. Ellis, G. M. Rosair, A. J. Welch and I. B. Sivaev, *Dalton Trans.*, 2016, **45**, 1127.
17 Y. O. Wong, M. D. Smith and D. V. Peryshkov, *Chem. – Eur. J.*, 2016, **22**, 6764.
18 Y. O. Wong, M. D. Smith and D. V. Peryshkov, *Chem. Commun.*, 2016, **52**, 12710.
19 K. O. Kirlikovali, J. C. Axtell, A. Gonzalez, A. C. Phung, S. I. Khan and A. M. Spokoyny, *Chem. Sci.*, 2016, **7**, 5132.
20 P. E. Behnken, T. B. Marder, R. T. Baker, C. B. Knobler, M. R. Thompson and M. F. Hawthorne, *J. Am. Chem. Soc.*, 1985, **107**, 932.
21 M. F. Hawthorne, D. A. Owen and J. W. Wiggins, *Inorg. Chem.*, 1971, **10**, 1034.
22 M. J. Manning, C. B. Knobler, M. F. Hawthorne and Y. Do, *Inorg. Chem.*, 1991, **30**, 3589.
23 M. F. Hawthorne, D. C. Young, T. D. Andrews, D. V. Howe, R. L. Pilling, A. D. Pitts, M. Reintjes, L. F. Warren Jr. and P. A. Wegner, *J. Am. Chem. Soc.*, 1968, **90**, 879.
24 The overall stereochemistries of **3**α and **4**α are the same, as are those of **3**β and **4**β.
25 *E.g.* M. Bown, J. Plešek, K. Baše, B. Štibr, X. L. R. Fontaine, N. N. Greenwood and J. D. Kennedy, *Magn. Reson. Chem.*, 1989, **27**, 947.
26 These are the H···H distances as measured by X-ray diffraction. However, because of the systematic underestimation of A–H distances by this technique, true internuclear H···H distances are likely to be somewhat shorter.
27 M. A. Bennett, T.-N. Huang, T. W. Matheson and A. K. Smith, *Inorg. Synth.*, 1982, **21**, 74.
28 S. A. Frith and J. L. Spencer, *Inorg. Synth.*, 1990, **28**, 273.
29 *Bruker AXS APEX2, version 2009-5*, Bruker AXS Inc., Madison, Wisconsin, USA, 2009.
30 O. V. Dolomanov, L. J. Bourhis, R. J. Gildea, J. A. K. Howard and H. Puschmann, *J. Appl. Crystallogr.*, 2009, **42**, 339.
31 G. M. Sheldrick, *Acta Crystallogr., Sect. A: Fundam. Crystallogr.*, 2008, **64**, 112.
32 G. M. Sheldrick, *Acta Crystallogr., Sect. A: Fundam. Crystallogr.*, 2015, **71**, 3.
33 A. McAnaw, G. Scott, L. Elrick, G. M. Rosair and A. J. Welch, *Dalton Trans.*, 2013, **42**, 645.
34 A. McAnaw, M. E. Lopez, D. Ellis, G. M. Rosair and A. J. Welch, *Dalton Trans.*, 2014, **43**, 5095.

Inorganic Chemistry

Article

Cite This: *Inorg. Chem.* 2018, 57, 8002–8011

pubs.acs.org/IC

Heterometalation of 1,1′-Bis(*ortho*-carborane)

Antony P. Y. Chan, Georgina M. Rosair, and Alan J. Welch*

Institute of Chemical Sciences, Heriot-Watt University, Edinburgh EH14 4AS, U.K.

Supporting Information

ABSTRACT: Deboronation of [8-(1′-*closo*-1′,2′-$C_2B_{10}H_{11}$)-*closo*-2,1,8-$MC_2B_9H_{10}$] affords diastereoisomeric mixtures of [8-(7′-*nido*-7′,8′-$C_2B_9H_{11}$)-*closo*-2,1,8-$MC_2B_9H_{10}$]$^-$ anions (**1**, M = Ru(*p*-cymene); **2**, M = CoCp) isolated as $[HNMe_3]^+$ salts. Deprotonation of **1** and reaction with $CoCl_2$/NaCp followed by oxidation yields [8-(1′-3′-Cp-*closo*-3′,1′,2′-$CoC_2B_9H_{10}$)-2-(*p*-cymene)-*closo*-2,1,8-$RuC_2B_9H_{10}$] isolated as two separable diastereoisomers, namely, **3***α* and **3***β*, the first examples of heterometalated derivatives of 1,1′-bis(*ortho*-carborane). Deprotonation of [7-(1′-*closo*-1′,2′-$C_2B_{10}H_{11}$)-*nido*-7,8-$C_2B_9H_{11}$]$^-$, metalation with $CoCl_2$/NaCp* and oxidation affords the isomers [1-(1′-*closo*-1′,2′-$C_2B_{10}H_{11}$)-3-Cp*-*closo*-3,1,2-$CoC_2B_9H_{10}$] (**4**) and [8-(1′-*closo*-1′,2′-$C_2B_{10}H_{11}$)-2-Cp*-*closo*-2,1,8-$CoC_2B_9H_{10}$] (**5**) as well as a trace amount of the 13-vertex/12-vertex species [12-(1′-*closo*-1′,2′-$C_2B_{10}H_{11}$)-4,5-Cp*$_2$-*closo*-4,5,1,12-$Co_2C_2B_9H_{10}$] (**6**). Reduction then reoxidation of **4** converts it to **5**. Deboronation of either **4** or **5** yields a diastereoisomeric mixture of [8-(7′-*nido*-7′,8′-$C_2B_9H_{11}$)-2-Cp*-*closo*-2,1,8-$CoC_2B_9H_{10}$]$^-$ (**7**), again isolated as the $[HNMe_3]^+$ salt. Deprotonation of this followed by treatment with $[RuCl_2(p\text{-cymene})]_2$ produces [8-(1′-3′-(*p*-cymene)-*closo*-3′,1′,2′-$RuC_2B_9H_{10}$)-2-Cp*-*closo*-2,1,8-$CoC_2B_9H_{10}$] (**8**) as a mixture of two diastereoisomers in a 2:1 ratio, which could not be separated. Diastereoisomers **8** are complementary to **3***α* and **3***β* in which {CoCp} and {Ru(*p*-cymene)} in **3** were replaced by {Ru(*p*-cymene)} and {CoCp*}, respectively, in **8**. Finally, thermolysis of mixture **8** in refluxing dimethoxyethane yields [8-(8′-2′-(*p*-cymene)-*closo*-2′,1′,8′-$RuC_2B_9H_{10}$)-2-Cp*-*closo*-2,1,8-$CoC_2B_9H_{10}$] (**9**), again as a 2:1 diastereoisomeric mixture that could not be separated. All new species were characterized by multinuclear NMR spectroscopy, and **3***α*, **3***β*, **4**, **5**, **6**, and **9** were also characterized crystallographically.

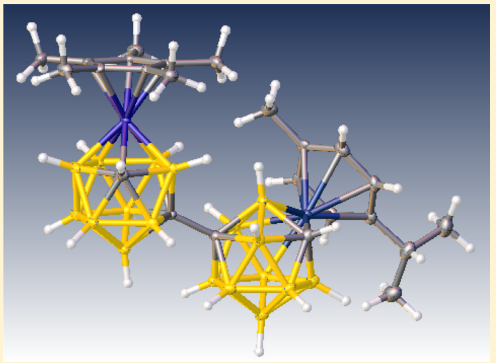

INTRODUCTION

The principles of removal of a {BH} vertex from a closo carborane and its subsequent replacement by an isolobal metal fragment {ML_n} to afford a metallacarborane (polyhedral subrogation) were established by Hawthorne and co-workers more than 50 years ago,[1−4] and now a vast range of metallacarboranes of differing polyhedral shapes and sizes containing metal atoms from across a broad spectrum of the periodic table is known.[5] Such species find application in catalysis, medicine, metal-ion extraction, and advanced materials, among others.[5]

The compound [1-(1′-*closo*-1′,2′-$C_2B_{10}H_{11}$)-*closo*-1,2-$C_2B_{10}H_{11}$], trivial name 1,1′-bis(*ortho*-carborane) (Figure 1), has a scaffold that offers extensive potential for derivatization. In particular, products could be envisaged in which a metallacarborane is connected to a carborane by a C_{cage}−C_{cage} bond or in which two metallacarborane units are connected by a C_{cage}−C_{cage} bond. We previously reported single-cage metalation of 1,1′-bis(*ortho*-carborane) affording metallacarborane−carborane species[6] and double-cage metalation yielding metallacarborane−metallacarborane compounds.[7] In the latter case metalation followed double deboronation, so the final products were necessarily homometalated. However, the potential utility of double-cage metalated derivatives of 1,1′-bis(*ortho*-carborane) would be greatly enhanced if controlled routes to heterometalated species were developed. In this contribution we report the stepwise deboronation and metalation of 1,1′-bis(*ortho*-carborane) to afford the first examples of heterometalated metallacarborane−metallacarborane species.

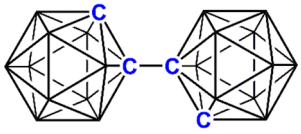

Figure 1. 1,1′-bis(*ortho*-carborane).

EXPERIMENTAL SECTION

Synthesis. Experiments were performed under dry, oxygen-free N_2 using standard Schlenk techniques, although subsequent manipulations were sometimes performed in the open laboratory. Solvents were freshly distilled under nitrogen from the appropriate drying agent [tetrahydrofuran (THF) and 40−60 petroleum ether (petrol); sodium wire: CH_2Cl_2 (DCM); calcium hydride] and were degassed (three freeze−pump−thaw cycles) before use. Deuterated solvents for NMR spectroscopy [$CDCl_3$, $(CD_3)_2CO$, CD_3CN] were stored over 4 Å molecular sieves. Preparative thin-layer chromatography (TLC) employed 20 × 20 cm Kieselgel F_{254} glass plates, and column

Received: April 27, 2018
Published: June 20, 2018

DOI: 10.1021/acs.inorgchem.8b01166
Inorg. Chem. 2018, 57, 8002–8011

chromatography used 60 Å silica as the stationary phase. Elemental analyses were conducted using an Exeter CE-440 elemental analyzer. NMR spectra at 400.1 MHz (^{1}H) or 128.4 MHz (^{11}B) were recorded on a Bruker AVIII-400 spectrometer at room temperature (Supporting Information). Electron ionization mass spectrometry (EIMS) was performed using a Finnigan (Thermo) LCQ Classic ion trap mass spectrometer at the University of Edinburgh. The starting materials 1,1′-bis(*ortho*-carborane),[8] [$RuCl_2$(*p*-cymene)]$_2$,[9] [8-(1′-*closo*-1′,2′-$C_2B_{10}H_{11}$)-2-(*p*-cymene)-*closo*-2,1,8-$RuC_2B_9H_{10}$] (**IIa**),[6] [8-(1′-*closo*-1′,2′-$C_2B_{10}H_{11}$)-2-Cp-*closo*-2,1,8-$CoC_2B_9H_{10}$] (**IIb**),[6] and [$HNMe_3$][7-(1′-*closo*-1′,2′-$C_2B_{10}H_{11}$)-*nido*-7,8-$C_2B_9H_{11}$] (**III**)[6,10] were prepared by literature methods or slight variations thereof. All other reagents were supplied commercially.

*[$HNMe_3$][8-(7′-nido-7′,8′-$C_2B_9H_{11}$)-2-(p-cymene)-closo-2,1,8-$RuC_2B_9H_{10}$] (**1**).* Compound **IIa** (0.200 g, 0.392 mmol) and KF (0.114 g, 1.962 mmol) were dissolved in a mixture of THF (50 mL) and deionized water (5 mL), and the solution was heated to reflux overnight. After it cooled to room temperature solvents were removed in vacuo, and the resultant white residue was redissolved in deionized water (20 mL) and filtered. To the filtrate was added an aqueous solution of excess [$HNMe_3$]Cl, which immediately resulted in the precipitation of a white solid, [$HNMe_3$][8-(7′-*nido*-7′,8′-$C_2B_9H_{11}$)-2-(*p*-cymene)-*closo*-2,1,8-$RuC_2B_9H_{10}$] (**1**). This was collected by filtration, washed with water, and dried in vacuo. Yield 0.188 g, 0.336 mmol, 86%. $C_{17}H_{45}B_{18}NRu$ requires C 36.5, H 8.11, N 2.50; found C 35.6, H 8.23, N 3.06%. ^{1}H NMR [$(CD_3)_2CO$], essentially equimolar mixture of diastereoisomers; δ 6.00−5.87 [m, 4H+4H, $CH_3C_6H_4CH(CH_3)_2$], 3.21 [s, 18H, $HN(CH_3)_3$], 2.79 [overlapping app septets, 1H+1H, $CH_3C_6H_4CH(CH_3)_2$], 2.64 (br s, 1H+1H, C1′H), 2.26 [s, 3H+3H, $CH_3C_6H_4CH(CH_3)_2$], 1.93 (br s, 1H+1H, C8′H), 1.30−1.27 [overlapping pairs of d, 6H+6H, $CH_3C_6H_4CH(CH_3)_2$], −2.66 (1H) and −2.81 (1H) (overlapping br singlets, μ-H). ^{11}B{^{1}H} NMR [$(CD_3)_2CO$] (relative integrals given); δ −1.1 (1B), −2.8 (2B), −4.9 (1B), −7.9 (1B), −10.2 (3B), −13.8 (2B), −16.7 (2B), −19.5 (1B), −21.0 (2B), −25.5 (1B), −33.5 (1B), −35.9 (1B).

*[$HNMe_3$][8-(7′-nido-7′,8′-$C_2B_9H_{11}$)-2-Cp-closo-2,1,8-$CoC_2B_9H_{10}$] (**2**).* Similarly, compound **IIb** (0.200 g, 0.502 mmol) was deboronated with KF (0.146 g, 2.513 mmol) in THF/water and then metathesized with [$HNMe_3$]Cl affording the product [$HNMe_3$][8-(7′-*nido*-7′,8′-$C_2B_9H_{11}$)-2-Cp-*closo*-2,1,8-$CoC_2B_9H_{10}$] (**2**) as a yellow solid. Yield 0.192 g, 0.429 mmol, 85%. $C_{12}H_{36}B_{18}CoN$ requires C 32.2, H 8.11, N 3.13; found C 32.3, H 8.18, N 3.01%. ^{1}H NMR [$(CD_3)_2CO$], equimolar mixture of diastereoisomers; δ 5.50 (s, 5H, C_5H_5), 5.49 (s, 5H, C_5H_5), 3.19 [s, 18H, $HN(CH_3)_3$], 2.84 (br s, 1H+1H, C1′H), 1.88 (br s, 1H+1H, C8′H), −2.70 (1H) and −2.85 (1H) (overlapping br singlets, μ-H). ^{11}B{^{1}H} NMR [$(CD_3)_2CO$] (relative integrals given); δ −0.4 (3B), −1.2 (1B), −5.9 (2B), −9.6 (1B), −10.1 (1B), −12.7 (1B), −14.1 (2B), −17.3 (2B), −18.3 (1B), −20.4 (1B), −24.3 (1B), −33.3 (1B), −35.7 (1B).

*α-[8-(1′-3′-Cp-closo-3′,1′,2′-$CoC_2B_9H_{10}$)-2-(p-cymene)-closo-2,1,8-$RuC_2B_9H_{10}$] (**3α**) and β-[8-(1′-3′-Cp-closo-3′,1′,2′-$CoC_2B_9H_{10}$)-2-(p-cymene)-closo-2,1,8-$RuC_2B_9H_{10}$] (**3β**).* ^{n}BuLi (0.15 mL of a 2.5 M solution, 0.375 mmol) was added dropwise to a cooled (0 °C) solution of **1** (0.100 g, 0.179 mmol) in THF (20 mL), and the reagents were stirred at room temperature for 0.5 h. The solution was then frozen at −196 °C, and $CoCl_2$ (0.081 g, 0.624 mmol) and NaCp (0.27 mL of a 2.0 M solution, 0.540 mmol) were added. The reaction mixture was stirred overnight. Following aerial oxidation (0.5 h) and filtration through silica, solvents were removed in vacuo, and the residue was purified by column chromatography using a DCM/petrol eluent (1:1) to afford a mobile orange band. This crude product was further purified by preparative TLC using the same eluent system to yield two mobile orange bands. Note that in this and the following metalation reactions isolated yields of products (following purification by chromatography) are relatively modest. After chromatography nonmobile components removed from silica with MeCN have ^{11}B NMR spectra that typically include resonances between −30 and −40 ppm, characteristic of *nido*-7,8-C_2B_9 fragments, so we ascribe the low isolated yields of metallacarborane products to poor conversion as opposed to decomposition.

*α-[8-(1′-3′-Cp-closo-3′,1′,2′-$CoC_2B_9H_{10}$)-2-(p-cymene)-closo-2,1,8-$RuC_2B_9H_{10}$] (**3α**).* R_f 0.51. Yield 0.024 g, 0.039 mmol, 22%. $C_{19}H_{39}B_{18}CoRu$ requires C 36.7, H 6.32; found C 37.3, H 6.77%. ^{1}H NMR ($CDCl_3$); δ 5.93−5.82 [m, 4H, $CH_3C_6H_4CH(CH_3)_2$], 5.80 (s, 5H, C_5H_5), 4.27 (br s, 1H, C2′H), 2.81 [app sept, 1H, $CH_3C_6H_4CH(CH_3)_2$], 2.63 (br s, 1H, C1′H), 2.32 [s, 3H, $CH_3C_6H_4CH(CH_3)_2$], 1.31 [d, 3H, $CH_3C_6H_4CH(CH_3)_2$], 1.29 [d, 3H, $CH_3C_6H_4CH(CH_3)_2$]. ^{11}B{^{1}H} NMR ($CDCl_3$); δ 5.2 (1B), 2.3 (1B), −0.9 to −10.0 multiple overlapping resonances with maxima at −0.9, −3.8, −5.2, −6.8, −8.5, −10.0 (total integral 11B), −14.6 (2B), −16.2 (1B), −17.9 (1B), −20.7 (1B). EIMS; envelope centered on m/z 622 (M^+).

*β-[8-(1′-3′-Cp-closo-3′,1′,2′-$CoC_2B_9H_{10}$)-2-(p-cymene)-closo-2,1,8-$RuC_2B_9H_{10}$] (**3β**).* R_f 0.56. Yield 0.027 g, 0.043 mmol, 24%. $C_{19}H_{39}B_{18}CoRu$ requires C 36.7, H 6.32; found C 35.9, H 6.65%. ^{1}H NMR ($CDCl_3$); δ 5.93−5.80 [m, 4H, $CH_3C_6H_4CH(CH_3)_2$], 5.82 (s, 5H, C_5H_5), 4.12 (br s, 1H, C2′H), 2.79 [app sept, 1H, $CH_3C_6H_4CH(CH_3)_2$], 2.63 (br s, 1H, C1′H), 2.31 [s, 3H, $CH_3C_6H_4CH(CH_3)_2$], 1.30 [d, 3H, $CH_3C_6H_4CH(CH_3)_2$], 1.28 [d, 3H, $CH_3C_6H_4CH(CH_3)_2$]. ^{11}B{^{1}H} NMR ($CDCl_3$); δ 5.0 (1B), 2.2 (1B), −0.9 to −10.4 multiple overlapping resonances with maxima at −0.9, −3.9, −5.6, −7.5, −8.7, −10.4 (total integral 11B), −14.6 (2B), −16.5 (1B), −17.4 (1B), −20.7 (1B). EIMS; envelope centered on m/z 622 (M^+).

[1-(1′-closo-1′,2′-$C_2B_{10}H_{11}$)-3-Cp-closo-3,1,2-$CoC_2B_9H_{10}$] (**4**), [8-(1′-closo-1′,2′-$C_2B_{10}H_{11}$)-2-Cp*-closo-2,1,8-$CoC_2B_9H_{10}$] (**5**), and [12-(1′-closo-1′,2′-$C_2B_{10}H_{11}$)-4,5-Cp*$_2$-closo-4,5,1,12-$Co_2C_2B_9H_{10}$] (**6**).* ^{n}BuLi (0.60 mL of a 2.5 M solution, 1.500 mmol) was added dropwise to an ice-cooled solution of **III** ([$HNMe_3$]$^+$ salt, 0.250 g, 0.745 mmol) in THF (25 mL), and the products were stirred for 1 h at room temperature. The pale yellow solution was then frozen at −196 °C, $CoCl_2$ (0.320 g, 2.465 mmol) and NaCp* (4.2 mL of a 0.5 M solution, 2.100 mmol) were added, and the reaction mixture was stirred overnight at room temperature. Following aerial oxidation (0.5 h) and filtration through silica, volatiles were removed in vacuo, and the residue was purified by column chromatography using a DCM/petrol eluent, 2:3, to afford red, yellow, and green (trace) bands, compounds **4**, **5**, and **6**, respectively.

[1-(1′-closo-1′,2′-$C_2B_{10}H_{11}$)-3-Cp-closo-3,1,2-$CoC_2B_9H_{10}$] (**4**).* R_f 0.41. Yield 0.120 g, 0.256 mmol, 34%. $C_{14}H_{36}B_{19}Co$ requires C 35.9, H 7.74; found C 35.8, H 7.83%. ^{1}H NMR ($CDCl_3$); δ 4.10 (br s, 1H, C2′H), 3.37 (br s, 1H, C2H), 1.84 [s, 15H, $C_5(CH_3)_5$]. ^{11}B{^{1}H} NMR ($CDCl_3$); δ 10.1 (1B), −1.9 (2B), −3.8 (4B), −6.0 (2B), −9.6 (6B), −12.4 (3B), −15.0 (1B). EIMS; envelope centered on m/z 469 (M^+).

[8-(1′-closo-1′,2′-$C_2B_{10}H_{11}$)-2-Cp-closo-2,1,8-$CoC_2B_9H_{10}$] (**5**).* R_f 0.68. Yield 0.033 g, 0.070 mmol, 9%. $C_{14}H_{36}B_{19}Co$ requires C 35.9, H 7.74; found C 36.3, H 7.86%. ^{1}H NMR ($CHCl_3$/CD_3CN, 1:10); δ 4.01 (br s, 1H, C2′H), 2.09 (br s, 1H, C1H), 1.84 [s, 15H, $C_5(CH_3)_5$]. ^{11}B{^{1}H} NMR ($CDCl_3$); δ 3.2 (1B), 1.1 (2B), −2.6 (1B), −4.1 (2B), −4.9 (1B), −7.2 (1B), −9.9 (6B), −13.3 (2B), −13.9 (1B), −18.0 (1B), −18.6 (1B). EIMS; envelope centered on m/z 469 (M^+).

[12-(1′-closo-1′,2′-$C_2B_{10}H_{11}$)-4,5-Cp$_2$-closo-4,5,1,12-$Co_2C_2B_9H_{10}$] (**6**).* R_f 0.31. Yield 0.004 g, 0.006 mmol, <1%. ^{1}H NMR ($CDCl_3$); δ 3.80 (br s, 1H, C2′H), 1.68 [s, 30H, $C_5(CH_3)_5$], 1.26 (br s, 1H, C1H). ^{11}B{^{1}H} NMR ($CDCl_3$); δ 7.6 (1B), 3.0 (5B), −3.1 (2B), −4.7 (2B), −5.9 (1B), −10.6 (6B), −13.4 (2B). EIMS; envelopes centered on m/z 663 (M^+) and 469 (M^+−{CoCp*}).

*Redox Isomerization of **4** to **5**.* To a frozen solution of **4** (0.020 g, 0.043 mmol) in THF (10 mL) was added sodium naphthalenide (1 mL of a 0.043 M solution in THF, 0.043 mmol). The reagents were warmed to room temperature, stirred under nitrogen for 1 h, and then aerially oxidized for 0.5 h. Purification by preparative TLC using a DCM/petrol eluent, 2:3, afforded the starting material **4** (R_f 0.40, 0.008 g, 0.017 mmol, 40%) and a yellow product (R_f 0.65, 0.009 g, 0.019 mmol, 45%) identical to **5** by ^{1}H and ^{11}B{^{1}H} NMR spectroscopies.

[$HNMe_3$][8-(7′-nido-7′,8′-$C_2B_9H_{11}$)-2-Cp-closo-2,1,8-$CoC_2B_9H_{10}$] (**7**).* Compound **5** (0.100 g, 0.213 mmol) and KF (0.062 g, 1.067

DOI: 10.1021/acs.inorgchem.8b01166
Inorg. Chem. 2018, 57, 8002−8011

Table 1. Crystallographic Data

	3α	3β·0.5CH_2Cl_2	4	5	6·$CHCl_3$	9·CH_2Cl_2
CCDC	1828646	1828647	1828648	1828649	1828650	1828651
formula	$C_{19}H_{39}B_{18}CoRu$	$C_{19.5}H_{40}B_{18}ClCoRu$	$C_{14}H_{36}B_{19}Co$	$C_{14}H_{36}B_{19}Co$	$C_{15}H_{52}B_{19}Cl_3Co_2$	$C_{25}H_{51}B_{18}Cl_2CoRu$
M	622.08	664.54	468.75	468.75	782.26	777.13
crystal system	triclinic	triclinic	orthorhombic	orthorhombic	triclinic	triclinic
space group	$P\bar{1}$	$P\bar{1}$	*Pbca*	$Pca2_1$	$P\bar{1}$	$P\bar{1}$
a/Å	9.0526(3)	13.0896(9)	14.0429(3)	13.2177(3)	8.3035(5)	9.3895(2)
b/Å	16.0530(5)	15.6050(11)	18.3107(5)	13.9889(4)	15.0776(9)	12.4982(2)
c/Å	19.5784(7)	16.1374(11)	19.0533(4)	27.0886(7)	16.2446(10)	16.5176(3)
α/deg	82.385(3)	64.491(3)	90	90	72.909(4)	97.171(2)
β/deg	87.118(3)	85.635(4)	90	90	75.995(4)	98.157(2)
γ/deg	78.086(3)	85.818(4)	90	90	89.479(4)	110.914(2)
U/Å^3	2758.55(16)	2963.4(4)	4899.27(19)	5008.7(2)	1882.0(2)	1759.77(6)
Z, Z'	4, 2	4, 2	8, 1	8, 2	2, 1	2, 1
F(000)/e	1256	1340	1936	1936	804	792
D_{calc}/Mg m^{-3}	1.498	1.490	1.271	1.243	1.380	1.467
X-radiation	Cu Kα	Mo Kα	Mo Kα	Mo Kα	Mo Kα	Mo Kα
λ/Å	1.541 78	0.710 73	0.710 73	0.710 73	0.710 73	0.710 73
μ/mm^{-1}	9.190	1.174	0.705	0.690	1.116	1.073
θ_{max}/deg	68.24	33.10	29.79	32.84	27.05	27.48
data measured	39 206	77 809	51 637	67 177	37 219	39 431
unique data	10 028	21 546	6532	14 322	8078	8068
R_{int}	0.0414	0.0430	0.0479	0.0488	0.0588	0.0266
R, wR_2 (obs data)	0.0430, 0.1172	0.0367, 0.0810	0.0469, 0.1032	0.0459, 0.1037	0.0512, 0.1145	0.0213, 0.0529
S	1.086	1.049	1.140	1.060	1.027	1.058
variables	850	856	375	750	539	494
E_{max}, E_{min}/e Å^{-3}	1.32, −0.80	1.07, −1.32	0.61, −0.41	0.42, −0.32	0.77, −0.81	0.84, −0.75
Flack parameter				0.469(19)		

mmol) were dissolved in a mixture of THF (50 mL) and deionized water (5 mL), and the resulting yellow solution was heated to reflux overnight. After it cooled to room temperature, solvents were removed in vacuo, and the yellow residue was redissolved in deionized water (20 mL) and filtered. To the filtrate was added an aqueous solution of excess $[HNMe_3]Cl$ resulting in the precipitation of a yellow solid, $[HNMe_3][8\text{-}(7'\text{-}nido\text{-}7',8'\text{-}C_2B_9H_{11})\text{-}2\text{-}Cp^*\text{-}closo\text{-}2,1,8\text{-}CoC_2B_9H_{10}]$ (**7**). This was collected by filtration, washed with water, and dried in vacuo. Yield 0.078 g, 0.151 mmol, 71%. $C_{17}H_{46}B_{18}NCo$ requires C 39.4, H 8.95, N 2.70; found C 40.2, H 8.81, N 2.75%. ^{1}H NMR [$(CD_3)_2CO$], essentially equimolar mixture of diastereoisomers; δ 3.18 [s, 18H, $HN(CH_3)_3$], 1.96 (br s, 1H+1H, C1*H*), 1.88 (br s, 1H+1H, C8′*H*), 1.85 [s, 15H, $C_5(CH_3)_5$], 1.84 [s, 15H, $C_5(CH_3)_5$], −2.68 (1H) and −2.84 (1H) (overlapping br singlets, μ-H). $^{11}B\{^1H\}$ NMR [$(CD_3)_2CO$] (relative integrals given); δ 1.3 (3B), −4.2 (2B), −7.1 (1B), −9.4 (1B), −10.1 (1B), −13.9 (3B), −17.2 (1B), −18.0 (1B), −19.1 (1B), −20.5 (1B), −24.3 (1B), −33.4 (1B), −35.7 (1B).

[8-(1′-3′-(p-cymene)-closo-3′,1′,2′-$RuC_2B_9H_{10}$)-2-Cp-closo-2,1,8-$CoC_2B_9H_{10}$] (**8**, Major and Minor Diastereoisomers).* ^{n}BuLi (0.17 mL of a 2.5 M solution, 0.425 mmol) was added dropwise to a cooled (0 °C) solution of **7** (0.100 g, 0.193 mmol) in THF (20 mL). After it warmed to room temperature, the dark yellow solution was frozen at −196 °C, and $[RuCl_2(p\text{-cymene})]_2$ (0.059 g, 0.096 mmol) was added. The reaction mixture was rewarmed and stirred overnight. Following filtration through silica, volatiles were removed in vacuo, and the residue was purified by column chromatography using a DCM/petrol eluent (3:7) to afford a mobile yellow band (R_f 0.34), which ultimately yielded $[8\text{-}(1'\text{-}3'\text{-}(p\text{-cymene})\text{-}closo\text{-}3',1',2'\text{-}RuC_2B_9H_{10})\text{-}2\text{-}Cp^*\text{-}closo\text{-}2,1,8\text{-}CoC_2B_9H_{10}]$ (**8**) as a yellow solid. NMR spectroscopy reveals **8** to be a mixture of the two diastereoisomers in a ∼2:1 ratio. In spite of exhaustive chromatography these isomers could not be separated. Yield 0.032 g, 0.046 mmol, 24%. $C_{24}H_{49}B_{18}CoRu$ requires: C 41.6, H 7.13. Found: C 41.0, H 7.16%. ^{1}H NMR ($CDCl_3$, major diastereoisomer); δ 6.04−5.78 [m, 4H, $CH_3C_6H_4CH(CH_3)_2$], 3.75 (br s, 1H, C2′*H*), 3.03 [app sept, 1H, $CH_3C_6H_4CH(CH_3)_2$], 2.46 [s, 3H, $CH_3C_6H_4CH(CH_3)_2$], 1.847 [s, 15H, $C_5(CH_3)_5$], 1.79 (br s, 1H, C1*H*), 1.35−1.26 [m, 6H, $CH_3C_6H_4CH(CH_3)_2$]. ^{1}H NMR ($CDCl_3$, minor diastereoisomer); δ 6.04−5.78 [m, 4H, $CH_3C_6H_4CH(CH_3)_2$], 3.88 (br s, 1H, C2′*H*), 3.03 [app sept, 1H, $CH_3C_6H_4CH(CH_3)_2$], 2.44 [s, 3H, $CH_3C_6H_4CH(CH_3)_2$], 1.852 [s, 15H, $C_5(CH_3)_5$], 1.79 (br s, 1H, C1*H*), 1.35−1.26 [m, 6H, $CH_3C_6H_4CH(CH_3)_2$]. $^{11}B\{^1H\}$ NMR ($CDCl_3$); δ 2.7 to 0.3 multiple overlapping resonances with maxima at 2.7, 1.9, 0.3 (total 5B), −3.8 to −7.6 multiple overlapping resonances with maxima at −3.8, −6.1, −7.6 (total 7B), −13.1 to −19.6 multiple overlapping resonances with maxima at −13.1, −14.8, −17.2, −19.6 (total 6B). EIMS; envelope centered on m/z 692 (M^+).

*Thermal Isomerization of **8** to **9**.* Mixture **8** (0.020 g, 0.029 mmol) was dissolved in dimethoxyethane (DME, 10 mL) and heated to reflux overnight. After it cooled, solvent was removed in vacuo, and the residue was purified by preparative TLC using a DCM/petrol eluent (2:3) to afford a mobile yellow band (R_f 0.36) from which $[8\text{-}(8'\text{-}2'\text{-}(p\text{-cymene})\text{-}closo\text{-}2',1',8'\text{-}RuC_2B_9H_{10})\text{-}2\text{-}Cp^*\text{-}closo\text{-}2,1,8\text{-}CoC_2B_9H_{10}]$ (**9**) was afforded as a yellow solid. By ^{1}H NMR spectroscopy **9** was shown to be a mixture of two diastereoisomers in a ∼2:1 ratio. Exhaustive chromatography failed to separate these components. Yield 0.017 g, 0.025 mmol, 85%. $C_{24}H_{49}B_{18}CoRu$ requires: C 41.6, H 7.13. $C_{24}H_{49}B_{18}CoRu{\cdot}0.5CH_2Cl_2$ requires: C 40.1, H 6.86. Found: C 40.1, H 6.98%. ^{1}H NMR ($CDCl_3$, major diastereoisomer); δ 5.86−5.71 [m, 4H, $CH_3C_6H_4CH(CH_3)_2$], 2.81 [app sept, 1H, $CH_3C_6H_4CH(CH_3)_2$], 2.59 (br s, 1H, C1′*H*), 2.30 [s, 3H, $CH_3C_6H_4CH(CH_3)_2$], 1.84 [s, 15H, $C_5(CH_3)_5$], 1.74 (br s, 1H, C1*H*), 1.29−1.26 [m, 6H, $CH_3C_6H_4CH(CH_3)_2$]. ^{1}H NMR ($CDCl_3$, minor diastereoisomer); δ 5.86−5.71 [m, 4H, $CH_3C_6H_4CH(CH_3)_2$], 2.81 [app sept, 1H, $CH_3C_6H_4CH(CH_3)_2$], 2.62 (br s, 1H, C1′*H*), 2.30 [s, 3H, $CH_3C_6H_4CH(CH_3)_2$], 1.83 [s, 15H, $C_5(CH_3)_5$], 1.77 (br s, 1H, C1*H*), 1.29−1.26 [m, 6H, $CH_3C_6H_4CH(CH_3)_2$]. $^{11}B\{^1H\}$ NMR ($CDCl_3$); δ 2.4 to −7.9 multiple overlapping resonances with maxima at 2.4, 1.0, −1.7, −4.9, −6.6, −7.9 (total 12B), −14.3 to −20.5 multiple overlapping resonances with maxima at −14.3, −16.2, −19.1, −20.5 (total 6B). EIMS; envelope centered on m/z 692 (M^+).

DOI: 10.1021/acs.inorgchem.8b01166
Inorg. Chem. 2018, 57, 8002−8011

Crystallography. Single crystals of **3**α, **3**β·0.5CH_2Cl_2, **4**, **5**, and **9**·CH_2Cl_2 were grown by diffusion of a DCM solution of the appropriate compound and petrol at −20 °C, while single crystals of **6**·$CHCl_3$ were afforded by slow evaporation of a $CHCl_3$ solution at room temperature. Diffraction data from **3**α were collected at 100 K on a Rigaku 007-HF diffractometer equipped with Cu Kα X-radiation; data from **3**β·0.5CH_2Cl_2 and **6**·$CHCl_3$ were collected at 100 K on a Bruker X8 APEXII diffractometer operating with Mo Kα radiation; data from **4** and **5** were obtained at 120 K on a Rigaku Oxford Diffraction SuperNova diffractometer, using Mo Kα radiation; data from **9**·CH_2Cl_2 were collected at 100 K on a Rigaku FR-E+ diffractometer, also using Mo Kα radiation. Compound **5** crystallizes as a two-component twin, but all other samples were single crystals. With *OLEX2*,[11] structures were solved by direct methods using the *SHELXS*[12] or *SHELXT*[13] program and refined by full-matrix least-squares using *SHELXL*.[14] In **3**α the ^{i}Pr group of the *p*-cymene of one of the two crystallographically independent molecules is partially disordered, and there is multiple disordering of the $CHCl_3$ molecule of solvation in **6**·$CHCl_3$. In **9**·CH_2Cl_2 application of the Vertex-Centroid Distance (VCD) and Boron−Hydrogen Distance (BHD) methods[15−17] revealed partial disorder between two cage {CH} and {BH} vertices in each metallacarborane cage, since the two diastereoisomeric forms of **9** are both present, but in all other structures cage C atoms bearing only H substituents were clearly distinguished from B atoms by the VCD and BHD approaches. H atoms bound to cage B or cage C atoms were allowed positional refinement, but all other H atoms were treated as riding on their respective C atom, with $C_{primary}$−H 0.98 Å, $C_{secondary}$−H 0.99 Å, $C_{tertiary}$−H 1.00 Å, C_{arene}−H 1.00 Å, and C_{Cp}−H 1.00 Å. H atom displacement parameters were constrained to 1.2 × U_{eq} (bound B or C) except for Me H atoms, 1.5 × U_{eq} (C_{methyl}). Table 1 contains unit cell data and further experimental details.

RESULTS AND DISCUSSION

Singly metalated 1,1′-bis(*ortho*-carborane) is known in four isomeric forms,[6,18,19] of which [1-(1′-*closo*-1′,2′-$C_2B_{10}H_{11}$)-*closo*-3,1,2-$MC_2B_9H_{10}$] (**I**) and [8-(1′-*closo*-1′,2′-$C_2B_{10}H_{11}$)-*closo*-2,1,8-$MC_2B_9H_{10}$] (**II**) (Figure 2) are the most common.

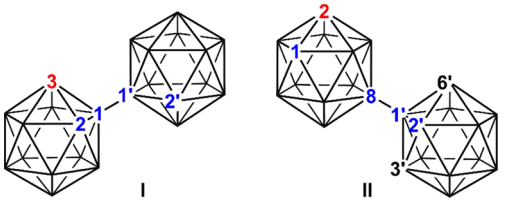

Figure 2. Two common isomers of singly metalated 1,1′-bis(*ortho*-carborane) demonstrating the atom numbering schemes. Carbon vertices in blue, metal (M) vertices in red, boron vertices in black. **I**a and **II**a, M = Ru(*p*-cymene). **I**b and **IIb**, M = CoCp.

We chose the latter as our starting point for the synthesis of heterometalated derivatives to minimize possible steric congestion between the two metal fragments. Deboronation of carboranes is classically performed by alkoxide,[1,2] but this approach is unsuitable for **II** because of the limited solubility of **II** in EtOH. Although the parent species 1,1′-bis(*ortho*-carborane) has been successfully deboronated in MeCN/H_2O[10] we found that this approach affords only slow and incomplete deboronation of **II**. However, "wet" fluoride ion, also recognized as a mild and selective deboronating agent,[20] proved to be successful. Thus, compound **II**a (M = Ru{*p*-cymene})[6] was successfully deboronated by KF in THF/water at reflux and metathesized to the trimethylammonium salt [$HNMe_3$][8-(7′-*nido*-7′,8′-$C_2B_9H_{11}$)-2-(*p*-cymene)-*closo*-2,1,8-$RuC_2B_9H_{10}$] (**1**), obtained in 86% isolated yield (Scheme 1). Note that deboronation of **II** occurs exclusively at the C_2B_{10} cage and not the MC_2B_9 cage and gives rise to a diastereoisomeric mixture, since either B3′ or B6′ could be lost. Salt **1** was characterized by elemental analysis and NMR spectroscopy.

Microanalytical results were consistent with the empirical formula $C_{17}H_{45}B_{18}NRu$. Although the existence of diastereoisomers could not be detected in the $^{11}B\{^1H\}$ NMR spectrum (which consists of 12 resonances with relative integrals 1:2:1:1:3:2:2:1:2:1:1:1, total 18B, from δ −1 to −36 ppm) nor from the two broad resonances in the ^1H spectrum assigned to cage C*H* atoms (δ 2.64 ppm, C1*H*; δ 1.93 ppm, C8′*H*; assignments by reference to related species, see Table 2) clear evidence is found in the ^1H resonances associated with the *p*-cymene ligand, where the signal for the C*H*(CH_3)$_2$ proton appears as two overlapping apparent septets, and the CH(CH_3)$_2$ protons give rise to two pairs of doublets. In addition the bridging protons on the nido carborane cages appears as two overlapping singlets at low frequency. On the basis of the integrals of these resonances the two diastereoisomers of **1** are formed in almost equal amounts.

Similarly, deboronation of **II**b (M = CoCp) and workup led to the isolation of [$HNMe_3$][8-(7′-*nido*-7′,8′-$C_2B_9H_{11}$)-2-Cp-*closo*-2,1,8-$CoC_2B_9H_{10}$] (**2**) in 85% yield. Once again the presence of a diastereoisomeric mixture could not be detected from either the ^{11}B NMR spectrum or the broad $C_{cage}H$ resonances in the ^1H spectrum (δ 2.84 ppm, C1*H*; δ 1.93 ppm, C8′*H*; assignments based on Table 2), but it is clearly evident from the existence in the latter of two very close (and equal integral) singlets at δ 5.50 and 5.49 ppm due to the C_5H_5 protons. As with **1** the B-*H*-B protons of the deboronated cage appear as broad overlapping singlets, this time at δ −2.70 and −2.85 ppm.

Salts **1** and **2** are potential precursors for hetero-bimetallic 1,1′-bis(*ortho*-carborane) derivatives. Deprotonation of **1** with ^{n}BuLi then reaction with a mixture of $CoCl_2$ and NaCp followed by aerial oxidation afforded the ruthenacarborane−cobaltacarborane species **3** as a mixture of diastereoisomers, separated into components **3**α and **3**β by TLC (Scheme 2). Compounds **3**α and **3**β are orange solids isolated in yields of 22% and 24%, respectively, and afford satisfactory microanalytical results. Unsurprisingly as diastereoisomers their NMR spectra are very similar. In their ^1H spectra, as well as the expected resonances for the *p*-cymene and Cp ligands, are one high-frequency resonance (δ ca. 4.2 ppm) and one relatively low-frequency resonance (δ ca. 2.6 ppm) assigned to $C_{cage}H$ atoms. By comparison with the $C_{cage}H$ resonances summarized in Table 2 we assign the high-frequency signal to a (new) 3,1,2-CoC_2B_9 cobaltacarborane cage and the low-frequency signal to the (existing) 2,1,8-RuC_2B_9 cage. We therefore formulate **3**α and **3**β as diastereoisomers of [8-(1′-3′-Cp-*closo*-3′,1′,2′-$CoC_2B_9H_{10}$)-2-(*p*-cymene)-*closo*-2,1,8-$RuC_2B_9H_{10}$], the first examples of heterometalated derivatives of 1,1′-bis(*ortho*-carborane). The $^{11}B\{^1H\}$ NMR spectra of **3**α and **3**β suffer from multiple overlapping resonances that cannot easily be individually integrated, but nevertheless signals could be integrated at high frequency [δ ca. 5 (1B) and 2 (1B) ppm] and at low frequency [δ ca. −15 (2B), −16 (1B), −17 (1B), and −21 (1B) ppm], between which is a group of resonances integrating for a combined total of 11 B atoms.

The structures of **3**α and **3**β were confirmed crystallographically. Crucial to the correct characterization of these diastereoisomers was our ability to distinguish between cage

DOI: 10.1021/acs.inorgchem.8b01166
Inorg. Chem. 2018, 57, 8002−8011

Scheme 1. Deboronation of II to Afford a Diastereoisomeric Mixture of Either 1 or 2; Deboronation of 5 to Afford a Diastereoisomeric Mixture of 7

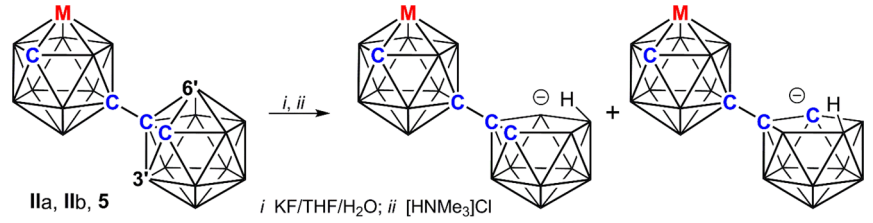

Table 2. Cage C*H* Chemical Shifts in 1−9 and Related Species

species	δ(C*H*)/ppm (assignment)	solvent	ref
[*closo*-1,2-$C_2B_{10}H_{12}$]	4.40 (C1*H*, C2*H*)	$(CD_3)_2CO$	21
[*nido*-7,8-$C_2B_9H_{12}$]$^-$	1.88 (C7*H*, C8*H*)	CD_2Cl_2	22
[3-(*p*-cymene)-*closo*-3,1,2-$RuC_2B_9H_{11}$]	3.70 (C1*H*, C2*H*)	$CDCl_3$	23
[3-Cp-*closo*-3,1,2-$CoC_2B_9H_{11}$]	4.26 (C1*H*, C2*H*)	CD_3CN	4
[2-Cp-*closo*-2,1,8-$CoC_2B_9H_{11}$]	2.73, 2.47 (not assigned)	$CDCl_3$	18, 24
[1-(1′-*closo*-1′,2′-$C_2B_{10}H_{11}$)-*closo*-1,2-$C_2B_{10}H_{11}$]	5.05 (C2*H*, C2′*H*)	$(CD_3)_2CO$	25
[7-(1′-*closo*-1′,2′-$C_2B_{10}H_{11}$)-*nido*-7,8-$C_2B_9H_{11}$]$^-$	4.36 (C8*H*), 1.99 (C2′*H*)	$(CD_3)_2CO$	6
[1-(1′ *closo*-1′,2′-$C_2B_{10}H_{11}$)-3-(*p*-cymene)-*closo*-3,1,2-$RuC_2B_9H_{10}$] (**Ia**)	4.03, 3.91 (not assigned)	$CDCl_3$	6
[1-(1′-*closo*-1′,2′-$C_2B_{10}H_{11}$)-3-Cp-*closo*-3,1,2-$CoC_2B_9H_{10}$] (**Ib**)	4.24, 4.03 (not assigned)	$CDCl_3$	6
[8-(1′-*closo*-1′,2′-$C_2B_{10}H_{11}$)-2-(*p*-cymene)-*closo*-2,1,8-$RuC_2B_9H_{10}$] (**IIa**)	3.64 (C2′*H*), 2.63 (C1*H*)	$CDCl_3$	6
[8-(1′-*closo*-1′,2′-$C_2B_{10}H_{11}$)-2-Cp-*closo*-2,1,8-$CoC_2B_9H_{10}$] (**IIb**)	3.59 (C2′*H*), 2.73 (C1*H*)	$CDCl_3$	6
[8-(7′-*nido*-7′,8′-$C_2B_9H_{11}$)-2-(*p*-cymene)-*closo*-2,1,8-$RuC_2B_9H_{10}$]$^-$ (**1**)	2.64 (C1*H*), 1.93 (C8′*H*)	$(CD_3)_2CO$	this work
[8-(7′-*nido*-7′,8′-$C_2B_9H_{11}$)-2-Cp-*closo*-2,1,8-$CoC_2B_9H_{10}$]$^-$ (**2**)	2.84 (C1*H*), 1.88 (C8′*H*)	$(CD_3)_2CO$	this work
α-[8-(1′-3′-Cp-*closo*-3′,1′,2′-$CoC_2B_9H_{10}$)-2-(*p*-cymene)-*closo*-2,1,8-$RuC_2B_9H_{10}$] (**3*α***)	4.27 (C2′*H*), 2.63 (C1*H*)	$CDCl_3$	this work
β-[8-(1′-3′-Cp-*closo*-3′,1′,2′-$CoC_2B_9H_{10}$)-2-(*p*-cymene)-*closo*-2,1,8-$RuC_2B_9H_{10}$] (**3*β***)	4.12 (C2′*H*), 2.63 (C1*H*)	$CDCl_3$	this work
[1-(1′-*closo*-1′,2′-$C_2B_{10}H_{11}$)-3-Cp*-*closo*-3,1,2-$CoC_2B_9H_{10}$] (**4**)	4.10 (C2′*H*), 3.37 (C2*H*)	$CDCl_3$	this work
[8-(1′-*closo*-1′,2′-$C_2B_{10}H_{11}$)-2-Cp*-*closo*-2,1,8-$CoC_2B_9H_{10}$] (**5**)	4.01 (C2′*H*), 2.09 (C1*H*)	CD_3CN[a]	this work
[12-(1′-*closo*-1′,2′-$C_2B_{10}H_{11}$)-4,5-Cp*$_2$-*closo*-4,5,1,12-$Co_2C_2B_9H_{10}$] (**6**)	3.80 (C2′*H*), 1.26 (C1*H*)	$CDCl_3$	this work
[6-(1′-*closo*-1′,2′-$C_2B_{10}H_{11}$)-4-(*p*-cymene)-5-(mesitylene)-*closo*-4,5,1,6-$Ru_2C_2B_9H_{10}$]	4.10 (C2′*H*), 2.27 (C1*H*)	$CDCl_3$	26
[$HNMe_3$][8-(7′-*nido*-7′,8′-$C_2B_9H_{11}$)-2-Cp*-*closo*-2,1,8-$CoC_2B_9H_{10}$] (**7**)	1.96 (C1*H*), 1.88 (C8′*H*)	$(CD_3)_2CO$	this work
[8-(1′-3′-(*p*-cymene)-*closo*-3′,1′,2′-$RuC_2B_9H_{10}$)-2-Cp*-*closo*-2,1,8-$CoC_2B_9H_{10}$] (**8**, major)	3.75 (C2′*H*), 1.79 (C1*H*)	$CDCl_3$	this work
[8-(1′-3′-(*p*-cymene)-*closo*-3′,1′,2′-$RuC_2B_9H_{10}$)-2-Cp*-*closo*-2,1,8-$CoC_2B_9H_{10}$] (**8**, minor)	3.88 (C2′*H*), 1.79 (C1*H*)	$CDCl_3$	this work
[8-(8′-2′-(*p*-cymene)-*closo*-2′,1′,8′-$RuC_2B_9H_{10}$)-2-Cp*-*closo*-2,1,8-$CoC_2B_9H_{10}$] (**9**, major)	2.59 (C1′*H*), 1.74 (C1*H*)	$CDCl_3$	this work
[8-(8′-2′-(*p*-cymene)-*closo*-2′,1′,8′-$RuC_2B_9H_{10}$)-2-Cp*-*closo*-2,1,8-$CoC_2B_9H_{10}$] (**9**, minor)	2.62 (C1′*H*), 1.77 (C1*H*)	$CDCl_3$	this work

[a] $CHCl_3/CD_3CN$, 1:10

Scheme 2. Formation of 3*α* and 3*β* from 1

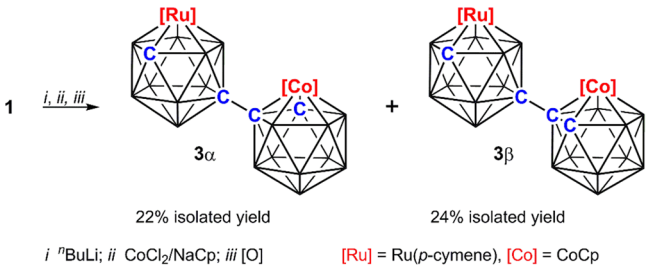

{CH} fragments and {BH} fragments, but this was achieved unambiguously for both crystallographically independent molecules of both species by application of the VCD and BHD methods.[15−17] Perspective views of single molecules of **3*α*** and **3*β*** are shown in Figure 3. These structural studies confirm that the ruthenacarborane cage is of 2,1,8-RuC_2B_9 architecture, while the cobaltacarborane cage is 3,1,2-CoC_2B_9. This latter finding is somewhat surprising, since we have previously shown that "in situ" metalation of singly deboronated 1,1′-bis(*ortho*-carborane) (supplying the {CoCp} fragment from $CoCl_2$/NaCp followed by oxidation) affords predominantly the 2,1,8-CoC_2B_9-1′,2′-C_2B_{10} species **II**, the result of facile 3,1,2- to 2,1,8- isomerization of the initially formed [3,1,2-CoC_2B_9-1′,2′-C_2B_{10}]$^-$ anion.[6] Clearly in the case of **3*α*** and **3*β*** the presence of a 2,1,8-RuC_2B_9 substituent prevents isomerization of the adjacent cobaltacarborane cage.

The two crystallographically independent molecules of **3*α*** effectively differ only in respect of the orientation of the *p*-cymene ligand on the ruthenacarborane cage relative to C2′ of the cobaltacarborane cage. In both molecules the *p*-cymene ligand is essentially parallel to the plane defined by atoms C8B4B5B10B12 (the lower pentagonal belt, the usual reference plane for icosahedral metallacarboranes)[27] as

DOI: 10.1021/acs.inorgchem.8b01166
Inorg. Chem. 2018, 57, 8002−8011

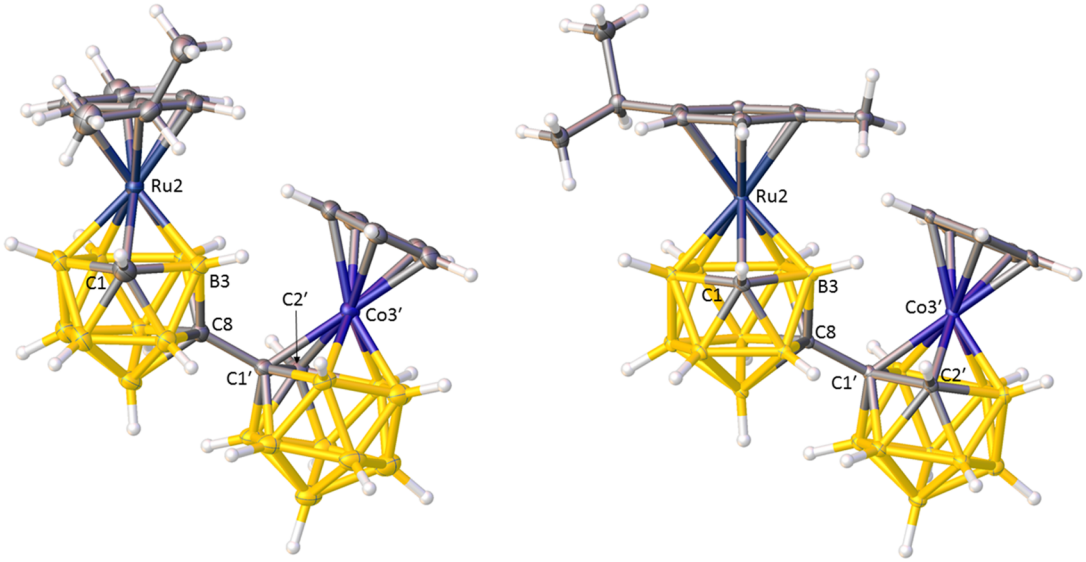

Figure 3. (left) Perspective view of one of the two crystallographically independent molecules of compound **3***α*. (right) Perspective view of one of the two crystallographically independent molecules of compound **3***β*.

expected given that the ruthenacarborane has a 2,1,8-RuC_2B_9 architecture. In contrast the Cp ligand on the 3′,1′,2′-CoC_2B_9 cage is clearly inclined away from the adjacent ruthenacarborane substituent to minimize steric crowding, subtending bend-back angles θ of 13.93(18) and 13.97(18)° with the B5′B6′B11′B12′B9′ lower pentagonal belt. In independent molecules of the related species [1-(1′-*closo*-1′,2′-$C_2B_{10}H_{11}$)-3-Cp-*closo*-3,1,2-$CoC_2B_9H_{10}$] the angles θ are 15.8 and 16.3°.[6] The two independent molecules of **3***β* are practically superimposable, including the orientation of the *p*-cymene ligand. Once again this lies effectively parallel to its reference plane, while the Cp ligand of the cobaltacarborane is inclined by θ values of 13.57(8) and 13.08(7)°.

Having successfully prepared hetero-bimetallic Ru/Co derivatives of 1,1′-bis(*ortho*-carborane) by subrogating {BH} vertices first with a Ru-ligand fragment and second with a Co-ligand fragment, we then considered the reverse approach. However, treatment of salt **2** in THF with ^{n}BuLi resulted in considerable darkening of the solution, and no mobile products were afforded following subsequent reaction with $[RuCl_2(p\text{-cymene})]_2$. Reasoning that this was probably the result of attack on the Cp ligand by ^{n}BuLi we switched attention to the Cp* analogue. The precursor **II** (M = CoCp*) is unknown, so we attempted to prepare it in an analogous way to that which afforded **IIb**,[6] namely, deprotonation of the $[HNMe_3]^+$ salt of singly deboronated 1,1′-bis(*ortho*-carborane) **III**, reaction with $CoCl_2$/NaCp*, and finally aerial oxidation (Scheme 3). Somewhat to our surprise, however, while the anticipated product [8-(1′-*closo*-1′,2′-$C_2B_{10}H_{11}$)-2-Cp*-*closo*-2,1,8-$CoC_2B_9H_{10}$] (**5**) was afforded by this approach the major reaction product was, in fact, the isomeric species [1-(1′-*closo*-1′,2′-$C_2B_{10}H_{11}$)-3-Cp*-3,1,2-$CoC_2B_9H_{10}$] (**4**). A trace amount of the 13-vertex bimetallacarborane/12-vertex carborane species [12-(1′-*closo*-1′,2′-$C_2B_{10}H_{11}$)-4,5-Cp^*_2-*closo*-4,5,1,12-$Co_2C_2B_9H_{10}$] (**6**) was also isolated.

Compound **4** was isolated as a red solid in 34% yield, and its chemical composition was established by elemental analysis and mass spectrometry. The $^{11}B\{^1H\}$ NMR spectrum is largely uninformative because of significant peak overlap between δ 0 and −16 ppm, but the presence of a single 1B resonance at

Scheme 3. Formation of 4, 5, and 6 from Deprotonation and Metalation of III with {CoCp*}

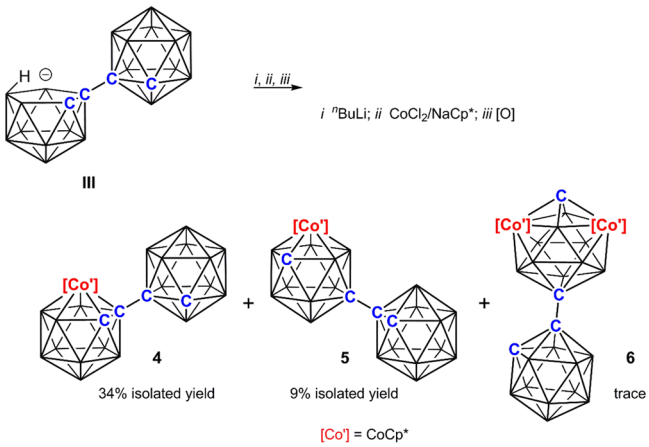

relatively high frequency (δ 10.1 ppm) is consistent with a 3,1,2-CoC_2B_{10}-1′,2′-C_2B_{10} structure by reference to its Cp analogue **I** (M = CoCp). In the ^1H NMR spectrum, in addition to a singlet due to the Cp* protons, are broad $C_{cage}H$ resonances at δ 4.10 and 3.37 ppm. In the Cp analogue the two $C_{cage}H$ resonances are very close and cannot be easily assigned (see Table 2), but in **4** the $C_{cage}H$ of the cobaltacarborane cage is shielded by the inductive effect of the Cp* ligand and shifted ca. 0.6 ppm to lower frequency. The identity of compound **4** was confirmed crystallographically, and a perspective view of a single molecule is shown in Figure 4 (left). The structure is directly comparable with that of its Cp analogue,[6] albeit somewhat more distorted to accommodate the larger steric bulk of the Cp* ligand. Thus, Cp* is more bent away from the C_2B_{10} substituent with a θ value of 21.58(8)° (Cp analogue 15.8, 16.3°), the carborane substituent is less elevated with respect to the C1C2B7B8B4 plane at 16.07(12)° (Cp analogue 19.1, 19.5°), and the C1−Co3 distance is extended at 2.1670(19) Å (Cp analogue 2.118, 2.124 Å).

Yellow compound **5** was afforded in 9% isolated yield, and elemental analysis and mass spectrometry are fully consistent

DOI: 10.1021/acs.inorgchem.8b01166
Inorg. Chem. 2018, 57, 8002−8011

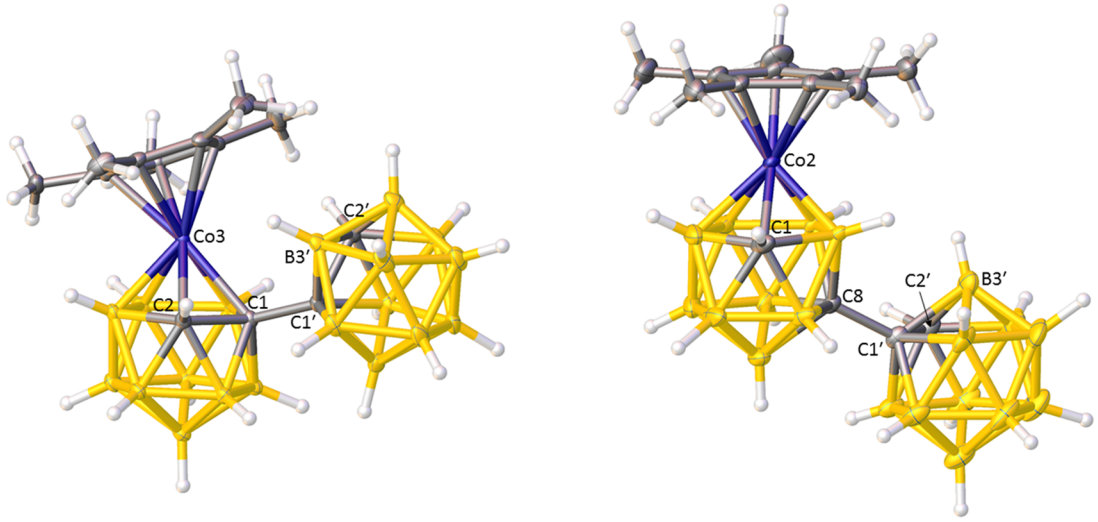

Figure 4. (left) Perspective view of compound **4**. (right) Perspective view of one of the two crystallographically independent molecules of compound **5**.

with **5** being an isomer of **4**. There are two $C_{cage}H$ resonances in the ^{1}H NMR spectrum, but in $CDCl_3$ the lower frequency one (due to the cobaltacarborane) is partially obscured by the signal due to the Cp* protons. Using a mixed solvent of $CHCl_3/CD_3CN$ (1:10), however, shifts the C1*H* resonance somewhat, such that it is now close to, but distinguished from, that of a trace of water. With a frequency of δ 2.09 ppm we again note that the C1*H* resonance in **5** is downfield-shifted by ca. 0.6 ppm with respect to that in the Cp analogue **II** (Table 2). The structure of a single molecule of **5**, established crystallographically, is shown in Figure 4 (right). In marked contrast to the situation in the 3,1,2-CoC_2B_9-1′,2′-C_2B_{10} species **4**, the Cp* ligand in the 2,1,8-CoC_2B_9-1′,2′-C_2B_{10} isomer **5** is now essentially parallel with lower pentagonal belt of the cobaltacarborane, since steric crowding with the carborane substituent is no longer a serious issue.

As previously noted it is somewhat surprising (based on precedence with CoCp[6]) that a significant amount of the 3,1,2-CoC_2B_9-1′,2′-C_2B_{10} species **4** was afforded by in situ metalation of singly deboronated 1,1′-bis(*ortho*-carborane). Nevertheless, **4** may be converted to **5** by a simple redox process. After 1 h of stirring of **4** with 1 equiv of $Na[C_{10}H_8]$ in THF at ambient temperature followed by aerial oxidation conversion is ca. 50%. Note that under the same conditions the Cp analogue of **4** is completely converted to the Cp analogue of **5**.[6]

A minor coproduct in the initial synthesis of **4** and **5** is green compound **6**, whose limited availability (4 mg) resulted in characterization only by mass spectrometry, NMR spectroscopy, and single-crystal X-ray diffraction (Figure 5). Compound **6** consists of a 13-vertex docosahedral dicobaltacarborane in which the metal atoms occupy vertices 4 and 5, and the carbon atoms occupy vertices 1 and 12, with a 1′,2′-$C_2B_{10}H_{11}$ substituent bound at C12. A handful (<20) of docosahedral $MM'C_2B_9$ metallacarboranes are known, and in all structurally established cases[23,28−30] the metal atoms occupy the degree-6 vertices 4 and 5, with the carbon atoms either at vertices 1 and 6 or at vertices 2 and 3. Compound **6** is therefore the first proven example of a 13-vertex bimetallacarborane with a 4,5,1,12-$M_2C_2B_9$ architecture, although this motif has previously been suggested for one isomer of $(CoCp)_2C_2B_9H_{11}$.[31] We suggest that the origin of the

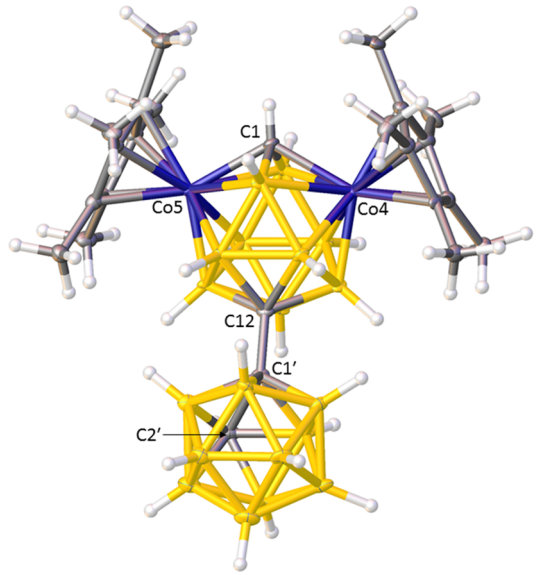

Figure 5. Perspective view of compound **6**.

unexpected product **6** is Direct Electrophilic Insertion (DEI) of a $\{CoCp^*\}^+$ fragment into the anionic species $[4]^-$ or, more likely, $[5]^-$ prior to aerial oxidation. DEI was first recognized as a route to bimetallacarboranes by Kudinov and coworkers,[29] and we have previously used it to deliberately prepare 14-vertex bimetallacarboranes from 13-vertex monometallacarborane anions.[16,26,32] In the ^{1}H NMR spectrum of **6** there are, in addition to the singlet arising from the 30 Cp* protons, two broad integral-1 $C_{cage}H$ resonances at δ 3.80 and 1.26 ppm. By analogy with [6-(1′-*closo*-1′,2′-$C_2B_{10}H_{11}$)-4-(*p*-cymene)-5-(mesitylene)-*closo*-4,5,1,6-$Ru_2C_2B_9H_{10}$],[26] the closest fully characterized compound in the literature, we assign the lower-frequency $C_{cage}H$ resonance in **6** to C1*H*.

Deboronation of **5** with KF in THF/water followed by metathesis afforded the yellow solid $[HNMe_3][8$-(7′-*nido*-7′,8′-$C_2B_9H_{11}$)-2-Cp*-*closo*-2,1,8-$CoC_2B_9H_{10}]$ (**7**) as an equal mixture of diastereoisomers (Scheme 1). Salt **7** gave satisfactory elemental analysis. In the ^{1}H NMR spectrum the C1*H* resonances of the diastereoisomers cannot be resolved

DOI: 10.1021/acs.inorgchem.8b01166
Inorg. Chem. 2018, 57, 8002−8011

and neither can the C8′*H* resonances. By analogy with the $C_{cage}H$ chemical shifts for anion **2** (Table 2), the most similar species, we tentatively assign the resonance at δ 1.96 ppm to C1*H* (shielded relative to that in **2** by the presence of the Cp* ligand) and that at δ 1.88 ppm to C8′*H*. Evidence for a diastereoisomeric mixture is provided by the observation of two close and equal singlets assigned to the Cp* protons at δ 1.85 and 1.84 ppm and a broad low-frequency signal due to the bridging protons of the deboronated cage, which clearly shows partial resolution, with maxima at δ −2.68 and −2.84 ppm.

Interestingly, KF/H_2O deboronation of compound **4** followed by metathesis yields an orange solid that, spectroscopically, appears to be a mixture of salt **7** and another species. We tentatively identify this second species as [HNMe$_3$][1-(7′-*nido*-7′,8′-$C_2B_9H_{11}$)-3-Cp*-*closo*-3,1,2-$CoC_2B_9H_{10}$], that is, the simple B3′ (or B6′) deboronated variant of **4**. Presumably partial isomerization of the cobaltacarborane cage from 3,1,2-CoC_2B_9 to 2,1,8-CoC_2B_9, yielding **7**, accompanies deboronation. When this mixture is treated with ^{n}BuLi and then metalated with [$RuCl_2$(*p*-cymene)]$_2$ a diastereoisomeric mixture of a single species **8** is afforded, exactly the same mixture that is produced by deprotonation/metalation of salt **7** alone. This suggests that deprotonation of [1-(7′-*nido*-7′,8′-$C_2B_9H_{11}$)-3-Cp*-*closo*-3,1,2-$CoC_2B_9H_{10}$]$^-$ results in its complete isomerization to the 2,1,8-CoC_2B_9 isomer, a conclusion that is fully consistent with the reduction-induced isomerization of 3,1,2-MC_2B_9 species we observed previously.[6]

When prepared from salt **7** (Scheme 4), compound **8** [8-(1′-3′-(*p*-cymene)-*closo*-3′,1′,2′-$RuC_2B_9H_{10}$)-2-Cp*-*closo*-2,1,8-$CoC_2B_9H_{10}$] is afforded (as a yellow solid) in 24% isolated yield. Elemental analysis and mass spectrometry are fully consistent with the molecular formula $C_{24}H_{49}B_{18}CoRu$. As anticipated from the fact that precursor **7** exists as two diastereoisomers, compound **8** is also a diastereoisomeric mixture, but, somewhat to our surprise, not an equal one. Although the $^{11}B\{^1H\}$ NMR spectrum is largely uninformative due to multiple overlapping resonances, in the ^1H spectrum are clear resonances for two high-frequency $C_{cage}H$ atoms, two CH_3 groups of the *p*-cymene ligand, and two separate resonances for the Cp* protons (although the chemical shifts here are only distinguished in the third place of decimals). In all cases these pairs of resonances suggest that the two diastereoisomers are present in a ratio of ca. 2:1. The identity of compound **8** is revealed from the ^1H NMR spectrum. We know that the cobaltacarborane cage is of 2,1,8-CoC_2B_9 architecture, since that is what it was in precursor **7**, but the ruthenacarborane cage in **8** must be 3′,1′,2′-RuC_2B_9, since the high-frequency $C_{cage}H$ resonances present (major isomer δ 3.75 ppm, minor isomer δ 3.88 ppm) are much more reminiscent of that in [1-(1′-*closo*-1′,2′-$C_2B_{10}H_{11}$)-3-(*p*-cymene)-*closo*-3,1,2-$RuC_2B_9H_{10}$] (**Ia**, δ 4.03 or 3.91 ppm) than that in [8-(1′-*closo*-1′,2′-$C_2B_{10}H_{11}$)-2-(*p*-cymene)-*closo*-2,1,8-$RuC_2B_9H_{10}$] (**IIa**, δ 2.63 ppm). See Table 2. Note that **8** is the complement of **3** in which {CoCp} in **3** has been replaced by {Ru(*p*-cymene)} and {Ru(*p*-cymene)} in **3** has been replaced by {CoCp*}. Unlike **3**, however, the diastereoisomeric components of **8** could not be separated in spite of exhaustive attempts by TLC, and neither could crystals of either diastereoisomer be grown from the mixture. The final experiment, thermal isomerization of **8**, was therefore performed on the isomeric mixture.

Scheme 4. Formation of 8 and then 9 from Deprotonation and Metalation of 7 with {Ru(*p*-cymene)} Followed by Thermolysis[a]

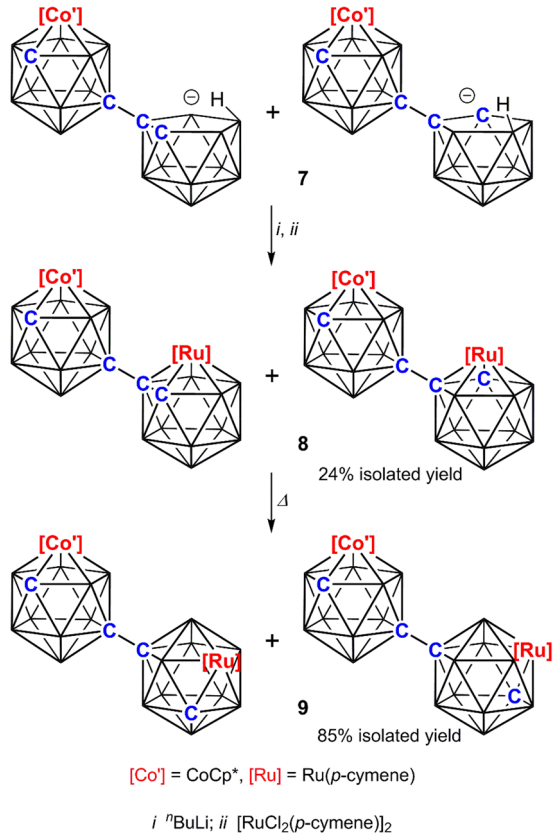

[a]**7**, **8**, and **9** are all mixtures of two diastereoisomers; for **7** this mixture is 1:1, but for **8** and **9** the mixture is 2:1, although in these cases the identities of the major and minor components are not known.

With the indication that the ruthenacarborane cage of **8** was of 3′,1′,2′-RuC_2B_9 form, we investigated its possible thermal isomerization. Compound **8** was recovered unchanged from heating to reflux in THF, but in refluxing DME for 1 h there was clear evidence from ^1H NMR spectroscopy of a change, and isomerization was complete after overnight reflux (Scheme 4). The product, compound **9**, was obtained as a yellow solid and was shown to be an isomer of **8** by elemental analysis and mass spectrometry. As was the case with **8**, compound **9** is a mixture of two diastereoisomers (approximate ratio 2:1) that unfortunately we could not separate in spite of exhaustive attempts to do so.

Compound **9** is [8-(8′-2′-(*p*-cymene)-*closo*-2′,1′,8′-$RuC_2B_9H_{10}$)-2-Cp*-*closo*-2,1,8-$CoC_2B_9H_{10}$], that is, an isomer of **8** in which the ruthenacarborane cage has isomerized from 3′,1′,2′-RuC_2B_9 to 2′,1′,8′-RuC_2B_9. This is clear from the chemical shift of the higher-frequency $C_{cage}H$ resonances in the ^1H NMR spectrum assigned to the ruthenacarborane cage (major isomer δ 2.59 ppm, minor isomer δ 2.62 ppm), which is in accord with the $C_{cage}H$ chemical shift in [8-(1′-*closo*-1′,2′-$C_2B_{10}H_{11}$)-2-(*p*-cymene)-*closo*-2,1,8-$RuC_2B_9H_{10}$] (**IIa**), δ 2.63 ppm (Table 2). In contrast the lower-frequency $C_{cage}H$ resonances in **9**, assigned to the 2,1,8-CoC_2B_9 cage, is barely changed from those in **8**. A clear indication of the approximate 2:1 ratio of the two diastereoisomers of **9** comes from the well-resolved resonances due to the Cp* protons at δ 1.84 (major)

DOI: 10.1021/acs.inorgchem.8b01166
Inorg. Chem. 2018, 57, 8002−8011

and δ 1.83 (minor) ppm. This ratio is effectively the same as that in **8**.

Crystallization of **9** from DCM/petrol affords yellow block crystals of **9**·CH_2Cl_2, and crystallographic study reveals that the two diastereoisomers crystallize together to give a partially disordered structure. Initially this was evident from both VCD and BHD analyses of the prostructure,[15−17] and it was ultimately confirmed by successful refinement. In the cobaltacarborane cage vertices 1 and 11 are essentially 50:50 C/B disordered [occupancy factors of 0.52(2) for C1 and 0.48(2) for B1, with complementary occupancy factors for vertex 11], while in the ruthenacarborane cage vertex 1′ is 0.69(2):0.31(2) C/B, and vertex 11′ is 0.31(2):0.69(2) C/B. The 50:50 disorder in the cobaltacarborane cage means that both diastereoisomers are present in the crystal in equal amounts. Several crystals were successively mounted on the diffractometer, but the unit-cell dimensions of all were identical within experimental error. Figure 6 shows a perspective view of one arbitrary diastereoisomer of **9**.

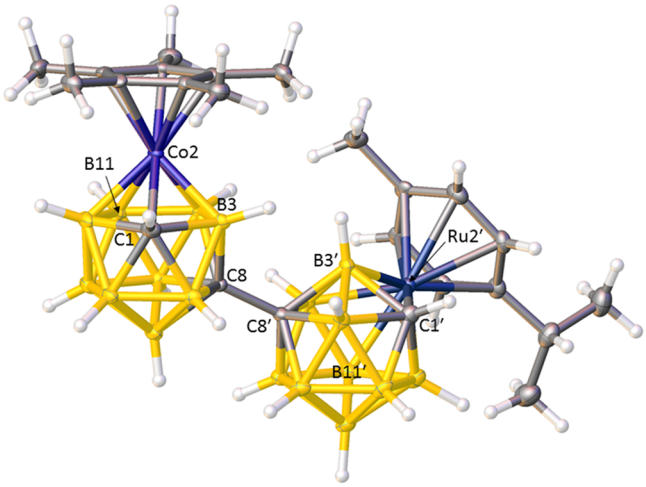

Figure 6. Perspective view of one arbitrary diastereoisomer of compound **9**.

Notwithstanding the disorder, the crystallographic study confirms that in **9** the ruthenacarborane cage has isomerized from the 3′,1′,2′-RuC_2B_9 form in **8** to 2′,1′,8′-RuC_2B_9 in **9**, as inferred by analysis of the ^{1}H NMR spectrum. Just as compounds **3**α and **3**β are the first examples of hetero-bimetallic derivatives of 1,1′-bis(*ortho*-carborane) with 2,1,8-MC_2B_9-3′,1′,2′-M′C_2B_9 structures, so compound **9** is the first hetero-bimetallic derivative with a 2,1,8-MC_2B_9-2′,1′,8′-M′C_2B_9 structure. Exopolyhedral ligand bend-back angles θ in **9** are 1.32(6)° (cobaltacarborane) and 5.54(7)° (ruthenacarborane), close to zero as expected for 2,1,8-MC_2B_9 cages.

CONCLUSIONS

Stepwise deboronation-metalation-deboronation-metalation has allowed isolation of the first examples of heterometalated derivatives of 1,1′-bis(*ortho*-carborane) with both 2,1,8-MC_2B_9-3′,1′,2′-M′C_2B_9 and 2,1,8-MC_2B_9-2′,1′,8′-M′C_2B_9 architectures. Critical to the success of this approach has been the use of the relatively mild reagent KF in THF/H_2O for the second deboronation step. Products are afforded as a mixture of diastereoisomers, since the second deboronation occurs at both the 3′ and 6′ positions of the C_2B_{10} cage. In one case these diastereoisomers could be separated by chromatography.

ASSOCIATED CONTENT

Supporting Information

The Supporting Information is available free of charge on the ACS Publications website at DOI: 10.1021/acs.inorgchem.8b01166.

^{1}H and ^{11}B{^{1}H} NMR spectra of all new products (PDF)

Accession Codes

CCDC 1828646−1828651 contain the supplementary crystallographic data for this paper. These data can be obtained free of charge via www.ccdc.cam.ac.uk/data_request/cif, or by emailing data_request@ccdc.cam.ac.uk, or by contacting The Cambridge Crystallographic Data Centre, 12 Union Road, Cambridge CB2 1EZ, UK; fax: +44 1223 336033.

AUTHOR INFORMATION

Corresponding Author

*E-mail: a.j.welch@hw.ac.uk.

ORCID

Alan J. Welch: 0000-0003-4236-2475

Notes

The authors declare no competing financial interest.

ACKNOWLEDGMENTS

We thank the Engineering and Physical Sciences Research Council and the CRITICAT Centre for Doctoral Training for financial support (Ph.D. studentship to A.P.Y.C.; Grant No. EP/L016419/1). We also thank the U.K. National Crystallography Service, for data collection of compounds **3**α and **9**·CH_2Cl_2, and Dr G. S. Nichol (Univ. of Edinburgh) for data collection of compounds **4** and **5**.

REFERENCES

(1) Wiesboeck, R. A.; Hawthorne, M. F. Dicarbaundecaborane(13) and Derivatives. *J. Am. Chem. Soc.* **1964**, *86*, 1642−1643.

(2) Hawthorne, M. F.; Young, D. C.; Garrett, P. M.; Owen, D. A.; Schwerin, S. G.; Tebbe, F. N.; Wegner, P. A. Preparation and characterization of the (3)-1,2- and (3)-1,7-dicarbadodecahydroundecaborate(−1) ions. *J. Am. Chem. Soc.* **1968**, *90*, 862−868.

(3) Hawthorne, M. F.; Young, D. C.; Wegner, P. A. Carbametallic Boron Hydride Derivatives. I. Apparent Analogs of Ferrocene and Ferricinium Ion. *J. Am. Chem. Soc.* **1965**, *87*, 1818−1819.

(4) Hawthorne, M. F.; Young, D. C.; Andrews, T. D.; Howe, D. V.; Pilling, R. L.; Pitts, A. D.; Reintjes, M.; Warren, L. F.; Wegner, P. A. π-Dicarbollyl derivatives of the transition metals. Metallocene analogs. *J. Am. Chem. Soc.* **1968**, *90*, 879−896.

(5) Grimes, R. N. *Carboranes,* 3rd ed.; Elsevier: Amsterdam, The Netherlands, 2016.

(6) Thiripuranathar, G.; Man, W. Y.; Palmero, C.; Chan, A. P. Y.; Leube, B. T.; Ellis, D.; McKay, D.; Macgregor, S. A.; Jourdan, L.; Rosair, G. M.; Welch, A. J. Icosahedral metallacarborane/carborane species derived from 1,1′-bis(*o*-carborane). *Dalton Trans.* **2015**, *44*, 5628−5637.

(7) Thiripuranathar, G.; Chan, A. P. Y.; Mandal, D.; Man, W. Y.; Argentari, M.; Rosair, G. M.; Welch, A. J. Double deboronation and homometalation of 1,1′-bis(*ortho*-carborane). *Dalton Trans.* **2017**, *46*, 1811−1821.

(8) Ren, S.; Xie, Z. A Facile and Practical Synthetic Route to 1,1′-Bis(*o*-carborane). *Organometallics* **2008**, *27*, 5167−5168 The ^{1}H NMR chemical shift (δ = 5.51 ppm) reported in this paper for the C2*H* and C2′*H* atoms of 1,1′-bis(*ortho*-carborane) in $(CD_3)_2CO$ is at

DOI: 10.1021/acs.inorgchem.8b01166
Inorg. Chem. 2018, 57, 8002−8011

variance with the value (δ = 5.05 ppm) that we and others (e.g., ref 25) record.
(9) Bennett, M. A.; Huang, T.-N.; Matheson, T. W.; Smith, A. K.; et al. (η^6-Hexamethylbenzene)Ruthenium Complexes. *Inorg. Synth.* **2007**, *21*, 74−78.
(10) Kazakov, S.; Sivaev, I. B.; Suponitsky, K. Yu.; Kirilin, A. D.; Bregadze, V. I.; Welch, A. J. Facile synthesis of *closo-nido* bis(carborane) and its highly regioselective halogenation. *J. Organomet. Chem.* **2016**, *805*, 1−5.
(11) Dolomanov, O. V.; Bourhis, L. J.; Gildea, R. J.; Howard, J. A. K.; Puschmann, H. *OLEX2*: a complete structure solution, refinement and analysis program. *J. Appl. Crystallogr.* **2009**, *42*, 339−341.
(12) Sheldrick, G. M. A short history of *SHELX*. *Acta Crystallogr., Sect. A: Found. Crystallogr.* **2008**, *A64*, 112−122.
(13) Sheldrick, G. M. *SHELXT* − Integrated space-group and crystal-structure determination. *Acta Crystallogr., Sect. A: Found. Adv.* **2015**, *A71*, 3−8.
(14) Sheldrick, G. M. Crystal structure refinement with *SHELXL*. *Acta Crystallogr., Sect. C: Struct. Chem.* **2015**, *C71*, 3−8.
(15) McAnaw, A.; Scott, G.; Elrick, L.; Rosair, G. M.; Welch, A. J. The VCD method − a simple and reliable way to distinguish cage C and B atoms in (hetero)carborane structures determined crystallographically. *Dalton Trans.* **2013**, *42*, 645−664.
(16) McAnaw, A.; Lopez, M. E.; Ellis, D.; Rosair, G. M.; Welch, A. J. Asymmetric 1,8/13,2,*x*-$M_2C_2B_{10}$ 14-vertex metallacarboranes by direct electrophilic insertion reactions; the VCD and BHD methods in critical analysis of cage C atom positions. *Dalton Trans.* **2014**, *43*, 5095−5105.
(17) Welch, A. J. What Can We Learn from the Crystal Structures of Metallacarboranes? *Crystals* **2017**, *7*, 234.
(18) Man, W. Y.; Zlatogorsky, S.; Tricas, H.; Ellis, D.; Rosair, G. M.; Welch, A. J. How to Make 8,1,2-*closo*-MC_2B_9 Metallacarboranes. *Angew. Chem., Int. Ed.* **2014**, *53*, 12222−12225.
(19) Mandal, D.; Man, W. Y.; Rosair, G. M.; Welch, A. J. Steric *versus* electronic factors in metallacarborane isomerisation: nickelacarboranes with 3,1,2-, 4,1,2- and 2,1,8-NiC_2B_9 architectures and pendant carborane groups, derived from 1,1′-bis(*o*-carborane). *Dalton Trans.* **2016**, *45*, 15013−15025.
(20) Fox, M. A.; Gill, W. R.; Herbertson, P. L.; MacBride, J. A. H.; Wade, K.; Colquhoun, H. M. Deboronation of *C*-substituted *ortho*- and *meta-closo*-carboranes using "wet" fluoride ion solutions. *Polyhedron* **1996**, *15*, 565−571.
(21) Siedle, A. R.; Bodner, G. M.; Garber, A. R.; Beer, D. C.; Todd, L. J. Antipodal shielding effects in the boron-11, carbon-13 and phosphorus-31 nuclear magnetic resonance spectra of icosahedral carborane derivatives. *Inorg. Chem.* **1974**, *13*, 2321−2324.
(22) Buchanan, J.; Hamilton, E. J. M.; Reed, D.; Welch, A. J. The structure of $[7,8\text{-}C_2B_9H_{12}]^-$; correction of a popular misconception. *J. Chem. Soc., Dalton Trans.* **1990**, 677−680.
(23) Lopez, M. E.; Edie, M. J.; Ellis, D.; Horneber, A.; Macgregor, S. A.; Rosair, G. M.; Welch, A. J. Symmetric and asymmetric 13-vertex bimetallacarboranes by polyhedral expansion. *Chem. Commun.* **2007**, 2243−2245.
(24) Kaloustian, M. K.; Wiersema, R. J.; Hawthorne, M. F. Thermal rearrangement of π-cyclopentadienyl-π-dicarbollyl derivatives of cobalt. *J. Am. Chem. Soc.* **1972**, *94*, 6679−6686.
(25) Yang, X.; Jiang, W.; Knobler, C. B.; Mortimer, M. D.; Hawthorne, M. F. The synthesis and structural characterization of carborane oligomers connected by carbon-carbon and carbon-boron bonds between icosahedra. *Inorg. Chim. Acta* **1995**, *240*, 371−378.
(26) Man, W. Y.; Ellis, D.; Rosair, G. M.; Welch, A. J. Carborane Substituents Promote Direct Electrophilic Insertion over Reduction-Metalation Reactions. *Angew. Chem., Int. Ed.* **2016**, *55*, 4596−4599.
(27) Mingos, D. M. P.; Forsyth, M. I.; Welch, A. J. Molecular and crystal structure of 3,3-bis(triethylphosphine)-1,2-dicarba-3-platinadodecaborane(11), and molecular-orbital analysis of the 'slip' distortion in carbametallaboranes. *J. Chem. Soc., Dalton Trans.* **1978**, 1363−1374.
(28) Kudinov, A. R.; Rybinskaya, M. I.; Perekalin, D. S.; Meshcheryakov, V. I.; Zhuravlev, Yu. A.; Petrovskii, P. V.; Korlyukov, A. A.; Golovanov, D. G.; Lyssenko, K. A. Structures of cationic metallacarborane complexes $[(\eta\text{-}9\text{-}Me_2S\text{-}7,8\text{-}C_2B_9H_{10})Ni(\mu\text{-}Cp)Ni(\eta\text{-}9\text{-}Me_2S\text{-}7,8\text{-}C_2B_9H_{10})]^+$ and $[Cp^*Ru(Me_2S\text{-}C_2B_9H_{10})\text{-}RuCp^*]^+$. *Russ. Chem. Bull.* **2004**, *53*, 1958−1962.
(29) Kudinov, A. R.; Perekalin, D. S.; Rynin, S. S.; Lyssenko, K. A.; Grintselev-Knyazev, G. V.; Petrovskii, P. V. Direct Electrophilic Insertion into a Twelve-Vertex Metallacarborane. *Angew. Chem., Int. Ed.* **2002**, *41*, 4112−4114.
(30) Grüner, B.; Štíbr, B.; Kivekäs, R.; Sillanpää, R.; Stopka, P.; Teixidor, F.; Viñas, C. Diferratricarbaboranes of the *subcloso*-$[(\eta^5\text{-}C_5H_5)_2Fe_2C_3B_8H_{11}]$ Type, the First Representatives of the 13-Vertex Dimetallatricarbaborane Series. *Chem. - Eur. J.* **2003**, *9*, 6115−6121.
(31) Dustin, D. F.; Hawthorne, M. F. New 13-atom bimetallocarboranes prepared by polyhedral subrogation. *J. Am. Chem. Soc.* **1974**, *96*, 3462−3467.
(32) Robertson, A. P. M.; Beattie, N. A.; Scott, G.; Man, W. Y.; Jones, J. J.; Macgregor, S. A.; Rosair, G. M.; Welch, A. J. 14-Vertex Heteroboranes with 14 Skeletal Electron Pairs: An Experimental and Computational Study. *Angew. Chem., Int. Ed.* **2016**, *55*, 8706−8710.

DOI: 10.1021/acs.inorgchem.8b01166
Inorg. Chem. 2018, 57, 8002−8011